A MULTIPLE PARAMETER APPROACH

TO LOG ANALYSIS: A PETROPHYSICAL STUDY

by

GEORGE A. ANDERSON III, B.S., M.S.

A DISSERTATION

IN

GEOSCIENCE

Submitted to the Graduate Faculty
of Texas Tech University in
Partial Fulfillment of
the Requirements for
the Degree of

DOCTOR OF PHILOSOPHY

Approved

Co-Chairperson of the Committee

Co-Chairperson of the Committee

Accepted

Dean of the Graduate School

May, 2003

ACKNOWLEDGEMENTS

I want to express my appreciation to Burlington Resources, Midland, TX, for bringing this project to the Center for Applied Petrophysical and Reservoir Studies at Texas Tech University and for providing the data to examine the problem and complete the research. I want to further express my appreciation to Burlington Resources for funding the study, and for the time and effort of the Burlington technical professionals in providing the support to initiate the study and for their continuing support for data base questions and needs. Burlington was an excellent corporate sponsor of this research project.

The breadth and depth of knowledge in petrophysical analysis of reservoir character and value of Dr. George B. Asquith and Dr. Scott M. Frailey, co-chairs of my dissertation committee, was vital to the success of my research. My own personal, nearly quarter-century professional experience in the petroleum industry would not have led me to the awareness and the methods upon which my research ultimately was founded. I was fortunate to find these two experts working together at Texas Tech and I look forward to using what I have learned from them to further the effectiveness of interpreting reservoir value in the successful exploitation of oil and gas reserves.

My courses and discussions with my committee members, Dr. James E. Barrick and Dr. Thomas M. Lehman, have been helpful in improving my understanding of the fundamental concepts and processes in geology and in planning research projects. I leave Texas Tech with a usefully expanded awareness of the interaction of geologic processes operating within the hierarchy of scales embedded in natural earth systems.

My fellow geoscience graduate students were a pleasure for an old guy to be around. They helped make the experience enjoyable, and often, quite funny. It was also a valuable lesson in the quality of the young people moving into adulthood today. They are a talented, capable group, ready for the challenges ahead.

I want to acknowledge my former colleague at Mobil Oil and great friend, Elizabeth Baker Elliott. Betty rests now on a shaded, grassy hill north of her birthplace in

Cordell, Oklahoma, that looks out over the Granite Wash reservoirs of the deep Anadarko Basin (of which she spoke often and which I had no idea would one day become so important to me). Many years ago, Betty made the effort to provide an opportunity to a young man she only met on a Mobil "Farm-Out" in Arkansas. She thought I worked hard to do a good job of wellsite geology under adverse conditions, and that I could make a good Mobil geologist, a group of professionals she respected and brought respect to. Her effort and friendship changed the direction of my life at a critical time, leading to my professional career and ultimately to my studies here at Texas Tech. Selfless individuals can have important effect on the lives of others, and Betty was one of those kinds of folks. I never thanked her enough when I could and I certainly want to remember to thank her now. Thank you so very much for helping to give me a chance, Betty.

My parents, George and Romaine Anderson, grew up in a time when work was often deemed more important than education, and neither finished high school before starting the work of their adult lives. As parents of a daughter and son, though, they never failed to express their insistence that their kids had to work hard at school and their belief that their kids were going to go to college. They put their money where their mouth was, and supported the expense of eight straight years of college tuition and room and board to see their daughter and son graduate from college. Their belief in the value of education grew from the hard work and responsibility of their own lives, and they drew honor and pleasure from the educational and professional accomplishments of their children. I have arrived at this time and place because of the values imbued in both my sister and me by two honorable people, our parents. They have been an inspiration.

I spent over three years living in Lubbock while working on my degree. My wife, Thena Anderson, supported me in pursuing my goal (and dream) of a Ph.D. at a time when perhaps it would have been better to focus on preparing our finances for retirement. She endured those years when I was not home to talk about how our days went and to lock the doors at night. It has taken more years than I thought it would, but she has been steadfast in her support. Pursuit of this degree has not been easy for me, but my wife, Thena, has made it easier, and we have done it together, and I thank her dearly for that.

Finally, I would like to express my appreciation to Ms. Joan Blackmon, Petroleum Engineering, Business Manager, for her invaluable support in editing this manuscript to Texas Tech University Graduate School standards. I would also like to express my appreciation to the Petroleum Engineering Department, under Dr. James F. Lea, in providing facilities and support to permit me to complete this manuscript on campus.

TABLE OF CONTENTS

ABSTRACT

Standard Archie water saturation and formation porosity are the two key parameters determined from wireline logs that are used in the evaluation of a subsurface reservoir as a potential hydrocarbon producer. They are measures of reservoir content but not reservoir performance, and by themselves do not provide an actual indication of the hydrocarbon productivity of a reservoir.

The Desmoinsian Prue Sands, in the granite wash facies of the deep Anadarko Basin in southwestern Oklahoma, are established gas reservoirs that have proven difficult to evaluate petrophysically in order to distinguish hydrocarbon productive and non-productive reservoirs. This study is intended to develop a different approach to log analysis in the texturally and mineralogically variable Prue Sands to improve the reliability of log analysis as an indicator of Prue hydrocarbon productivity.

A suite of petrophysical parameters from a basic log package was used to examine reservoir characteristics in addition to Archie water saturation and formation porosity. These include the resistivity of the connate water in the reservoirs, reservoir quality, hydrocarbon movability and alternate methods to calculate water saturation values for the reservoir. Bulk volume water values were used to assess the relationship of water saturation of the reservoir to irreducible water saturation and to the grain size distribution that comprises the reservoir framework. Selected parameters can indicate reservoir characteristics that suggest the presence of excess conductivity associated with reservoir shaliness, a condition that is otherwise difficult to determine in the Prue granite wash.

Logs from a series of wells with a range of established Prue production characteristics, from excellent to poor, were examined using the suite of petrophysical parameters included in this study. Results from the analysis of this suite of parameters were grouped into ranges of values representing the range of hydrocarbon production from the wells analyzed. The groups of values were ranked with a series of integer

scores from 5 to 1 to represent the range of hydrocarbon productivity. Outlier scores of 0 and –1 represented conditions outside the normally expected ranges.

A petrophysical analysis program was developed on a personal computer using the spreadsheet program Microsoft Excel to compute the multiple parameters used in the petrophysical analysis of the Prue. Results are extracted from the program and a series of charts generated in Excel are used to display and interpret the results. This study has demonstrated that production-calibrated ranking of multiple petrophysical parameters can be used to evaluate the hydrocarbon productivity of the Prue.

LIST OF TABLES

LIST OF FIGURES

NOMENCLATURE LIST FOR EQUATIONS

A = container area, m^2

BHT = Bottom hole Temperature (recorded on Log Header), °F

a = Tortuosity Factor

c_{cl} = excess conductance from counter-ions concentrated on clay plate surface area in pore system, mhos

c_o = total conductance of a fluid filled pore, mhos

c_w = conductance of the pore electrolyte, mhos

CW = Connate Water

d_h = Borehole Diameter, inches

d_i = Electrically Equivalent Invaded Zone Diameter, inches

DOI = Depth (Radius) of Investigation of each Resistivity Log

ϕ = Formation Porosity

F = the Faraday, coulumbs

F_{DN} = Formation Resistivity Factor Developed from Density - Neutron Porosity, as Expressed in Equation 6.3.

F_R = Empirical Formation Resistivity Factor

F_{Rd} = Uninvaded Zone Formation Rexsistivity Factor: Developed using Rd & Rw

F_{Ri} = Invaded Zone Formation Resistivity Factor: Developed using Ri & Rz

F_{Rxo} = Flushed Zone Formation Resistivity Factor: Developed using Rxo & Rmf

F_{Rxoc} = Flushed Zone Formation Resistivity Factor: Developed using Calculated Rxo & Rmf

FZ = Flushed Zone part of the Invaded Zone

h = Permeable Bed Thickness, ft

I = Formation Resistivity Index

I = current, amperes

ILD = Deep Induction Log

ILM = Medium Induction Log; measures resistivity @ about half the DOI of the ILD log

I_o = current flow through the brine-filled sand, amperes

I_w = current through the brine, amperes

IZ = Invaded Zone: Combination of FZ & TZ

L = container length, m

LL8 = Laterolog 8

Logger's TD = Total Depth Reached by Logger to record the BHT (recorded on Log Header), ft

m = Cementation Exponent

MAST = Mean Annual Surface Temperature (Assumed 60° F for this study)

MC = Mud Cake

MF = Mud Filtrate

ML = Microlog

MSFL = MicroSpherically Focused Log

n = Saturation Exponent

Oil = Oil

PL = Proximity Log

R = Universal Gas Constant, joules

R_d = Resistivity of Uninvaded Zone, Ω-m

R_i = Measured Resistivity of the Invaded Zone, Ω-m

R_m = Resistivity of the mud in the well bore, Ω-m

R_{mc} = Resistivity of the Mud Cake, Ω-m

R_{med} = Medium DOI Resistivity, Falls Between R_d and R_i, Ω-m

R_{mf} = Measured Resistivity of the Mud Fltrate, Ω-m

r_o = resistance of the brine-filled sand, Ohms (Ω)

R_o = resistivity of a 100% water saturated formation, Ω-m

R_o = resistivity of the brine-filled sand, Ω-m

R_o = resistivity of the brine-filled sand, Ω-m.

R_t = Formation Resistivity, Ω-m

R_t = resistivity of partly water saturated formation (saturation remainder is non-conducting fluid), Ω-m

R_w = Measured Resistivity of the Connate Water, Ω-m

r_w = brine resistance, Ohms (Ω)

R_w = Connate Water Resistivity, Ω-m

R_{xo} = Measured Resistivity of the FZ, Ω-m

R_{xoc} = Calculated Resistivity of Flushed Zone, Ω-m, Using Equations 1.2, 1.3.

R_z = Resistivity of IZ saturating water for Shallow DOI: weighted average of $R_{mf} + R_w$, Ω-m

r_w = Wellbore Radius, in.

r_i = Mud Filtrate Invaded Radius, in.

R_{T1} = Resistivity at Measured Temperature recorded on Log Header

R_{T2} = Resistivity at Formation Temperature

SFL = Spherically Focused Log

S_i = Water Saturation in the shallow portion of IZ; Mud Filtrate + Connate Water

SP = Spontaneous Potential Curve; Permeable Zone Log

S_w = Water Saturation in the UIZ; all Connate Water (CW)

S_w = Water Saturation,

S_{xo} = Water Saturation in the FZ; all Mud Filtrate (MF)

τ = Tortuosity = L' / L

Tgrad = Geothermal Gradient, °F / 100 ft

T_1 = Temperature Recorded on Log Header for Rmf Measurement, °F

T_2 = Formation Temperature, °F

T_2 = Absolute Temperature, °K

TZ = Transition Zone part of the Invaded Zone

UZ = Uninvaded Zone

V = Potential difference, volts

WBA = Well Bore Axis

u = Mobility of the Chloride ion

v = Mobility of the Sodium ion

ψ = Conductive Area Ratio = A' / A

NOMENCLATURE FOR PETROPHYSICAL PARAMETERS

SP Parameter to Assess SP Response Across a Reservoir Using a Ratio, $SP_{PRUEZONE}$ / $SP_{PRUEMAX}$, to Normalize Each SP Curve with the Maximum SP Across a Prue Reservoir in a Well

Density – Neutron Porosity Parameter to Assess Formation Porosity Values Calculated Using the Root-Mean Square Formula,

$$\phi_{DN} = \left(\left(\phi_D^2 + \phi_N^2\right)/2\right)^{0.5}$$

Ri / Rd Parameter to Assess Invasion Profile Factor as a Ratio of Shallow and Deep Formation Resistivity

Gas Effect Parameter to Assess Gas Effect in a Reservoir by the Difference Between Density Porosity and Neutron Porosity

FMOP_Rxoc Comparison of Ratios (F_{DN}/F_{Rxoc}), (F_{DN}/F_{Rd}), and (F_{Rxoc}/F_{Rd}) to Assess Hydrocarbon Saturation in the Flushed Zone and Uninvaded Zone as Parameter to Characterize Movable Hydrocarbons and Detect Excess Conductivity

FMOP_Ri Comparison of Ratios (F_{DN}/F_{Ri}), (F_{DN}/F_{Rd}), and (F_{Ri}/F_{Rd}) to Assess Hydrocarbon Saturation in the Invaded Zone and Uninvaded Zone as Parameter to Characterize Movable Hydrocarbons and Detect Excess Conductivity

PhiRes_Rxoc Comparison of Ratios (Phi_{Rxoc}/Phi_{DN}), (Phi_{Rd}/Phi_{DN}), and (Phi_{Rd}/Phi_{Rxoc}) to Assess Hydrocarbon Saturation in the Flushed Zone and Uninvaded Zone as Parameter to Characterize Movable Hydrocarbons. Strict Flushing Assumption Applied

PhiRes_Ri Comparison of Ratios (Phi_{Ri}/Phi_{DN}), (Phi_{Rd}/Phi_{DN}), and (Phi_{Rd}/Phi_{Ri}) to Assess Hydrocarbon Saturation in the Invaded Zone and Uninvaded Zone as Parameter to Characterize Movable Hydrocarbons. Strict Flushing Assumption Applied

PhiResA_Rxoc Comparison of Ratios (Phi_{Rxoc}/Phi_{DN}), (Phi_{Rd}/Phi_{DN}), and (Phi_{Rd}/Phi_{Rxoc}) to Assess Hydrocarbon Saturation in the Flushed Zone and Uninvaded Zone as Parameter to Characterize Movable Hydrocarbons and Detect Excess Conductivity

PhiResA_Ri Comparison of Ratios (Phi_{Ri}/Phi_{DN}), (Phi_{Rd}/Phi_{DN}), and (Phi_{Rd}/Phi_{Ri}) to Assess Hydrocarbon Saturation in the Invaded Zone and Uninvaded Zone as Parameter to Characterize Movable Hydrocarbons and Detect Excess Conductivity

MHI(Ri) Quotient of Ratios of Formation Resistivities and Saturating Aqueous Solution Resistivities, $[(Ri/Rt) / (Rz/Rw)]^{0.5}$, in the Invaded Zone and Uninvaded Zone as Parameter to Characterize Movable Hydrocarbons

MHI(Rxoc) Quotient of Ratios of Formation Resistivities and Saturating Aqueous Solution Resistivities, $[(Rxoc/Rt) / (Rmf/Rw)]^{0.5}$, in the Flushed Zone and Uninvaded Zone as Parameter to Characterize Movable Hydrocarbons

Kr Ratio (krw/krg) as Parameter to Characterize Relative Permeability to Gas

Swa Calculated Archie Water Saturation Parameter

Swpat Ratio (Sw_a / $Sw_{Patchett}$) as Parameter to Assess Affect of SP on Calculated Archie Water Saturation.

Swr1/2 Calculated Ratio Water Saturation Parameter using ($Si = Swa^{0.5}$) Assumption

Swr1/5 Calculated Ratio Water Saturation Parameter using ($Si = Swa^{0.2}$) Assumption

Swr : Swa Parameter Using Quotient of Differences, (Swr1/5-Swa) / (Swr{1/5-1/2}), to Compare the Consistency Between Range of Values of Calculated Ratio Water Saturation Values and Calculated Archie Saturation Values

BVW_SD Parameter to Assess BVW Data Scatter Based on Results of Standard Deviation Screen as an Indicator of Irreducible Water Saturation

BVW Parameter to Assess Reservoir Grain Size Distribution, Based on Asquith (1982) Table 8, Using Calculated BVW Value and Assuming the Reservoir is at Irreducible Water Saturation

CHAPTER I

INTRODUCTION

Location of Study

The study area lies in the deep basin axis of the asymmetrical Anadarko Basin, in T. 9-10 N., R. 19-20 W., in Washita County in southwestern Oklahoma. It is approximately 6 – 7 miles north of the fault system along which granitic provenance terrain of the Wichita Mountains was uplifted (Fig. 1.1, modified from Andrews, 1996).

Purpose of Study

Burlington Resources, of Midland, Texas, brought this project to The Center for Applied Petrophysical and Reservoir Studies at Texas Tech University. The problem arose from Burlington's efforts to develop the natural gas reserves contained in the upper Desmoinesian, upper Cherokee, Prue sandstones in the Anadarko Basin that lies within their leasehold position in Washita County, Oklahoma. Burlington found that results of Prue production tests in new wells, successful or unsuccessful, could not be explained in terms of the results from the petrophysical analysis Burlington completed on the tested Prue sands. The results of petrophysical analysis of wells with successful production tests looked similar to the results of petrophysical analysis of wells with unsuccessful production tests. It was difficult to make effective decisions on which new wells to test and which to plug and abandon without testing. This is an important distinction because in order to achieve commercial production rates from this tight gas reservoir, expensive hydraulic fracture stimulation procedures are required. Assuming this additional completion expense unnecessarily, in addition to the dry hole expense of an 11,000-ft well burdens the economics of a drilling program and further reduces operating unit profitability.

Prue sands are viable objectives in the study area, but the identification of Prue test candidates can confound routine petrophysical analysis. The purpose of this study is to determine how to recognize producible hydrocarbon accumulations in the Prue from a

standard logging suite. This must be performed in a rock-fluid system with common mud log gas shows, complex mineralogy, textural variability, and the potential for variable R_w in stacked sands.

The production-calibrated multiple parameter approach to petrophysical analysis was developed as part of this study in order to improve the effectiveness of decisions made in selecting zones to test in a wellbore drilled to find and produce hydrocarbons from the Prue. A suite of petrophysical parameters has been applied to the analysis of the hydrocarbon potential of the Prue sands in the Anadarko Basin. Outcomes from the analysis of all the petrophysical parameters were ranked in terms of their interpreted relationship to a range of hydrocarbon producibility representative of the Prue within the study area.

The Prue wells that were examined exhibit a wide range of production-test results and the ranked outcomes were compared to actual production test results. The comparison demonstrated that the production-calibrated multiple parameter approach provided a ranked assessment of the hydrocarbon potential of individual reservoirs that properly characterized the Prue sand potential for a successful test. A review of the production-calibrated petrophysical parameter method for the Prue was described in Anderson et al. (2002a).

In order to assess the flexibility of the multiple parameter approach to petrophysics beyond its application in Pennsylvanian siliciclastics of the Anadarko Basin, the method was applied to two carbonate reservoirs in the Permian Basin. It is not intended as a rigorous, production-calibrated interpretation, but rather as a scoping examination of the application of multiple parameters in the petrophysical analysis of carbonate reservoirs. Two parameters developed for the analysis of granite wash gas reservoirs had to be replaced, and selected changes were made to the ranges of analytical outcomes for the petrophysical parameters relative to the scores for the carbonates. A review of the multiple parameter approach to log analysis in carbonates was described in Anderson et al. (2002b).

Previous Work

Burlington Resources, as Meridian Oil Company, drilled the *Flying J 3-11* well in 1995 for lower Cherokee objectives, stratigraphically below the Prue. Two cores, each about 58-ft long, were recovered in the lower Cherokee. Sample information from a mudlog through this lower Cherokee formation, as well as the cores, indicates that the lower Cherokee in this well is part of the granite wash depositional sequence. Frost et al. (1982, p. 121) indicate that granite wash sandstones historically have proven a difficult petrophysical challenge because the presence of naturally radioactive framework mineral grains complicates the determination of variable clay content that affects reservoir quality.

Burlington (Meridian) engaged a consulting firm to prepare a petrophysical analysis of the *Flying J 3-11* wireline logs to detect and evaluate productive zones in the lower Cherokee section (Petrophysical Evaluation of Meridian Oil Flying J No. 3-11, S. Burns Flat Field, Washita Co., Oklahoma; Meridian Oil undated consultant report). After completing core-log calibration, the consultant determined shale volume using the minimum value computed from the spontaneous potential (SP), the shallow guard log, apparent grain density from density-neutron logs, or the neutron log. No specific equations were reported by the consultant to characterize any of these shale volume relationships.

Values for porosity were computed using only the density log, because an accurately determined shale volume proved elusive, and shale corrections for the neutron and acoustic logs could not be applied. It appears there was little confidence in the calculated shale volumes, yet that parameter is critical in shaly sand analysis. Furthermore, chlorite was identified as an authigenic clay in sands in the core, and this clay can affect porosity calculated from density logs.

According to that same consultant's report, a value of 0.15 Ωm at 75 °F was determined for connate-water resistivity, R_w, using the minimum R_{wa} method. This single value was used, corrected for temperature, for all zones analyzed in that report, which extended over 1000 ft of vertical section, from about 12,500 ft to 13, 500 ft. Choosing

one R_w value over an extensive interval in a sedimentary section deposited in an environment of interfingering marine and non-marine conditions apparently was not considered a cause for concern in the analysis.

Water saturation was calculated in the consultant's report using the Dual Water Method, which requires values for shale volume, as well as the assumption that petrophysical properties of adjacent shales reflect the petrophysical properties of the clays in the sands. Dewan (1983, pp. 57-258) provides a summary of the calculations involved in the Dual Water Method. The values used for Archie's empirical parameters, *a*, *m*, and *n* were 1, 2, and 2, respectively.

The consultant calculated permeability values from log data as a function of density porosity and shale volume using a variation of an unreferenced Core Lab equation (Equation 1.1). The values computed using Equation 1.1 are in terms of permeability to air at surface conditions, however the consultant's report does not provide the units, darcies or millidarcies, in which the permeability values are computed. Since the millidarcy is the permeability unit used in core analysis (Core Lab, 1973, pp. 2-13), it is assumed the units developed from the equation are millidarcies.

$$Log(Perm) = (9.6 \times \phi_{Total}) - (6.5 \times V_{Shale}) - 1.635 \qquad 1.1$$

In order to select zones to test, the consultant ultimately focused on calculated values of permeability in combination with calculated values of water saturation. The methods are assumption-intensive, cumbersome to complete and depend on shale volume determination that may not be reliable in the granite wash. Ultimately, the value to Burlington of the method developed by the consultant is reflected in Burlington's decision to bring the problem to the Center for Applied Petrophysical and Reservoir Studies at TTU. Burlington felt compelled to get a second study to address their objective: to develop a petrophysical method that provides for more effective decisions on which granite wash wells to complete and which wells to abandon without testing.

Available Data

Prue Sand data available to this study included 16 wells that tested the Prue. Log data included copies of log prints from each of the wells and digital log data over the Prue interval, along with formation tops picked by Burlington. Log data from each well examined in this study represents basic openhole logging data. Each well has a spontaneous potential curve, a gamma ray curve and dual induction-laterolog (or SFL) curves. Calculated R_{xo} curves were also generated for each well using relationships from Schlumberger (1989a, p. 8-11) and are cited as R_{xoc} to denote they are calculated and not measured curves. The relationships used to compute [R_{xo}/R_t] from [R_{LL8}/R_{ID}] and [R_{SFL}/R_{ID}] are shown below as Equation 1.2 and Equation 1.3, respectively.

$$\frac{R_{xo}}{R_t} = \left[1.85 \left(\frac{R_{LL8}}{R_{ID}} \right) - 0.85 \right] \qquad 1.2$$

$$\frac{R_{xo}}{R_t} = \left[1.45 \left(\frac{R_{SFL}}{R_{ID}} \right) - 0.45 \right] \qquad 1.3$$

Density-Neutron data was available in each well examined from which to determine formation porosity. Sonic log data was available only inconsistently in the wells examined and was not used in any of the petrophysical calculations.

Information on intervals tested, test results, and cumulative production through April 1999 was obtained from scout ticket data provided by Burlington. Burlington also provided Prue structure maps and completion zone maps over the study area. There were no Prue core samples available from any of the 16 wells, but sample description and mudlog show information was available in those wells with mudlogs.

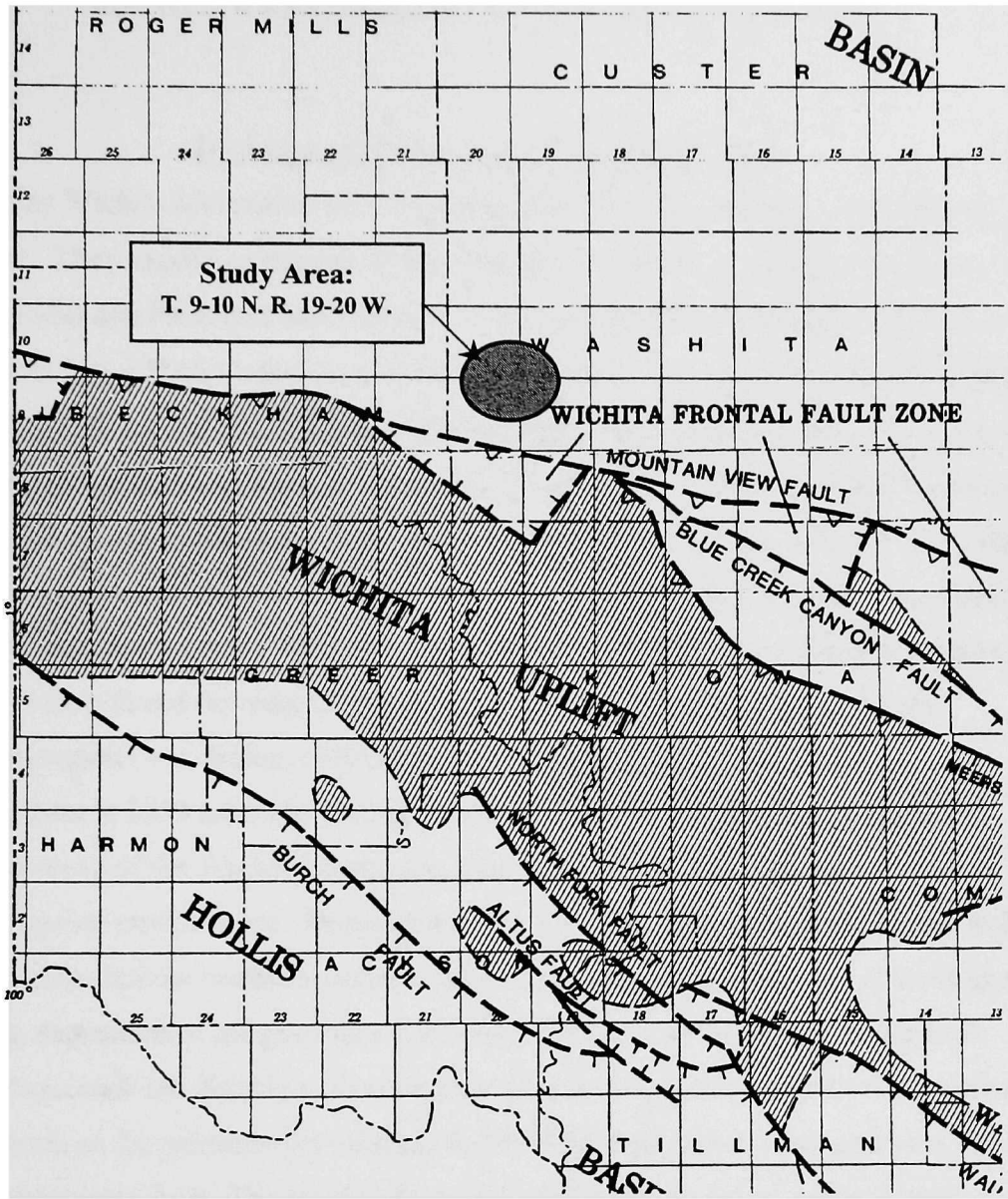

Figure 1.1. Study Area Location Map (Adapted from Andrews, R. D., et al., 1996).

CHAPTER II

GRANITE WASH GEOLOGY OF THE ANADARKO BASIN

Tectonics and Deposition of the Granite Wash

The Wichita Mountains are a system of low relief hills that represent uplifted basement. They expose a complex of late Precambrian to early - middle Cambrian igneous rocks and Paleozoic sedimentary cover in southwestern Oklahoma (Chase, et al, 1956, table 1, p. 37; McConnell and Gilbert, 1986, table 1, p. 16). The Amarillo Uplift is a buried mountain range that continues this uplifted basement trend west into the Texas Panhandle. Together, the Wichita – Amarillo Uplift constitutes the southern border of the Anadarko Basin (Ball et al., 1991, p. 1; GRI, 1991, fig. 1; Evans, 1979, p. 97). These two fault-bounded tectonic features are elements of the early Pennsylvanian Ancestral Rockies. They are a part of a system of intracratonic, fault-bounded basement uplifts and adjacent basins found throughout the western Midcontinent and adjoining Rocky Mountain region (Ver Weibe, 1930; Dutton, 1982; Rascoe and Adler, 1983).

Edwards 1959 indicated that igneous rock fragments eroded from exposed basement rocks of the Wichita Mountains were transported from the highlands into a fringing marine environment. Deposition resulted in a broad alluvial-deltaic front with interfingering shallow marine sediments in the southern Anadarko Basin. According to Edwards, deposition of the gravelly-sandy-silty sediments derived from the adjacent granitic highlands led directly to development of mineralogically and texturally complex granite wash as the principle depositional facies of Pennsylvanian sediments near the Wichita Mountain front. The results of a sedimentological study by Dutton (1982) supported Edwards' conclusion and indicated that Atokan through Wolfcampian granite washes accumulated as thick fan-delta wedges along the fault-bounded uplifts that form the southern border the Anadarko Basin.

Stratigraphy of the Granite Wash

In this setting, upper Demoinesian terrigenous clastics fall within the stratigraphic range of granite wash development. Consequently, the upper Cherokee Prue Sands (Figure 2.1.) should be expected to exhibit textural and mineralogical characteristics of granite wash sands and conglomerates deposited in a fan-delta environment.

System	Series	Group		Formation
Permian	**Wolfcampian**	Chase Council Grove		Brown Dolomite
Pennsylvanian	**Virgilian**	Cisco	Wabaunsee	
			Shawnee	Heebner Sh.
			Douglas	Douglas
				Tonkawa
	Missourian	Hoxbar	Ochelata	Avant
				Cottage Grove
			Skiatook	Hogshooter
				Checkerboard
				Cleveland SS
	Des Moinesian	Deese	Marmaton Group	Big Lime
				Oswego
			Cherokee Group	**Prue SS**
				Verdigris LS
				Skinner SS
				Pink Lime
				Red Fork SS
	Atokan			Atoka
				Clinton Lake
				13 Fingers Lime
	Morrowan			Upper Morrow
				Lower Morrow
				Primrose
	Springeran			Cunningham
				Springer

Figure 2.1. Generalized Stratigraphy: Anadarko Basin (Adapted from Burlington Resources: Generalized Stratigraphic Column for the Anadarko Basin).

CHAPTER III

STATEMENT OF PROBLEM

Textural and Mineralogical Complexities

The Prue is 800 to 900 ft thick in the study area. Eight or more individual sands can be recognized on SP logs, supported by defining Rate of Penetration (ROP) breaksand sample descriptions where available, across the stratigraphic extent of the Prue. Mudlog samples in these intervals are described variously as granite wash, conglomerate wash, quartz wash and sandstone, and they commonly exhibit gas shows rising distinctly above background gas measurements. Commercial gas production has been established in several of the Prue sands encountered at different stratigraphic levels in the study area.

Prue Sands have demonstrated productive potential in the study area. However, completing these sands requires expensive hydraulic fracturing. Successful identification of which, if any, of the stacked Prue Sands are viable test candidates is critical to avoid the expense burden of unnecessary testing and failed completions on a Prue drilling program. Effective petrophysical analysis and interpretation are imperative to achieve this end. There were no Prue cores available to this study to provide the opportunity for rock-log calibration.

The log suite typically available for each well in this study includes density-neutron and gamma-ray logs and dual induction-laterolog (or SFL) and spontaneous–potential (SP) logs. Frost et al. (1982) indicated that granite-wash reservoirs throughout the southwestern United States are complex reservoirs that standard logging suites cannot reliably evaluate due to the complexity of their mineralogy. Mineral groups represented include feldspar and mica (as grains and in rock fragments) and commonly a significant clay volume. Potassium in the alkali feldspar and mica framework grains deprives the petrophysicist of a key shaliness indicator, the conventional gamma-ray log.

Garber (1999) described the Pennsylvanian granite wash of North America's Midcontinent as exhibiting tremendous textural variance, with diverse mineralogical composition. Evaluating its reservoir potential is a daunting challenge, according to Garber, that requires combined technologies to properly address the analytical difficulties. Garber recommended a combination of formation-imaging and magnetic-resonance tools as the solution leading to improved interpretation of productive zones in granite-wash reservoirs. Frost et al. (1982) also concluded that interpretation in granite-wash formations does not yield satisfying results when approached with conventional techniques and that natural gamma-ray spectral logs are critical to successful petrophysical interpretation in granite wash.

These tools could add useful information to petrophysical interpretation in granite washes, but they're not routinely available in the study area. However, the basic strategy noted by Garber and Frost et al. is sound in recommending reliance on a variety of petrophysical measurements to produce better interpretations. This study has shown that a complete analysis of all the important information contained in a standard logging suite is an effective method in granite-wash evaluation. Extracting as much information as possible from a standard log suite leads to the development of multiple petrophysical parameters that provide more information pertinent to evaluating Prue hydrocarbon productive potential than calculated water saturation only.

Variable R_w

In one well analyzed early in the study, SP deflection amplitude was observed to be different among separate Prue Sands over a 300-ft interval. The mudlog for the well, however, showed uniform ROP development in those same sands, with minor clay content noted in the samples. If all the sands are reasonably clean, then something else is affecting SP development in Prue Sands in this well. Analysis of R_w from SP showed that calculated R_w varied by a factor of two in different sands over the 300-ft interval. This indicated that R_w variability could be a critical issue in petrophysical analysis in Prue Sands in the study area. Simply assuming a constant base R_w, corrected only for

temperature, in all calculations for the entire study could yield ineffective analysis leading to poor completion decisions in Prue evaluation. Connate water resistivity values for unspecified granite wash reservoirs in the vicinity of the study area, reported in a published water resistivity survey (SPE, 1975), shows a range of values from 0.04 to 0.4 Ω·m at 100 ° F.

Zanier and Timko (1970) reported significant differences in connate water salinity in Morrow sands in the Anadarko Basin, in Blaine, Canadian and Dewey counties, east and north of Washita County. In 27 wells examined in that study, a ratio of water salinity values, in PPM NaCl, ranging from 1.25 to 5.88 was noted in two vertically adjacent Morrow sands. Zanier and Timko attributed the salinity changes to effects of overpressuring in the Morrow sands.

In a short geologic note, Breeze (1972) reported that a map of bottom-hole pressure data in Morrow sands in the western Anadarko Basin exhibited a trend from abnormal to subnormal pressures in a northwesterly direction. Breeze reported changes in formation water salinity associated with the trend, and large salinity contrasts between permeable sands within the trend.

Dickey and Soto (1974) reported relatively fresh connate water in Morrow sands in Blaine County, Oklahoma, characterized by total dissolved solids (TDS) ranging from 10,000 to 30,000 PPM. Dickey and Soto also reported that Morrow connate water salinity in the surrounding area of the western Anadarko Basin ranged from 100,000 to 200,000 PPM TDS. Dickey and Soto attributed the dilute character of the Morrow connate waters in Blaine County to influx of meteoric water, or to the effect of abnormal pressuring as is found in the Gulf Coast Tertiary section.

The three studies in the western Anadarko Basin cited directly above, document the occurrence of vertical and lateral variability in the salinity of connate waters in Morrow sands, possibly associated with overpressure trends. Al-Shaieb et al. (1994) documented the presence of overpressure in Morrowan, Atokan and Desmoinesian sections in the Anadarko Basin, suggesting overpressure could be a mechanism affecting connate water salinity and variable R_w in the Prue as well. An example of such a change

was reported by Dickey (1986, figure 12-11, p. 269), who illustrated connate water salinity trends with depth in a sand-shale section from a Gulf Coast well. The trend of increasing salinity with depth was interrupted by an abrupt salinity decrease from about 150,000 PPM TDS to about 20,000 PPM TDS in sands at the top of overpressure.

In sediments coeval with Prue granite wash, Patchett and Rausch (1967, table 1) reported significant connate water salinity differences in Minnelusa sands in the Powder River Basin. According to Patchett and Rausch, in one well, the salinity varied from 3,500 PPM to 35,000 PPM between two sands with about 50-ft vertical separation, and from 35,000 PPM to 200,000 PPM between two wells with about six miles lateral separation. Wichmann (1986) reported a petrophysical interpretation that failed to distinguish productive from non-productive Minnelusa sands because of a five-fold change in connate water salinity between two sands separated by about 25 ft vertically had not been recognized. Wichmann stated that, although it was not known before the initial interpretation, the salinity difference was the result of the fact that the two vertically adjacent sands were deposited under significantly different environmental conditions, with consequent effect on connate water composition and R_w. The Minnelusa in the Powder River Basin was deposited in cyclically alternating marine and non-marine environments (Desmond et al., 1984).

Dutton and Land (1985) used isotopic and diagenetic evidence to investigate connate water composition of Pennsylvanian granite wash sands in Mobeetie Field, in that part of the Anadarko Basin located in the Texas Panhandle. They concluded that the composition might have been influenced by the inflow of meteoric water along recharge conduits adjacent to the fault-bounded provenance highlands of the Amarillo Uplift. Connate water salinity of affected sand beds would certainly be altered, depending on the amount of flushing by any meteoric inflow, as well as any compositional changes resulting from further diagenetic reactions in the sands. Differences in degree of communication with recharge conduits could produce variable salinity changes in vertically stacked sand beds in a single well, as well as salinity differences developed

between wells because of differences in distance from the uplift and laterally variable transmissibility properties.

Three separate processes described in this section could potentially lead to the development of intervals of variable salinity in granite wash reservoirs in the Anadarko Basin. They include fluid transfers associated with development of overpressured sections, interfingering marine and non-marine depositional environments and meteoric recharge of reservoir sands along the adjacent Wichita-Amarillo uplift. Variable connate water salinity, hence variable R_w, must be considered as a potential challenge in any complete petrophysical analysis of the Prue in the study area.

Gas Effect on Density-Neutron Logs

The density tool measures the electron density of a clean formation through the attenuation of gamma rays between a source and detector caused by collisions of the gamma rays with electrons in the formation that cause energy loss and absorption of the gamma rays (Dewan, 1983, p. 97). Formation electron density is related directly to formation bulk density. Knowing the formation matrix density and the density of the fluid in the pores, formation porosity can be determined from bulk density. Shale content affects bulk density of a formation based on the type of clay in the formation. Two clays, kaolinite and illite, exhibit the same density as quartz (Dewan, 1983, table 7-1, p. 231) and have little effect on porosity calculation from the density log. Chlorite density is greater than quartz and smectite is less dense, hence these two clays can affect porosity calculation from the density log.

The neutron tool measures the hydrogen content of a formation, and in a clean formation, the hydrogen is associated with pore fluids so that hydrogen content is related to formation porosity. The clay content in shale includes hydrogen in its crystal lattice and the neutron tool "sees" that lattice-hydrogen as porosity, therefore, shale content causes the neutron to read much higher porosity than is actually represented by liquid-filled pores. Shale content has a greater effect on neutron porosity than it does on density porosity. According to Dewan (1983, p. 248), a gas-free, shaly sand will always read

higher neutron porosity than density porosity. As the amount of shale increases, the porosity difference also increases in a linear relationship, which is the basis of the density-neutron combination as a shale volume indicator.

$$(V_{Sh})_{ND} = \left[(\phi_n - \phi_d) / (\phi_{nsh} - \phi_{dsh}) \right] \qquad 3.1$$

However, the density-neutron method cannot be used for shale volume analysis when gas is present in a formation (Dewan, 1983, pp. 248). Density logging tools are calibrated in freshwater-filled limestone (Schlumberger, 1989a, pp. 5-11). Gas, as a low-density pore fluid, lowers formation bulk density to a greater extent than does liquid-filled porosity. The presence of gas in a reservoir therefore causes the density log to read lower formation bulk density than would be found in an equivalent liquid-filled reservoir, and, hence, higher apparent porosity than an equivalent liquid-filled reservoir. As with the density tool, the neutron tool is calibrated in water-filled limestone (Schlumberger, 1989a, p. 5-19). Hydrogen concentration is much higher in water and hydrocarbon liquids than in hydrocarbon gases: therefore, the neutron tool measures much less hydrogen in a gas-filled reservoir than would be found in an equivalent liquid-filled reservoir. Consequently, the neutron log reads much lower apparent porosity in a gas-bearing reservoir than an equivalent liquid-filled reservoir.

The effect of gas-filled pores on neutron log porosity in sandstone is counterbalanced by shaliness; the counterbalancing magnitude is a function of actual gas saturation. The effect of shaliness on density porosity is a function of clay type, but gas saturation increases density porosity. Gas in the pores of shaly sandstone alters whatever effect the presence of clay exerts on the density log. The fact that these Prue Sands are gas reservoirs negates the value of the density-neutron log combination as a reliable shale volume indicator because the numerator in Equation 3.1 is rendered unreliable. The loss of the GR and density-neutron tools as shale volume indicators, taken together, make identification of a clean reservoir difficult in the Prue granite wash gas reservoirs using conventional logging suites.

CHAPTER IV
BASIC RESISTIVITY CONCEPTS

Development of Archie's Equation

In 1942, Gus Archie, an engineer at Shell Oil Co. in Houston, published what has been called "the most influential paper in petrophysics" (Schlumberger, 1988). Historically, evaluating lease reserves had required expensive cores recovered using oil-based mud to obtain the porosity and water saturation information necessary to determine the volume of hydrocarbons-in-place. At that time, electrical logs, providing information on formation resistivity, had been in use by the petroleum industry for almost 15 years. However, their application was stubbornly qualitative as laboratory researchers pursued the relationship between formation resistivity and water saturation in reservoir rocks. It was understood qualitatively that an oil-saturated reservoir rock was more resistive than a brine-saturated reservoir, but the relationships to quantify actual degrees of water saturation, and hence, degrees of oil saturation, were not available.

Archie recognized that the key to the problem would be in first being able to recognize the resistivity of a reservoir that is 100% wet. With the knowledge of that value, it would be possible to compare actual reservoir resistivity to wet resistivity, and thereby quantitatively evaluate degrees of water saturation. Archie developed the concept of the *formation resistivity factor* to provide the relationship that would enable the determination of the resistivity of a reservoir when it is wet. Then he applied existing research to develop the *formation resistivity index* to determine the degree of water saturation, based on the resistivity of a wet reservoir. These two fundamental relationships were combined in Archie's water saturation equation, which has provided the petroleum industry one of the requisite tools instrumental in the industry's commercial success over the last half of the 20^{th} century, and into the 21^{st}. Schlumberger's accolade to Archie was proper and fitting and frames the need to review the development and application of the Archie water saturation equation.

Historical Background

Schlumberger introduced the electrical log as a petroleum industry tool in 1927 in an oil well in the Pechelbronn field in France (Schlumberger, 1989a, p. 1-1). Conrad Schlumberger was a physics instructor at *Ecole des Mines* in 1911 (JPT, 1999, p. 20) and developed an interest in the application of surface electrical measurements in prospecting for subsurface metal ore deposits. Schlumberger began his geophysical career in 1911-1912, applying electrical surveying methods to develop equipotential maps along the surface of the earth in metals prospecting. The assumption was that the electrical method could be used to distinguish more conductive metal ore deposits from the less conductive, non-metalliferous host rocks surrounding the ore deposit (Johnson, 1961; JPT, 1999).

By 1920, Conrad Schlumberger had recognized the potential that the resistivity data he collected could be used in tectonic studies as well as in metals prospecting (Johnson, 1961, p. iii). In 1921, Marcel Schlumberger, Conrad's brother, used a 2500-ft. borehole to test downhole resistivity measurements as part of a surface seismic interpretation project. The results demonstrated that electrical measurements were useful in characterizing variation in subsurface formations penetrated by a wellbore (JPT, 1999, p. 20).

After a discussion with a friend who managed a Franco-Belgian oil drilling company, Conrad Schlumberger considered the idea that the electrical character of earth formations could also be of use in boreholes drilled for oil and gas exploration (Johnson, 1961, p. 2). Schlumberger recognized subsurface electrical surveying could provide information on resistivity variation between formations penetrated by a borehole that would permit stratigraphic correlation of subsurface beds between wells, which at that time required time-consuming, expensive cores. The Schlumberger method was initially called "electrical coring" and permitted definition of subsurface structures. An early Schlumberger project dealing with the location of coal beds in a borehole demonstrated the potential for lithofacies analysis when log data was combined with representative earth sample descriptions (Johnson, 1961, p. 4).

Using subsurface electrical surveying information to assist in defining structural and lithofacies trends to delineate traps was an important contribution to the industry. However, locating producible accumulations of oil in new wells was still the primary objective of the operators who drilled the wells. Over the course of several years of commercial use, the electrical surveying method was refined to overcome problems inherent in a drilled well that affect the quality of electrical measurements as representative of true formation resistivity. By 1936, the standard electric log included the SP curve, short and long normal resistivity curves, and a long lateral resistivity curve (Hamilton, 1961, p. 9). This suite of information provided the means to locate permeable beds, to assess invasion effects on resistivity measurements and to determine a value indicative of actual formation resistivity, providing a qualitative idea of fluid content in subsurface zones.

According to the Houston Geological Society (HGS) Electrical Well Logging Study Group (1939, p. 1297), the electrical resistivity of a porous and permeable formation is dependent on the water volume in the formation and the nature and amount of salts dissolved in the water. Further, the study group indicated that, because hydrocarbons are not conductive, as the hydrocarbon content of a formation increased to the exclusion of the electrolytic formation water, a higher resistance would characterize the formation. The oil and gas industry recognized the usefulness of subsurface formation resistivity measurements in the identification of potential hydrocarbon-bearing strata encountered in a wellbore.

The fundamental importance of resistivity measurements in well log analysis is unchanged today. Tiab and Donaldson (1999, p. 138) reiterate the concept stated by the HGS 60 years earlier, that the resistivity of a rock saturated with hydrocarbons will be greater than the resistivity of that same rock completely saturated with formation water. This relationship is an *essential concept* in the detection of hydrocarbons in the subsurface.

What is Resistivity?

In an electrical circuit, the ratio of the *electrical potential difference* between two ends of a conductor and the *electrical current* flowing through the conductor is a constant. The constant of proportionality of the ratio is called the *resistance* and represents the property inherent in any material object to oppose the flow of electrical current through it. The relationship is stated as Ohm's Law (White, 1966, p. 247).

$$r = \frac{Potential\ Difference}{Current} = \frac{V}{I} \qquad 4.1$$

When the potential difference, V, is measured in volts and current, I, is measured in amperes, then resistance, r, is measured in units called *ohms*.

According to Bassiouni (1994, p. 1) the reciprocal of resistance is called conductance, c, and represents the current-carrying ability of a material object referred to as a conductor. It is expressed by the following relationship.

$$c = \frac{Current}{Potential\ Difference} = \frac{I}{V} = \frac{1}{r} \qquad 4.2$$

Resistance is constant for a fixed conductor geometry and material, however, if the conductor length is increased, the conductor resistance will increase and if the conductor cross-sectional area is increased, resistance will decrease (Bassiouni, 1994, p. 1). Resistance is directly proportional to conductor length and inversely proportional to conductor area.

$$r = R\left(\frac{L}{A}\right) \qquad 4.3$$

The constant of proportionality in this relationship, R, is the specific resistance, or, *resistivity,* of the conductor. Bassiouni (1994, p. 1) likened the relationship between resistance and resistivity as similar to the relationship between mass and density. Mass is

a characteristic of an entire geometrically defined body, while density is the mass per unit volume within the body and is constant throughout a homogeneous body. Resistivity is an intrinsic property of a conducting material, analogous to density, and represents the resistance of a unit volume of a particular material; it is constant throughout a homogeneous body.

The relationship between resistance and resistivity can be rearranged to explicitly represent resistivity:

$$R = \left[r \left(\frac{A}{L} \right) \right] \qquad 4.4$$

When resistance, r, is measured in ohms, length, L, in meters (m) and area, A, in square meters (m^2), the unit of resistivity, R, is [Ohm m^2 / m] or [Ohm m]. Conductivity is the reciprocal of resistivity: therefore Equation 4.4 can be inverted to demonstrate that conductivity is expressed in units of [mhos per meter] where a [mho = 1 / ohm].

$$C = \frac{1}{R} = \frac{M}{Ohm\, M^2} = \frac{1}{Ohm} \times \frac{M}{M^2} = \frac{Mho}{M} \qquad 4.5$$

Rocks are not good conductors of electricity, therefore in electric logging measurements, the inverse ohm would be a very small number. Consequently, the conductivity unit in electric logging is based on one-thousandth of a mho, [0.001 mho]. The practical conductivity unit in electric logging is the *millimho per meter* (Bassiouni, 1994, p.1). The relationship between formation resistivity and conductivity in electrical logging terms is expressed by Equation 4.6.

$$R = \frac{1000}{C} \qquad 4.6$$

Flow of Electrical Current through a Rock

Outside the petroleum industry, conduction of electrical current is normally considered the property of a metal wire, such as copper, used to carry electrical energy throughout a home or business. A generator or battery supplies electrical current, and electrons flow through the copper wire, along the potential gradient producing the electric current. However, as Schlumberger demonstrated, measurement of the resistivity of electrical currents flowing in subsurface rock formation is fundamentally important in evaluating potential reservoir formations as hydrocarbon accumulations. How does electrical current flow through a rock?

A reservoir formation is the product of an accumulation of sedimentary detritus deposited in a basin. Distances of detrital transport may be significant or nil. Initially the formation consists of particles of various sizes, shapes and composition stacked on top of one another. As deposition proceeds and the accumulation thickens, grain to grain packing adjusts under the increasing overburden. The individual particles begin to bind into a coherent framework through the processes of lithification, changing the identity of the accumulation from individual particles to a sedimentary rock.

The grain framework of the reservoir rock contains intergranular voids, which are the rock pores. The volume, geometry and distribution of the pores are controlled by the geometrical character of the framework grains and their packing response to increasing burial or tectonism. As deposition and burial proceed, the pores are filled with connate water of variable salinity that, in part, is a function of depositional environment, chemical interaction between the connate water and the framework grains during burial history and hydrodynamic conditions imposed on the rock during its burial history.

Solid rock material of a formation is generally resistive and acts as an electrical insulator. A clean, dry core plug of a reservoir rock will not carry any significant current because the rock matrix and the air in its pores are not good conductors (Bassiouni, 1994, p. 2). If the core sample is saturated with distilled water, it still will not carry any current because pure water is also a poor conductor. How, then, can electrical current be conducted through a non-conducting rock matrix?

Salt water (brine), with ions in solution, is a conductor; current is conducted in salt water by movement of the ions and can be termed an electrolytic conductor (Hassan et al., 1994, p. 42). As the salinity of a brine increases, its ability to conduct electrical current also increases. Therefore, because resistivity is the inverse of conductivity, brine resistivity decreases in proportion to its increase in conductivity.

Brine in the pore system of a formation can electrolytically carry the flow of electrical current through the formation. Electrolytic current flow through a formation is not as straightforward and predictable as electronic conduction in standard copper wire, the length and cross section of which can be measured directly. Electrical current flow through a rock must be considered in two parts. First, the electrolytic potential of the saturating brine, which is a function of brine salinity, must be determined. Second, the effect of the formation on the distribution and continuity of the electrolytic brine must be assessed for its effect on the overall current flow pattern through the rock.

The distribution and continuity of the saturating brine is controlled by the texture of the formation. Texture is one of the principle defining characteristics of a sedimentary rock and includes the shape, size and surface features of the sedimentary grains as well as the grain-to-grain fabric of the formation (Pettijohn et al., 1972, p. 68, 89). Formation texture controls the geometry of the interstitial rock pore network and, hence, the geometry of the pore-filling electrolyte.

The Effect of Formation Texture on Flow of Electrical Current Through a Rock

Electrolytic Current in a Brine

When an electrical potential difference is imposed on a container filled with brine, negative ions from salts dissolved in the brine, flow directly from negative to positive potential along the length of the brine-filled container. The case is shown schematically in Figure 4.1.

Tiab and Donaldson (1999, p. 138) noted that under an applied voltage, the resistance of brine, r_w, to electrical current flow is represented by Ohm's Law.

$$r_w = \frac{V}{I_w} \tag{4.7}$$

When the brine is in a container, as in Figure 4.1, then the resistivity of the brine, R_w, can be represented by Equation 4.8.

$$R_w = r_w\left(\frac{A}{L}\right) = \left(\frac{V}{I_w}\right)\left(\frac{A}{L}\right) \tag{4.8}$$

Electrolytic Current in a Brine-Filled Sand

Mineral constituents in rocks are generally non-conductors, and current flow through a brine-filled rock formation is therefore more tortuous than current flow in a simple brine-filled container. The insulating mineral grain matrix forces the current into a convoluted path through the brine-filled rock pore network, as illustrated schematically in Figure 4.2.

Current is the quantity of charge passing any point in a circuit in a particular unit of time, under a specific potential difference (White, 1966, p. 243). Assume the potential difference across the brine-filled sand is the same as the potential difference across the brine-filled container. The more convoluted current path in the brine-filled sand will diminish the amount of charge passing any point in unit time along that container length. By definition, the current along the length of the brine-filled sand container will decrease from the value in the brine-filled container.

Ohm's law for the brine-filled sand is shown in Equation 4.9. Voltage in Equation 4.9 equals the voltage in Equation 4.7. Because the voltage across the two containers is the same, but the current is diminished in the brine-filled sand, then, according to Ohm's Law, the resistance of the brine-filled sand system must increase relative to the brine-filled container.

$$r_o = \frac{V}{I_o} \tag{4.9}$$

The same relationship that was used to describe the brine resistivity, Equation 4.8, can also be used to describe the resistivity of the brine-filled sand, shown as Equation 4.10. Container dimensions are assumed the same in both Figure 4.1 and Figure 4.2.

$$R_O = r_O\left(\frac{A}{L}\right) = \left(\frac{V}{I_O}\right)\left(\frac{A}{L}\right) \qquad 4.10$$

Although container dimensions are assumed the same in both Figures 4.1 and 4.2, and the brine conductor is the same, the electrolytic current path length through the brine-filled sand is greater than the current path in the brine-filled container. The conductor in Figure 4.2 is no longer the simple brine-only system; it is now a rock-brine system in which the rock texture imposes a more complex conductive geometry than that of the simple brine-only system. The increased path length per unit conductor volume increases the resistance and hence the resistivity of the brine-filled sand conductor, R_o, over the value of the brine-only conductor, R_w, in the container.

Note that if the same voltage is applied to produce electrical current flow through a brine-filled container and brine-filled sand container of the same dimensions, the resulting current, I_w, will be greater than I_o. The current in the brine-filled sand must overcome greater resistance across the same potential drop, and according to Ohm's law, current through the sand will have to be less then through the brine alone.

The ratio of the resistivity values in each of the two systems eliminates the common voltage and dimensions from the relationship, showing it is equal to the inverse ratio of the currents flowing through each system. Therefore, for any given voltage, the ratio of the resistivity of a brine-saturated sand and the resistivity of the saturating brine will always be greater than one (Tiab and Donaldson, 1999, p. 139):

$$\frac{R_O}{R_W} = \frac{I_W}{I_O} \qquad 4.11$$

Formation Resistivity Factor

As the character of the electrical log evolved and resistivity measurements across permeable formations more reliably indicated actual formation resistivity, it permitted qualitative interpretation of formation fluid content in formations penetrated by a wellbore. Interpretations such as "sand, possible gas or oil" or "water sand" were common (HGS, 1939, fig. 14, p. 1308). The *essential concept* was, as noted above, that the resistivity of a rock saturated with hydrocarbons will be greater than the resistivity of that same rock completely saturated with formation water.

Archie (1942) published the results of his empirical investigations into the relationship of formation resistivity to formation porosity and to hydrocarbon saturation. The objective of his study was the development of relationships that could be used in quantitative analysis of formation resistivity data applied in the detection and evaluation of subsurface hydrocarbon accumulations. If quantitative values for water saturation could be determined for a reservoir, then hydrocarbon saturation was also known because water and hydrocarbons are the two fluids most commonly found saturating the pore volume of subsurface reservoirs. Rarely, carbon dioxide, nitrogen or helium gas can be found in subsurface reservoirs, but this case requires special geologic conditions and is atypical.

Archie (1942, p. 310) said "A study of the resistivity of formations when all the pores are filled with water is of basic importance in the detection of oil or gas by the use of an electrical log. Unless this value is known, the added resistivity due to oil or gas in a formation cannot be determined." Archie's initial premise was based on the *essential concept*. In order to recognize the resistivity added to a hydrocarbon-bearing formation, R_t, it is first necessary to recognize the resistivity of that formation when its pores are 100% saturated with water, R_o. Archie identified the following relationship for the resistivity of a rock with its pores brine-saturated.

$$R_O = F_R R_W \qquad 4.12$$

Archie called the parameter the formation resistivity factor, which represents the effect of the rock pore network on the distribution of the electrolytic brine in the formation and the consequence of that effect on the overall formation resistivity. Wyllie (1963, p. 13) called the formation resistivity factor "perhaps the most important single relationship in electric log interpretation."

Archie empirically investigated the relationship between the formation resistivity factor, F_R, and formation porosity using a series of "clean" (clay-free) Gulf Coast sands. Porosity values of these sandstones ranged from 10% to 40% and salinities of saturating brine ranged from 20,000 to 100,000 PPM NaCl. For that range of porosity and salinity, Archie found a linear relationship between F_R and porosity when they were plotted on log-log coordinates. That relationship is illustrated schematically on Figure 4.3.

The empirical results indicated that as porosity increased, the formation resistivity factor decreased. Varying the salinity of the saturating brine did not affect the relationship. Archie expressed the empirical relationship the between the formation resistivity factor, F_R, and porosity, ϕ, as shown in Equation 4.13.

$$F_R = \phi^{-m} \tag{4.13}$$

The exponential parameter, $-m$, represents the negative slope of the trend line in the plotted relationship (Figure 4.3).

Archie found that the absolute value for the exponential factor, m, ranged from 1.8 to 2.0 for consolidated sandstones, while the value for m in clean, unconsolidated sands was about 1.3. Archie concluded Gulf Coast sands might expect a value of m ranging from 1.3 to 2.0. Archie's formation resistivity factor relationship factor can be rewritten as shown in Equation 4.14.

$$F_R = \frac{1}{\phi^m} \tag{4.14}$$

This form of the relationship emphasizes the fact that the negative slope of the trendline on Figure 4.3 passes through the intercept, noted as point *a* on Figure 4.3, where $F_R = 1.0$ and porosity = 1.0. When porosity = 1.0, then $R_o = R_w$ because the system where porosity = 1.0 represents an open container with no mineral grains present to affect current flow (as shown in Figure 4.1). Since [$F_R = R_o/R_w$], then F_R should theoretically equal 1.0 when porosity equals 1.0. As was shown by Tiab and Donaldson, and cited in Equation 4.11, because of electrical current considerations, the ratio [R_o/R_w] can never be less than 1.0.

While Archie (1942) developed the formation resistivity factor from empirical evidence, Winsauer et al. (1952), examined the formation resistivity factor theoretically. Winsauer et al. (1952, p. 253-254) found that the formation resistivity factor varied as a function of formation porosity and a geometrical parameter called tortuosity, which referred to the complexity of pore channels in porous rocks. Tortuosity was defined as the ratio of two distinct lengths in a rock pore system: the pore channel path-length between two parallel planes and the straight-line distance between the two planes.

Winsauer et al. examined the relationship between the flow of electric current in a brine-filled container and the flow of electric current in a brine-filled sand container, as illustrated in Figures 4.1 and 4.2. In the brine-filled container, electrical current flow could be characterized in terms of the straight-line path length, L, of the entire container and the area of conductive flow, A, through the entire container. However, in the brine-filled sand container, electrical current flow would be characterized in terms of the more tortuous path length, L', and the reduced conductive area of brine-filled pores through the sand matrix, A'. Winsauer et al., found that the formation resistivity factor could be represented by the general relationship shown in Equation 4.15.

$$F_R = \frac{\tau}{\psi} \qquad 4.15$$

According to Winsauer, et al., rock texture controls the rock pore geometry and is important in characterizing electrical current flow through a rock. Winsauer, et al., (p. 274), concluded that pore channel tortuosity, in particular, affects the path of current flow through a rock, but is very difficult to measure and, therefore, it is not a readily useful parameter in electrical log interpretation. Winsauer et al. indicated it would be useful to have a relationship between formation resistivity factor and porosity and repeated Archie's experiment. Winsauer et al. examined about 40 sandstone samples from Ordovician to Tertiary in age and from basins across the United States, from Pennsylvania to California. A relationship, Equation 4.16, was developed for the formation resistivity factor, in the general form established by Archie, which reasonably matched the results from Winsauer et al.'s tortuosity experiments on those sands.

$$F_R = \frac{0.62}{\phi^{2.15}} \qquad 4.16$$

During the course of this study, Winsauer et al. were employees of Humble Oil Company and Equation 4.16 became known as the Humble Equation. It illustrated that parameter values for Archie's empirical expression, shown in Equation 4.14, for the formation resistivity factor may not consistently apply to formations and lithologies from basins beyond the texturally uniform Gulf Coast sands Archie examined. Indeed, Archie (1942, p. 310), had indicated caution was necessary in applying his empirical relationships to more complex reservoir rocks. The formation resistivity factor relationship is now generally written as shown in Equation 4.17.

$$F_R = \frac{a}{\phi^m} \qquad 4.17$$

Compare Equations 4.15 and 4.17, the parameter, a, in the numerator of Equation 4.17 is a function of tortuosity and represents the intercept of the negatively-sloping trend

line with the *y*-axis. This is illustrated on Figure 4.3, where the trendline intercepts the y-axis where y = 1.0, at 100% porosity on the x-axis. The trendline that was fit to the graph of the data from Winsauer et al. (figure 14, p. 275) crosses the x-axis at 80% porosity, and intercepts the y-axis at 0.62, below the x-axis. The parameter, *a*, in Equation 4.17 is called the tortuosity factor.

The parameter in the denominator of Equation 4.17 is a function of conductive area in a rock pore system and the exponent, *m*, is called the cementation exponent or cementation factor. Hilchie (1982, p. 1-4) wrote that the parameters *a* and *m* are both related to pore geometry. Winsauer et al. (1952, p. 255) showed that the formation resistivity factor is a ratio of conductive path tortuosity (in the numerator) and apparent conductive area in a rock pore system (in the denominator).

Adisoemarta et al. (2000), in a theoretical examination of the two empirical parameters, also found that *a* represents the tortuosity of the current path length and, in addition, found that its value is reasonably constrained between 1.0 and 1.4. The cementation factor, *m*, represents the contrast between the area of the pore bodies and the area of the pore throats in a rock. Formation porosity is a volume parameter associated with a large intergranular area, but interconnecting pore throats, with much smaller intergranular area, control the flow of electrical current through the brine-saturated pore system. The cementation factor mathematically compensates for the difference between pore body and pore throat areas in characterizing the electrical conductivity in a rock pore system, validating the empirical relationship between formation resistivity factor and porosity.

Adisoemarta et al. (2000) found that a value for *m* of 2.0 represents the electrical current flow conditions in a cubic pack of uniform spheres in which the geometry of pore bodies and pore throats are uniformly consistent throughout the pack. The flow of electrical current through brine in this system would be predictably uniform through all pores and pore throats. As the ratio of [pore body area] to [pore throat area] increases, the value of the cementation exponent *m* will also increase (Adisoemarta et al., 2000, table 2) to mathematically compensate for the effects of pores that are accounted for in

formation porosity but contribute little to formation conductivity because they are isolated and lack average interconnecting pore throats. An ever-larger cementation exponent factored with fractional porosity, results in an ever-smaller effective conductive area in the denominator of the formation resistivity factor ratio (Equation 4.17).

Wyllie (1963, p. 12) indicated that two formations with the same porosity can have different formation resistivity factors. This means two different formations can have the same porosity, be 100% saturated with the same brine, and yet have different formation resistivity values, i.e. [$F_R = R_o/R_w$]. If the textures and consequent pore geometries of the two formation are significantly different, requiring different values for Archie's empirical parameters a and m, then different values of F_R will be developed for each formation. With the correct F_R value, the correct R_o value will be predicted for each of the two formations.

The formation resistivity factor serves to characterize the distinct resistivity contribution of each texturally distinct formation to total formation resistivity. This certainly reinforces Wyllie's 1963 observation on the critical importance of the concept of formation resistivity factor in log interpretation. It illustrates the importance of formation texture as a control on formation resistivity and serves to reinforce the awareness of the importance of actual sample description and analysis in log interpretation.

To recognize the resistivity that is added to a formation by replacing a portion of the saturating connate water with hydrocarbons, it is first necessary to be able to recognize the resistivity of a formation when it is water saturated. The fundamental objective guiding Archie's initial investigation was achieved, and it is represented by Equation 4.18.

$$F_R = \frac{R_O}{R_W} = \frac{a}{\phi^m} \qquad 4.18$$

Therefore, if formation porosity and brine resistivity are known and appropriate values for the empirical parameters a and m are used, then the resistivity of a water-saturated formation can be determined through the formation resistivity factor (Archie, 1942, p.

311). With the formation resistivity factor, it is possible to predict the resistivity of a water-saturated reservoir.

The Effect of Hydrocarbons on Formation Resistivity

Formation Resistivity Index

With the means to characterize the resistivity of a water saturated formation, Archie (1942) proceeded to develop an empirical relationship that would serve to characterize a formation with pore spaces partly filled with brine and the remainder filled with hydrocarbons. Archie used data from several investigators who had previously examined the variation in resistivity of sands with the variation in water saturation of the sands. These prior investigations were accomplished by first measuring the resistivity of a sand sample fully saturated with conductive water and then displacing varying amounts of the conductive water with non-conducting fluids. The relationship, shown as Equation 4.19, is called the *formation resistivity index* and is expressed as a ratio of two distinct resistivity values: the resistivity of sands that are partly water saturated and sands that are 100% water saturated.

$$I = \frac{R_t}{R_o} \tag{4.19}$$

In a manner similar to the formation resistivity factor, Archie plotted the formation resistivity index against water saturation on log-log coordinates. The relationship is illustrated schematically on Figure 4.4. The empirical relationship indicates that the resistivity index, I, decreases in value as the value for water saturation, S_w, increases, and can be expressed as follows in Equation 4.20.

$$I = \frac{R_t}{R_o} = S_w{}^{-n} \tag{4.20}$$

Equation 4.20 can be rewritten as Equation 4.21.

$$\frac{1}{S_w{}^n} = \frac{R_t}{R_o} \Rightarrow S_w{}^n = \frac{R_o}{R_t} \qquad 4.21$$

When the value for $S_w = 1.0$, then $R_t = R_o$ because there are no hydrocarbons in the formation. Therefore, when $S_w = 1.0$, the resistivity index $(R_t/R_o) = 1.0$, and it can not have a value less than 1.0 (Figure 4.4).

According to Archie (1942, p. 312), the value for the empirical parameter, n, called the Saturation Exponent, is close to 2.0. Adisoemarta et al. (2001) indicate that the nature of Archie's empirical parameter n in hydrocarbon-bearing formations is a function of the diminished cross-sectional area of conductive water in pore throats because non-conducting hydrocarbons are also present in the pore throats. Like the empirical parameter, m, the parameter n compensates for the fact that formation saturation is a pore body property while formation resistivity is a pore throat property.

Archie's Water Saturation Equation

Archie combined the formation resistivity factor (Equation 4.12) and formation resistivity index relationships (Equation 4.20), to get the Archie water saturation equation (Equation 4.22).

$$S_w = \left(F_R \left(\frac{R_w}{R_t} \right) \right)^{1/n} = \left[\left(\frac{a}{\phi^m} \right) \left(\frac{R_w}{R_t} \right) \right]^{1/n} \qquad 4.22$$

Unless otherwise indicated by sample examination, general practice in log analysis is to use standard values for the Archie empirical parameters. Usually values of $a = 1.0$ and $m = 2.0$ are used for moderately to highly cemented formation (Amyx et al., 1960, figure 2-61, p. 117), and a value of $n = 2.0$, as suggested by Archie (1942).

Formation Mineral Constituents as Conductors

Clay Minerals

When clay minerals are included in the mineralogical composition of a sandstone, it creates a condition that was not considered when Archie developed the fundamental water saturation equation in 1942. Archie considered the grain framework of sandstones to be non-conductive. In the subsurface, the two most common fluid types in the pores of sandstones are water and hydrocarbons. Water with dissolved salts is electrolytic, hence conductive; hydrocarbons are not electrolytes and are non-conductive. In Archie's model, therefore, only salt water in the pore system of sandstones contributes to the rock-fluid system conductivity.

The assumption of non-conductive grains is valid for most common sedimentary rock-forming minerals such as quartz, feldspar, calcite and dolomite, but the assumption fails with clays. The platy sheet structure of clay minerals engenders two properties that provide clay minerals the ability to contribute to conductivity in rock formations.

The crystal structure and composition of certain clay minerals promotes common ionic substitution in the clay crystal lattice, and the substitution can create a net negative charge along the clay mineral surface. In the presence of water, clays with the net negative surface charge will adsorb a thin layer of water along the clay mineral surface that is essentially immovable (Dewan, 1983, p. 238) and is called *clay water* or *bound water*. Cations, called counter-ions, are adsorbed from pore water into the bound water layer and counteract the net negative charge on the clay mineral surface. These ions, generally Na^{+} and Ca^{+2}, are loosely held to the clay structure and are readily replaced by other ions, providing the mechanism for the property called *Cation Exchange Capacity* (CEC). The counter-ions are loosely held in the clay structure because an *exchange site* is not *a lattice site* (Mason, 1966, p. 160). These loosely held counter-ions are free to move under an impressed electric field (Bassiouni, 1994, p. 15) and hence represent a current-carrying mechanism separate from the ions in solution in the pore-saturating brine.

Dewan (1983, p. 238) indicates that the specific surface area of clays in [(m^2 / gm)] is hundreds of times greater than that for sands, and when clays are present in sandstones, it results in an extensive concentration of mobile cations on clay surface areas in the sandstones. Consequently, the counter-ions associated with the clay surfaces in sandstones result in conductance in excess of that contributed by the electrolytic brine in the sandstone pores, and is represented by Equation 4.24 (Bassiouni, 1994, p. 15).

$$c_O = c_{cl} + c_W \qquad 4.23$$

Therefore, in those reservoir rocks that include clay minerals in their compositional mode that are susceptible to common ionic substitution, Archie's assumption of a non-conducting grain framework in the analysis of formation resistivity fails. The contribution of the mobile cations on clay surfaces to overall conductivity in such a rock-fluid system is called Excess Conductivity (Schlumberger, 1989b, p. 43). Excess conductivity is that conductivity of a formation in excess of the conductivity that can be accounted for by electrolytic character of the brine-filled pores of the formation.

Excess conductivity can contribute to the mischaracterization of the formation resistivity factor, which is empirically based on clean, water-filled sands. The excess conductivity from the clay in shaly sand diminishes overall formation resistivity from the value that would be found in a clean sand of the same measured porosity, (R_o shaly sand < R_o clean sand). If the standard value for the empirical parameter m were used with the wireline log value of formation porosity in a shaly sand, $m = 2.0$, then the calculated value for the formation resistivity factor would be incorrect. It could not be used to correctly predict the wet formation resistivity measured for the shaly sand; it would predict an R_o value that is too large. Consequently, the value calculated for water saturation in the formation would be very pessimistic.

The practical effect of excess conductivity from shaliness in a sandstone is to diminish the apparent contrast in pore body and pore throat area in shaly sand from the contrast in a correlative clean sand. If this condition is met, then a value for the empirical

parameter *m* less than 2.0 would be more appropriate in the empirical relationship between porosity and formation resistivity factor in a shaly sand.

Microporous Grains

Pore Size

Pore geometry is often described with reference to a particular pore type, such as interparticle, intraparticle or fracture, however, pore size is another way to classify pore geometry that is not often discussed. Choquette and Pray (1970, p. 224) in a study on the classification of porosity in carbonates, developed a three-part system to classify pore size, including micropores, mesopores, and megapores. Pores with dimensions exceeding those of megapores were described as cavernous.

Coalson et al. (1987, p. 61) presented a tripartite system of pore size classification that included micropores, mesopores, and macropores. Luo and Machel (1995) used a four-part classification system that added the term megapore to the three terms used by Coalson et al. In terms of size, megapores in Luo and Machel's system correspond exactly to cavernous pores in Choquette and Pray's system, and, therefore, Choquette and Pray's megapores correspond to macropores in Luo and Machel's classification system.

The Table 4.1 illustrates, with unified nomenclature, the size ranges of the three pore-size classification systems just discussed. The term *cavernous* has a genetic connotation directly related to carbonates, while megapore is more generally applicable to all sedimentary rocks. Any pore space exceeding macropore dimensions could be called a megapore.

Table 4.1 Pore Size Classification System

Reference	Macroporosity	Mesoporosity	Microporosity
Choquette and Pray (1970, fig. 2, p. 224)	4000 to 256,000 μm	62.5 - 4000 μm	< 62.5 μm
Coalson et al. (1987, p. 60-61)	> 15 μm	5 - 15 μm	< 5 μm
Luo and Machel (1995, fig. 3, p. 1706)	1000 to 256,000 μm	1 to 1000 μm	< 1 μm

There are significant differences in the size ranges listed in each of the classification systems. Choquette and Pray (1970) were focused on visible porosity in their classification and indicated that micropores can be assessed by a hand lens or microscope (p. 233). The studies of Coalson et al. and Luo and Machel, each recognize the effect on pore description developed through the application of instrumentation with much finer resolution than that provided by standard optics.

Luo and Machel indicated that instrumentation provides a range of *observation domains* with which to examine pore size. The scanning electron microscope (SEM) and mercury-injection capillary pressure analysis are important tools in pore size classification, beyond the range of the unaided eye and the light microscope. If pore size classification includes methods beyond the resolution of standard optics, it would indicate that the microporosity size class is considered to be about 1 to 5 microns (μm) or less.

Keike and Hartmann (1974, p. 1080) indicate that while there are no recognized limits to pore size classification, it has been accepted that a micropore cannot be seen at less than *50x* magnification. Keike and Hartmann further stated that, for detailed resolution of the structure of micropores, at least *100x* magnification is required, and in some cases, an SEM with up to *5000x* magnification is required. Pittman (1971, p. 1873) and Worthington et al. (1989, p. 203) each defined the dimensions of microporosity as one micron or less. Swanson (1985, p. 1) defined micropores in terms of mercury injection capillary pressure curves and characterized micropores more generally as pores

whose dimensions are significantly less than those pores contributing to the rock permeability.

A standardized definition of microporosity is not available, but a minimum dimension on the order of one to five microns is representative of values reported in the literature for those classification schemes that go beyond the range of visible porosity. This is the pore size range in which capillary binding of excess pore water is possible (Swanson, 1985, p. 2, fig. 2, p. 9).

Clay Minerals

Clay minerals are very fine particles, less than 4 microns in diameter, and in sandstones generally assume a platy or fibrous habit or cluster as very fine, shaly masses (Scholle, 1979, p. 64-72, 130-138). Swanson (1985, p. 6) indicated that capillary water within clay micropores in sandstones contributes to formation electrical conductance. Capillary-bound water in a rock-fluid pore system is distinct from the layer of adsorbed bound water in which the counter-ions reside on the surfaces of clay minerals. Capillary bound water is a normal part of the pore water system and is present as irreducible water saturation in clean sands as well as shaly sands.

Because of the extremely fine size of clay particles, microporosity is a characteristic property of clays regardless of their CEC potential. Thus, electrical conductance through a rock formation can be enhanced because of the associated capillary-bound water within clay micropores. The presence of clays in sands promotes higher irreducible water saturation values than in clean sands. Higher values of irreducible water means greater electrolyte content and hence greater conductivity of the rock–fluid system in a shaly sand than in a clean sand of the same effective porosity.

Carbonates

Pittman (1971) described a system of dual porosity in carbonate rocks, with microporosity that can hold irreducible water, while coexisting larger pores hold and transmit fluids. Asquith (1985, p. 29-31) described the water saturation relationships in

oolitic reservoirs in which microporosity had been diagenetically created in ooids. The micropores are associated with very high capillary pressures and consequently hydrocarbons that migrate into the oolitic reservoirs are generally unable to displace the capillary bound water in the micropores. Essentially, microporous grains are themselves water saturated, and act as conductors of electric current. When microporosity is present, the current path through the formation is less tortuous and excess conductivity is added to the formation by the water-saturated, microporous ooids (Asquith, 1985, p. 30, fig. 10).

Chert

Microporous chert is found as clastic framework grains in hydrocarbon productive sandstones (Swanson, 1985, p. 6; Kenyon et al., 1989). Productive microporous chert is also found in bedded to nodular form associated with carbonate shelf deposits (Watney et al., 2001). Productive chert reservoirs can be associated with high irreducible water saturations and low resistivity log readings when depositional and diagenetic conditions are conducive to development of microporous chert (Watney et al., 2001, p. 106).

Excess Conductivity

Formations that include microporous grains can exhibit excess conductivity associated with the capillary- water bound in the micropores (Asquith, 1985, p. 31). If a reservoir is characterized by a bimodal pore system, it includes macropores capable of storage and transmission of contained fluids and micropores that are saturated with capillary-bound brine. Log analysis in a reservoir with a bimodal pore system will reflect the total water saturation in the reservoir, both immobile and mobile. In such a case, water-free hydrocarbon production can accompany misleading values of calculated water saturation that appear to be high based on an assumption of a uniformly macroporous pore system. An operator who is unaware of the presence of a bimodal pore system could overlook the productive potential of a reservoir with a bimodal pore system.

Invasion

Field Relationships

The formation resistivity relationships in the Archie water saturation equation desribed above are based on laboratory experiments on core plugs of reservoir formations. Porosity and pore fluid concentrations are known and controlled to suit the requirements of the experiments; a single resistivity measurement can be used to represent the actual resistivity of the plug and saturating fluids. However in an actual wellbore, the nature and concentrations of the reservoir pore fluids are less certain quantities. Further, the presence of drilling mud in the wellbore, at controlling hydrostatic pressures in excess of the reservoir pressure, causes infiltration of the watery component of the drilling mud (called mud filtrate) into permeable formations penetrated by the wellbore. The concentration of the in-situ reservoir pore fluids is affected by the invading mud filtrate and a radial zone of modified fluid saturation, called the *invaded zone*, is created around the wellbore.

Figure 4.5 schematically illustrates mud filtrate invading a water-filled porous and permeable formation. Immediately behind the wellbore wall, the formation is completely flushed of all original connate water. Then the concentration of mud filtrate in the formation begins to diminish further away from the source of mud filtrate, the wellbore mud, until a point is reached in which there is no mud filtrate in the formation. Diminishing mud filtrate volume with distance from the wellbore is compensated through a transitional zone where ever-smaller volumes of connate water have been displaced by mud filtrate along the invasion profile, until the point is reached where there is no mud filtrate and the undisturbed pores are filled with connate water.

According to Campbell and Martin (1955, p. 233), during invasion, formation connate water is completely removed from the near wellbore region because originally irreducible water is mobile in the presence of a water phase (mud filtrate). Further according to Campbell and Martin, in a reservoir that contains displaceable hydrocarbons, some of the hydrocarbon pore fluids will be swept away from the near wellbore region, along with the connate water, by the invading mud filtrate, leaving

behind a residual saturation of immobile hydrocarbons. Gondouin and Heim (1964) refer to the interaction between the invading mud filtrate and original connate water as miscible deplacement and the interaction between the mud filtrate and oil as immiscible deplacement.

Depth of Invasion

The depth (or, radius) to which a permeable formation is invaded by mud filtrate is a function of the volume of mud filtrate that penetrates into the formation. For a given volume of invaded mud filtrate, invasion depth is a function of formation porosity. According to Dewan (1983, p. 11-13), invasion depth will be maximized in lower porosity formations and minimized in higher porosity formations, and is approximately proportional to ϕ^{-2}, shown mathematically as Equation 4.24.

$$Depth\,of\ Invasion \sim \propto \frac{1}{\sqrt{\phi}} \qquad 4.24$$

Dewan provides an example of this relationship; invasion depth doubles as porosity is reduced from 36% to 9%, and, the inverse of the square root of 9 is twice the value of the inverse of the square root of 36.

$$\frac{1}{\sqrt{36}} = \frac{1}{6} \Rightarrow \frac{1}{\sqrt{9}} = \frac{1}{3} \qquad 4.25$$

Therefore, across an individual reservoir zone with a normal porosity range, for instance, from 16% to 10%, one should not expect more than about 26% difference in the depth of invasion across the reservoir zone, as illustrated in Equation 4.26.

$$\frac{1}{\sqrt{16}} = \frac{1}{4} = 0.25 \Rightarrow \frac{1}{\sqrt{10}} = \frac{1}{3.16} = 0.316 \qquad 4.26$$

Depth of invasion should, therefore, be reasonably uniform across reservoirs with a reasonable scatter in the range of reservoir porosity.

The volume of mud filtrate lost to a permeable formation is the result of the interaction among several fundamental characteristics of the drilling mud system. These characteristics include the measured fluid loss of the mud, the differential pressure at the formation face, the permeability of the mud cake, and the length of time the face of a permeable formation is exposed to the mud (Bassiouni, 1994, p. 71). The differential pressure is a function of mud density, and mud cake permeability is a function of mud solids content that are deposited on the wellbore wall as a residue from the mud, after filtrate is lost to the permeable formation. Therefore, for a given differential pressure, fluid loss character, and mudcake permeabilty, the same volume of filtrate will be lost to an invaded formation in any given time, regardless of formation porosity or permeability (Dewan, 1983, p. 11). A lack of textural uniformity across a reservoir, with variable pore types and geometries, should, therefore, have little effect on the volume of mud filtrate invaded as long as the key mud properties are uniform.

Wyllie (1954, p. 57) also stated that formation permeability has little influence on the volume of mud filtrate that invades a permeable bed, in agreement with Dewan. However, Wyllie further stated that as formation permeability approaches the permeability of the mudcake, approximately 10^{-3} md, formation permeability itself will begin to effectively limit invasion. What is a practical range of mudcake permeability, and would a formation with minimal invasion retain sufficient permeability to allow development of an SP response? What would minimal invasion mean regarding the commercial productive capacity of a hydrocarbon-bearing formation? Can invasion be evaluated petrophysically?

A tornado chart, such as Chart Rint-2a (Schlumberger, 1989c, p. 89), includes depths of invasion, shown as d_i, as explained on Chart Rint-1 (Schlumberger, 1989c, p. 88). This "depth" refers to an electrically equivalent diameter of invasion determined from formation resistivity measurements (Schlumberger, 1958, p. 16). Doll et al. (1960,

p. 858) characterize this electrically equivalent invasion diameter as a cylindrical boundary in a formation, separating two homogeneous media of constant resistivity, R_{xo} and R_t. The defining cylinder is concentric with the borehole.

This invasion geometry describes the most simple invasion relationship in which the transitional zone of diminishing mud filtrate content shown in Figure 4.5 is replaced by a uniform invasion front, shown schematically on Figure 4.6. This conceptual analog is comprised of two zones separated by a planar front oriented vertically through the permeable bed. Each of the two zones exhibits distinct pore fluid content, and hence, distinct and constant formation resistivity. The planar front separating the zones is located at an electrically equivalent diameter of invasion that is representative of the average resistivity of the actual transitional invaded zone, and would have the same effect on formation resistivity measurements as the actual invaded zone (Schlumberger, 1958, p. 16). This is illustrated schematically in Figure 4.7, and reduces the complexity of a transitional invasion profile to a system of three unknowns, R_{xo}, R_t and d_i (Singer and Barber, 1988, p. 2). In this simplified form, formation resistivity measurements can be used in charts such as Rint-2a to assess the invasion diameter, d_i.

Chart Rint-2a (Schlumberger, 1989c, p. 89) includes d_i values from 15 to 90 in, which, according to Figure 4.7, would represent a diameter that includes the diameter of the borehole. Doll et al. (1960, p. 860-861), show that to get the actual depth (or, radius) of invasion from the borehole wall, it is first necessary to subtract the borehole diameter, d_h, from d_i, and divide the remainder by two. For instance, if $d_h = 8$ inches and d_i is determined to be 40 inches, then the depth of invasion from the borehole wall would be 16 inches.

Bassiouni (1994, p. 71, *Equations* 4.10 and 4.11) examines the relationship between the volume of filtrate invasion behind the formation face and d_i in more detail. Bassiouni Equations 4.10 and 4.11 are shown below as Equations 4.27 and 4.28, respectively. The mathematical construction of Equations 4.27 and 4.28 demonstrates the assumption that the formation volume invaded by mud filtrate is a porous cylinder concentric with the borehole. Equations 4.27 and 4.28 can be followed mathematically

through Equation 4.29 to Equation 4.30, which illustrates the foundation for Dewan's proportionality relationship shown in Equation 4.24.

$$V_{mf} = \left(\frac{\pi}{4}\right)\left(d_i^{\,2} - d_h^{\,2}\right) h\phi S_{xo} \qquad 4.27$$

$$d_i = \left[\left(\frac{4V_{mf}}{\pi h\phi S_{xo}}\right) + d_h^{\,2}\right]^{1/2} \qquad 4.28$$

$$d_i = \left[\left(\frac{1}{\phi}\right)\left(\frac{4V_{mf}}{\pi h S_{xo}}\right) + d_h^{\,2}\right]^{1/2} \qquad 4.29$$

$$d_i \sim\propto \frac{1}{\sqrt{\phi}} \qquad 4.30$$

In reference to values obtained from Equation 4.24, Dewan (1983, p. 13) states that typical depths to which a formation is invaded is about 1-2 ft., with a range from a few inches to a few feet. These values are not characterized by Dewan in terms of *di*, but rather, they represent invasion radii behind the formation face.

In Table 4.2, Asquith (1982, p. 3) relates the diameter of invasion in the more general terms of a ratio between diameter of invasion and borehole diameter. The invasion diameter relationships presented by Asquith are a product of the development of electric log departure curves by logging service companies from 1947 to 1959, to correct electric log measurements for the effects of invasion. Examples of departure curves with invasion diameter ratios noted below, for a 7 7/8" borehole, are illustrated in Hilchie (1979, p. 91-98).

Table 4.2 Departure Curve Invasion Diameter Ratios

Reservoir Character	Invasion Diameter / Borehole Diameter
Low Porosity	10
Intermediate Porosity	5
High Porosity	2

Depth of invasion concerns in any particular reservoir requires an individual assessment for that reservoir, although the ratios from Asquith indicate that reasonable generalities can be made in general rock types. However, because values for all the variables involved in determining the actual volumes of mud filtrate lost to a formation are difficult to routinely quantify in a drilling well, the most useful method for determining the diameter of invasion in a drilled formation is based on formation resistivity measurements to determine d_i.

Invasion Profile

The composition of drilling mud, including salinity, is generally distinct from the composition of formation fluids, hence the electrical properties of drilling muds are generally different than those of the formation fluids (Bassiouni, 1994, p. 66). The resistivity of a formation that is saturated with mud filtrate will be different than the resistivity of that same formation saturated with connate water. Consequently the mud filtrate invaded zone of a reservoir will exhibit resistivity values different from true formation resistivity, which is unaffected by mud filtrate. A resistivity profile, called the *invasion profile*, develops across the mud filtrate-invaded formation as a function of changing fluid saturation characteristics across the invaded zone.

Immediately behind the borehole wall of a wellbore that has traversed a 100% water-bearing permeable formation, displacement of original water in the pores of the formation is practically complete (Schlumberger, 1958, p. 13). This zone of practically complete displacement is called the *flushed zone* (Schlumberger, 1958). As noted in the

preceding section on depth of invasion, mud filtrate ceases its invasive penetration at some distance into the permeable formation, and a transitional zone of diminishing mud filtrate exists between the flushed and uninvaded zones of the permeable formation. Collectively, these two parts of the permeable formation, the flushed zone and the transition zone, are known as the *invaded zone* of the formation (Asquith, 1982, p. 3).

The flushed zone represents about the first 3 inches (Frank, 1986, p. 10) to 6 inches (Dewan, 1983, p. 26) around the wellbore. If the reservoir is water-bearing, the pores are completely filled with mud filtrate (Frank, 1986, p.10). If the reservoir is hydrocarbon-bearing, then the pores are filled with mud filtrate and residual oil. In an intermediate porosity reservoir, the transition zone could extend to a diameter of several feet of diminishing mud filtrate concentration beyond the wellbore wall, until the volume of invaded mud filtrate has been completely expended in filling available pore space across the invaded zone.

Wyllie (1963, p. 75) describes the invasion profile as a *curse* of those seeking to determine true formation resistivity. The process of mud filtrate invasion in the near-wellbore region of a formation means that measured values of formation resistivity will not represent true formation resistivity. Industry has not developed a single formation resistivity tool that will read deeply enough into the formation to reach the uninvaded zone because of associated problems relating to vertical resolution (Dewan, 1983, p. 26). Consequently, industry has resorted to using three formation resistivity logs, each with a different depth of investigation, shallow, medium and deep, to define the invasion profile (Suau et al., 1972, p. 122). Resistivity values recorded at these different depths of investigation can be used together to correct the deep resistivity measurements for the effects of changing resistivity across the invasion profile and provide a formation resistivity value indicative of true formation resistivity.

Figure 4.8 schematically illustrates the relationship between formation resistivity values recorded and the changing fluid saturation conditions across the invaded zone. The different formation resistivity values are obtained from logs that are designed to measure resistivity at incremental depths of investigation of across the invaded zone. The

resistivity of the flushed zone is known as R_{xo} (Schlumberger, 1989a, p. 2-6). Tixier (1949, p. 145) labeled the resistivity of the invaded zone, R_i., at the level under investigation, while Wyllie (1963, p. xiv), described R_i as the average resistivity of the invaded zone. Asquith (1982, p. 42, table 4) includes five different logs to measure R_i, which supports the "level of investigation" characterization of Tixier. Deep-reading resistivity logs, labeled R_d, are designed to detect that part of the formation unaffected by mud filtrate invasion. A third resistivity log is designed to read between R_i and R_d, and is referred to as R_{med}.

It is important to note that values from resistivity tools are not "point source" values, measured at the limiting point of a tools depth of investigation. Rather, resistivity measurements represent a cumulative value that can be attributed to the current passing through the invaded zone, approaching the non-invaded zone to various degrees based on tool configuration. This explains why, even if the depth of investigation of a deep resistivity log, R_d, reaches into the non-invaded zone, the measurement must still be invasion-corrected to reduce or eliminate the effects of the current's traverse across the invaded zone, hence, *Wyllie's Curse*.

It was noted above that the simplified conceptual analog of invasion, illustrated on Figures 4.6 and 4.7, reduces the complexity of a transitional invasion profile to a system of three unknowns, R_{xo}, R_t and d_i. Because R_{xo} logs are seldom run with induction logs, the response of the R_i log on Figure 4.8, is designed to be mostly affected by R_{xo}, while the R_d log is designed to be mostly affected by true formation resistivity, R_t. The third log, R_{med} is designed to be mostly affected by variations in d_i (Schlumberger, 1989a, p. 7-36). The resistivity measurements from these three curves, therefore, provide values for the three unknowns on Figure 4.7, and can be used in a tornado chart for the determination of R_t , R_{xo}, and d_i (Schlumberger, 1989a, p. 7-36 - 7-37).

The relative contribution of each zone of the simplified invasion profile, with no transition zone (Figure 4.6), to the total measured signal of individual resistivity logging tools is illustrated on Figure 4.9, a schematic representation of a radial geometric factor chart. According to Schlumberger (1989a, p. 7-11), this type of chart can be used to

compare the relative effects of the invaded zone on the response of different logging tools, and hence, provides information on relative depths of investigation of individual resistivity logging tools.

Figure 4.10 is a schematic example of a log with the three resistivity curves generated from the formation resistivity values recorded across the invasion profile of a wet reservoir, as illustrated in Figure 4.8. Flushed zone resistivity values, R_{xo}, are not routinely recorded in standard fresh water mud ($R_{mf} >> R_w$) logging programs, but can be recorded in place of the invaded zone resistivity log, R_i, or in addition to R_i, on a separate logging run. This example assumes fresh mud whose mud filtrate resistivity is much greater than the resistivity of the connate water in the formation. The SP curve is used to distinguish permeable formations, which can be invaded, from impermeable formations that are not invaded. Negative deflection of the SP curve to the left, away from the values in the shale, indicates permeable formation.

The R_i curve on Figure 4.10 indicates that formation resistivity in the near-wellbore part of the transition zone, which is almost totally saturated with mud filtrate, is greater than formation resistivity deeper in the invaded zone. This is a result of the fact that the resistivity of the mud filtrate, R_{mf}, is greater than R_w, and, as is illustrated on Figure 4.8, there is much greater concentration of mud filtrate shallower in the invaded zone. Because the R_{med} curve is close to the R_d curve rather than being close to the R_i curve, it indicates shallow invasion and a possibly porous formation. If R_{med} were closer to R_i, then invasion would be much deeper than the case illustrated in Figure 4.8, and mud filtrate saturation would be similar across both the shallow and medium depths of investigation. The relative position of the R_{med} curve with respect to the R_i and R_d curves can be a qualitative indicator of invasion depth (Dewan, 1983, p. 28). This reaffirms the context of the R_{med} curve noted above, as one designed to be affected by variations in d_i.

Also, according to Dewan (1983, p. 28), when R_d is nearly the same as, or less than the resistivity of interbedded or adjacent shales, as is illustrated on Figure 4.10, experience indicates the sands are water-bearing. Furthermore, according to Dewan (1983, p. 13), because the permeability of shale is very poor, mud filtrate will not invade

shale. Consequently, when R_i is low, and all three resistivity curves nearly overlay, it could be interpreted as the invasion profile across a shale interval. Shales do not exhibit the resistivity curve separation seen in a permeable formation that has been invaded. If, instead, the measured R_i value is relatively high, with negligible separation of the resistivity curves, the non-invaded profile could represent a tight, non-porous formation rather than a shale. As the permeability of a tight formation vanishingly approaches that of mudcake, it will inhibit invasion and prevent development of an invasion profile and could affect SP development as well.

Figure 4.11 schematically illustrates the changing fluid saturation conditions across a hydrocarbon-bearing formation invaded by mud filtrate and the associated formation resistivity values recorded at different depths of investigation across the invaded zone. The in-situ formation fluids, oil and connate water, are displaced from the wellbore wall by the invading mud filtrate. Oil is reduced to residual saturation values and connate water is removed from the flushed zone. Filtrate concentration diminishes outward across the transition zone. This is compensated in the reservoir pore volume through the displacement of ever-smaller volumes of connate water and oil along the invasion profile, until the point of unaltered saturation is reached.

Figure 4.12 is a schematic example of a log with an invasion profile representing the formation resistivity values measured across the invaded zone with the changing fluid saturation conditions illustrated on Figure 4.11. Formation resistivity shallow in the transition, R_i, "sees" nearly all mud filtrate and residual oil and records the highest formation resistivity value of the three curves. Medium and deep resistivity measurements see the effect of increasing saline connate water saturation, which increasingly diminishes the formation resistivity, leading to the invasion resistivity profile illustrated on Figure 4.12.

The presence of non-conducting hydrocarbons in the formation drives the medium and deep formation resistivity curves to values much higher than in the wet formation. If the reservoir illustrated in Figure 4.12 is considered to be the same formation illustrated in Figure 4.10, then the two figures together illustrate the essential concept noted by the

HGS in 1939. The resistivity of a hydrocarbon-saturated reservoir is greater than the resistivity of the same reservoir completely saturated with formation water.

Movable Hydrocarbons

As noted by Wyllie (1963), mud filtrate invasion complicates the process required to measure a formation resistivity value indicative of the true formation resistivity using wireline logs in a mud-filled borehole. However, according to Dewan (1983, p. 30) invasion also has a redeeming value; hydrocarbons swept out of the invaded zone provide an indication of hydrocarbon producibility. Wyllie's curse is Dewan's redemption.

The difference between hydrocarbon saturation values in the flushed zone and the uninvaded zone represents a direct indication of the presence and movability of hydrocarbons in the formation and, therefore, an assessment of potential hydrocarbon producibility. Examine the oil saturation curve in the invasion profile illustrated in Figure 4.11. The residual oil saturation, S_{or}, in the FZ is much lower than oil saturation, S_o, in the UZ. The difference between these two values illustrates the relationship between the changing oil saturation across the invaded zone and *movable hydrocarbons.* Using formation resistivity measurements in the evaluation of the amount of oil swept out of the invaded zone by filtrate invasion provides a valuable tool in petrophysical analysis.

The focus of the *essential concept* noted by the HGS in 1939 was on distinguishing water-saturated and hydrocarbon-bearing formations. The concept was quantified empirically by Archie in 1942, whose experiments provided the means to determine the percent water saturation in a formation when formation porosity and resistivity are known. However, there is more resistivity information developed from wireline logs in a mud filtrate invaded wellbore than in evaluating oil-saturated core plugs under laboratory conditions. The added information is a barrier to be overcome in the determination of true formation resistivity and calculation of water saturation using Archie's relationships. In overcoming the barrier, there is important information that can be extracted from the invaded zone and used in support of the Archie method to calculate water saturation values in a reservoir. Invaded zone data such as formation resistivity,

saturating brine resistivity, formation resistivity factors, and water saturation values, can be used in identifying the presence of moved hydrocarbons in a formation. When these data are considered quantitatively, they can be applied in a reservoir to assess the quality of hydrocarbon movability relative to a producible accumulation of hydrocarbons.

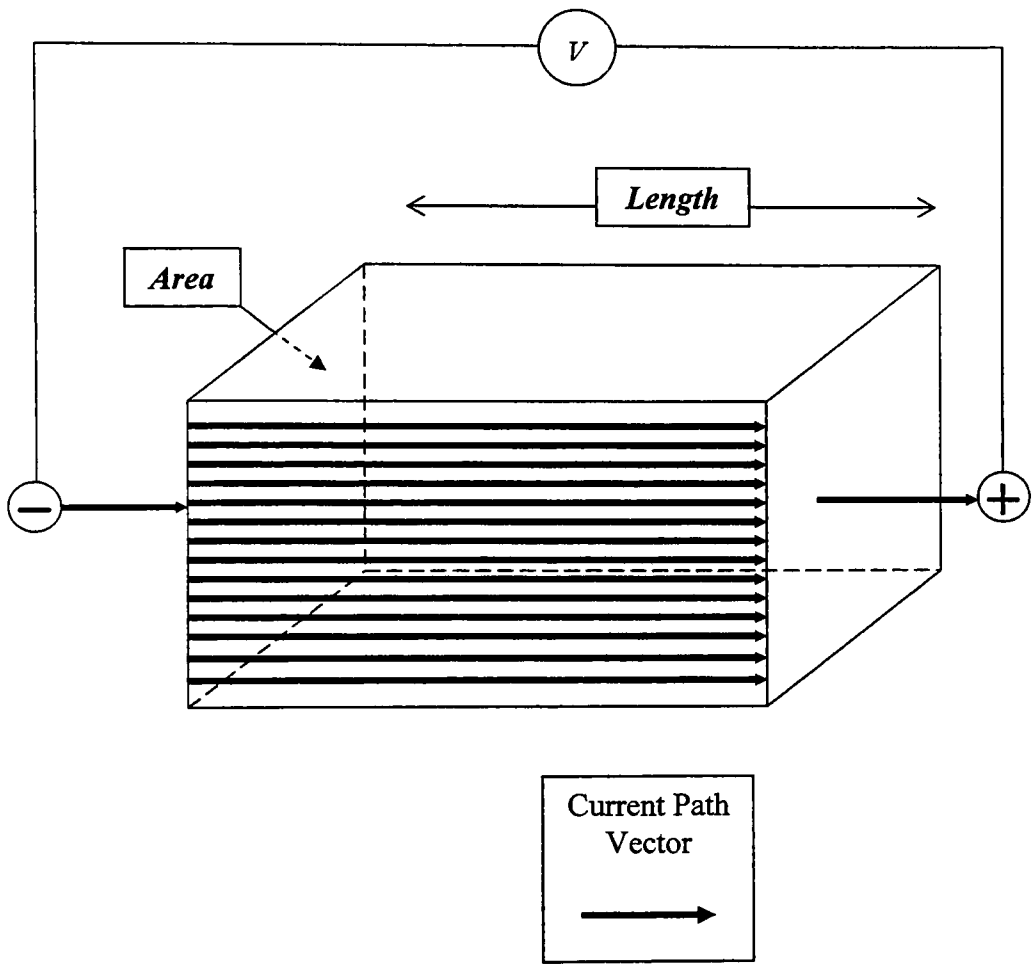

Figure 4.1 Linear Electrical Current Flow through Brine-Filled Container of Length, L, and Area, A, under an Applied Voltage, V, to Experimentally Measure the Brine Resistance, r_w and Calculate the Brine Resistivity, R_w. Current Path Vector Arrows on the Container Face Represent Unobstructed Flow through the Brine-Filled Container Volume.

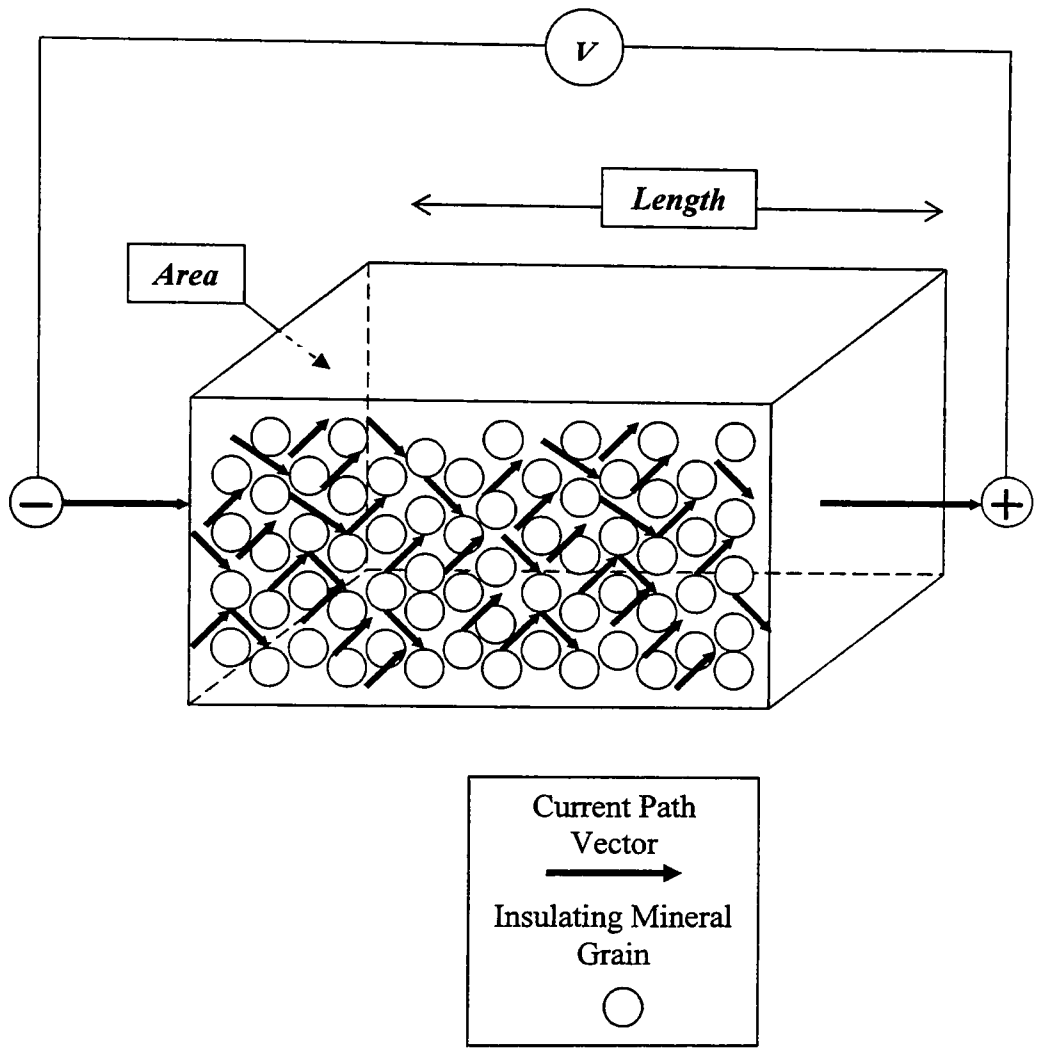

Figure 4.2 Tortuous Electrical Current Flow through Brine-Filled Sand in Container of Length, L, and Area, A, under an Applied Voltage, V, to Experimentally Measure the Resistance of the Brine-Filled Sand, r_o and Calculate the Brine-Filled Sand Resistivity, R_o. Current Path Vector Arrows on the Container Face Represent Tortuous Flow through the Brine-Filled Sand Container Volume.

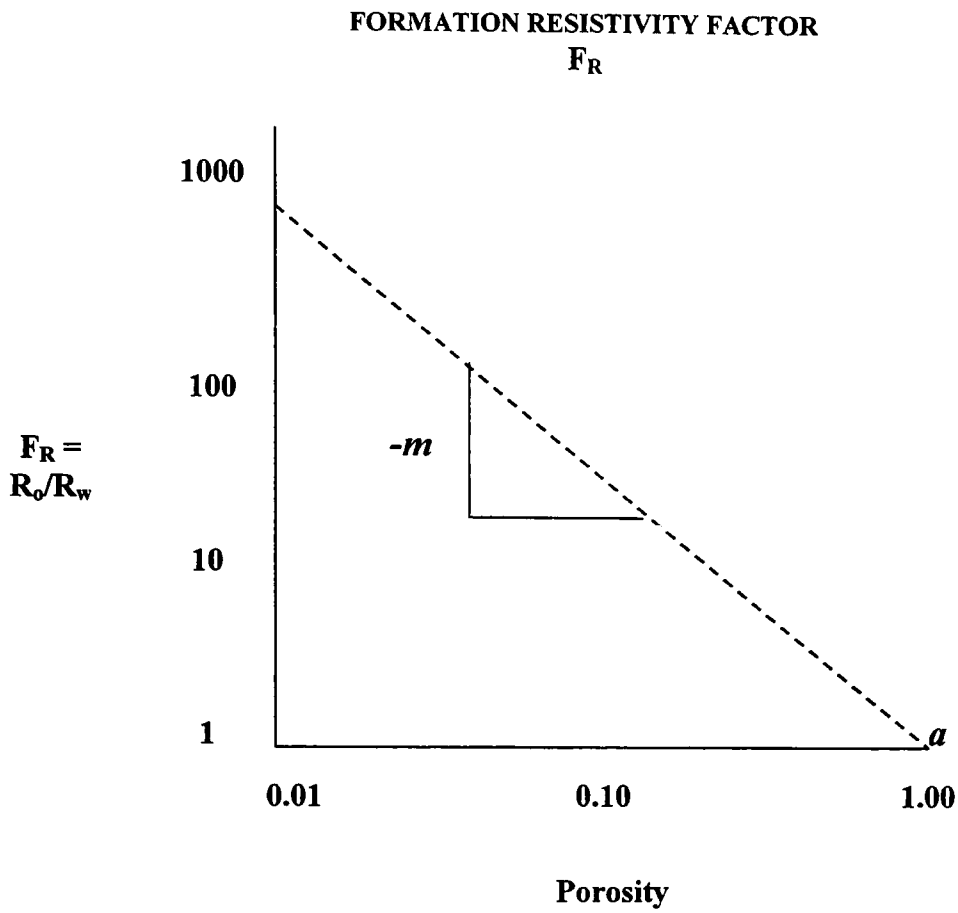

F_R: Formation Resistivity Index
R_w: Resistivity of the Connate Water
R_o: Resistivity of the Uninvaded Zone 100% Water Saturated
m: Archie Cementation Exponent
a: Tortuosity Factor

Figure 4.3 Empirical Relationship between Formation Resistivity Factor and Formation Porosity.

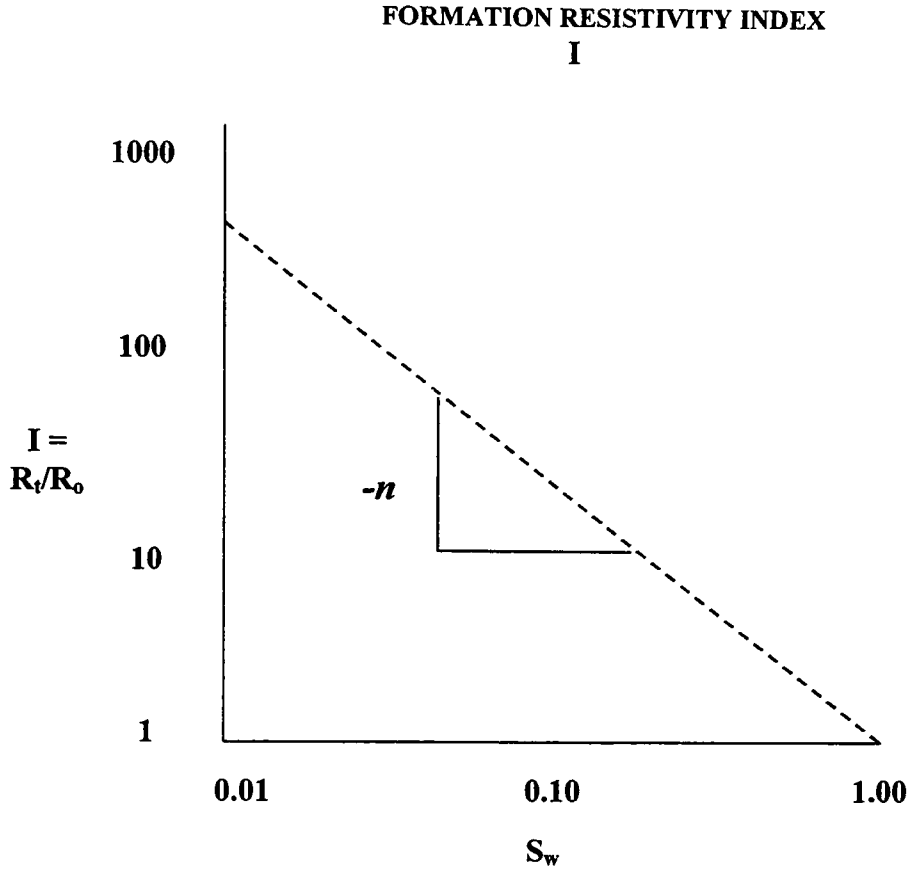

I: Formation Resistivity Index
R_o: Resistivity of the Uninvaded Zone 100% Water Saturated
R_t: Resistivity of the Uninvaded Zone < 100% Water Saturated
n: Archie Saturation Exponent

Figure 4.4 Empirical Relationship between the Formation Resistivity Index and Formation Water Saturation.

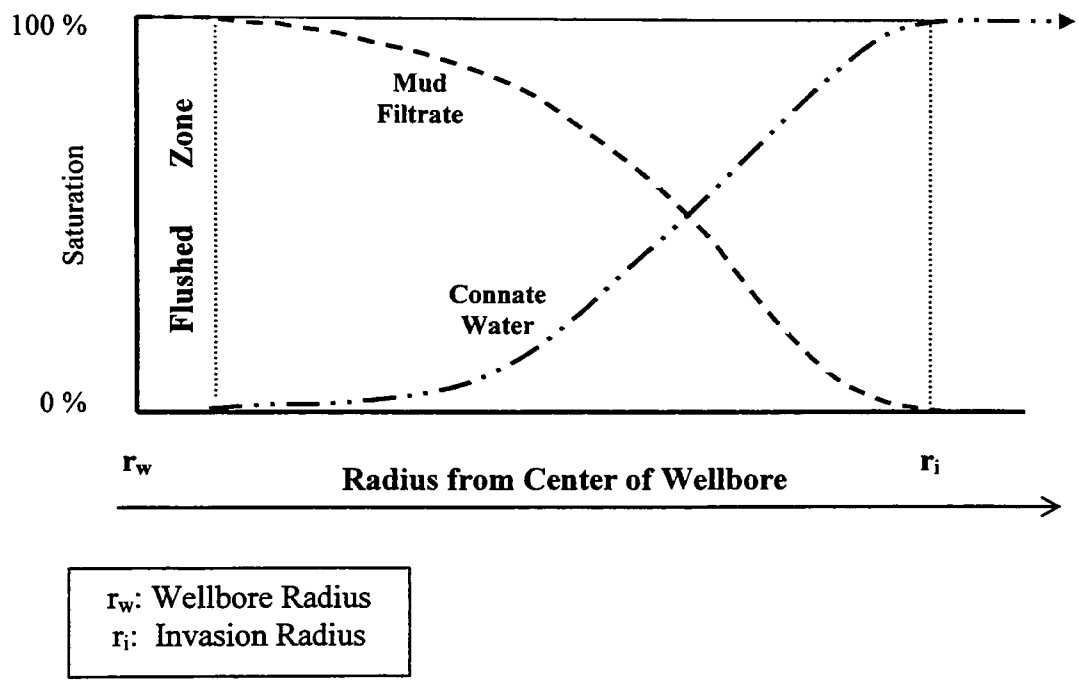

Figure 4.5 Changing Pore Fluid Saturation through the Invaded Zone of a Permeable Formation, in a 100 % Wet Interval.

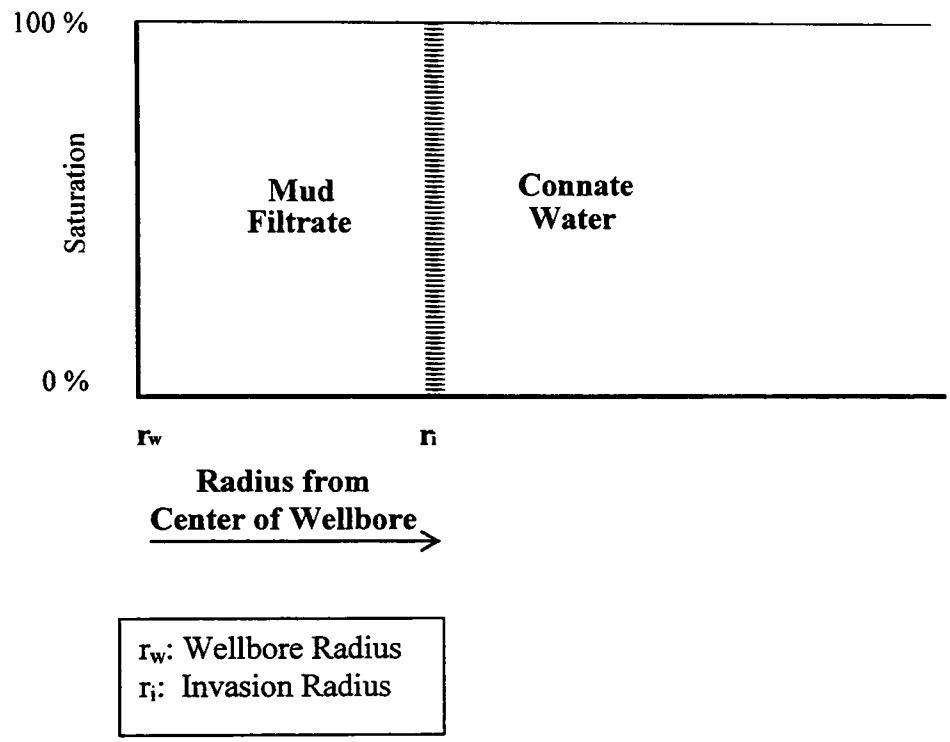

Figure 4.6 Zones of Uniform Pore Fluid Content to Represent the Electrically Equivalent Diameter of the Invaded Zone in a 100 % Wet Interval.

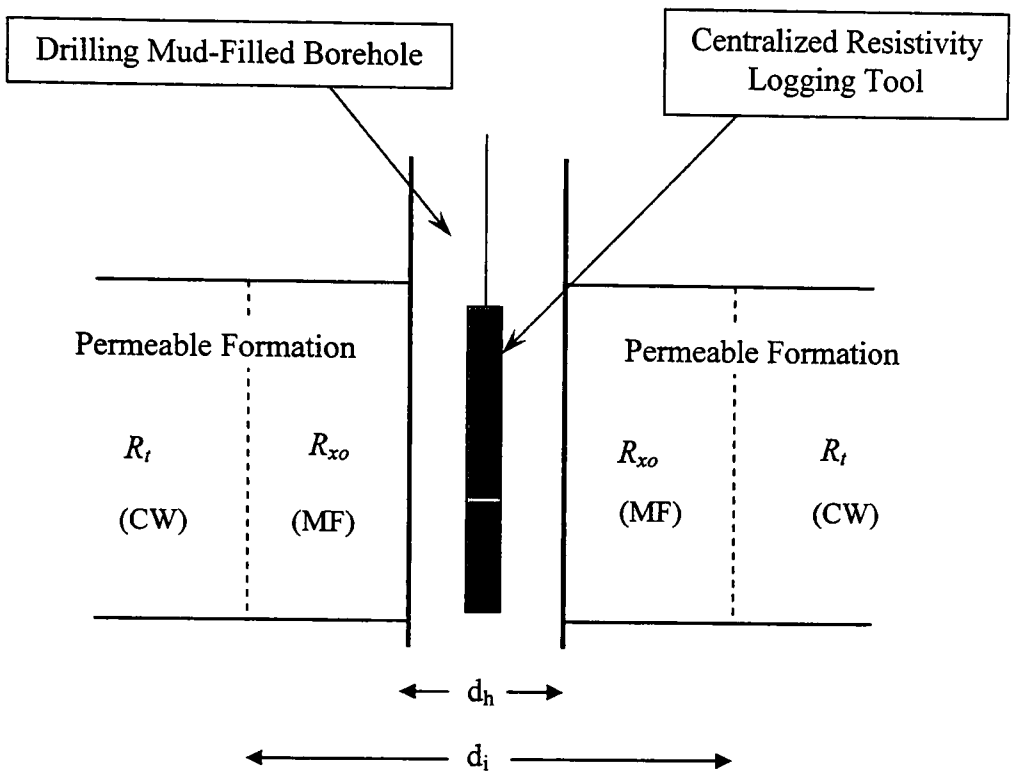

R_{xo}: Resistivity of the Flushed Zone
R_t: Resistivity of the Uninvaded Zone
MF: Mud Filtrate
CW: Connate Water
d_i: Borehole Diameter
d_i: Electrically Equivalent Invasion Diameter

Figure 4.7 Two Zones of Uniform Pore Fluid Content Representing the Electrically Equivalent Diameter of the Invaded Zone in a 100 % Wet Interval.

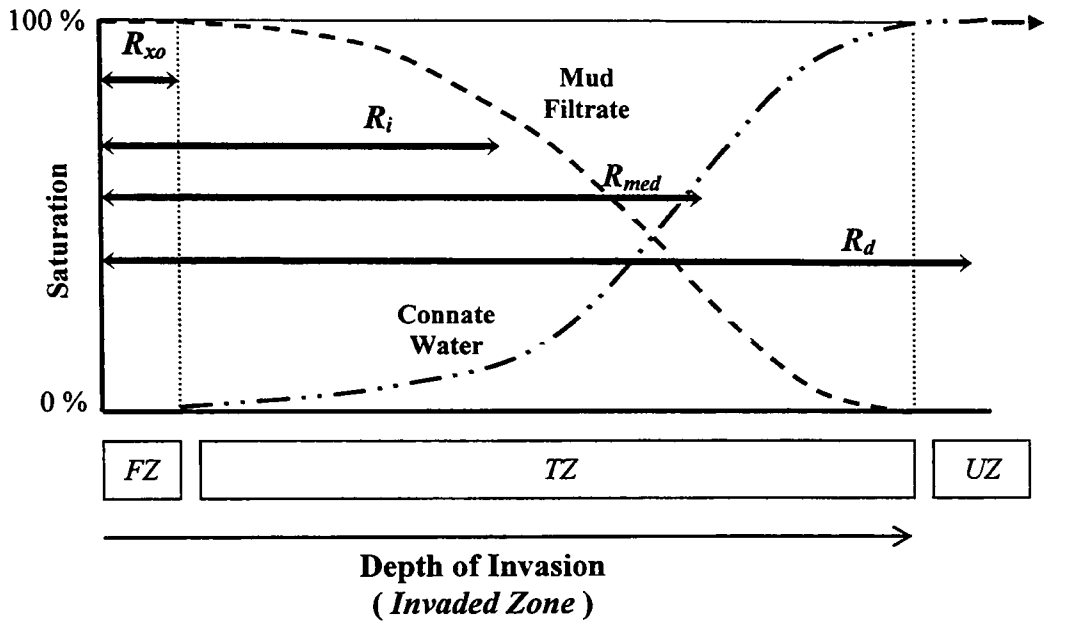

FZ: Flushed Zone portion of the Invaded Zone
TZ: Transition Zone portion of the Invaded Zone
UZ: Uninvaded Zone
R_{xo}: Measured Resistivity of the FZ
R_i: Measured Resistivity of the Shallow-Depth TZ
R_{med}: Measured Resistivity of the Medium-Depth TZ
R_d: Measured Resistivity of the Deep UZ

Resistivity Logging Tool and Relative Depth of Investigation Producing Measured Resistivity Values

R_i

Figure 4.8 Formation Resistivity Logs: Depth of Investigation vs. Pore Fluid Content through the Flushed and Transition Zones, to the Uninvaded Zone, in a 100 % Wet Interval.

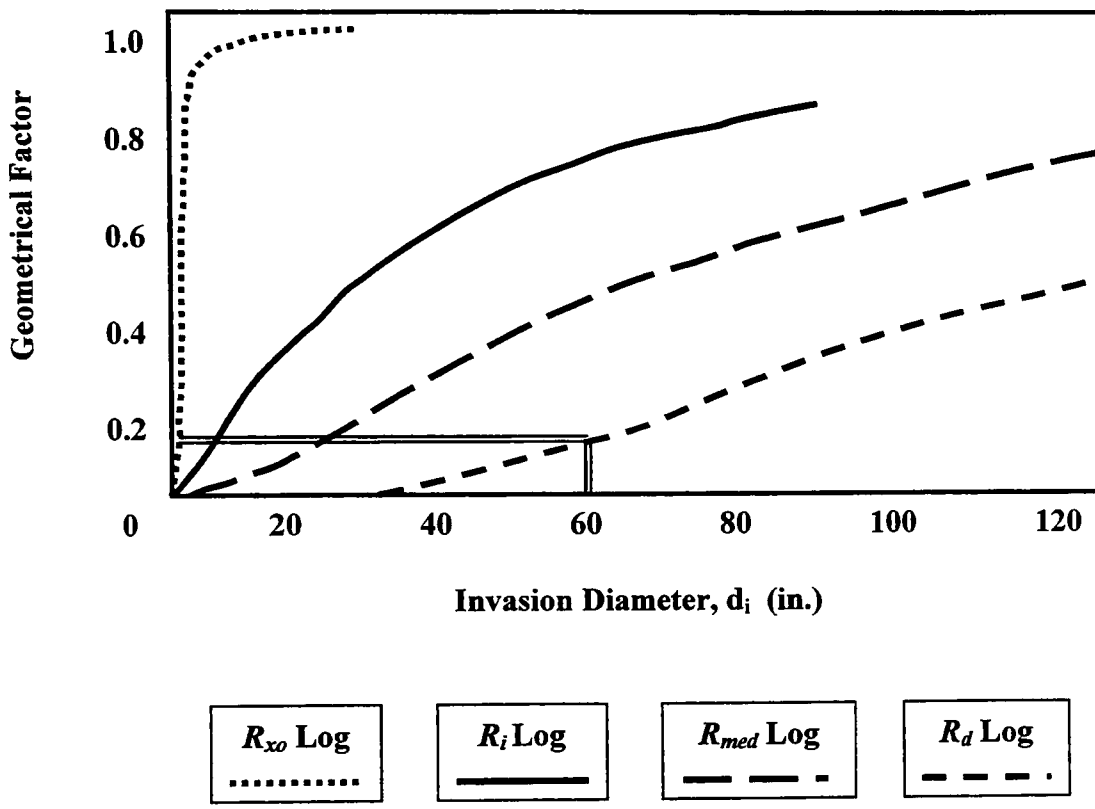

Figure 4.9 Schematic Geometrical Factor: Comparison of the Contribution of the Invaded Zone to the Signal Response in Logging Tools with Different Depths of Investigation. An example is shown by the double line that connects the 60 in. invasion diameter to the R_d log Geometrical Factor response curve, which demonstrates that with a 60 in. invasion diameter, about 20% of the reading from the R_d log would be responding to formation resistivity in the invaded zone less than 60 in. from the wellbore wall. Therefore, 80% of the R_d reading is responding to formation resistivity in the uninvaded zone greater than 60 in. from the wellbore wall.

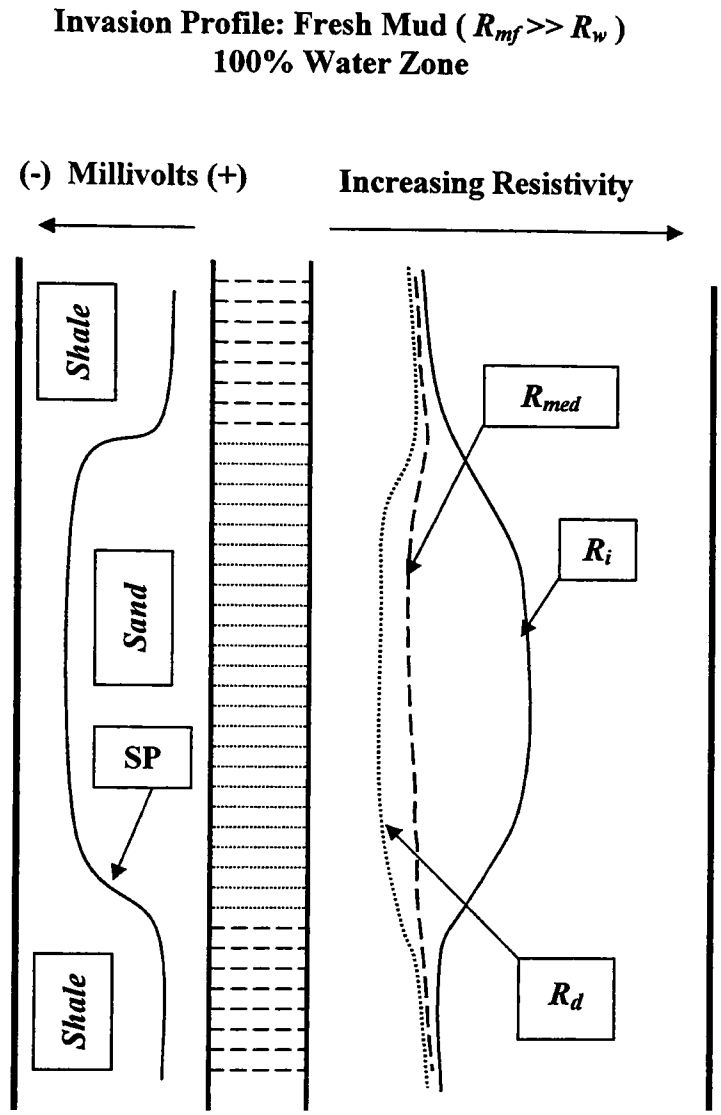

Figure 4.10 Invasion Profile: R_i, R_{med}, and R_d Curves Reflect Changing Fluid Saturation Conditions across the Invaded Zone.

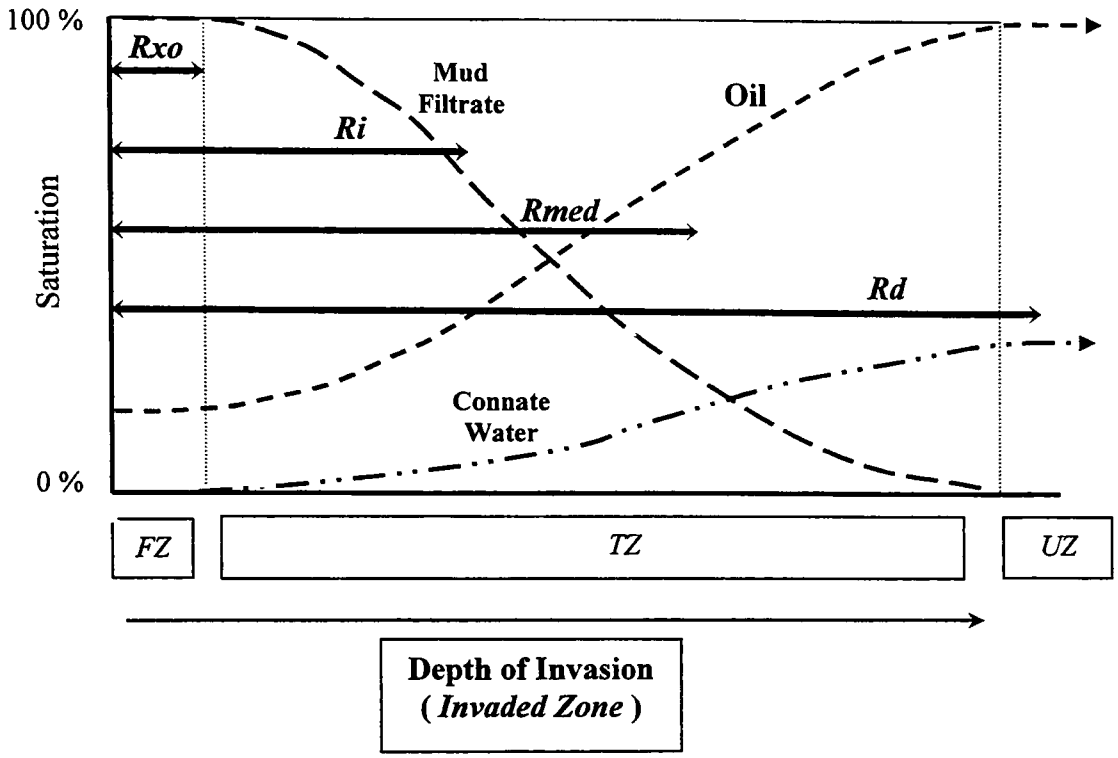

FZ: Flushed Zone portion of the Invaded Zone
TZ: Transition Zone portion of the Invaded Zone
UZ: Uninvaded Zone
R_{xo}: Measured Resistivity of the FZ
R_i: Measured Resistivity of the Shallow-Depth TZ
R_{med}: Measured Resistivity of the Medium-Depth TZ
R_d: Measured Resistivity of the Deep UZ

Resistivity Logging Tool and Relative Depth of Investigation Producing Measured Resistivity Values

R_i

Figure 4.11 Formation Resistivity Logs: Depth of Investigation vs. Pore Fluid Content through the Flushed and Transition Zone, to the Uninvaded Zone, in a Hydrocarbon – Bearing Interval.

Invasion Profile: Fresh Mud ($R_{mf} >> R_w$)
Hydrocarbon – Bearing Zone

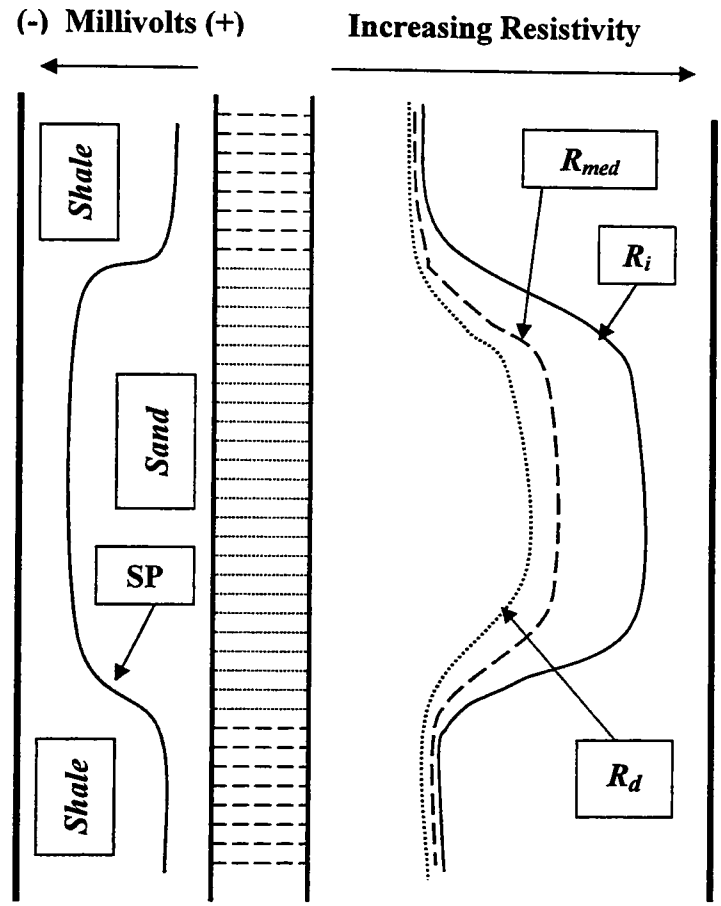

Figure 4.12 Invasion Profile: R_i, R_{med}, and R_d Curves Reflect Changing Fluid Saturation Conditions across the Invaded Zone

CHAPTER V
PETROPHYSICAL PARAMETERS

Petrophysical Analysis

As Archie continued his work on the relationship of electrical log data to the quantitative analysis of rock-fluid systems, he considered that there was a need for a term to express the physics of rocks as a function of their petrologic character. Archie (1950) introduced the general term petrophysics to describe the physics of particular rock types that would represent a finer scale of study distinct from the geophysics of larger rock systems in the earth. Archie characterized the petrophysics of reservoir rocks as the study of the physical properties of rocks related to pore and fluid distribution as it applies to the detection and evaluation of hydrocarbon accumulations in formations penetrated by a wellbore.

Identification of a reservoir and detection of the presence of hydrocarbons in the reservoir represent the initial steps in petrophysical analysis. Once the presence of a reservoir with an accumulation of hydrocarbons is identified, it must be evaluated relative to a producible accumulation. In petrophysics, evaluation refers to the analysis and interpretation of the petrophysical properties of an accumulation of hydrocarbons relative to the properties of an accumulation that is producible. The elements used in such detection and evaluation are petrophysical parameters. Hydrocarbon volume in-place is also a critical commercial evaluation parameter, but involves measurements of trap size, reservoir geometry and extent, and formation pressure data that are not the province of petrophysics.

Petrophysical analysis and interpretation in granite wash has been recognized as a problem that requires information beyond that contained in a standard approach (Frost et al., 1982; Garber, 1999). Acquisition of extra information from non-standard logging tools such as the spectral gamma-ray log (Frost et al.), or a formation-imaging log combined with a magnetic resonance log (Garber) has been recommended to provide a possible solution to understand the effects of complex mineralogy and variable texture in

granite wash reservoirs. The log database available in this study largely lacks that extra information, therefore it was necessary to find a way to more broadly apply the standard petrophysical data that is available. A strategy of combined methods was sought that would provide information to characterize Prue reservoirs beyond water saturation values calculated using the standard Archie method.

A suite of petrophysical parameters was applied to reservoir identification, hydrocarbon detection and assessment of hydrocarbon movability. Self-potential, in combination with mudlog data where available, provided initial indications of permeable beds. Initial assessments of reservoir quality were examined using formation porosity and the appearance of gas-effect, computed from a density-neutron log combination. The invasion profile, using the shallow and deep resistivity curves, was also examined as an indicator of reservoir quality. Dual induction–laterolog resistivity log data provided the foundation for many of the key analytical parameters used to identify productive hydrocarbon zones and distinguish them from wet or marginally productive zones in the Prue granite wash reservoirs.

Formation Resistivity Data in Petrophysical Analysis

Resistivity measurements in subsurface formations penetrated by a wellbore reflect the textural and fluid saturation characteristics of a formation; they interact as properties of a rock-fluid system to produce a measurable characteristic, formation resistivity. These formation properties include the volume and geometric nature of the pore system, electrolytic properties and volume of the connate water included in the pores and any conductive properties of the rock matrix.

Archie water saturation analysis is commonly applied in assessing the value of individual reservoir zones as potential candidates for testing as hydrocarbon producers. Water saturation analysis is based on true formation resistivity and porosity measurements, connate water resistivity, and a general assumption concerning the values of critical empirical parameters relating formation resistivity and porosity. Water saturation and porosity are components of a static reservoir. However, in the context of

moved hydrocarbons in an invaded reservoir, formation resistivity data can be applied as components of a dynamic reservoir in the detection and evaluation of producible subsurface hydrocarbon accumulations.

Examination of a series of petrophysical parameters developed from resistivity data in the invaded zone can provide a broader analysis of indications of hydrocarbon presence and the transmissibility properties of reservoir rock-fluid systems. Evaluation of these parameters can extend petrophysical analysis beyond calculated Archie water saturation and porosity. In addition to examining the properties of a static reservoir, petrophysical analysis in terms of a dynamic rock-fluid system provides the opportunity to interpret log response in relation to reservoir performance, not just reservoir content (Bateman, 1985, p. 105).

Historical Application of Invaded Zone Resistivity Data in Petrophysical Analysis

Formation porosity and Archie water saturation are the essential parameters developed in standard petrophysical analysis. By themselves however, these two parameters do not provide a direct indication of the productive potential of a reservoir. If values calculated for these petrophysical parameters fall within an appropriate range, generally based on local cutoffs, then a decision is made to run and cement casing and the reservoir is tested. The decision to test is based on the comparison of calculated water saturation to local cutoffs to determine if it actually represents a commercially producible accumulation of hydrocarbons.

Fluid saturation information leading to the testing decision is calculated using deep resistivity data from the uninvaded zone of the reservoir surrounding the borehole, corrected for the effects of invasion using shallow resistivity data measurements in the invaded zone. However, according to Dewan (1983, p. 30), in addition to complicating the use of deep resistivity data, invasion has a redeeming feature. The invasion process provides a petrophysicist the opportunity to assess the hydrocarbon producibility of a reservoir by comparing hydrocarbon saturation conditions in the invaded and uninvaded zones of the reservoir. The difference between these two reservoir conditions is an

indication of the volume of hydrocarbons moved by invading mud filtrate and, therefore, represents hydrocarbons available to be moved in production operations.

Early log analysts, often out of necessity, routinely included resistivity data from the invaded zone as an important source of petrophysical information. Tixier (1949) developed the ratio water saturation method as a means to determine water saturation in a reservoir at a time when the necessary formation porosity data was not readily available. Tixier realized that a ratio of Archie-type water saturation equations in the invaded zone and uninvaded zone of a reservoir caused the formation resistivity factor, and hence, formation porosity, to be factored out of the relationship. Then, using an estimate of the volumetric relationship between water saturation in the invaded and uninvaded zones and mathematical substitution, Tixier was able to calculate a useful value for water saturation in the uninvaded zone of a reservoir.

Doll (1950) considered that flushed zone resistivity measurements from the newly developed microlog provided the means to determine formation porosity based on Archie's empirical correlation between formation porosity and the formation resistivity factor. The ready availability of measured R_{mf} values facilitated the application of this method. Formation porosity developed from formation resistivity measurements represents water filled porosity in the formation. Therefore, in any hydrocarbon-bearing reservoir, a correction was required in the porosity calculation to account for the effects of residual hydrocarbons in the flushed zone on flushed zone resistivity used in Doll's resistivity porosity method.

Doll and Martin (1954) used water-filled porosity values developed from flushed zone and uninvaded zone resistivity data to develop a relationship that characterized the amount of producible oil in a unit volume of reservoir. The concept is based on detection of oil moved by mud filtrate flushing during invasion by calculating the resistivity porosity values in the flushed and uninvaded zones without applying a correction for residual oil saturation. The method essentially compares residual oil saturation and original oil saturation values in an invaded reservoir.

Millican et al. (1964) extended the work of Doll and Martin and proposed that "effective log interpretation requires more than evaluating oil saturation, it requires identification of movable oil." Log analysis consisting only of water saturation computation was not sufficient to evaluate a reservoir. Many apparently oil saturated formations they examined in the Permian Basin did not produce hydrocarbons because of poor hydrocarbon mobility. Millican et al. used a combination of resistivity porosity from the flushed and uninvaded zones and formation porosity from sonic log measurements to develop a movable oil plot, a method that encouraged assessment of residual and movable oil saturation in addition to water saturation in a reservoir.

Millican et al. described several examples where the movable oil plot was used successfully in petrophysical analysis of a range of formations. The examples included the Devonian and San Andres of West Texas, as well as the Lansing-Kansas City formation in Kansas and a Penn sand from the Texas Panhandle. Interpretation of the movable oil plot was able to distinguish zones with greater productive potential from those with less productivity. The movable oil plot recognized restricted layers of movable oil distributed across a thicker zone in which water saturation was not a useful indicator of productivity. The movable oil plot was used for selective perforation and to avoid perforating zones that could include water-cut oil.

Burke et al. (1966) applied the movable oil plot method in the tight (porosity = 5%-10%) San Andres of the Chaveroo pool in southeast New Mexico. The San Andres pay zone at Chaveroo was described by Burke et al. as fractured, vuggy dolomite with some intercrystalline and oolitic porosity. Formation porosity determination was complicated by a variable content of anhydrite, gypsum, chert, silt and limestone included with the dolomite. Because of the generally low San Andres porosity at Chaveroo, accurate porosity determination was important. The logging program required density, neutron and sonic logs to assess variable mineralogy in the porosity calculations. However, the variable pore geometry described for the Chaveroo San Andres also affected formation permeability, and Burke et al. (p. 5) considered an absence of movable oil to represent insufficient permeability for oil production. Burke et al. described how

the movable oil plot, developed using the method of Millican et al. was used with improved formation porosity calculations to provide improved completion history in the Chaveroo San Andres.

Maxson (1969) described how a movable oil plot based on the formation resistivity factor (FMOP) and resistivity porosity was used successfully in the Clearfork in Wasson field in Yoakum Co. According to Maxson, Clearfork wells completed based on movable hydrocarbon analysis had good initial potentials and low water cuts. These wells appeared to exhibit higher sustained producing rates than wells completed based on the analysis of the standard logging program, which often included just a sonic and gamma ray log. The improved production justified the extra expenditure on the expanded logging program required for the analysis of movable oil in the Clearfork carbonates. The additional logs included varying combinations of density, sonic and sidewall neutron logs along with a laterolog-microlaterolog combination.

Raymer and Salisch (1970) reported on a log analysis study of South American shaly sandstone reservoirs, in which shaliness could be an impediment to productive permeability. Raymer and Salisch stated that the most important advantage gained by including flushed zone measurements in petrophysical analysis of shaly sands is the capacity to evaluate hydrocarbon movability and thereby assess hydrocarbon producibility. Furthermore, Raymer and Salisch concluded from the results of their study that saturation values based only on resistivity data from the uninvaded zone can be misleading and result in costly errors in testing decisions. Apparently "good" hydrocarbon saturation values were not sufficient for the identification of hydrocarbon productive test candidates in these South American shaly sandstone reservoirs. Analysis of hydrocarbon movability was often critically important in identifying zones with the best opportunity for successful completion, and was proven through production or wireline testing.

These early petrophysical studies demonstrate that, despite the complications of variable texture and mineralogy, there is a range of petrophysical information contained in a standard logging suite that can be effective in the evaluation of the productive

potential of a reservoir that resists standard analysis. Extracting the information requires a strategy of combining several petrophysical methods to provide an assessment of reservoir quality and the detection of movable hydrocarbons, included within the framework of water saturation calculation. The strategy follows the conclusion of Millican et al. (1964), that water saturation calculations alone are not sufficient in the analysis of a hydrocarbon productive reservoir; it is necessary to examine a reservoir for indications of movable oil.

The value of indications of movable hydrocarbons in petrophysical analysis is evident today, even with the advent of modern logs such as those described by Frost, et al (1982) and Garber (1999). Walsh et al. (1994) developed commercially available software that is dependent on a series of cross plots based on the resistivity information contained in the invaded and uninvaded zones of a reservoir to identify the presence of movable hydrocarbons. Cheng et al. (1999) combined reservoir engineering and petrophysics to determine a pseudo-mobility profile in the texturally complex Cretaceous Qishn Clastics in the Masila Block of the Republic of Yemen on the Arabian Peninsula. Conventional evaluation methods of log data proved unreliable in the Masila development area, and application of modern logging technology such as nuclear magnetic resonance was constrained by the high cost required to operate in such a remote location. Necessity forced reevaluation of available standard openhole log data and a simple, cost-effective productivity indicator based on movable hydrocarbon analysis was developed to evaluate the hydrocarbon potential of the texturally variable Qishn reservoir. Production history has supported the conclusion that the pseudo-mobility profile, based on movable hydrocarbon analysis in the invaded zone, has been a reliable estimator of Qishn productivity.

There is a breadth of data available in a standard logging suite that provides the opportunity to extend petrophysical analysis beyond Archie water saturation calculations. In an interpretation based only on calculated water saturation values, there is no opportunity to evaluate how well the input parameters and assumptions used in the calculation produces values that actually represent saturation conditions in the reservoir.

Petrophysical methods based on a combination of information from the invaded and uninvaded zones provides the opportunity to detect the presence and assess the movability of hydrocarbons in the reservoir without calculating water saturation. Further, it affords an opportunity to evaluate the calculated Archie water saturation values as a reasonable representation of actual fluid saturation conditions in the reservoir. This broadened assessment should be completed as an essential part of petrophysical analysis in the Prue, providing input to water saturation evaluation and hydrocarbon producibility lacking in Archie water saturation analysis alone.

Petrophysical Analysis Parameters

Figure 5.1 shows the suite of parameters compiled into the petrophysical analysis spreadsheet developed for this study. The overall approach is a four-fold system. To begin the petrophysical analysis of an identified reservoir, it was first necessary to obtain an R_w value for the reservoir. Because of the potential for variable salinity in separate Prue reservoirs, an R_w value was computed from the log data for each sand examined in the study. Then, parameters representing different aspects of reservoir quality are evaluated. Next, additional parameters are computed that provide information on the presence and movability of hydrocarbons in a reservoir, but do not require an explicit water saturation calculation. These parameters can also provide indications of excess conductivity in the reservoir. Finally, water saturation values are computed by different methods to examine and evaluate the calculated values. Each water saturation calculation method is based on different assumptions. Together, they provide the opportunity to compare saturation values based on different input information to gain insight about the effects of the different assumptions. When the results are comparable, it provides confidence in the values; when the results are different, it encourages examination of all the variables and assumptions used to calculate the different water saturation values.

Analysis of Connate Water Resistivity: R_w

To begin the petrophysical analysis of a reservoir that has been identified, it was necessary to obtain an R_w value for the reservoir. Because of the potential for variable salinity in separate Prue reservoirs, an R_w value was computed from the log data for each sand examined in the study.

When a drilling mud-filled wellbore traverses the contact between a shale and a permeable bed, a naturally-occurring electromotive force (*emf*) can be found at the contact. The mechanism responsible for development of the natural *emf* is a function of the salinity contrast between the mud filtrate and connate water in the permeable bed. The presence and magnitude of the *emf* is recorded on the SP log, and this information provides the opportunity to examine the resistivity of the connate water in the permeable bed.

In order to be able to compute R_w values, a spreadsheet was developed that included two separate algorithms based on the SP. The first of the two relationships is from Dresser Atlas (1985, p. 16-17) and the second is from Bateman and Konen (1977), which was referenced in Asquith (1982, p. 29), where the algorithm developed by Bateman and Konen was reviewed.

Computed R_w values from the Dresser Atlas relationship follow the curves for "mostly NaCl solutions" (Dresser Atlas, 1985, Chart 2-3, p. 17) while the results from Bateman and Konen follow the curves on Chart 2-3 for fresh formation waters containing divalent cations. Computed values of R_w from the Dresser Atlas method for mostly NaCl solutions were used in the petrophysical analyses completed in this study. The algorithms from both methods are shown in Appendix A.

Assess Reservoir Quality

SP

The first step in log analysis is to locate potentially permeable beds by distinguishing impermeable shales from non-shales (Dewan, 1983, p. 35) and generally the Gamma Ray and SP logs are used for this initial purpose. The presence of radioactive

grains in non-shale facies renders the Gamma Ray less effective for this purpose in granite wash. However, the Spontaneous Potential (SP) log measures electrical currents that flow naturally in borehole mud at the contact between a shale and a permeable sand or carbonate and is used to identify potentially permeable beds. Where available, Rate of Penetration (ROP) curves and sample descriptions confirm that the SP is useful in recognizing potential permeable beds in Prue granite wash sands.

The amplitude of SP deflection is used as a Prue reservoir quality indicator by normalizing the SP development in each individual Prue reservoir against the maximum SP in the entire Prue interval in the well being studied.

$$\frac{Prue\ SP\ Amplitude}{Prue\ Interval\ Maximum\ SP} = Normalized\ SP\ Factor \qquad 5.1$$

A value near 1.0 is interpreted to represent a clean reservoir with a minimum R_w value. Values that decrease from 1.0 indicate a reservoir that is shaly and less clean, or a reservoir with a higher R_w, either of which could decrease the potential for a successful completion.

Formation Porosity

Formation porosity is calculated using density and neutron log data and the standard root mean square relationship (Asquith, 1982, p. 68).

$$\phi_{DN} = \sqrt{\frac{\phi_D^{\,2} + \phi_N^{\,2}}{2}} \qquad 5.2$$

Formation porosity is evaluated as a reservoir-quality indicator based on where individual zonal porosity values fall in a range of values interpreted to represent poor to excellent Prue reservoirs.

Invasion

In overbalanced drilling, hydrostatic pressure of the mud column is designed to remain measurably higher than formation pressure to maintain safe well control. The pressure differential forces mud filtrate into the formation, pushing *in situ* reservoir pore fluids away from the wellbore creating a radial invaded zone around the wellbore. Depending on relative values of mud filtrate resistivity (R_{mf}), connate water resistivity (R_w), and the depth of invasion, a resistivity invasion profile develops around the wellbore. The invaded zone can be detected in a reservoir by standard resistivity logging tools with three different depths of investigation.

There is no invasion across impermeable shale intervals. Therefore, no resistivity invasion profile develops in shale intervals (Dewan, 1983, p. 13, 28-29). The three resistivity curves overlay in a shale because they are measuring the same rock-fluid system, undisturbed by invasion, at all three depths of investigation. In contrast, permeable beds are invaded by mud filtrate, a resistivity invasion profile develops and the shallow, medium and deep log curves separate because each log measures different saturation conditions. The amount of separation between the shallow and deep resistivity curves is measured by a ratio of the two values. Greater separation is interpreted to represent better reservoir permeability as it is further removed from the lack of curve separation in impermeable rocks represented by uninvaded shales.

Gas Effect

Gas effect refers to a characteristic curve crossover of the density and neutron porosity logs in gas-bearing reservoirs. The density tool measures the electron density of a formation, which is related directly to formation bulk density. Gas, as a low-density pore fluid, lowers formation bulk density to a greater extent than does liquid-filled porosity. The presence of gas in a reservoir therefore causes the density log to read lower formation bulk density than would be found in an equivalent liquid-filled reservoir and, hence, higher apparent porosity than an equivalent liquid-filled reservoir.

The neutron tool measures the hydrogen content of a fluid-filled formation and relates that to formation porosity. Hydrogen concentration is much higher in water and hydrocarbon liquids than in hydrocarbon gases, therefore the neutron tool measures much less hydrogen in a gas-filled reservoir than would be found in an equivalent liquid-filled reservoir. Consequently, the neutron log reads much lower apparent porosity in a gas-bearing reservoir than an equivalent liquid-bearing reservoir.

Gas effect represents the opposing response of the density-neutron log combination due to the presence of gas-filled pores. As density porosity increases in gas-bearing reservoirs, neutron porosity simultaneously decreases, and the two curves cross. The amount of curve separation is measured by simple subtraction of neutron from density porosity. Shaliness in a reservoir will lessen gas-effect curve separation. As this measure of curve separation increases, it is considered to represent a cleaner reservoir, with greater gas saturation and less risk of water in the production stream; increased gas-effect indicates a stronger potential for a high quality, gas-productive reservoir.

Detection of Hydrocarbon Presence and Movability

The response of a reservoir rock-fluid system to the mud filtrate invasion process can be detected and measured by a suite of formation resistivity logs designed to investigate the breadth of the invaded zone. The log response of the individual resistivity tools combined with formation porosity data provides an opportunity in petrophysical analysis and interpretation to detect the presence and movability of hydrocarbons in a reservoir. Several of the traditional methods described in the preceding section are applied to this purpose: to broaden the analysis in this study beyond calculation of a water saturation value as the primary indicator of reservoir potential. These methods are based on long-standing petrophysical fundamentals. They provide indications of hydrocarbon presence and the transmissibility properties of a reservoir rock-fluid system to expand a multiple parameter interpretation in Prue granite wash reservoirs.

FMOP: Formation Factor Movable Oil Plot

Tixier et al. (1960. p. 154), described a method to detect a hydrocarbon-bearing reservoir without using a value for R_w or R_t. Residual hydrocarbons in the invaded zone of a reservoir increase the invaded zone resistivity to values in excess of those in a purely water-saturated reservoir. Consequently, the formation resistivity factor determined from shallow resistivity measurements, using R_i or R_{xo} and R_{mf}, will be greater than the formation resistivity factor calculated from sonic porosity, based on Archie's empirical correlation of F_R to formation porosity. Comparison of the values of the two different formation resistivity factors provides indications of the presence of hydrocarbons in the invaded zone of a reservoir, without using values for R_w or R_t.

While the method of Tixier et al. (1960) can be used to detect hydrocarbon presence, it provides no evidence of hydrocarbon movability. Later investigators, such as Maxon (1969) and Raymer and Salisch (1970) added the formation resistivity factor from deep resistivity measurements to the method described by Tixier et al. and thereby included the effects of hydrocarbon saturation undiminished by the flushing-effects of invasion to the method. By comparing three different values of the formation resistivity factor, the component of hydrocarbon movability was added to the hydrocarbon detection method of Tixier et al. (1960), illustrating the usefulness of the FMOP as a tool in the detection of hydrocarbon presence and movability in a reservoir.

Dresser Atlas (1982, p. 161-164) described the method used to construct and interpret the formation resistivity factor movable oil plot (FMOP). The FMOP essentially applies Archie's original concept that it is first necessary to recognize a formation when it is wet in order to be able to recognize when the formation is hydrocarbon bearing. The *empirical* formation resistivity factor, F_R, by definition represents a wet reservoir. Values for F_R developed from core analysis are not available in this study; therefore values developed from the empirical correlation to formation porosity, shown in Equation 5.3, are used. Formation porosity values are calculated from density–neutron log data, and the formation resistivity factor developed from porosity is labeled F_{DN}.

$$F_R = \frac{R_O}{R_W} = \frac{a}{(\phi_{DN})^m} = F_{DN} \qquad 5.3$$

In the FMOP, the *empirical* formation resistivity factor is compared to *apparent* formation resistivity factors, F_{Rxoc}, F_{Ri}, and F_{Rd}, developed from resistivity measurements across the invaded zone (Equations 5.4, 5.5, 5.6). The comparison represents the FMOP, which provides the means to identify zones with residual and movable hydrocarbons.

$$F_{Rxoc} = \frac{R_{xoc}}{R_{mf}} \qquad 5.4$$

$$F_{Ri} = \frac{R_i}{R_z} \qquad 5.5$$

$$F_{Rd} = \frac{R_d}{R_w} \qquad 5.6$$

As was noted in chapter II, calculated R_{xo} data are labeled R_{xoc} to denote they are calculated and not measured data. Consequently, petrophysical parameters based on the calculated R_{xoc} data are labeled with the same lower case *c* reference.

The empirical formation resistivity factor, F_{DN}, was defined at the condition where $S_w = 1.0$, and is a function of formation texture as a control on the volume and geometry of interconnected water-filled pores in the formation. It provides the means to determine the resistivity of a water-saturated formation. The apparent formation resistivity factors, F_{Rxoc}, F_{Ri}, and F_{Rd}, in the invaded and uninvaded zones are inherently a function of formation texture and hydrocarbon volume as a control on the volume and geometry of water-filled pores. Because these parameters are based on formation resistivity measurements, interconnected, water-filled pores remain a critical conceptual element of

the apparent formation resistivity factors, as it is for the empirical formation resistivity factor.

The apparent formation resistivity factors provide the means to assess formation resistivity associated with diminished water-filled porosity in the invaded and uninvaded zones. As movable hydrocarbon saturation increases and water-filled porosity decreases across the invaded zone of a hydrocarbon bearing reservoir, the apparent formation resistivity factors represent the changing volume and geometry of interconnected water-filled pores across the invaded zone.

An FMOP was computed for each of the Prue Sand reservoirs examined in this study. If a reservoir is wet, then water-filled porosity extends across the invaded zone as mathematically shown below:

$$F_{DN} = F_{Rxoc} = F_{Ri} = F_{Rd} \tag{5.7}$$

Because they are equal in value, the empirical and apparent formation resistivity factor curves will overlay across the stratigraphic extent of a wet reservoir. If a reservoir contains movable hydrocarbons, the four resistivity factor curves will separate as follows:

$$F_{DN} \leq F_{Rxoc} < F_{Ri} < F_{Rd} \tag{5.8}$$

Values of the F_{Rxo} curve exceed those of F_{DN} because of the insulating effects of the residual hydrocarbons in the flushed zone and F_{Ri} is greater than F_{Rxo} because insulating hydrocarbon saturation in the transition zone is greater than residual saturation in the flushed zone. However, if there is a strong mud filtrate flushing effect in a reservoir, and filtrate saturation is high in the invaded zone, then the apparent formation resistivity factor from the flushed zone, F_{Rxoc}, could nearly overlay the empirical curve, F_{DN}. The F_{Rd} curve exceeds the apparent curves in the invaded zone because of the greater insulating effects of total hydrocarbon saturation in the uninvaded zone. As the

hydrocarbon saturation is increasing across the invaded zone, interconnected water-filled porosity is decreasing.

Bassiouni (1994, p. 255) described the FMOP as an effective method in locating movable hydrocarbons, while Schlumberger (1989, p. 8-12) described it as a tool to show a hydrocarbon saturation and movability. The amount of separation of the apparent formation resistivity factor curves from the empirical formation resistivity factor curve, F_{DN}, is directly related to values for water saturation in the flushed zone S_{xo}, the transition zone S_i, and the uninvaded zone S_w. Residual hydrocarbon saturation is related to the separation of the F_{DN} curve and the two invaded zone curves, while movable hydrocarbon saturation is directly related to the separation of the F_{Rd} curve and the two invaded zone curves. The FMOP provides a qualitative assessment of hydrocarbon saturation and movable hydrocarbons as a function of formation porosity and the Archie empirical parameters, m and a. All of this relative saturation information can be shown without having to calculate any water saturation values.

In cases where the F_{Rxo} or F_{Ri} curve plots below (less than) the F_{DN} curve, it indicates the formation is less resistive than when its pore system is 100% water saturated, and conductivity in the rock-fluid system is in excess of that which can be accounted for by water-filled porosity. In that case, the rock matrix must contribute to electrical conductivity, either through the presence of clay minerals, with their inherent property of electrical conductivity through cation exchange capacity, or the presence of water-filled, microporous grains. This represents a condition termed "excess conductivity" (Schlumberger, 1989b, p.43).

The method assumes that the formation porosity measurements are not similarly affected by the presence of clay. Dewan (1983, p. 249) states that there is a poor correlation between volume of shale calculations from the density – neutron log and CEC values measured on cores. This suggests that the effects exerted by the volume of shale in a reservoir on density – neutron porosity measurements is smaller than the effects exerted by the CEC in the volume of shale on formation resistivity measurements.

The FMOP provides a qualitative assessment of hydrocarbon saturation and movable hydrocarbons as a function of formation porosity and the Archie empirical parameters, a and m. This qualitative saturation information can be shown without having to calculate any water saturation values. The FMOP can be used quantitatively if an assumption is made for the value of Archie's empirical parameter, n. Figure 6.2 illustrates that the separation between the FMOP curves, represented mathematically by ratios between the empirical formation resistivity factor and the individual apparent formation resistivity factors, is equal to square of water saturation (when n = 2) in the zones represented by each respective apparent formation resistivity factor. Building on the relationships illustrated in Figure 6.2, the relationships on Figure 6.3 illustrates how the FMOP represents movable hydrocarbons.

A parameter, R_z is indicated in Equation 5.5, in association with the apparent formation resistivity factor for the invaded zone, F_{Ri}. In the transition zone of the invaded zone, R_z represents the average resistivity of the mixture of connate water and mud filtrate in the invaded zone (Frank, 1986, p. 10, 50; Schlumberger, 1989a, p. 8-7). It represents the resistivity of the saturating brine in that zone, analogous to R_{mf} and R_w in the flushed and uninvaded zones, respectively. The calculations associated with development of a value for R_z are reviewed in Appendix B.

Resistivity Porosity

Millican et al. (1964, p. 3) indicated that porosity computed from resistivity data in the flushed and uninvaded zones represented water-filled porosity in each of those respective segments of the invasion profile. Water-filled porosity computed from resistivity data is called resistivity-derived porosity (Asquith, 1982, p. 44) or, more simply, resistivity porosity. Because it is based on formation resistivity measurements, resistivity porosity represents the porosity in a clean formation that is interconnected and saturated with conductive brine. The interconnected, water-filled pore volume, defined as resistivity porosity, represents the conductive pathway for the transit of electrical current through a non-conducting formation matrix.

In the time between the advent of quantitative log analysis in 1942 and the common availability of formation porosity logging tools, porosity determination was considered one of the main applications of resistivity logs (Schlumberger, 1958, p. 18, 109, 111-116). The electrical log parameter critical to formation porosity determination was flushed zone resistivity, and if the formation was hydrocarbon bearing, the resulting value was called *apparent* formation porosity. Residual hydrocarbons in the flushed zone reduced the volume of saturating brine, and consequently, the water-filled, apparent porosity value was less than total formation porosity. To determine actual formation porosity, a correction factor was necessary in the calculation, based on knowledge of water saturation in the flushed zone, S_{xo}, shown below as Equation 5.9 (Schlumberger, 1958, p. 18).

$$\phi = \left(\frac{R_{mf}}{R_{xo}} \right)^{1/2} \times \frac{1}{S_{xo}} \qquad 5.9$$

A value for S_{xo} of 0.8 was suggested for use in formations with intergranular porosity, saturated with high API gravity oil. Reservoirs characterized by pore systems with low or irregular permeability or containing heavy oil should use a value of 0.6 for S_{xo} because flushing will be less complete than in reservoirs with intergranular porosity (Schlumberger, 1958, p. 18).

Millican et al. (1964) demonstrated that if apparent porosity values from resistivity are not corrected for residual hydrocarbons, but are compared directly to sonic log formation porosity, the difference represents the pore volume of residual hydrocarbons in the invaded zone. Invaded zone resistivity porosity would be less than the total formation porosity by the volume of conductive brine that has been replaced by non-conducting hydrocarbons in the reservoir pore system. Furthermore, uncorrected resistivity porosity from the deep resistivity data can be included in the analysis to represent water-filled porosity in the uninvaded zone. Examination of the three porosity curves represents a movable oil plot (MOP). It provides the means to identify residual

and movable hydrocarbons by the separation of the shallow and deep resistivity porosity from density-neutron porosity.

A resistivity porosity MOP has been computed for each Prue Sand examined in this study following the procedures described by Millican et al. (1964) and Dresser Atlas (1982, p. 152-160). Values for resistivity porosity parameters, based on formation resistivity measurements across the invaded zone, have been calculated as shown in Equations 5.10, 5.11 and 5.12.

$$\phi_{Rxoc} = \left(\frac{a \times R_{mf}}{R_{xoc}} \right)^{1/m} \qquad 5.10$$

$$\phi_{Ri} = \left(\frac{a \times R_z}{R_i} \right)^{1/m} \qquad 5.11$$

$$\phi_{Rd} = \left(\frac{a \times R_w}{R_t} \right)^{1/m} \qquad 5.12$$

The method in the derivation of the resistivity porosity relationships are shown in Appendix C.

Resistivity porosity information is interpreted in this study based on ratios of the total formation porosity (Equation 5.2) and resistivity porosity from the flushed, invaded and uninvaded zones. In a wet reservoir, 100% water-filled porosity extends across the invaded zone, consequently, resistivity porosity values are equal across the invaded zone (Equation 5.13), and the four porosity curves would overlay.

$$\phi_{DN} = \phi_{Rxoc} = \phi_{Ri} = \phi_{Rd} \quad 5.13$$

In a hydrocarbon-bearing reservoir, water-filled porosity diminishes across the invaded zone (Equation 5.14), as a function of the movable hydrocarbon volume in the reservoir.

$$\phi_{DN} \geq \phi_{Rxoc} > \phi_{Ri} > \phi_{Rd} \quad 5.14$$

Separation of the resistivity porosity curves from the flushed and invaded zone from total formation porosity is a function of water saturation in the invaded zone. Separation of the deep resistivity porosity curve and total formation porosity is related to water saturation in the uninvaded zone. If the separation between resistivity porosity and total formation porosity is considered as a ratio, then a quantitative value for water saturation can be developed (Asquith, 1982, p. 100).

Comparing the separation relationship of all four porosity curves illustrates conditions of presence and movability of hydrocarbons in the reservoir. Figure 6.4 illustrates that the separation between resistivity porosity and formation porosity, represented mathematically by ratios of the respective porosity values, is equal to water saturation in each respective zone. These relationships can then be used to represent movable hydrocarbons in the reservoir.

Asquith et al. (1992) in a petrophysical study of the shaly Tannehill sandstone in Knox County, Texas, documented a case in which shallow resistivity porosity was greater than total formation porosity (Equation 5.15).

$$\phi_{Rxoc} > \phi_{Ri} > \phi_{DN} > \phi_{Rd} \quad 5.15$$

Having a value of water-filled porosity in the invaded zone in excess of total formation porosity represents a seemingly impossible condition. It was determined to be the result of excess conductivity contributed to the Tannehill rock-fluid system by the presence of illite-smectite clays in the reservoir rock.

MHI: Movable Hydrocarbon Index

Schlumberger (1972, p. 85) states that the ratio $[S_w / S_{xo}]$ is an index of oil movability. In a 100% wet reservoir, water saturation in the uninvaded zone (S_w) is equal to water saturation in the flushed zone (S_{xo}). Even after flushing by the invasion process, the reservoir remains 100% water saturated, and $[S_w = S_{xo} = 1.0]$. If the ratio $[S_w / S_{xo} < 1.0]$ then S_{xo} is $> S_w$ because movable hydrocarbons were flushed out of the invaded zone and replaced by mud filtrate water, hence S_{xo} is greater than S_w. This also indicates the converse, that residual oil saturation (ROS) in the flushed zone is less than oil saturation (S_o) in the uninvaded zone because $[S_w + S_o = 1.0]$ and $[S_{xo} + ROS = 1.0]$.

The underlying concept for this petrophysical parameter is that oil that was originally present in the flushed zone of a reservoir was swept away from the near-wellbore region by invading mud filtrate. The ratio $[S_w / S_{xo}]$ is therefore a function of the volume of hydrocarbons moved out of the flushed or invaded zones during invasion and is called the Movable Hydrocarbon Index (Asquith, 1982, p. 97).

Comparing water saturation in the uninvaded zone with water saturation in the invaded zone provides the opportunity to evaluate movable hydrocarbons. Moreover, a ratio of the two values causes the formation resistivity factor to be canceled out of the relationship. Asquith (1982, p. 96-97) illustrates the calculations required to determine the MHI and the ratio values associated with a producible accumulation of hydrocarbons. Equations 5.16 through 5.19 illustrate the development of the movable hydrocarbon index.

$$\left(S_{w_{Archie}} \right)^n = \left[\frac{F \times R_W}{R_t} \right] \qquad 5.16$$

$$S_{xo}{}^n = \left[\frac{F \times R_{mf}}{R_{xo}} \right] \qquad 5.17$$

$$\frac{Sw^2}{Sxo^2} = \frac{F_R \times \frac{Rw}{Rt}}{F_R \times \frac{Rmf}{Rxo}} = \frac{Rw}{Rt} \times \frac{Rxo}{Rmf} = \frac{Rxo}{Rt} \times \frac{Rw}{Rmf} = \frac{R_{xo}/R_t}{R_{mf}/R_w} \qquad 5.18$$

$$\left[\frac{S_w^{\,2}}{S_{xo}^{\,2}}\right]^{\frac{1}{2}} = \frac{S_w}{S_{xo}} = MHI = \left[\frac{R_{xo}/R_t}{R_{mf}/R_w}\right]^{\frac{1}{2}} \qquad 5.19$$

The formation resistivity factor cancels out of the MHI relationship, therefore the MHI method does not require any values for formation porosity or the associated empirical empirical parameters, m, and a. It represents a petrophysical method that provides information on the presence and movability of hydrocarbons based on ratios of formation and saturating brine resistivity and the empirical parameter n (Equation 5.20).

$$MHI = \left[\frac{R_{xo}/R_t}{R_{mf}/R_w}\right]^{1/n} \qquad 5.20$$

Valid application of the MHI relationship depends on the presence of a normal invaded zone. If there is virtually no invasion in a formation, for instance in a shale or non-permeable, vuggy carbonate, then both the R_{xo} log and R_d logs would read the same formation rock-fluid condition, and hence, the same formation resistivity, where $[R_d \cong R_{xo}]$, whether the rock is wet or hydrocarbon saturated. There would be no mud filtrate in the pores investigated by the resistivity logs i.e. pore water would be all connate water. In theory, the non-invasion MHI relationship would actually be represented by Equation 5.21, which if substituted into Equation 5.20, yields a value of approximately one, and indicates there are no movable hydrocarbons in the reservoir.

This is what would be expected if there were no invasion in a wet or hydrocarbon saturated reservoir.

$$\left(R_{xo} \approx R_t\right) and \left(R_w \approx R_{mf}\right) \qquad 5.21$$

In fact, in the case of minimal invasion, using the relationships from Equation 5.21, the numerator in Equation 5.20 would be valid because logged R_d and R_{xo} curves would be of very similar value in a non-invaded formation, and the ratio in the numerator would be approximately 1.0. However, the denominator would not be valid if the assumed R_{mf} value is used in the calculated relationship, instead of an approximate R_w value; in that case, the value of the denominator would be much greater than 1.0.

For example, if $R_w = 0.05\Omega$-m and $R_{mf} = 0.15\Omega$-m, then the denominator of the overall MHI relationship will be $0.15/0.05 = 3.0$. If the ratio in the numerator of the overall MHI relationship is approximately 1.0 because the logged formation resistivity values are similar, then the overall MHI relationship will become approximately $(1/3)^{\frac{1}{n}} = 0.33^{\frac{1}{n}} = 0.33^{0.5} = 0.5745$. The result is an MHI value indicating hydrocarbon movability that is invalid because the assumption of mud filtrate in the pores of the logged lithology at the depth of investigation of the R_{xo} log is invalid. There would actually be very little mud filtrate in the flushed zone pores due to very limited invasion. An assumption of normal invasion, forced on conditions of minimal invasion, invalidates the numerator of the brine resistivity ratio in the denominator of the overall MHI relationship.

If, instead of no invasion, the reservoir were very deeply invaded, then the deep resistivity log would be measuring nearly the same rock-fluid conditions as the shallow resistivity log, and a condition analogous to that described in Equation 5.21 would occur, where $\left(R_t \approx R_{xo}\right) and \left(R_{mf} \approx R_w\right)$. If this condition is entered into Equation 5.20, it would indicate no moved hydrocarbons or a wet reservoir. However, if the assumed values of R_{mf} and R_w were entered into the denominator, the result would indicate moved

hydrocarbons, as it did in the shallow invasion assumption. Application of the MHI parameter to a deeply invaded wet reservoir could lead to erroneous results. It would not be possible to use the MHI relationship to determine if the reservoir is saturated with movable hydrocarbons that were uniformly swept by deep invasion or if the reservoir is wet.

As the difference between R_w and R_{mf} increases, the consequent apparant *MHI* value decreses and the apparent hydrocarbon movability in the permeable formation increases. The validity of the *MHI* indicator should be evaluated in the context of other petrophysical parameters that provide indications of shaliness or a predominance of secondary, non-interconnected porosity.

Analysis of movable hydrocarbons as an indicator of hydrocarbon presence and producibility is an important part of the multiple parameter approach to log analysis in Prue Sands in the deep Anadarko Basin. Were the method applied in reservoirs in other basins, such as highly porous Gulf Coast Tertiary sands, where invasion may be intrinsically shallow, hydrocarbon movability could be difficult to detect. In order to be effective, it is important to understand the rock-fluid mechanisms that underlie the petrophysical parameters prior to application of the multiple parameter approach. Alternate parameters or altered assumptions for the current parameters may be required as the method is used in different reservoirs with different petrophysical characteristics.

Relative Permeability to Gas

In this study, relative permeability in the reservoirs is evaluated in terms of a relative permeability ratio of water and gas. As the value of the ratio decreases below 1.0, the potential for movable hydrocarbons in the reservoir are interpreted to increase.

Pirson et al. (1963) recommended two relationships to describe two-phase flow of gas and liquid in a reservoir. These relationships were used to calculate values for relative permeability to gas and water in each Prue Sand reservoir evaluated in this study. The relationships are a function of calculated Archie water saturation in the reservoir as well as a value of calculated irreducible water saturation in the reservoir. As is shown

below in Equation 5.24, the irreducible water saturation values used in Equations 5.22 and 5.23 are not calculated as a function of the water saturation values used in the equations.

$$K_{rg} = \left[1.0 - \left(\frac{(S_w - S_{wirr})}{(1.0 - S_{wirr})}\right)\right] \times \left\{1.0 - \left[\frac{(S_w - S_{wirr})}{(1.0 - S_{wirr})}\right]^{\frac{1}{4}} \times (S_w)^{\frac{1}{2}}\right\}^{\frac{1}{2}} \qquad 5.22$$

$$k_{rw} = \left(\frac{R_o}{R_t}\right)^{\frac{3}{2}} \times \left(\frac{S_{wa} - S_{wirr}}{1 - S_{wirr}}\right)^{\frac{3}{2}} \qquad 5.23$$

There were no irreducible water saturation values available for the Prue reservoirs examined in this study. Asquith (1980, p. 76; and 1982, p. 142) provided a relationship that can be used to estimate irreducible water saturation in a reservoir.

$$S_{wirr} = \sqrt{\frac{F_R}{2000}} \qquad 5.24$$

The relationship is based on a grain size class assumed for the reservoir and the bulk volume water in the reservoir consequent to that assumption. Asquith (1982, p. 98, table 8) lists ranges of bulk volume water as a function of grain size in siliciclastic reservoirs or pore type in carbonate reservoirs that are at irreducible water saturation. Equation 5.24 was developed for clastic reservoirs of assumed coarse grain size, and was found to produce satisfactory results in the Rocky Mountains and the Anadarko Basin (Asquith, 1980, p. 76). Asquith indicates the constant in the relationship can vary from area to area. Development of the relationship in Equation 5.24 to estimate irreducible water saturation is reviewed in Appendix D.

As an example, if the reservoir under evaluation is more fine-grained than the assumed grain size, then actual irreducible water saturation will be higher than the value

calculated with this method. Consequently, the calculated relative permeability to gas will be less than 100% in the reservoir, even if the reservoir is at irreducible water saturation. However, in hydrocarbon productive reservoirs, the ratio of calculated values for [Water RelPerm/Gas RelPerm] will still be much less than 1.0, even in very fine grained reservoirs. Values of this ratio increasingly less than 1.0 are considered to represent reservoirs with increasingly greater potential to produce a water-free gas stream. Finally, any concern that the reservoir is not at irreducible water saturation can be evaluated through examination of other petrophysical parameters.

Evaluation of Water Saturation

Water saturation is one of the most critically important parameters in petrophysical analysis because it provides a direct indication of hydrocarbon saturation. Archie recognized that general application of the empirical relationships he developed for computing water saturation from electric log data required caution and an awareness of the properties of the rock-fluid system that affect the response of the electric logs. Any change in geologic facies from the Gulf Coast sands he studied would have an effect on the electrical properties of the formation, which could result in analysis that falls outside useful accuracy.

Archie was pointing out that it is necessary to evaluate calculated water saturation values developed from his empirical relationships in terms of the characteristics of a formation that affect the electrical properties of that formation. Archie's *caveat* can be approached two ways. First, in developing an approach to petrophysical analysis, the means to assess the water saturation values calculated using standard Archie parameters should be found. Second, the means to determine if the calculated Archie water saturation values can be explained in the context of depositional facies should be found.

Archie S_w

Water saturation values are calculated across each reservoir using density-neutron porosity and invasion-corrected deep resistivity in the Archie relationship as shown in Equation 5.21. Standard assumptions for the values of the Archie empirical parameters, a = 1.0 and $m = n = 2.0$ are used to complete the equation.

Water saturation as a petrophysical parameter is evaluated based on where individual saturation values fall within a range of water saturation values. Values that fall higher in the range are considered less likely to represent a producible accumulation of hydrocarbons than those values that fall lower in the range.

Patchett S_w

Patchett and Rausch (1967) examined a variety of cases of shaly sand analysis based on different sets of available input data, in Basins complicated by rapid vertical and lateral changes in water resistivity. The objective of their study was to develop an improved value of calculated water saturation in shaly sands by incorporating the SP log response into Archie's standard water saturation relationship. In this way, the effects of shaliness on SP development compensate for the effects of shaliness on resistivity data used in the water saturation calculation (Tixier et al., 1968). The method developed by Patchett and Rausch (Equation 5.25) was used in this study to calculate a value for water saturation that can be compared to the standard calculated Archie water saturation value. This theoretical relationship provides an opportunity to detect any effects of shaliness on Archie water saturation.

$$Sw_{Patchett} = \left[\left(\frac{F_R R_w}{R_t} \right) \left(\frac{R_{mf}}{R_{mf} - R_w} \right) \left(\frac{10^{(PSP/K)} - 1}{10^{(PSP/K)}} \right) \right]^{0.5} \qquad 5.25$$

The Patchett equation used in this study was examined further in several other sources, including Tixier et al. (1968, p. 19), Fertl and Hammack (1972, p. 15-16), Dresser Atlas (1982, p.181) and Hilchie (1982, p. VII-17). These references provide useful insights into development and application of the Patchett equation used in this study. Water saturation values calculated from Patchett were compared to Archie water saturation values based on a ratio of Patchett and standard Archie. The closer the ratio is to unity is considered an indication that the reservoir is cleaner, and shaliness has less effect on the Archie saturation values.

Ratio S_w

Ratio water saturation (S_{wr}) is a method developed by Tixier (1949) to calculate a value for S_w in low permeability sandstones in the Rocky Mountains. This was a time when the formation porosity data required in standard Archie was not readily available, therefore the Archie method for calculating S_w using the formation resistivity factor was often not an option. Like the movable hydrocarbon index, this method is based on a ratio of Archie water saturation in the uninvaded zone (S_{wa}) and the flushed zone (S_{xo}) or invaded zone (S_i), which eliminated the formation resistivity factor from the calculation.

The basic concept in S_w *Ratio* is that in a hydrocarbon-bearing reservoir, there is a distinction between water saturation in the invaded zone and the uninvaded zone. If there are hydrocarbons in a reservoir that falls within certain permeability constraints (Tixier, 1949), the hydrocarbons will be flushed by the invasion of mud filtrate. The effects of the process of invasion and flushing on hydrocarbon saturation produce consequent effects on water saturation in the flushed zone (Figures 5.9 and 5.11).

A generalized assumption on the degree of flushing can be made based on reservoir quality. In turn, this permits an assumption of the volumetric relationship between water saturation in the flushed or invaded zone (S_{xo} or S_i) and the uninvaded zone (S_w). Based on assumption, a valid relationship between formation resistivity values and saturating-fluid resistivity values in the invaded and uninvaded zones is expected. It is then possible, through mathematical substitution, to determine water saturation in the

uninvaded zone based entirely on ratios of formation resistivity and saturating fluid resistivity between the invaded and uninvaded zones.

If a value for S_{xo} or S_i is known or can be assumed in terms of S_{wa}, then, with substitution, the S_{wr} equation is reduced to just one unknown water saturation value. Two separate relationships have appeared in the literature to assuage this need. Tixier (1949) examined a suite of logs from productive sands in the Rocky Mountains and developed the relationship, $S_i = S_w^{1/2}$, and Schlumberger (1989, p. 8-7) reported a strictly empirical relationship, $S_{xo} = S_w^{1/5}$.

Equation 5.18 illustrates mathematical development of the ratio of Archie water saturation equations in the flushed and uninvaded zones, and Equation 5.26 mathematically summarizes the result. To develop the S_w *Ratio* relationship, begin by inserting the assumptions on invaded and uninvaded saturation noted above into the relationships for the flushed and invaded zones. Equation 5.27 represents the mathematical substitution involved using the $S_{xo} = S_w^{1/5}$ invasion assumption, and Equation 5.28 is the actual S_w *Ratio* equation that results from that assumption.

$$\left(\frac{S_w}{S_{xo}}\right)^2 = \frac{\frac{R_{xo}}{R_t}}{\frac{R_{mf}}{R_w}} \qquad 5.26$$

$$\frac{(S_w)^2}{\left(S_w^{1/5}\right)^2} = \frac{(S_w)^2}{(S_w)^{2/5}} = \frac{(S_w)^{10/5}}{(S_w)^{2/5}} = (S_w)^{8/5} = \frac{\frac{R_{xo}}{R_t}}{\frac{R_{mf}}{R_w}} = S_{wr} = \left(\frac{\frac{R_{xo}}{R_t}}{\frac{R_{mf}}{R_w}}\right)^{5/8} \qquad 5.27$$

Take the 5/8th root of each side of Equation 5.27 to get S_{wr}, which can be rewritten as Equation 5.28.

$$S_{wr} = \left(\frac{\left(\frac{R_{xo}}{R_t} \right)}{\left(\frac{R_{mf}}{R_w} \right)} \right)^{0.625} \qquad 5.28$$

Now assume: $S_i = S_w^{(1/2)}$. Equation 5.29 represents the ratio of Archie water saturation equations in the invaded and uninvaded zones. Equation 5.30 illustrates the mathematical relationships involved in the second invasion assumption, $S_i = S_w^{1/2}$ and Equation 5.31 is the S_{wr} equation based on that invasion assumption.

$$\left(\frac{S_w}{S_i} \right)^2 = \frac{\frac{R_i}{R_t}}{\frac{R_z}{R_w}} \qquad 5.29$$

$$\frac{(S_w)^2}{\left(S_w^{1/2}\right)^2} = \frac{\frac{R_i}{R_t}}{\frac{R_z}{R_w}} = \frac{S_w^{\,2}}{S_w} = S_{wr} \qquad 5.30$$

$$S_{wr} = \left[\left(\frac{R_i}{R_t} \right) \Big/ \left(\frac{R_z}{R_w} \right) \right] \qquad 5.31$$

If $S_w = 0.35$, then in the Tixier (1949) relationship, $S_i = 0.35^{1/2} = 0.592$ and in the Schlumberger, 1989a, relationship $S_{xo} = 0.35^{1/5} = 0.811$. The second relationship indicates greater flushing than the first, and, consequently, more movable hydrocarbons. In this study, S_{wr} calculations are based on a comparison of S_{wa} values to S_i values, and make use of both flushing assumptions noted above in Equations 5.28 and 5.31. Two S_{wr} values are therefore calculated at each data point and are labeled $S_{wr}(1/2)$ and $S_{wr}(1/5)$, respectively.

It is interesting to note that if water saturation in a reservoir is about 0.35, then the resulting invaded zone water saturation values are the same as those suggested by Schlumberger (1958) for different quality reservoirs, as cited above. Including the inference of reservoir quality in the S_{wr} investigation is what is intended in this study with the use of the two invasion assumptions. Ratio water saturation as a petrophysical parameter, is evaluated in the same way and in the same range that Archie water saturation values are evaluated.

Comparison of Archie and Ratio Water Saturation

Water saturation is an important parameter in petrophysical analysis. Similar calculated results from two methods that rely on different assumptions provide confidence in data, assumptions and results. Calculation of S_{wa} values requires a value for formation porosity and assumptions concerning values for the empirical parameters, m, n, and a. Calculation of S_{wr} values does not require formation porosity, nor the empirical parameters m and m, but does require an assumption concerning the volumetric relationship between water saturation in the invaded and uninvaded zones.

If calculated S_{wa} values fall within the range of values developed from the *Swr(1/2)* and *Swr(1/5)* relationships, it provides confidence in the calculated water saturation values. If calculated values for S_{wa} are less than $S_{wr}(1/2)$, or are greater than *Swr1/5*, then confidence in all calculated water saturation values should be suspect, and should direct the interpreter to inspect the input data and assumptions used in both Archie and Ratio water saturation calculations. When S_{wa} values are less than $S_{wr}(1/2)$ it could indicate that the value of the empirical parameter m used in the S_{wa} calculation (and not in S_{wr}) is too low, possibly because of vuggy porosity with very poor hydrocarbon movability. When S_{wa} values are greater than $S_{wr}(1/5)$, it could indicate that the value of the empirical parameter m used in the S_{wa} calculation is too high, possibly because of excess conductivity associated with shaliness or microporous grains in the reservoir. However, it also could indicate that the invasion assumptions used in the S_{wr} calculations (and not in S_{wa}) are not applicable in the reservoir being studied and the S_{wr} values are incorrect. The Archie-Ratio comparison promotes an examination of analytical parameters used and consideration of the petrophysical character of the rock-fluid system under study.

The [Archie/Ratio] comparison parameter is evaluated in terms of the relation of S_{wa} values to the range of S_{wr} values bracketed by $S_{wr}(1/5)$ and $S_{wr}(1/2)$. When S_{wa} falls within the range of S_{wr} values, that is interpreted positively as support for the validity of the water saturation calculations because two separate methods, dependent on different assumptions, arrive at very similar answers. However, for S_{wa} values that do fall within the range of Sw Ratio values, those that align more closely to *Swr (1/2)* values should be expected to exhibit less movability, and would be ranked lower than those S_{wa} values that align more closely to *Swr (1/5)* values, which would be expected to exhibit more favorable movability. When the S_{wa} values fall outside the range of S_{wr} values, it is interpreted as a lack of confidence in all the computed water saturation values, because one does not know which value is most representative of actual reservoir saturation conditions. The comparison requires the petrophysicist to evaluate the validity of the computed results, and, if necessary, to reexamine input data and assumptions used in each

method. The Archie-Ratio comparison addresses Archie's caveat that application of the empirical relationships he developed requires caution and an awareness of the petrophysical characteristics of the reservoir rock-fluid system, itself.

BVW: Bulk Volume Water

Porosity and water saturation are two of the most critical values determined from log analysis. However, porosity and water saturation alone are not adequate to specify whether productive hydrocarbons are present in a reservoir, so they must be characterized in terms of a relationship with expected fluid production.

Buckles (1965) was concerned about the accuracy of connate water saturation values used in volumetric reserve calculations for fields or pools he worked as a reservoir engineer at Imperial Oil in Canada. Commonly an average porosity for a field was determined and then an average S_w value was picked from a [Porosity - Water Saturation] correlation developed for the field. Buckles' concern was based on his realization that connate water saturation cannot be directly correlated to porosity. In a study of a series of uniform spherical grain packs with the same porosity but different particle sizes, irreducible water saturation was found to vary with particle size and surface area, despite constant porosity.

Buckles found that if he made a minor adjustment to a previously hand-drawn curve that had been fit through porosity and connate water saturation data for a field, it produced an equilateral hyperbola with an excellent representation of the data. In the form of a hyperbola, the product of porosity and water saturation, was a constant. Buckles called the constant the Bulk Volume Water (BVW) saturation and is represented mathematically below as Equation 5.32. BVW is essentially a porosity-normalized water saturation value.

$$BVW = \phi S_w \qquad 5.32$$

Having established that the term (ϕ S_w) is a constant, then in all ensuing volumetric calculations, hydrocarbon porosity could be readily determined by subtracting BVW values from total effective porosity. This value could be used with area and thickness information to quickly calculate volumetric reserves.

$$Hydrocarbo\ n\ Porosity = \phi \times (1 - S_w) = \phi - \phi\, S_w \qquad 5.33$$

Buckles minimized his concern about using a questionable *Sw* value picked from a faulty correlation to average porosity. Now the data could be fit to a hyperbolic representation of porosity and water saturation for a field (e.g., Buckles, 1965, figure 5, p. 46), and the BVW value determined.

Buckles' work was based on cores taken in wells drilled with oil-base mud. Morris and Biggs (1967) demonstrated that log-derived values of porosity and water saturation could be used the same way. They found that when plots of porosity and water saturation data calculated from well logs show increasing scatter about a hyperbolic trend, it reflected entering a transition zone in the reservoir, with increasingly greater water production. The increased scatter in BVW values indicates deviation from the constant value that represents the reservoir at irreducible water saturation. Asquith (1982, p. 107) used examples from the Ordovician Red River Formation to illustrate how increasing data scatter in [Porosity-Water Saturation] plots represents decreasing oil cuts in the production stream.

BVW_SD, Bulk Volume Water Standard Deviation Parameter

A petrophysical parameter, *BVW_SD*, has been used to assess if a reservoir is at irreducible water saturation by analyzing the amount of scatter in calculated BVW data. The calculated BVW data was filtered through a standard deviation screen developed through standard deviation scatter tests on a series of synthetic reservoirs shown in Appendix E. Reservoirs at irreducible water saturation exhibit essentially constant values of BVW. Therefore, increasing scatter in the BVW data, measured by the standard

deviation screen, *BVW_SD*, is considered to represent increasing risk to the reservoir's hydrocarbon productive capacity through increasing water cut.

BVW, Bulk Volume Water Parameter

A second petrophysical parameter, *BVW*, has been used to examine the range of actual calculated BVW values for a reservoir, as distinct from *BVW_SD*, which is purely a measure of the scatter in calculated BVW data. The calculated BVW values are grouped into ranges identified by Asquith (1982, table 8, p. 98), in reservoirs at irreducible water saturation. The groups of BVW values listed by Asquith represent a range of grain sizes in clastic rocks and pore types in carbonate rocks. As noted by Buckles (1965), irreducible water saturation is a function of grain size and grain surface area. Therefore, in a reservoir at irreducible water saturation, calculated BVW values can be used to estimate the sediment grain size or carbonate pore type.

If a reservoir at irreducible water saturation exhibits variable texture, such as grain size graded bedding or changes in pore geometry, or lithology breaks, the reservoir could still show moderate scatter in its BVW data, despite being at irreducible water saturation. On a Buckles-type BVW plot, the condition of textural variability at irreducible water saturation would be represented by a series of data clusters in which each cluster could be fairly represented by an individual hyperbolic trendline. For example, on Figure E.1, if a second data population were found to define a hyperbolic trend of about 0.045, between the two standard curves, 0.04 and 0.06, in addition to the existing trend between standard curves 0.06 and 0.08, it would indicate a reservoir at irreducible water saturation that is comprised of two separate grain size populations. However, if the plotted BVW data comprise a heterogeneous mix that can not be fairly represented by several distinct hyperbolic trendlines, the data is better explained by scatter due to deviation from irreducible water saturation rather than textural variability. An example of such scatter is illustrated on Figure E.5.

BVW Evaluation

Evaluation of BVW calculated for a reservoir should look for indications of minimal scatter using the *BVW_SD* parameter. If there is minimal scatter, it indicates the reservoir is at or near irreducible water saturation and should be expected to produce water-free hydrocarbons. The associated *BVW* parameter will provide an estimate of the grain size in the reservoir. Coarser grain size indicates better permeability for the same porosity.

If the *BVW_SD* parameter indicates moderate or high scatter in calculated BVW data, the indication is not necessarily a function of entering a transition zone. The distribution of the scatter can be assessed by examining the *BVW* parameter. If scatter is moderate to high, but is contained within one or two adjacent grain size groups, then the data may represent a texturally variable reservoir at irreducible water saturation. In that case, a follow-up plot is necessary to determine if the data can be represented by a series of individual hyperbolic trendlines.

If the *BVW_SD* parameter indicates high scatter, and the groups represented by the *BVW* parameter indicate the presence of a grain size distribution from shale to coarse grain size, it quite likely represents a reservoir that is not at irreducible water saturation and will not produce water-free hydrocarbons. A BVW plot of this type of reservoir should not be expected to produce a series of hyperbolically defined data clusters.

To assess BVW data in a depositional relationship, individual BVW values are multiplied by 1000 to get the BVW data to a common scale in which can it be plotted with standard log data. If BVW data is not constant, but the trends make depositional sense when plotted with depth, it could represent a texturally or lithologically variable reservoir at irreducible water saturation.

Analysis of Prue Reservoirs Exhibiting Excess Conductivity

Some Prue reservoir zones examined in this study exhibit the condition where resistivity porosity from the flushed zone, ϕ_{Rxoc}, and the invaded zone, ϕ_{Ri}, exceed total formation porosity. This represents the condition expressed in Equation 5.15, suggesting

the presence of excess conductivity in the Prue reservoir. As noted by Asquith et al. (1992), this condition can be associated with shaly reservoirs.

It was found in this study that the porosity excess separating ϕ_{Rxoc} and ϕ_{DN} in such Prue reservoirs could be significantly reduced if the value of the empirical parameter *m* was reduced through iterative testing in the petrophysical analysis spreadsheet. With an appropriately reduced value for the empirical parameter *m*, the ϕ_{Rxoc} curve was nearly equal to the ϕ_{DN} curve, and the compensating effect of the reduced *m* value had minimized the apparent excess conductivity.

Hilchie (1979, p. 11) stated that it was a common practice in the evaluation of shaly formations to compensate for shaliness by reducing the values of the parameters *m* and *n* from the standard value of 2.0. Hilchie provided a set of compensating values as an example.

Table 5.1 Hilchie Shale Volume Relationship to Empirical Parameters, *m*, *n*.

% Shale Volume	Empirical Parameter *m*	Empirical Parameter *n*
20	1.7	1.7
25	1.6	1.6
30	1.5	1.5

Tixier (1949, p. 145) described the *z* factor as the ratio of the volume of formation water to the volume of total pore water in the invaded zone, and the space occupied by formation water would be non-effective porosity while effective porosity would be saturated by mud filtrate. Furthermore, Tixier referred to core data in which the ratio of non-effective porosity to effective porosity was of the same order as the *z* factor.

The introduction of colloidal/clay particles into a clean formation would cause an increase in the ratio of non-effective porosity to total porosity. According to Tixier (Figure B.1), when the value of the *z* factor increases above 0.10, it represents a shaly reservoir. For example, if Ratio water saturation values were computed using a *z* factor

revised upward from 0.10 to reflect shaliness, it would yield *Swr* values that represent the water saturation in diminished effective porosity. In essence, the increase in the value of the *z* factor is a shaliness correction to the affected petrophysical parameters.

In this study, the value of the empirical parameter *m* was reduced to minimize an indicator of shaliness, apparent excess conductivity. The fractional amount of reduction in the empirical parameter *m* was added to the standard value of the *z* factor, 0.05, used in the Prue reservoirs examined in this study. For example, the fractional reduction in *m*, from 2.0 to 1.6, is 0.20, which, when added to 0.05, results in 0.25. As a percent, this value equals the same as the shale volume associated with $m = 1.6$ in the Hilchie Shale Volume table, 25%. It turns out that *z* values computed from this method are identical to the shale volumes listed as pairs with the empirical parameter *m* in the table from Hilchie (1979). The *z* factor exhibits values similar to the *q* shaliness parameter, also described as a relationship between effective and non-effective porosity in shaly sands (Asquith, 1991, p. 21).

Volume of shale is a difficult property to ascertain in these Prue granite wash sands. Therefore, in Prue reservoirs that exhibited the appearance of excess conductivity, the petrophysical data for the reservoir was reanalyzed using a reduced value for the parameter *m*, and a concomitantly increased value for the parameter *z*, developed as described above. The parameters that don't include R_z in their calculation, e.g. *PhiRes (Rxo)* and *Swa* values, will not be affected by a change in the *z* factor, but will respond to a reduction in the value of the empirical parameter *m*, which is a part of their calculation.

Petrophysical Analysis in Permian Basin Carbonates

In order to test the flexibility of the multiple parameter approach to petrophysical analysis developed in the Prue Sands, the method was tested on two carbonate reservoirs from the Permian Basin. Petrophysical analysis in carbonates presents different challenges than siliciclastic sands, and analysis of the Permian Basin carbonates will provide an opportunity to test the method in reservoirs with different petrophysical characteristics than granite wash sands.

Siliciclastic sediments are land-derived particles developed initially by weathering and erosion of pre-existing rocks in highland areas. The terrigenous detritus is then transported relatively long distances to a depositional basin. Carbonate sediments, on the other hand, are generally intrabasinal sediments produced near their site of deposition (Ham and Pray, 1962, p. 4; Dunham, 1962, p. 111). Initial development of carbonate sediments is generally a function of organic activity that varies with environmental habitat and geologic age. Consequently, there is a great diversity of carbonate grain types, shapes, sizes, and internal morphology, which can be further complicated by comminution of debris in skeletal deposits. An important addition to organic activity as the source of carbonate particles is inorganic carbonate accretions, such as oolites (Feray et al. 1962).

Carbonate minerals are generally more soluble than most siliciclastic minerals, and, therefore, are more susceptible to post-depositional alteration (Ham and Pray, 1962, p. 5). Furthermore, early in their depositional history, carbonate grains are also exposed to alteration that can be attributed to the biological-mechanical effects of organic activity extant in their depositional habitat.

The diversity of carbonate grains and their susceptibility to alteration generally leads to pore systems in carbonate reservoirs of greater complexity than the network of intergranular voids found in siliciclastic reservoirs. Choquette and Pray (1970, p. 222) identified fifteen basic pore types in carbonate rocks based on size, shape, genesis and position with respect to fabric elements in the rock. However, Lucia (1995, p. 1277, table 1) concluded that petrophysical characterization of carbonate pore systems could be accomplished through a two-fold system that encompasses most of the pore types recognized by Choquette and Pray. The Lucia system is comprised of interparticle porosity and non-interparticle porosity, called vuggy porosity, representing high interconnectivity and low interconnectivity, respectively. Lucia also explained that vuggy porosity must be subdivided into separate vugs and touching vugs. Asquith (1985, p. 29) demonstrated that intragranular microporosity can also exert significant influence on petrophysical analysis of carbonates.

Whether one considers fifteen pore types, or two pore types, the petrophysical characterization of carbonates requires an awareness of the complexity of pore genesis and geometry in carbonate reservoirs. With proper planning, logs can help to distinguish interconnected matrix porosity from isolated secondary porosity.

Permian Basin Carbonate Petrophysical Parameters

In the multiple parameter approach to log analysis in carbonates, two parameters from the analysis in Prue Sands relating to gas reservoirs and shaly reservoirs, *Gas Effect* and S*wPatchett*, respectively, have been replaced. Also, the relative permeability to gas parameter has been revised to relative permeability to oil for these Permian Basin carbonate reservoirs. The Pirson (1963) relative permeability to gas equations were replaced with two equations for relative permeability to water and oil developed by Park Jones and referenced in Morris and Biggs (1967, p. 20).

$$k_{rw} = \left(\frac{S_w - S_{wirr}}{1 - S_{wirr}} \right)^3 \qquad 5.34$$

$$k_{ro} = \left(\frac{0.9 - S_w}{0.9 - S_{wirr}} \right)^2 \qquad 5.35$$

Furthermore, the *BVW* parameter scores for carbonates are based on reservoir pore type groups (Asquith, 1982, table 8, p. 98) rather than sediment grain-size groups that were used in the Prue. Dorin et al. (1968), in studies of Devonian carbonate reservoirs in northwestern Alberta, provides actual field examples of pore type groups and associated BVW values similar to those defined by Asquith (1982). The remaining petrophysical parameters that were used in the analysis of the Prue were also used in the carbonate analysis. However, the range of values of some of the parameters developed for interpretation of Prue productivity had to be adjusted to fit the results from the carbonates.

Two new petrophysical parameters have been developed to replace *Gas Effect* and S*wPatchett*. The new parameters reflect the importance of recognizing the character of the porosity in petrophysical analysis in carbonates. A reservoir quality parameter, *Secondary Porosity*, has been used to replace *Gas Effect*, and a calculated water saturation value based on a variable *m*, *SwVar_m*, has been used to in place of S*wPatchett*.

Secondary Porosity

The petrophysical parameter *Secondary Porosity* is based on the nature of acoustic wave propagation in rocks. The acoustic waves of a sonic log propagate mainly through the matrix of a rock (Wang and Lucia, 1993, p. 2). Because a continuous path for acoustic energy exists through the rock matrix, acoustic waves can bypass and ignore isolated vugs, thereby transiting a vuggy carbonate rock more quickly than if the total porosity were all in the matrix (Schlumberger, 1974, p. 23). Therefore, the velocity of the acoustic waves in vuggy carbonate formations depends primarily on the amount of intergranular porosity in the matrix, and computed sonic porosity will be too low in vuggy carbonates (Schlumberger, 1989a, p. 5-7).

The equation used to compute sonic porosity is the Wyllie time-average equation, shown below as Equation 5.36 (Asquith, 1982, p. 66). As Δt_{log} decreases through more rapid transit in vuggy carbonates, ϕ_{sonic} will likewise decrease.

$$\phi_{Sonic} = \frac{\Delta t_{log} - \Delta t_{ma}}{\Delta t_f - \Delta t_{ma}} \qquad 5.36$$

Nuclear emissions from the density and neutron logging tools respond to bulk properties of a sedimentary rock, and are not fabric selective; they respond to bulk volume porosity (Schlumberger, 1974, p. 23). The signal response of density and neutron tools therefore is a measure of total formation porosity, including both interparticle and

vuggy porosity. A ratio between sonic log porosity and total porosity from the density-neutron combination calculated using the root-mean square equation, provides a measure of isolated secondary porosity in a formation.

$$Secondary\ Porosity = \frac{\phi_{Sonic}}{\phi_{DN}} \qquad 5.37$$

As the value of the ratio of sonic porosity to total porosity decreases from 1.0, it indicates that the content of interconnected porosity has decreased and the content of vuggy porosity has increased. Wang and Lucia (1993, p. 10) state that the value of Archie's empirical parameter *m*, increases as the ratio of separate-vug porosity to total porosity increases because separate vugs contribute little to electrical conductivity through a carbonate pore system. Furthermore, the reservoir should also be expected to exhibit less effective fluid transmissibility properties, and consequently, less movable hydrocarbons as the content of isolated vuggy porosity increases.

Variable *m*

Adisoemarta et al. (2000) showed theoretically that the correlation of Archie's formation resistivity factor to porosity should be $F_R = a/\phi$; a value for the empirical parameter *m* is not theoretically required in the relationship. However, Adisoemarta et al. demonstrated that Archie's parameter *m* is required in the empirical relationship developed through resistivity measurements because of the relationship between pore throats and pore bodies. Pore throats control electrolytic conduction in a pore system while the information available to the interpreter from logs is formation porosity, a volumetric parameter controlled by the pore body. The empirical parameter *m* is a function of the ratio of pore body area to pore throat area in an electrically conductive pore system.

Adisoemarta et al. (2000) showed mathematically that an *m* of 2 represents the pore throat - pore body relationship found in a cubic packing arrangement of uniform

spheres, essentially an interparticle porosity configuration. As the ratio of pore body area to pore throat area increases, the value of *m* also increases (Adisoemarta et al., 2000, table 2). This is exactly what would be expected in a dual pore system consisting of interparticle porosity and isolated vug porosity. The interparticle porosity consists of average pore bodies regularly interconnected by average pore throats, however isolated vugs contribute significantly to pore body area in the formation but very little to the pore throat area. Consequently, isolated vugs cause the pore body area to pore throat area ratio in a formation to increase, which requires an increased value for Archie's empirical parameter *m* when considering the electrical nature of the pore system. Theory from Adisoemarta et al. (2000) matches observation from Wang and Lucia (1993).

The petrophysical character of carbonate porosity can vary stratigraphically and areally across a carbonate reservoir zone or between different carbonate reservoirs as the nature of the carbonate sediments and their alteration history change. Several different methods have been proposed to account for the effects of variable pore geometry on log response and the empirical parameter *m*. Asquith (1985, p. 7) cited the Nugent method to determine variable *m* in vuggy carbonates when the log package includes neutron and/or density logs and a sonic log.

$$m = \frac{2[Log(\phi_{Sonic})]}{Log\phi_{Total}} \qquad 5.38$$

According to Walsh et al. (1994, p. 292), when no sonic log is available in vuggy carbonates, a variable *m* relationship can still be applied using the method of Focke and Munn (1987). Focke and Munn developed a series of relationships for variable *m* in carbonates based on a study of core samples from wells drilled offshore Qatar, in the Persian Gulf. Vuggy limestones in the Focke and Munn study were represented by Rock Type 4 (Focke and Munn, 1987, p. 158), described as lime grainstones with well-developed vuggy porosity. Four different equations for Rock Type 4 were developed to include four different permeability groups referred to as Permeability Classes 1-4.

Two of the Rock Type 4 equations for variable *m* are illustrated below. Rock type 4, Permeability Class 2 (Equation 5.39) includes reservoirs with measured permeabilities from 0.1 to 1.0 md, and Rock Type 4, Permeability Class 3 (Equation 5.40) includes reservoirs with a permeability range from 1.0 to 100.0 md.

$$m = 1.4 + 0.0857\phi \qquad 5.39$$

$$m = 1.2 + 0.0829\phi \qquad 5.40$$

SwVar_m, Water Saturation Calculated Using Variable *m*

The standard value for the empirical parameter *m* used in routine petrophysical analysis is 2.0. The table below (modified from Core Lab, 1973, p. 6-26) is designed to illustrate the effects of different values for *m* on calculated water saturation, assuming R_t = 80 Ω-m and R_w = 0.08 Ω-m. The table illustrates that in changing the standard value of the empirical parameter *m* from 2.0 to 3.0, the calculated values of water saturation using the Archie method are about doubled at higher values of porosity, 0.20 - 0.30. At lower values of porosity, 0.10, calculated water saturation values triple with the value for *m* increased from 2.0 to 3.0.

Table 5.2 The Effect of Variable *m* on Calculated Water Saturation Values.

Calculated Water Saturation Assuming Empirical Parameter *n* = 2.0					
	m = 2.0		*m* = 3.0		
Porosity	F_R	S_w	F_R	S_w	ΔS_w
0.30	11	0.10	37	0.19	0.09
0.20	25	0.16	125	0.35	0.19
0.10	100	0.32	1000	1.00	0.68

The value chosen for *m* can have a significant effect on water saturation calculated using the Archie method, and hence, the value chosen for *m* can also have a significant effect on the potential value assigned to a carbonate reservoir under investigation. Therefore, in the multiple parameter approach to petrophysical analysis in carbonates, two Archie water saturation parameters are used. The standard value of Archie S_w using $m = 2.0$, *Swa*, and a water saturation value calculated based on variable *m* determined using the Nugent or Focke and Munn methods, *SwVar_m*, are both included in the analysis. There are other methods to evaluate variable *m* reviewed in Wang and Lucia (1993) and Asquith (1995).

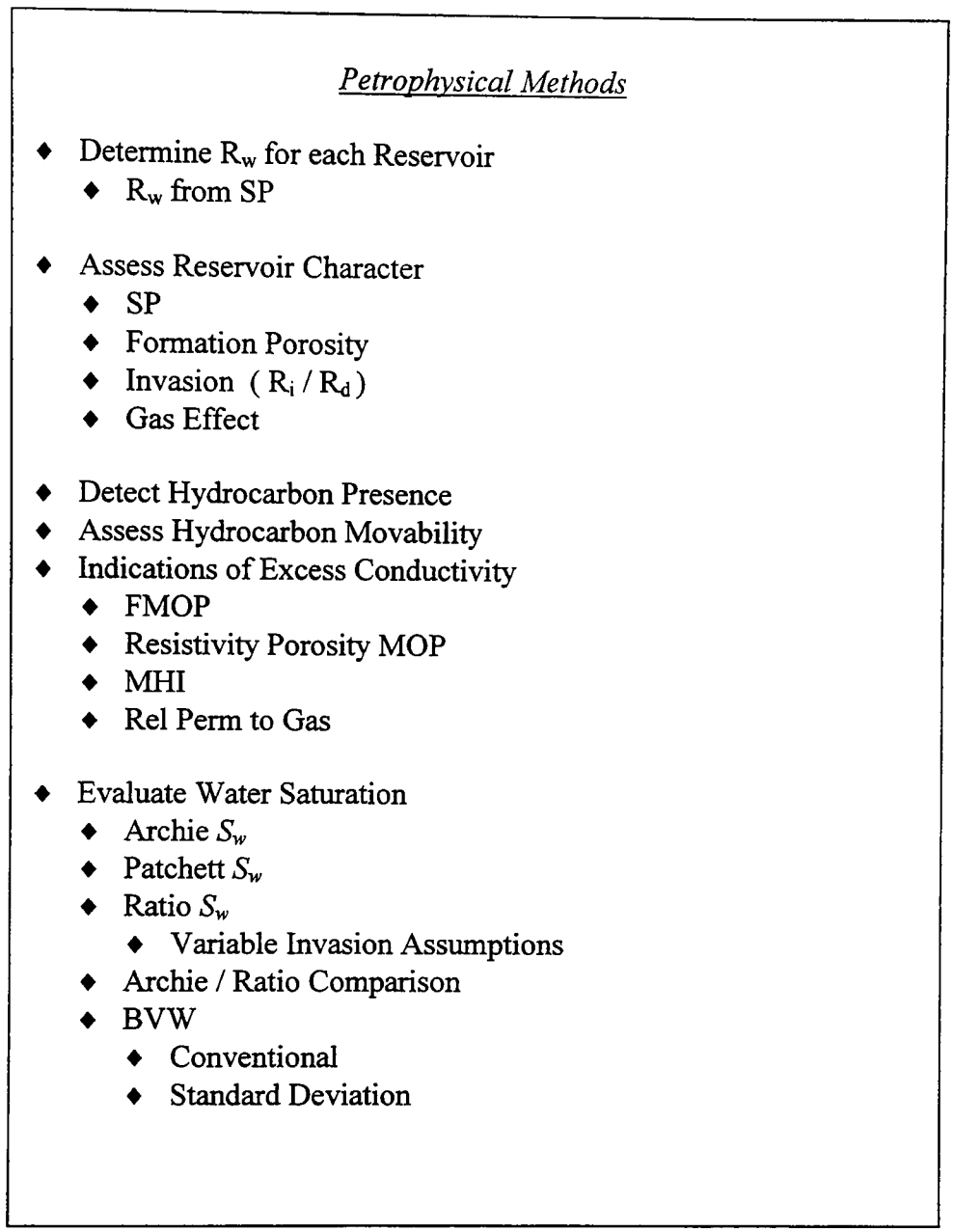

Figure 5.1 Petrophysical Methods used in the Analysis and Interpretation of the Hydrocarbon Potential of the Prue Sands.

Relationship of Apparent Formation Resistivity Factor to Empirical Formation Resistivity Factor and Water Saturation

$$S_w^{-n} = \frac{R_t}{R_o} \Rightarrow \frac{1}{S_w^n} = \frac{R_t}{R_o}$$

$$F_R = \frac{R_o}{R_w} \Rightarrow R_o = F_R R_w$$

Assume Archie Empirical Parameter $n = 2.0$

$$\frac{1}{S_w^2} = \frac{R_t}{F_R R_w} \Rightarrow \frac{F_R}{S_w^2} = \frac{R_t}{R_w} = F_{Rd}$$

$$F_{Rd} = \frac{R_d}{R_w} = \frac{F_R}{S_w^2} \Rightarrow S_w^2 = \frac{F_R}{F_{Rd}}$$

Rxo Analog to Above Derivation

$$F_{Rxo} = \frac{R_{xo}}{R_{mf}} = \frac{F_R}{S_{xo}^2} \Rightarrow S_{xo}^2 = \frac{F_R}{F_{Rxo}}$$

Figure 5.2 Development of the Relationship of the Empirical and Apparent Formation Resistivity Factors to Water Saturation.

FMOP Relates to MHI

$$F_R = \frac{R_o}{R_w} = \frac{a}{\phi^m} = F_{DN}$$

$$F_{Rd} = \frac{R_{Deep}}{R_w} = \frac{F_R}{S_w^2} \Rightarrow S_w^2 = \frac{F_R}{F_{Rd}}$$

$$F_{Rxo} = \frac{R_{xo}}{R_{mf}} = \frac{F_R}{S_{xo}^2} \Rightarrow S_{xo}^2 = \frac{F_R}{F_{Rxo}}$$

$$\frac{S_w^2}{S_{xo}^2} = \frac{F_R / F_{Rd}}{F_R / F_{Rxo}} = \frac{F_{Rxo}}{F_{Rd}} \Rightarrow \frac{S_w}{S_{xo}} = \left(\frac{F_{Rxo}}{F_{Rd}}\right)^{\frac{1}{2}}$$

$$\frac{S_w^2}{S_{xo}^2} = \frac{F_R / F_{Rd}}{F_R / F_{Rxo}} = [MHI]^2 \Rightarrow MHI = \left[\frac{F_R / F_{Rd}}{F_R / F_{Rxo}}\right]^{1/2} = \left[\frac{F_{Rxo}}{F_{Rd}}\right]^{1/2}$$

Figure 5.3 Development of the Relationship of the Elements of the FMOP to MHI.

Resistivity Porosity Relates to MHI

$$S_{xo} = \left(\frac{F_R \times R_{mf}}{R_{xo}} \right)^{\frac{1}{n}}$$

$$S_{xo} = \left(\frac{1}{\phi^m} \times \frac{aR_{mf}}{R_{xo}} \right)^{\frac{1}{n}} = \left[\left(\left(\frac{1}{\phi^m} \right)^{1/n} \right) \left(\left(\frac{aR_{mf}}{R_{xo}} \right)^{1/n} \right) \right]$$

$$\phi_{Rxo} = \left(\frac{a \times R_{mf}}{R_{xo}} \right)^{\frac{1}{m}}$$

When Archie Empirical Parameter $n = m$

$$S_{xo} = \frac{\phi_{Rxo}}{\phi} \qquad \frac{\phi_{Rxo}}{\phi_{Formation}} = S_{xo}$$

Sw Analog to Sxo

$$\frac{\phi_{Rd}}{\phi_{Formation}} = S_w$$

$$MHI = \frac{S_w}{S_{xo}} = \frac{\phi_{Rd} / \phi_{DN}}{\phi_{Rxo} / \phi_{DN}} = \frac{\phi_{Rd}}{\phi_{Rxo}}$$

Figure 5.4 Development of the Relationship of Resistivity Porosity to MHI.

CHAPTER VI
MULTIPLE PARAMETER APPROACH

General

The objective of the multiple parameter approach to petrophysical analysis and interpretation is to maximize the information extracted from a logging suite in order that the breadth of results can be calibrated against established production information. The goal of production-calibrated petrophysical analysis is to provide the means to make outcome-based decisions on reservoir value that reference a range of production potential.

Application of the multiple parameter approach in this study was intended to apply a variety of petrophysical methods that permit examination of reservoir quality, detection of movable hydrocarbons and evaluation of calculated water saturation values for the Prue. In order to develop a consistent, objective interpretation of the analyses in terms of a producible accumulation of hydrocarbons, it is necessary to extract the results of the analyses in such a way that it can be evaluated within a framework that relates analytical outcomes to potential hydrocarbon productivity. It is vitally important to be able to interpret the results calculated from all the methods, in terms of a producible accumulation of hydrocarbons in the Prue.

Rank the Petrophysical Parameters

If the results from the petrophysical analysis of a reservoir zone, e.g. water saturation calculations, are averaged in order to develop an interpretation, then details in water saturation trends across the reservoir can be lost to the interpretation. To address the issue of consistent, objective interpretation of analytical results without losing analytical detail, an alternative to averaging all the analytical results for a petrophysical parameter was needed.

Petrophysical data values were sampled every half-foot in the wellbore by the wireline logs, consequently an analytical data value was generated each half-foot across a

reservoir for each petrophysical parameter. A ranking system was developed in this study that is intended to examine each analytical result from each petrophysical parameter, at half-foot increments, through a series of logical arguments developed in Excel. A score is assigned to each result based on how each resultant value is interpreted to represent a producible accumulation of hydrocarbons (Frailey, personal communication). Instead of computing one average value for a petrophysical parameter in a reservoir, each separate result at half-foot increments was assigned a score. At the end of the analysis, each petrophysical parameter therefore included many scores to characterize a reservoir rather than a single average value.

Possible scores for the results from a petrophysical parameter range from *(5)* to *(1)*. A score of *(5)* indicates that analytical result provides a strong indication of a reservoir capable of water-free hydrocarbon production, at top rates. A score of *(1)* represents a reservoir least likely to produce water-free hydrocarbons because it is wet or tight. Two outlier scores, *(0)* and *(-1)* are also included in the ranking system. A score of *(0)* requires a second look at the analysis. Often it represents petrophysical characteristics that suggest the presence of excess conductivity or shaliness that can lead to an invalid interpretation, or it can simply represent very questionable hydrocarbon productive potential. A score of *(-1)* indicates the results fall outside a range that would normally be expected for the petrophysical parameter. It may indicate poor data quality that has been affected by poor hole conditions, or weak assumptions in the algorithms used in the method, or may simply represent incorrect data entry.

Table 6.1 is an example of the logical process in which analytical results from one particular petrophysical parameter, Movable Hydrocarbon Index (*MHI*), are grouped into a range of values considered to represent stronger to weaker hydrocarbon productive potential. When the value of the *MHI* ratio is about 1 (i.e., between 0.9 and 1.1), it indicates that the reservoir is either wet or is hydrocarbon bearing, but with absolutely no indication of moveable hydrocarbons (Schlumberger, 1989a, p. 8-7). As the value of the *MHI* ratio decreases from one, it indicates hydrocarbons are present in the reservoir with increasing movability. When the ratio is < 0.3, the values are considered to be "too good"

in the Prue, and the input calculations should be examined. If the ratio values are greater than 1.1, then no hydrocarbons can possibly have been moved, and it is ranked zero.

Tables 6.2 through 6.5 illustrate the logical process and ranks assigned to the range of analytical outcomes for the petrophysical parameters associated with assessing reservoir quality. Values for scores assigned to ranges of analytical outcomes were developed through examination of the petrophysical analyses completed on Prue Sands during this study (Asquith, personal communication).

Tables 6.6 through 6.15 illustrate the logical process and scores assigned to the range of analytical outcomes for the petrophysical parameters intended to detect the presence and movability of hydrocarbons, as well as provide indications of excess conductivity in the reservoir. The logical process included in Tables 6.8 and 6.9 is based on an assumption of excellent flushing conditions, while the process in Tables 6.10 and 6.11 is analogous to the FMOP, and based on a range of flushing conditions. Outcomes scores assigned to the range of values for the MHI parameter shown in Tables 6.12, 6.13 and 6.14 are based on limits provided by Asquith (1982, p. 97).

Tables 6.16 through 6.22 illustrate the logical process and assigned ranking for analytical outcomes from evaluation of water saturation values calculated for the Prue reservoirs examined in this study. The scores for the range of water saturation values are based on the petrophysical analysis of Prue Sands during this study. Scores for the BVW standard deviation parameter, Table 6.21, are based on the screens illustrated in Appendix E, while the range of values for the BVW parameter shown in Table 6.22 are based on Asquith (1982, Table 8, p. 98).

Relative Frequency of Scores

In the Prue Sands evaluated in this study, a score was generated for each analytical outcome of each petrophysical method at every half-foot data increment. Under this process, a large number of score values are generated for each petrophysical parameter across a reservoir. Computing a single average of all the scores is not desirable. If a reservoir includes zones of distinctly different quality, favorable and

unfavorable for hydrocarbon productivity, the distinction will be lost in the averaging, and the proper value of the reservoir will not be recognized.

To assess the productive value of the reservoir indicated by all the scored results from each method, it is necessary to determine the percent of individual scores in the overall score population for each method. To this end, a portion of the petrophysical analysis spreadsheet is designed to collect all the scores from each petrophysical parameter and to calculate the relative frequency value for each score in each parameter. The results are displayed in a chart that includes a series of relative frequency histograms, with one histogram generated for each petrophysical parameter.

The ranking method represents an Expert System approach to interpreting the results of petrophysical analysis. The ranking histograms are a quantitative summary of a complete petrophysical analysis. They provide an operator the means to rapidly and objectively assess the value of individual reservoir zones. As page-size summaries of a complete petrophysical analysis, they are suited to well file storage that would provide anyone reviewing the file a quick introduction to the nature and quality of the reservoirs in the well. In addition, petrophysical parameter charts and ranking histograms stored in the well file documenting uphole potential can significantly reduce reaction time to wellbore management questions when the original objective is depleted.

Calibrate to Production

In order to develop a ranking system to interpret analytical results from a suite of petrophysical methods, the range of analytical values and respective scores in each method must be calibrated against some established production results. The suite of petrophysical parameters described in the previous section has been applied in a group of wells that include Prue Sand intervals with a perforation and production test record available to the study. Final scores for a zone, from each petrophysical parameter applied are compared to initial potential (IP) or production test results for the zone to determine how well the ranked scores represent the known test results for the zone. The range of

initial potential groupings used to calibrate production test results is illustrated in Figure 6.1.

The wells best suited to the purpose of calibration to production are those wells that were tested in a single zone. When multiple zones are included in a test interval, with perforations across many tens of feet, it can be difficult to distinguish which zones (or subzones) contribute the bulk of the production. For effective calibration, it is vital that the petrophysical parameter scores effectively represent the production results. As multiple zones are included in a tested/abandoned or tested/produced interval, it becomes more difficult to ascertain how well the resulting population of scores represents the production results.

The intent of the production-calibrated ranking system of petrophysical interpretation developed in this study is to establish a working relationship in the Prue between log response and hydrocarbon productive potential. Application of a broad suite of petrophysical parameters rather than focusing on calculated water saturation provides the means to examine log response in terms of properties of a reservoir rock-fluid system that are characteristic of a producible accumulation of hydrocarbons. Using a ranked scoring system provides an understanding of the strengths and an awareness of the risks associated with those critical properties in each zone that is considered for testing. Zones that score predominantly 4s and 5s should be good test candidates. Zones that score predominantly 3s and 4s should be fair to good test candidates and those with 2s and 3s are risky test candidates. The quality and risk should vary within these groups depending on which actual single score is predominant in the zone's overall score. Zones with predominantly 0s, 1s and 2s should not be considered a viable test candidate.

Every operator should be an expert in calibrating his petrophysical interpretation to *expected* test results. The multiple parameter approach, using ranking histograms provides one way to do that.

Table 6.1 An Example of the Logical Process in which Analytical Outcomes from one Petrophysical Parameter, Movable Hydrocarbon Index (*MHI*), are Grouped into a Range of Values Considered to Represent Stronger to Weaker Hydrocarbon Productive Potential.

$MHI = [(R_i/R_t) / (R_{mf}/R_w)]^{0.5}$	
SCORE	RANGE OF VALUES OF ANALYTICAL OUTCOMES
-1	$MHI \leq 0.3$
5	$0.5 \geq MHI > 0.3$
4	$0.6 \geq MHI > 0.5$
3	$0.7 \geq MHI > 0.6$
2	$0.9 \geq MHI > 0.7$
1	$1.1 \geq MHI > 0.9$
0	$MHI\ (R_i) > 1.1$

Table 6.2 Range of Values of Analytical Outcomes and Associated Scores for the SP Normalization Factor.

$SP = SP_{PRUEZONE} / SP_{PRUEMAX}$	
SCORE	RANGE OF VALUES OF ANALYTICAL OUTCOMES
-1	$SP > 1.1$
5	$1.1 \geq SP > 0.9$
4	$0.9 \geq SP > 0.7$
3	$0.7 \geq SP > 0.5$
2	$0.5 \geq SP > 0.3$
1	$0.3 \geq SP > 0.1$
0	$SP \leq 0.1$

Table 6.3 Range of Values of Analytical Outcomes and Associated Scores for Formation Porosity.

$Phi_{DN} = [((Phi_D^2) + (Phi_N^2)) / 2]^{0.5}$	
SCORE	RANGE OF VALUES OF ANALYTICAL OUTCOMES
-1	$Phi_{DN} > 0.25$
5	$0.25 \geq Phi_{DN} > 0.18$
4	$0.18 \geq Phi_{DN} > 0.15$
3	$0.15 \geq Phi_{DN} > 0.10$
2	$0.10 \geq Phi_{DN} > 0.07$
1	$0.07 \geq Phi_{DN} > 0.04$
0	$Phi_{DN} \leq 0.04$

Table 6.4 Range of Values of Analytical Outcomes and Associated Scores for the Invasion Profile Factor.

Invasion Profile Factor = R_i / R_d	
SCORE	RANGE OF VALUES OF ANALYTICAL OUTCOMES
-1	$(R_i/ R_d) \geq 2.7$
5	$2.7 > (R_i/ R_d) \geq 2.3$
4	$2.3 > (R_i/ R_d) \geq 1.9$
3	$1.9 > (R_i/ R_d) \geq 1.5$
2	$1.5 > (R_i/ R_d) \geq 1.1$
1	$1.1 > (R_i/ R_d) \geq 0.9$
0	$(R_i/ R_d) < 0.9$

Table 6.5 Range of Values of Analytical Outcomes and Associated Scores for the Density – Neutron Porosity Separation Parameter to Demonstrate Gas Effect.

Gas Effect = DensityPhi - NeutronPhi	
SCORE	RANGE OF VALUES OF ANALYTICAL OUTCOMES
-1	(GE) > 20.0
5	20.0 ≥ (GE) > 10.0
4	10.0 ≥ (GE) > 7.0
3	7.0 ≥ (GE) > 4.0
2	4.0 ≥ (GE) > 1.0
1	1.0 ≥ (GE) > -1.0
0	(GE) ≤ -1.0

Table 6.6 Range of Values of Analytical Outcomes and Associated Scores for the FMOP_Rxoc Parameter to Demonstrate the Presence and Movability of Hydrocarbons and to Assess the Presence of Excess Conductivity.

FMOP_R_{xoc} [= FMOP as {F(DN) : F(R_{xoc}) : F(R_d)}]	
SCORE	RANGE OF VALUES OF ANALYTICAL OUTCOMES
-1	All Else
5	$F_{DN}/F_{Rxoc} \leq 1.1$; $F_{DN}/F_{Rd} \leq 0.9$; $0.25 \geq F_{Rxoc}/F_{Rd} > 0.09$
4	$F_{DN}/F_{Rxoc} \leq 1.1$; $F_{DN}/F_{Rd} \leq 0.9$; $0.36 \geq F_{Rxoc}/F_{Rd} > 0.25$
3	$F_{DN}/F_{Rxoc} \leq 1.1$; $F_{DN}/F_{Rd} \leq 0.9$; $0.49 \geq F_{Rxoc}/F_{Rd} > 0.36$
2	$F_{DN}/F_{Rxoc} \leq 1.1$; $F_{DN}/F_{Rd} \leq 0.9$; $0.9 \geq F_{Rxoc}/F_{Rd} > 0.49$
1	$1.1 \geq F_{DN}/F_{Rxoc} > 0.9$; $1.1 \geq F_{DN}/F_{Rd} > 0.9$
0	$(F_{DN}/F_{Rxoc}) > 1.1$

Table 6.7 Range of Values of Analytical Outcomes and Associated Scores for the FMOP_Ri Parameter to Demonstrate the Presence and Movability of Hydrocarbons and to Assess the Presence of Excess Conductivity.

FMOP_R_i [= FMOP as {F(DN) : F(R_i) : F(R_d)}]	
SCORE	RANGE OF VALUES OF ANALYTICAL OUTCOMES
-1	All Else
5	$F_{DN}/F_{Ri} \leq 1.1$; $F_{DN}/F_{Rd} \leq 0.9$; $0.25 \geq F_{Ri}/F_{Rd} > 0.09$
4	$F_{DN}/F_{Ri} \leq 1.1$; $F_{DN}/F_{Rd} \leq 0.9$; $0.36 \geq F_{Ri}/F_{Rd} > 0.25$
3	$F_{DN}/F_{Ri} \leq 1.1$; $F_{DN}/F_{Rd} \leq 0.9$; $0.49 \geq F_{Ri}/F_{Rd} > 0.36$
2	$F_{DN}/F_{Ri} \leq 1.1$; $F_{DN}/F_{Rd} \leq 0.9$; $0.9 \geq F_{Ri}/F_{Rd} > 0.49$
1	$1.1 \geq F_{DN}/F_{Ri} > 0.9$; $1.1 \geq F_{DN}/F_{Rd} > 0.9$
0	$(F_{DN}/F_{Ri}) > 1.1$

Table 6.8 Range of Values of Analytical Outcomes and Associated Scores for the PhiRes(*Rxoc*) Parameter to Demonstrate the Presence and Movability of Hydrocarbons and to assess the presence of Excess Conductivity.

PhiRes(R_{xoc}) [= PhiResMOP as {Phi(DN) : Phi(R_{xoc}) : Phi(R_d)}]	
SCORE	RANGE OF VALUES OF ANALYTICAL OUTCOMES
-1	All Else
5	$1.1 \geq Phi_{Rxoc}/Phi_{DN} > 0.9$; $0.5 \geq Phi_{Rd}/Phi_{DN} > 0.3$
4	$1.1 \geq Phi_{Rxoc}/Phi_{DN} > 0.9$; $0.7 \geq Phi_{Rd}/Phi_{DN} > 0.5$
3	$1.1 \geq Phi_{Rxoc}/Phi_{DN} > 0.9$; $0.9 \geq Phi_{Rd}/Phi_{DN} > 0.7$
2	$Phi_{Rxoc}/Phi_{DN} \leq 0.9$; $Phi_{Rd}/Phi_{DN} \leq 0.9$; $1.1 \geq Phi_{Rd}/Phi_{Rxoc} > 0.9$
1	$1.1 \geq Phi_{Rxoc}/Phi_{DN} > 0.9$; $1.1 \geq Phi_{Rd}/Phi_{DN} > 0.9$
0	$Phi_{Rxoc}/Phi_{DN} > 1.1$; $1.1 \geq Phi_{Rd}/Phi_{DN} > 0.9$

Table 6.9 Range of Values of Analytical Outcomes and Associated Scores for the PhiRes(R_i) Parameter to Demonstrate the Presence and Movability of Hydrocarbons and to Assess the Presence of Excess Conductivity.

PhiRes(R_i) [= PhiResMOP as {Phi(DN) : Phi(R_i) : Phi(R_d)}]	
SCORE	RANGE OF VALUES OF ANALYTICAL OUTCOMES
-1	All Else
5	$1.1 \geq Phi_{Ri}/Phi_{DN} > 0.9$; $0.5 \geq Phi_{Rd}/Phi_{DN} > 0.3$
4	$1.1 \geq Phi_{Ri}/Phi_{DN} > 0.9$; $0.7 \geq Phi_{Rd}/Phi_{DN} > 0.5$
3	$1.1 \geq Phi_{Ri}/Phi_{DN} > 0.9$; $0.9 \geq Phi_{Rd}/Phi_{DN} > 0.7$
2	$Phi_{Ri}/Phi_{DN} \leq 0.9$; $Phi_{Rd}/Phi_{DN} \leq 0.9$; $1.1 \geq Phi_{Rd}/Phi_{Ri} > 0.9$
1	$1.1 \geq Phi_{Ri}/Phi_{DN} > 0.9$; $1.1 \geq Phi_{Rd}/Phi_{DN} > 0.9$
0	$Phi_{Ri}/Phi_{DN} > 1.1$; $1.1 \geq Phi_{Rd}/Phi_{DN} > 0.9$

Table 6.10 Range of Values of Analytical Outcomes and Associated Scores for the PhiResA(R_{xoc}) Parameter to Demonstrate the Presence and Moveability of Hydrocarbons and to Assess the Presence of Excess Conductivity.

PhiResA(R_{xoc}) [= PhiResMOP as {Phi(DN) : Phi(R_{xoc}) : Phi(R_d)}]	
SCORE	RANGE OF VALUES OF ANALYTICAL OUTCOMES
-1	All Else
5	$Phi_{Rxoc}/Phi_{DN} \leq 1.1$; $Phi_{Rd}/Phi_{DN} \leq 0.9$; $0.5 \geq Phi_{Rd}/Phi_{Rxoc} > 0.3$
4	$Phi_{Rxoc}/Phi_{DN} \leq 1.1$; $Phi_{Rd}/Phi_{DN} \leq 0.9$; $0.6 \geq Phi_{Rd}/Phi_{Rxoc} > 0.5$
3	$Phi_{Rxoc}/Phi_{DN} \leq 1.1$; $Phi_{Rd}/Phi_{DN} \leq 0.9$; $0.7 \geq Phi_{Rd}/Phi_{Rxoc} > 0.6$
2	$Phi_{Rxoc}/Phi_{DN} \leq 1.1$; $Phi_{Rd}/Phi_{DN} \leq 0.9$; $0.9 \geq Phi_{Rd}/Phi_{Rxoc} > 0.7$
1	$1.1 \geq Phi_{Rxoc}/Phi_{DN} > 0.9$; $1.1 \geq Phi_{Rd}/Phi_{DN} > 0.9$
0	$Phi_{Rxoc}/Phi_{DN} > 1.1$

Table 6.11 Range of Values of Analytical Outcomes and Associated Scores for the PhiResA(R_i) Parameter to Demonstrate the Presence and Movability of Hydrocarbons and to Assess the Presence of Excess Conductivity.

PhiResA(R_i) [= PhiResMOP as {Phi(DN) : Phi(R_i) : Phi(R_d)}]	
SCORE	RANGE OF VALUES OF ANALYTICAL OUTCOMES
-1	All Else
5	$Phi_{Ri}/Phi_{DN} \leq 1.1$; $Phi_{Rd}/Phi_{DN} \leq 0.9$; $0.5 \geq Phi_{Rd}/Phi_{Ri} > 0.3$
4	$Phi_{Ri}/Phi_{DN} \leq 1.1$; $Phi_{Rd}/Phi_{DN} \leq 0.9$; $0.6 \geq Phi_{Rd}/Phi_{Ri} > 0.5$
3	$Phi_{Ri}/Phi_{DN} \leq 1.1$; $Phi_{Rd}/Phi_{DN} \leq 0.9$; $0.7 \geq Phi_{Rd}/Phi_{Ri} > 0.6$
2	$Phi_{Ri}/Phi_{DN} \leq 1.1$; $Phi_{Rd}/Phi_{DN} \leq 0.9$; $0.9 \geq Phi_{Rd}/Phi_{Ri} > 0.7$
1	$1.1 \geq Phi_{Ri}/Phi_{DN} > 0.9$; $1.1 \geq Phi_{Rd}/Phi_{DN} > 0.9$
0	$Phi_{Ri}/Phi_{DN} > 1.1$

Table 6.12 Range of Values of Analytical Outcomes and Associated Scores for the MHI(R_i) Parameter to Identify Hydrocarbon Presence and Movability based on the Ratio between Water Saturation Values in the Invaded and Uninvaded Zones. The Formation Resistivity Factor is Cancelled-Out of the Relationship. As ratio decreases, S_{xo} increases relative to S_{wa}, indicating Increasingly Flushed Hydrocarbons.

$MHI(R_i) = [(R_i/R_t) / (R_z/R_w)]^{0.5}$	
SCORE	RANGE OF VALUES OF ANALYTICAL OUTCOMES
-1	$MHI (R_{ij}) \leq 0.3$
5	$0.5 \geq MHI (R_i) > 0.3$
4	$0.6 \geq MHI (R_i) > 0.5$
3	$0.7 \geq MHI (R_i) > 0.6$
2	$0.9 \geq MHI (R_i) > 0.7$
1	$1.1 \geq MHI (R_i) > 0.9$
0	$MHI (R_i) > 1.1$

Table 6.13 Range of Values of Analytical Outcomes and Associated Scores for the MHI (R_{xoc}) Parameter to Identify Hydrocarbon Presence and Movability based on the Ratio between Water Saturation Values in the Invaded and Uninvaded Zones. The Formation Resistivity Factor is Cancelled-Out of the Relationship. As the Ratio Decreases, S_{xo} Increases Relative to S_{wa}, Indicating Increasingly Flushed Hydrocarbons.

$MHI(R_{xoc}) = [(R_{xoc}/R_t) / (R_{mf}/R_w)]^{0.5}$	
SCORE	RANGE OF VALUES OF ANALYTICAL OUTCOMES
-1	$MHI (R_{xoc}) \leq 0.3$
5	$0.5 \geq MHI (R_{xoc}) > 0.3$
4	$0.6 \geq MHI (R_{xoc}) > 0.5$
3	$0.7 \geq MHI (R_{xoc}) > 0.6$
2	$0.9 \geq MHI (R_{xoc}) > 0.7$
1	$1.1 \geq MHI (R_{xoc}) > 0.9$
0	$MHI (R_{xoc}) > 1.1$

Table 6.14 Range of Values of Analytical Outcomes and Associated Scores for the MHI (SP) Parameter to Identify Hydrocarbon Presence and Movability based on the Ratio between Water Saturation Values in the Invaded and Uninvaded Zones. The Formation Resistivity Factor is Cancelled-Out of the Relationship. As the Ratio decreases, S_{xo} increases relative to S_{wa}, indicating increasingly flushed Hydrocarbons.

MHI(SP) $= [(R_{xoc}/R_t) / (R_{mf}/R_w (SP))]^{0.5}$	
SCORE	RANGE OF VALUES OF ANALYTICAL OUTCOMES
-1	MHI (SP) ≤ 0.3
5	$0.5 \geq$ MHI (SP) > 0.3
4	$0.6 \geq$ MHI (SP) > 0.5
3	$0.7 \geq$ MHI (SP) > 0.6
2	$0.9 \geq$ MHI (SP) > 0.7
1	$1.1 \geq$ MHI (SP) > 0.9
0	MHI (SP) > 1.1

Table 6.15 Range of Values of Analytical Outcomes and Associated Scores for the (krw/krg) Parameter to Demonstrate the Presence and Movability of Hydrocarbons. Relative Permeability to Gas and Water is used to Assess the Expected Produced Fluid as S_{wa} Approaches S_{wirr}, krg Approaches 100% and krw Approaches 0%.

Kr [= Relative Permeability to Gas Indicator using (krw/krg) Ratio]	
SCORE	RANGE OF VALUES OF ANALYTICAL OUTCOMES
-1	[krw / krg] ≤ 0.001
5	$0.1 \geq$ [krw / krg] > 0.001
4	$0.3 \geq$ [krw / krg] > 0.1
3	$0.6 \geq$ [krw / krg] > 0.3
2	$0.9 \geq$ [krw / krg] > 0.6
1	$1.1 \geq$ [krw / krg] > 0.9
0	krg = 0; [krw / krg] > 1.1

Table 6.16 Range of Values of Analytical Outcomes and Associated Scores for the Archie Water Saturation Parameter, S_{wa}, to Evaluate the Calculated Water Saturation Value for the Reservoir.

S_{wa} [= Archie Water Saturation]	
SCORE	RANGE OF VALUES OF ANALYTICAL OUTCOMES
-1	$S_{wa} \leq 0.20$
5	$0.45 \geq S_{wa} > 0.20$
4	$0.55 \geq Swa > 0.45$
3	$0.65 \geq S_{wa} > 0.55$
2	$0.9 \geq S_{wa} > 0.65$
1	$1.1 \geq S_{wa} > 0.9$
0	$S_{wa} > 1.1$

Table 6.17 Range of Values of Analytical Outcomes and Associated Scores for the [Sw_a / $Sw_{Patchett}$] Parameter to Evaluate the Calculated Water Saturation Value for the Reservoir.

Swpat = [Sw_a / $Sw_{Patchett}$]	
SCORE	RANGE OF VALUES OF ANALYTICAL OUTCOMES
-1	[Sw_a / $Sw_{Patchett}$] < 0.9
5	0.9 ≤ [Sw_a / $Sw_{Patchett}$] < 1.1
4	1.1 ≤ [Sw_a / $Sw_{Patchett}$] < 1.2
3	1.2 ≤ [Sw_a / $Sw_{Patchett}$] < 1.3
2	1.3 ≤ [Sw_a / $Sw_{Patchett}$] < 1.5
1	1.5 ≤ [Sw_a / $Sw_{Patchett}$] < 2.0
0	[Sw_a / $Sw_{Patchett}$] ≥ 2.0

Table 6.18 Range of Values of Analytical Outcomes and Associated Scores for the $S_{wr}1/2$ Parameter to Evaluate the Calculated Water Saturation Value for the Reservoir.

Swr1/2 [= Ratio Water Saturation using ($S_i = S_{wa}^{0.5}$) Assumption]	
SCORE	RANGE OF VALUES OF ANALYTICAL OUTCOMES
-1	Swr1/2 ≤ 0.20
5	0.45 ≥ Swr1/2 > 0.20
4	0.55 ≥ Swr1/2 > 0.45
3	0.65 ≥ Swr1/2 > 0.55
2	0.9 ≥ Swr1/2 > 0.65
1	1.1 ≥ Swr1/2 > 0.9
0	Swr1/2 > 1.1

Table 6.19 Range of Values of Analytical Outcomes and Associated Scores for the $S_{wr}1/5$ Parameter to Evaluate the Calculated Water Saturation Value for the Reservoir.

$S_{wr}1/5$ [= Ratio Water Saturation using ($S_i = S_{wa}^{0.2}$) Assumption]	
SCORE	RANGE OF VALUES OF ANALYTICAL OUTCOMES
-1	$S_{wr}1/5 \leq= 0.20$
5	$0.45 \geq S_{wr}1/5 > 0.20$
4	$0.55 \geq S_{wr}1/5 > 0.45$
3	$0.65 \geq S_{wr}1/5 > 0.55$
2	$0.9 \geq S_{wr}1/5 > 0.65$
1	$1.1 \geq S_{wr}1/5 > 0.9$
0	$S_{wr}1/5 > 1.1$

Table 6.20 Range of Values of Analytical Outcomes and Associated Scores for the S_{wa}:S_{wr} Limits Parameter to Evaluate the Calculated Water Saturation Value for the Reservoir.

S_{wr} : S_{wa} [= (Ratio / Archie) Consistency Comparison]	
SCORE	RANGE OF VALUES OF ANALYTICAL OUTCOMES
-1	$[(S_{wr}1/5\text{-}S_{wa}) / (S_{wr}\{1/5\text{-}1/2\})] > 1.15$
5	$0.1 \geq [(S_{wr}1/5\text{-}S_{wa}) / (S_{wr}\{1/5\text{-}1/2\})] > -0.15$
4	$0.25 \geq [(S_{wr}1/5\text{-}S_{wa}) / (S_{wr}\{1/5\text{-}1/2\})] > 0.1$
3	$0.65 \geq [(S_{wr}1/5\text{-}S_{wa}) / (S_{wr}\{1/5\text{-}1/2\})] > 0.25$
2	$0.95 \geq [(S_{wr}1/5\text{-}S_{wa}) / (S_{wr}\{1/5\text{-}1/2\})] > 0.65$
1	$1.15 \geq [(S_{wr}1/5\text{-}S_{wa}) / (S_{wr}\{1/5\text{-}1/2\})] > 0.95$
0	$[(S_{wr}1/5\text{-}S_{wa}) / (S_{wr}\{1/5\text{-}1/2\})] \leq -0.15$

Table 6.21 Range of Values of Analytical Outcomes and Associated Scores for the BVW (Standard Deviation) Parameter to Evaluate the Calculated Water Saturation Value for the Reservoir.

BVW_SD [= BVW Data Scatter from Standard Deviation Screen]	
SCORE	RANGE OF VALUES OF ANALYTICAL OUTCOMES
-1	BVW_SD ≤ 0.00025
5	0.0025 ≥ BVW_SD > 0.00025
4	0.005 ≥ BVW_SD > 0.0025
3	0.008 ≥ BVW_SD > 0.005
2	0.01 ≥ BVW_SD > 0.008
1	0.015 ≥ BVW_SD > 0.01
0	BVW_SD > 0.015

Table 6.22 Range of Values of Analytical Outcomes and Associated Scores for the BVW Parameter to Evaluate the Calculated Water Saturation Value for the Reservoir.

BVW [= Grain Size Group Assuming Reservoir @ Swirr]	
SCORE	RANGE OF VALUES OF ANALYTICAL OUTCOMES
-1	BVW < 0.020
5	0.020 ≤ BVW_Cgr < 0.025
4	0.025 ≤ BVW_Mgr < 0.035
3	0.035 ≤ BVW_Fgr < 0.050
2	0.050 ≤ BVW_Vfgr < 0.070
1	0.070 ≤ BVW_Silty < 0.090
0	BVW_Shaly ≥ 0.090

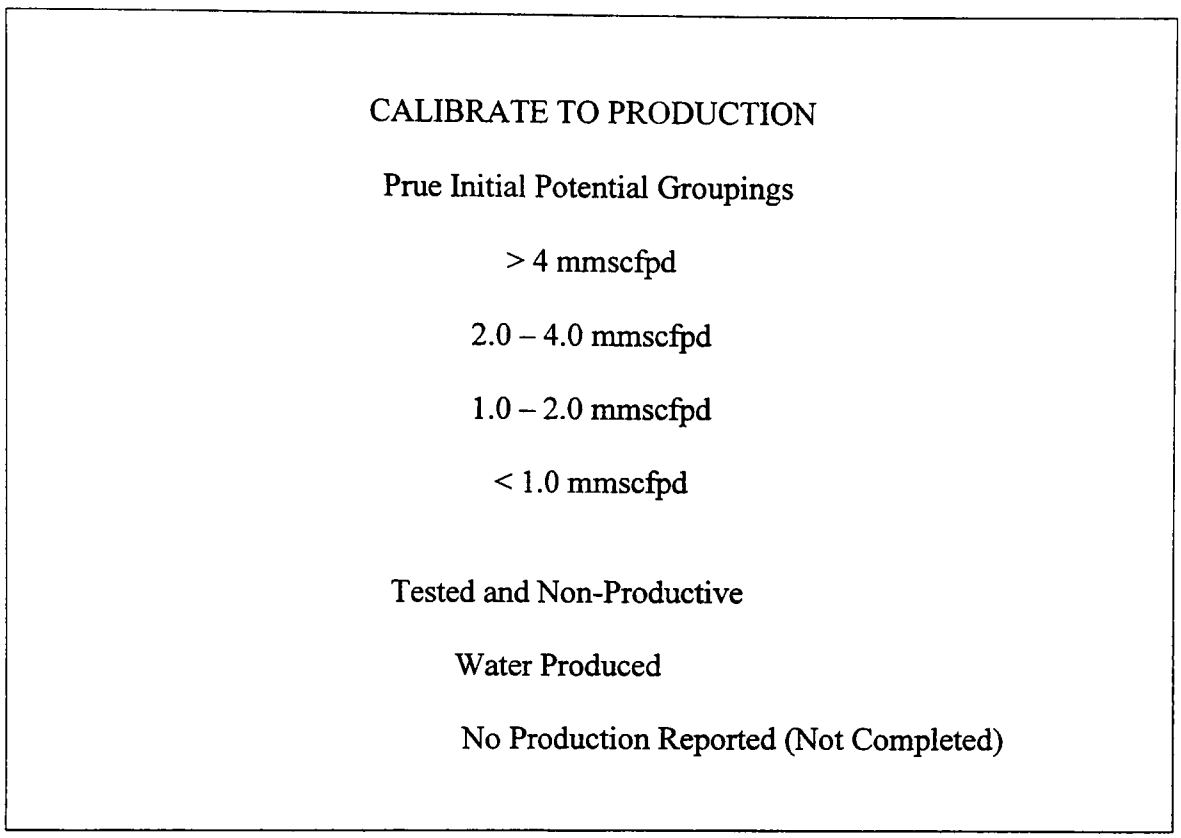

Figure 6.1 Initial Potential and Production Test Results in Prue Wells Examined in this Study used to Calibrate the Range of Analytical Outcomes from the Multiple Parameter Approach to Petrophysical Analysis and Interpretation.

CHAPTER VII
RESULTS

Prue Granite Wash

Petrophysical Parameter Charts

The results from three wells examined in this study, Wells A, B and C, are reviewed to illustrate the effectiveness of the method in using log response to assess the potential for hydrocarbon productivity in the Prue. A series of charts were developed in this study to illustrate the results calculated from the suite of petrophysical parameters used to evaluate Prue Sands. They illustrate the outcomes of the analysis of the petrophysical parameters in a depositional context and provide an opportunity to assess trends in reservoir quality, the presence and movability of hydrocarbons and examine the character of the calculated water saturation in the reservoir. Each petrophysical parameter chart includes a legend box that identifies the individual curves on the chart. The annotation CBS appended to a curve identifier indicates the curve is referenced to the chart bottom scale; all other curves refer to the chart top scale.

Well A

Prue Sand 1

Examples from Well A in the study are included to provide an opportunity to review the content of analytical data and interpretation significance of the charts. The charts are presented in wireline log format, with the depth scale to the left and two separate curve scales found at the top and bottom of each chart.

One Prue Sand in Well A was perforated from 11,359 ft to 11,370 ft and completed with an initial potential of 4.9 million standard cubic ft of gas per day (mmscfpd) + 37 barrels of condensate per day (bcpd), and no water. Cumulative production for Well A is 2.9 bcfg over 78 months. A red bar along the depth axis of each chart marks the perforated interval in Well A.

Standard Log Data Chart. The first chart of petrophysical parameters (Figure 7.1) is a plot of the standard log data acquired through the zone of interest. The character of the basic log data is as important as the analytical data. The log data curves included on this chart are the standard gamma ray (GR), the spontaneous potential (SP), the density porosity (PhiDen), the neutron porosity (PhiNeut) curves, and the shallow and deep resistivity curves (Rsfl and Rild, respectively). The only analytical curve on this plot is the *Amplified BVW* curve, which was generated by multiplying calculated *BVW* values (Equation 6.32) by 1000 to get to the proper scale to fit on the plot. The porosity and water saturation values used to calculate BVW were generated as indicated in the section on water saturation in Chapter VI. All individual curves are identified in the chart legend box. Curves whose identity labels are followed by "CBS" refer to the chart bottom scale; all other log data curves refer to the chart top scale.

Note the trends in the two curves used to identify permeable zones, the GR and SP curves. The SP curve appears to indicate the reservoir extends down to about 11,387 ft, but the GR curve shows a notable trend change, from clean to shaly (high gamma ray), at about 11,372 ft. The density-neutron curves show reasonably uniform separation representing gas effect over the GR-clean interval, which closes across the GR-shaly interval. A reasonable invasion profile and consequent indications of permeability is indicated by the separation of the shallow and deep resistivity curves across the GR-clean interval, which is significantly reduced across the GR-shaly interval.

Knowing that the zone was completed water-free indicates that it was at irreducible water saturation and that textural information in the BVW curve is valid. However, even if this were a new well with no completion data, the textural trend indicated by the BVW curve is sedimentologically reasonable and is supported by the correlative trends in the standard log data. It provides a petrophysical framework against which examination of cuttings samples can be characterized to provide petrologic information in support of the petrophysical analysis.

The *Amplified BVW* curve plots between about 60 and 65 (0.060 to 0.065 x 1000) across the GR-clean interval, but rises to about 90 across the GR-shaly zone. If the

reservoir is at irreducible water saturation, the *Amplified BVW* curve suggests the interval shown as potential reservoir by the SP curve is texturally bimodal. It is much finer, with more grain surface area, in the bottom half of the zone grading to a slightly coarsening-upward, very fine-grained, clean sand at the top. It suggests a textural or mineralogical change has diminished the apparent magnitude of the gas effect and the quality of the invasion profile in the bottom half of the zone and caused the *GR* curve to read higher. The overall character of the basic log data, supported by the *Amplified BVW* curve, suggests that, although porosity is nearly uniform, the texture of the section from 11,372 ft to 11,387 ft is different than that in the perforated interval. The base of the SP-defined zone could be shaly, very fine-grained sand, although it is not so shaly that it has caused the SP deflection to decrease significantly. Hilchie (1979, p. 69-70) has stated that SP deflection in low resistivity colloidal sands in Oklahoma and the Rocky Mountains is often not significantly reduced, attributing the effect to illite in the sandstone pores.

The standard-log curves and BVW curve provide a textural framework from which to examine the calculated petrophysical parameters and indicates different reservoir properties in the top half of the interval compared to those in the bottom half. Despite reasonably constant porosity, the character of the standard log data and the BVW data indicate that the perforated interval exhibits petrophysical properties that correspond to better reservoir quality than is found in the remainder of the interval.

FMOP Chart. Figure 7.2 is the example of the FMOP for Well A. There are five curves on this chart, the SP curve and four FMOP curves as were defined in Equations 6.3 through 6.6. Note that the apparent formation resistivity factor curves from shallow resistivity, F(*Ri*) and calculated flushed zone resistivity, F(*Rxo*c), very nearly overlay the empirical formation resistivity factor curve, the F(*DN*) curve. This indicates that the reservoir is either wet or very well flushed. Note also the magnitude of separation between the deep formation resistivity factor curve, F(R_d), and the empirical formation resistivity factor, F(*DN*); that separation indicates the presence of hydrocarbons in the uninvaded zone, while the separation between F(R_d) and F(R_i), and between F(R_d) and F(R_{xo}) indicates that the hydrocarbons in the reservoir are highly movable.

If the Prue Sand reservoir is at irreducible water saturation, the trend in the F(R_d) curve relative to the F(DN) curve indicates a textural change across the SP-defined reservoir interval that supports the information indicated by the *BVW* curve on Figure 7.1. The trends of the empirical and apparent deep formation resistivity factor curves demonstrate that formation properties in the lower half of the SP-defined interval contribute to a more conductive rock - fluid system than exists in the top half of the interval. Greater formation conductivity in a system at irreducible water saturation can be explained by an increased volume of capillary bound water, which requires greater grain surface area. The required textural change could be attributed to finer grain size or the presence of clay or microporous grains in the lower half of the zone. Note also that the F(R_i) and F(R_{xoc}) curves fall below the F(DN) curve, suggesting the presence of excess conductivity and possible shaliness or microporous grains in the lower half of the reservoir.

The trend in the F(R_d) and F(DN) curves in the bottom half of the SP-defined reservoir indicates that although the formation in the bottom half reservoir interval is not nearly as resistive as the top half, the F(R_d) curve still maintains separation from F(DN), signaling that hydrocarbon saturation continues into the lower half of the SP-defined reservoir. Only the top half of the SP-defined reservoir was perforated. However, completion by hydraulic fracture, as indicated on the scout data sheet, probably includes the lower half of the reservoir in the completion because no barrier to downward fracture propagation can be noted on the logs separating the top and bottom halves of the SP-defined reservoir zone. Water-free production reported in the IP suggests that the lower half of the reservoir is therefore also at irreducible water saturation. Although hydrocarbon saturation is less than in the top half, the finer texture (i.e., more clay) in the lower half holds more water at irreducible conditions.

The FMOP has qualitatively indicated the presence of a reservoir saturated with movable hydrocarbons without requiring any water saturation calculations. It has also provided information on the textural character of the reservoir that can be interpreted in a depositional context, presuming the reservoir is at irreducible water saturation. If the

context is unreasonable, then the reservoir might not be at irreducible water saturation. All the information on Figures 7.1 and 7.2 support the idea that the SP-defined reservoir is a clean, coarsening-upward very fine-grained sand in the top half (the perforated interval), and finer-textured, possibly shaly sand, in the bottom half.

Resistivity Porosity-Movable Hydrocarbon Index Chart. Figure 7.3 is the third example of a petrophysical parameters chart for Well A. It is the plot of resistivity porosity and movable hydrocarbon index (MHI) parameters. There are six curves on the chart, four porosity curves referenced to the chart top scale and two MHI curves referenced to the chart bottom scale. Porosity curves on the plot include the total formation porosity curve, Phi(*DN*), developed from density-neutron crossplot porosity, Equation 6.2, and three resistivity porosity curves, Phi(R_{xoc}) and Phi(R_i), and Phi(R_d), developed from Equations 6.10–6.12, respectively. The two *MHI* curves on the plot are calculated from the shallow resistivity data and the calculated R_{xoc} data. The red bar along the depth axis marks the perforated interval.

Resistivity porosity represents water-filled porosity and since the Phi(R_i) and Phi(R_{xoc}) curves nearly overlay total formation porosity across the perforated interval, it indicates that formation porosity in the invaded zone is nearly all water-filled. The interval that was perforated, therefore, is wet or highly flushed. The Phi(R_d) curve plots considerably lower porosity than total formation porosity, therefore formation porosity in the uninvaded zone contains little water, and hence the reservoir in the uninvaded zone is saturated with movable hydrocarbons. Separation of total formation porosity and deep resistivity porosity relates directly to S_{wa}, and separation of total formation porosity and resistivity porosity in the flushed and invaded zone relates to S_{xo} and S_i, respectively.

The *MHI* curves across the perforated interval are about 0.4, considerably less than 1.0. This indicates well-moved hydrocarbons, and supports the interpretation from the resistivity porosity curves that the perforated reservoir is saturated with movable hydrocarbons. Because *MHI* is a parameter based on a ratio of water saturation in the uninvaded and invaded zones, the formation resistivity factor and, consequently, formation porosity and Archie empirical parameters m and a are factored out of the

relationship. The *MHI* provides an indication of moved hydrocarbons separate from the indication based on resistivity porosity.

In the unperforated bottom half of the reservoir on Figure 7.3, the Phi(*Ri*) and Phi(*Rxo*c) curves increase to values greater than total formation porosity, seemingly an impossible condition. This indicates the presence of excess conductivity in the bottom half of the reservoir, suggesting the presence of clay or microporous grains not found in the perforated interval.

Water Saturation-Relative Permeability Chart. Figure 7.4 is the final example of the petrophysical parameters charts for the Prue Sand examined in Well A. It includes four water saturation curves referenced to the chart top scale, and two calculated relative permeability curves referenced to the chart bottom scale. Calculated Archie water saturation (S_{wa}) and Patchett water saturation (*Swptcht*) curves fall inside or outside the range of values defined by the two ratio water saturation curves, $S_{wr}(1/2)$ and $S_{wr}(1/5)$. Expected fluid production, based on calculated S_{wa} and S_{wirr} values, is illustrated by the relative permeability curves, *krg* and *krw*.

Calculated Archie and Patchett water saturation curves nearly overlay throughout the extent of the reservoir, reflecting the reasonably stable SP curve across the extent of the reservoir. This characteristic suggests limited shaliness across the extent of the reservoir, and represents conflicting information regarding shaliness in the bottom half of the reservoir. It provides an indication why Archie (1950, p. 961) concluded that good sample descriptions are an important part of petrophysical analysis. It could represent a further indication of the presence of colloids/clays noted by Hilchie (1979) in the bottom half of the reservoir that would exhibit a more limited effect on the SP. If not the type of clay described by Hilchie (1979), it could otherwise indicate increased modal content of microporous framework grains such as tripolitic chert or weathered igneous pebbles, pocked with microvoids in altered feldspars or volcanic rock fragments. Such microporous framework grains could still contribute to increased capillary bound water that would facilitate the flow of electrical current through the formation.

Archie water saturation tracks $S_{wr}(1/5)$ through the perforated interval of the reservoir. This provides confidence in the calculated value of S_{wa} and indicates good hydrocarbon movability in the perforated reservoir interval. In the bottom half of the reservoir, the S_{wa} curve increases to values greater than $S_{wr}(1/5)$, raising concern about the validity of the value of calculated water saturation in this interval of the reservoir. Other petrophysical parameters indicate finer texture in the bottom half of the reservoir, with excess conductivity in the interval. If the lower, unperforated interval is shaly, it could indicate that the value for the Archie empirical parameter *m* is too high in this interval, and calculated Archie water saturation is too high. Alternatively, it could indicate the invasion-flushing assumptions used to calculate S_{wr} are not applicable and the calculated values of Ratio water saturation are wrong.

Calculated relative permeability to water is virtually nil in the perforated interval of the reservoir, while calculated relative permeability to gas is about 60%. Because these are very fine-grained sands and not medium to coarse-grained sands, calculated *krg* will not go to 100% even though the reservoir produces water-free. The relationship of the two curves in the perforated interval suggests very little potential for water production.

The effect of increased water saturation in the lower half of the reservoir on the *krg-krw* curves appears to indicate the presence of some pore water of limited movability in this part of the reservoir. However, the apparent condition of limited movable water in the lower half of the reservoir should be considered in the context of irreducible water in the slightly coarser-textured sands in the perforated interval. The finer-textured character of the sands in the lower half of the reservoir would hold more irreducible water than the sands in the perforated interval. The indication of slightly movable water represents the effect of the assumption of coarse-grained sands on the estimate of irreducible water saturation in the unperforated interval, and the expectation of water-free production from this part of the reservoir is not unreasonable.

Depth of invasion across the interval 11,356 ft. to 11,387 ft. can be examined using a tornado chart, e.g., Schlumberger Chart Rint2-a (Schlumberger, 1989c, p. 89).

and the formation resistivity data. Results demonstrate that the diameter of invasion, d_i, in the perforated interval is about 40 inches, while diameter of invasion in the unperforated lower half of the reservoir is about 26 inches. The formation porosity is essentially constant across the overall interval, yet invasion is diminished in the part of the overall interval characterized by excess conductivity. The relationship of the *Swa* and *Swr* curves on Figure 7.4 suggest that assumptions for water saturation calculations used in the lower half of the reservoir should be changed from those used in the perforated interval and could indicate a change in the character of flushing in the lower half of the reservoir.

Minimize Excess Conductivity. The next four figures, 7.5 through 7.8, examine the effects of reducing the value of the empirical parameter *m* to minimize excess conductivity and using that value to increase the value of *z*. The value of *m* used in the lower half of the reservoir in Well A is 1.75. Figure 7.5 is a second plot of resistivity porosity and MHI parameters for the Prue reservoir in Well A. The value for the *z* factor used to calculate R_z was changed from 0.05 to 0.175, representing shallower invasion across the interval with excess conductivity. A comparison of Figures 7.3 and 7.5 illustrates the effect of that change on petrophysical parameters *PhiRes* (R_i) and *MHI* (R_i). *PhiRes* (R_i) has been reduced to values in line with those in the perforated interval and *MHI* (R_i) has increased by about 50%, from values near 0.40 to values near 0.60. Values for R_z are not included in the calculation of the other parameters on the chart and, hence, are unaffected by the change in *z*.

Figure 7.6 is a second plot of water saturation and relative permeability parameters for the Prue reservoir in Well A, constructed using the same values for the *z* factor as were used in Figure 7.5. A comparison of Figures 7.4 and 7.6 illustrates the effects of that change on the S_{wr} parameters, which are calculated using R_z. The S_{wr} curves have increased in value so that the S_{wa} curve now falls within the limits of S_{wr}, nearly tracking $S_{wr}1/5$.

It appears that the increased *z* factor has produced a response in affected petrophysical parameters that reflects the diminished invasion in the lower half of the

overall Prue reservoir interval in Well A. Tixier (1949, p. 145-146) indicated that the *z* factor should be greater than 0.10 in formations that contain a large amount of colloidal material, which represents very small interstitial particles such as clay particles. The applicability of using an increased *z* factor in this interval corresponds to the log character described by Hilchie (1979) of low resistivity colloidal sands that do not cause significant reduction in the SP. The parameters that don't include R_z in their calculation, e.g. *PhiRes* (R_{xo}) and S_{wa} values, have not been affected by the change in the *z* factor, but would respond to a reduction in the value of the empirical parameter *m*, which is a part of their calculation

Figure 7.7 is a third plot of resistivity porosity and MHI data for the Prue reservoir in Well A. In addition to the change in the *z* factor across the interval with excess conductivity, the value for the empirical parameter *m* has been reduced from 2.0 to 1.75. A comparison of Figures 7.5 and 7.7 shows that, with the reduced *m* value, the excess conductivity of the *Phi* (R_{xo}) parameter has been nearly eliminated, as it falls very close to total formation porosity. The values for the *PhiRes* (R_i) and *PhiRes* (R_d) curves are also reduced, but they retain about the same magnitude of separation as in Figure 7.5. The MHI parameters are unaffected by any change in the empirical parameter *m*.

Figure 7.8 is the third water saturation - relative permeability plot for this Prue reservoir, and illustrates the effects of the diminished empirical parameter *m*. Archie water saturation still falls within the limits of the corrected S_{wr} curves, but now falls close to $S_{wr}1/2$, which suggests less movable hydrocarbons, in support of the increase in the *MHI* (R_i) curve from 0.4 to 0.6 (Figure 7.5).

Figure 7.9 is a Buckles-type BVW plot for the SP-defined reservoir interval in Well A, constructed using standard values for the empirical parameters, *m*, *n*, and *a*. There are five standard BVW curves shown on the plot: 0.02 through 0.10. The cluster of red triangles represents the BVW values for the perforated interval, 11,359-ft to 11,387 ft, which plot with limited scatter about a trendline in red that nearly overlays the standard 0.06 curve. The BVW values for the interval from 11,371-ft to 11,387-ft plot with somewhat more scatter about a green trendline that falls clearly oblique to the

standard 0.08 curve. If the data range for the lower interval is examined within trendlines parallel to the trendline that fits the data, then scatter about the oblique trendline is less than apparent BVW data scatter about the standard trendline. It suggests the lower half of the SP-defined interval in Well A is at or near irreducible water saturation, although with an associated texture skewed from that found in a clean sand.

The unperforated bottom half of the Prue reservoir in Well A appears to contain movable hydrocarbons that could contribute to Well A's water-free production through hydraulic fracture communication to the perforations. The movability is less than in the perforated interval, but falls in the range of expected production. Ultimately, any contribution from additional unperforated Prue reservoir volume in Well A would appear in unrealistically large calculated volumetric recovery efficiency for the reservoir.

Summary: Petrophysical Parameters Charts

Examination of the petrophysical parameters charts, Figures 7.1-7.8, can lead to observations that promote qualitative assessment of petrophysical characteristics and hydrocarbon content of a reservoir. Using the information from the suite of petrophysical parameters to develop a consistent, objective interpretation is the critical next step in evaluating the productive potential of a subsurface accumulation of hydrocarbons in the Prue detected through petrophysical analysis.

The procedures described above and illustrated on Figures 7.5-7.8, demonstrate the importance of well-planned core acquisition and analysis in the Prue to examine the changes in the Archie empirical parameters, a, m, and n, as well as the Tixier z factor, with changes in mineralogy, texture and associated log character. Hilchie indicated such changes as were illustrated in the Hilchie (1979) data table, had no theoretical basis, but worked to produce reasonable calculated values of water saturation in shaly sands. Since shale volume is not readily available in the Prue, excess conductivity in a reservoir, apparently due to the presence of clay, has been used as a shaliness indicator in this study. Excess conductivity is not uncommon in Prue sandstones, and the analytical method described above should be evaluated further through core analysis

Production-Calibrated Ranking System Histograms

The effectiveness of the production-calibrated ranking system developed in this study for the interpretation of petrophysical data is illustrated using examples from three wells that include production tests in Prue sands. The relative frequency of scores for each petrophysical parameter are presented as a series of histograms included on a chart of histograms computed for each petrophysical parameter. Each petrophysical parameter listed across the bottom of a ranking system histogram chart is identified on Figure 7.10. Reservoir quality parameters are placed to the left side of the ranking system histogram charts. Petrophysical parameters to detect hydrocarbon presence, assess hydrocarbon movability, and provide indications of excess conductivity follow in the central portion of the charts. The parameters used to evaluate water saturation are located toward the right side of the charts. A legend box illustrating the color used to identify each score bar in the histogram has been placed in each chart. The arrangement of the vertical bars that represent the relative frequency of each score in the individual histograms on the chart, proceed left to right, from (5) to (–1).

Well A

Prue Sand 1

Figure 7.11 is the ranking system histogram chart for the overall SP-defined reservoir interval in Well A, 11,356-ft to 11,387-ft, which was represented by the petrophysical parameters charts in Figures 7.1–7.4. Figure 7.11 illustrates the relative frequency of the scored analytical outcome from the full suite of petrophysical parameters across that overall interval. Petrophysical parameters for reservoir quality, SP and Phi, are nearly 100% (4s) and (5s). Movable hydrocarbons show some strength with almost 40% or greater scores of (5s) from the FMOP and PhiResA parameters. However, these movability parameters also show (0s), reflecting the excess conductivity in the bottom half of the interval. The *MHI* and *Kr* parameters are very strong with 90% – 100% (5s). The water saturation values are all strong. The *BVW*_SD parameter indicates high scatter with a score of (1), but the *BVW* parameter shows the scatter is from two

adjacent grain size groups, (2s) and (1s), in silty to very fine grained sands (Asquith, 1982, p. 98, table 8). As can be seen on Figure 7.1, the amplified BVW curve appears to represent grain size grading in the reservoir. The zone scores are encouraging.

Figure 7.12 is the ranking system histogram for Well A across only the perforated interval, 11,359-ft to 11,370-ft. The initial potential in this zone was 4.9 mmscfpd + 37 bcpd and no water. The IP for Well A fits into the strongest initial potential production calibration group, > 4 mmscfpd. Most of the petrophysical parameters show over 75% of their scores as (5s). The S_{wr}:S_{wa} parameter indicates that about 80% of the Archie water saturation values fall within the range of Ratio water saturation values, which gives confidence to the calculated values of S_{wa}, which, itself has a score of 100% (5s). The score indicating the measured scatter, *BVW*_SD, has improved from (1) to (4) in going from the total SP-defined zone to the perforated interval alone. The reservoir is of uniform texture with a single grain size class in the *BVW* parameter. The scores are very good and the test results are very good, indicating the ranking system worked in this well.

Figure 7.13 is the ranking system histogram for the unperforated lower half of the SP-defined reservoir interval in Well A. Comparison of scores on Figures 7.12 and 7.13 demonstrates that the range of porosity is quite similar throughout the reservoir. However, the diminished scores for the SP, the invasion profile and gas effect parameters, clearly indicate that values for these parameters are diminished in the unperforated, lower interval.

The predominance of zero's in the FMOP and PhiRes parameters reflect the excess conductivity (and potential shaliness) in this lower interval. The predominance of scores of five for the MHI parameters, which are unaffected by the formation resistivity factor, represents excellent hydrocarbon movability in the reservoir. However, these scores must be considered in the context of the zero's scored by the other movability indicators that are affected by the formation resistivity factor. The potential shaliness could affect the invasion assumptions used in computing the MHI parameters, and the validity of the calculated result, as was explained in Equation 5.21. One hundred percent zero's in the S_{wa} : S_{wr} comparator indicates that there is no agreement between the water

saturation values computed using standard Archie conditions and standard Ratio conditions.

Figure 7.14 is a second-look at the ranking system histogram for the unperforated lower half of the SP-defined reservoir interval in Well A. The effects of potential shaliness represented by excess conductivity have been corrected in the analytical results summarized on this chart. The value of the empirical parameter *m* was reduced from 2.0 to 1.75 and the *z* factor, which was increased from 0.05 to 0.175 in order to compensate for the effects of shaliness on petrophysical properties in the formation. Currently, there is no method analogous to the *z* factor available to develop a correction to R_{mf} in the flushed zone. Filtrate flushing, though, even in the flushed zone, would be expected to be less complete in the more complex formation texture associated with shaliness or microporous grains. Therefore, parameters based on R_{mf}, such as *FMOP* (R_{xoc}), *PhiResA* (R_{xoc}) and *MHI* (R_{xoc}) are less reliable in such textures and have been excluded from the chart. The parameters based on *Rz* are more useful in quantitative analysis.

The scores for the movability parameters on Figure 7.14, *FMOP* (R_i), *PhiResA* (R_i) *and MHI* (R_i) are predominantly 4s and 3s, compared to the predominance of 5s for those parameters in the perforated interval shown on Figure 7.12. The water saturation values are all good and the S_{wr}:S_{wa} comparator indicates S_{wa} values fall within the range of S_{wr} values. This suggests these values represent the water saturation in the effective porosity of this part of the SP-defined Prue reservoir in Well A. The relative permeability parameter looks good for the interval 11,371-ft to 11,387-ft, at nearly all 5s on Figures 7.13 and 7.14. Taken together, the production-calibrated ranking system histograms for the unperforated lower half of the reservoir in Well A indicates potential for water-free hydrocarbon production, albeit not at rates as strong as those in the perforated interval. The interpretation that the lower half of the reservoir should produce water-free hydrocarbons helps to explain how the reported 1700 barrel hydraulic fracture stimulation across 11-ft of perforations avoided potential water production through the hydraulic fracture migrating down into the unperforated lower half of the SP-defined reservoir in Well A. Lacking any barrier, the stimulation fracture probably did go down

into the lower half of the reservoir, but encountered movable hydrocarbons with no movable water.

Well B

Prue Sand 1

Three separate Prue Sands were tested in Well B. The most shallow of the three sands was perforated from 11,237-ft to 11,251-ft and hydraulically fractured using 1044 barrels of Frac Fluid. The initial potential (IP) test from the zone was 2.46 MMCFGPD + 30 BCPD and no water; cumulative production from the zone was 1.45 BCFG over 112 months. The water-free completion indicates that the reservoir is at irreducible water saturation, and BVW data reflect textural properties of the reservoir. Figure 7.15 is the ranking system histogram for the interval 11,237-ft to 11,251-ft in Well B. Score frequencies for the SP parameter are about 65% (5s), with the remainder mostly (4s) and (3s), indicating generally well developed SP for this Prue Sand. The *Phi* reservoir quality parameter shows a bout 50% (5s) and (4s), the remainder (3s), indicating a range of porosity from very good to fair. Invasion and Gas Effect reservoir quality parameters are characterized by a predominance of (2s) and (3s), while including a wider range of scores, suggesting a hetereogenoeus reservoir.

The *FMOP* and *PhiResA* hydrocarbon presence and movability parameters show about 50% (5s) and (4s) and (3s), but also about 50% (0s), indicating apparent excess conductivity in the reservoir. The *MHI* parameter shows a predominance of (5s) and (4s), and the scores for *kr* indicate much of the interval should be capable of water-free production. However, the S_{wa} parameter exhibits a range of values with scores from (2s) to (5s), suggesting a heterogeneous reservoir. The *Swpatchett* parameter reflects the stable SP parameter and does not indicate shaliness in the reservoir, in contrast to the apparent excess conductivity indicated by the (0s) in the *FMOP* and *PhiRes* parameters. Values for the S_{wr}*1/2* and *Swr1/5* parameters are predominantly (5s), but the agreement between S_{wa} and S_{wr}, as measured by the S_{wr}:S_{wa} comparison parameter is almost 70 %

(0s), indicating poor correlation between the calculated Archie and Ratio water saturation values.

The score of (1) for the *BVW* standard deviation parameter indicates considerable scatter in the data. However, since the well completed water-free, the zone is at irreducible water saturation and the *BVW* scatter indicates there is textural heterogeneity across the interval. A potential difficulty associated with such heterogeneity is a non-uniform response to the stimulation treatment and less effective resource recovery than would be found in a more uniform reservoir. The range of grain size classes in the reservoir includes a predominance of silty material with some shaly material and minor very fine-grained sand.

Examination of the petrophysical parameters charts for this Prue Reservoir, followed by a review of the calculated scores for the zone in the petrophysical analysis spreadsheet, provided an opportunity to identify a subzone in the reservoir in which the petrophysical parameters indicate uniformly better reservoir potential, a high-graded subzone within the overall completion zone. Figure 7.16 represents the ranking scores for a seven-foot sub-interval in the perforated zone that appears to include more nearly uniform petrophysical characteristics. The SP is clearly improved, as is the Density-Neutron gas effect parameter. The zero scores and apparent excess conductivity shown in the FMOP and PhiResA parameters is clearly reduced from the effect in the overall interval illustrated in Figure 7.15. Over 50% of the scores in the hydrocarbon presence and movability parameters are (5s) and (4s). Almost 70% of the Archie water saturation values are ranked with (5s) and (4s), but over 40% of the S_{wa} values do not correlate with the range of S_{wr} values. There is still high scatter in the BVW data, but it is included within two adjacent size class groups, very fine grained and silty sands. The shaly component represented by a score including 30% (0s) in the overall perforated interval (Figure 7.15) has fallen out of the high graded interval, suggesting the subzone is more texturally uniform than the overall perforated interval.

If the perforated interval in Well B is reanalyzed and reevaluated by modifying Archie's empirical parameter m and the z factor of Tixier for shaliness, the results are

shown in Figure 7.17. The empirical parameter m required values of 1.85 and 1.65 to minimize excess conductivity from the ϕ_{Rxoc} curve across this zone, and consequent z factors were 0.125 and 0.225, respectively. Because the modified z factor does not affect the parameters controlled by R_{mf}, those parameters are excluded from the chart. The reservoir quality parameters illustrated on Figure 7.17 are not affected by these revisions and are unchanged from their values shown on Figure 7.15. The excess conductivity represented by the zero scores is nearly eliminated from the *FMOP* (R_i) and *PhiResA* (R_i) parameters. With the *MHI* (R_i) parameter, the predominance of (4s), backed up by (3s) indicates the presence and movability of hydrocarbons in the effective porosity in the interval. The S_{wr} : S_{wa} comparator shows that almost 80% of the S_{wa} values fall within the range of S_{wr} values, indicating the improved correlation of calculated water saturation values in the effective porosity of this reservoir, and improved confidence in the result.

Figure 7.18 represents the effects of the revised values for the two parameters, m and z, in the high graded interval in this productive Prue Sand in Well B. This subzone only required an m of 1.85 and z of 0.125 to minimize excess conductivity. The ranks of (4s) and (3s) for the hydrocarbon presence and movability parameters demonstrate that movability is good to fair in the interval. However, the (2s) demonstrate that even in the high graded interval, some of the hydrocarbons have limited movability and suggest less effective reserve recovery than in the Prue reservoir in Well A illustrated on Figure 7.12.

There are encouraging scores in this Prue zone in Well B, however, comparison of Figures 7.12 and 7.15 indicates that production rates and recovery are clearly not going to be as good as in Well A. Although the overall lengths of the perforated intervals are about the same in the productive Prue sands in Wells A and B, the IP in Well B is about half that in Well A. Further, cumulative gas production from Well A is about twice the volume from Well B, in about 30% less time. The petrophysical characteristics in Well B indicate the productive Prue Sand is very fine-grained to shaly, with textural heterogeneity complicating both stimulation treatment and reserve recovery. The ranking histograms for the productive Prue Sand in Well B clearly illustrate that it should not be expected to produce as well as the Prue Sand in Well A.

Prue Sand 2

The second Prue Sand tested in Well B was perforated from 11,313-ft to 11,352-ft and hydraulically fractured using 873 barrels of frac fluid. No results were reported from the test, and the zone was not completed. Figure 7.19 is the ranking histogram for the tested interval. The SP parameter is stable across the interval, but the scores indicate the SP in this Prue Sand has less deflection amplitude than the maximum for the Prue in this well. Overall porosity is fair, but the invasion and gas effect parameters are of lesser quality and are represented by scores predominantly (2s) and (1s). The *FMOP* and *PhiResA* hydrocarbon detection and movability parameters indicate 100% of the sand exhibits excess conductivity and potential shaliness. The *MHI* parameters are ranked with (3s) and (2s). Archie water saturation, nearly all (1s) and (0s), is very poor, and there is no correlation between S_{wa} and the range of S_{wr} values. It would be difficult to recommend this sand for testing based on these results.

Figure 7.20 shows the scores for the sand after the m and z factor parameters are revised to eliminate the excess conductivity and revise the content of ineffective porosity used in the *MHI* and S_{wr} ratio parameters. A range of values for the empirical parameter m, 1.7, 1.6, and 1.4, were required to minimize excess conductivity from the ϕ_{Rxoc} curve across this zone, with consequent z values of 0.20, 0.25 and 0.35, respectively. The absence of (0s) indicate that excess conductivity has been minimized from $FMOP(R_i)$ and $PhiResA(R_i)$ parameters. The $S_{wr} : S_{wa}$ parameter indicates that over 80% of the S_{wa} values correlate with the range of S_{wr} values, suggesting the S_{wa} values with about an 85% rank of (2) are reasonable values for calculated water saturation in the effective porosity in this Prue Sand. Almost 90% of the *kr* parameter scores are (2s), (1s) and (0s), which indicates that any fluid production from this sand would be expected to exhibit minimal potential for water-free hydrocarbons. Again, there is nothing to recommend this sand for testing and the scores on the ranking histogram accurately reflect the non-completion.

Prue Sand 3

Figure 7.21 is the ranking histogram for the third Prue Sand tested in Well B, from 11,552 ft to 11,578 ft. The zone was treated with 720 barrels of frac fluid, production tested and flowed 0.353 MMSCFPD + 336 BW. It was not completed. The ranking histogram shows that the SP, which exhibits a predominant score of (3) is not nearly as well developed as the best SP in the Prue in this well. The *FMOP* and *PhiResA* parameters include a predominance of (0s), indicating common excess conductivity in the reservoir, with very little indication of the presence of movable hydrocarbons in the sand. The *kr* parameter indicates calculated relative permeability to gas is poor and the S_{wa} scores are predominantly (2s). The $S_{wa} : S_{wr}$ parameter indicates little correlation between Ratio and Archie saturation values and the *BVW*_SD parameter indicates the most scatter seen in any of the zones tested in this well. The predominance of (0s) and dearth of (4s) and (5s) on the ranking histogram for this zone reflect the poor quality of hydrocarbon productivity that was established for the reservoir during testing. The scores would have made this sand too risky to be recommended for completion efforts and expenses.

Figure 7.22 is the ranking histogram for this sand, with revised values for the parameters *m* and *z*-factor, to correct for the shaliness indications represented by the excess conductivity. Excess conductivity was erratic, but limited in the upper third of the reservoir, and values for the empirical parameter *m* and *z* were unchanged from standard values. However, the value for *m* was reduced to 1.65 across the lower two-thirds of the reservoir to minimize the excess conductivity from the ϕ_{Rxoc} curve; the associated value for *z* was increased to 0.225. The revised movability indicators show a predominance of (3s) and (2s), indicating the reservoir is saturated with hydrocarbons of limited movability. Calculated Archie water saturation is also predominantly ranked with (3s) and (2s), and the $S_{wa} : S_{wr}$ parameter indicates over 60% of the S_{wa} values fall within the range of calculated S_{wr} values. This indicates the calculated S_{wa} values represent water saturation in the effective porosity in this Prue Sand, and there are hydrocarbons present

in the sand, but of limited movability. The ranking histogram reflects the minimal hydrocarbons recovered on test.

Well C

Prue Sand 1

Two separate Prue Sands were tested in Well C. The shallower sand was perforated from 11,098-ft to 11,114-ft and hydraulically fractured using 1900 barrels of frac fluid. The initial potential from this Prue Sand was 3.7 MMSCFPD + 43 BCPD and no water. Cumulative production from the sand was 1.95 BCFG over 78 months.

Figure 7.23 is the ranking histogram for this first Prue Sand in Well C. The ranking histogram shows a predominance of scores of (4s) and (5s). Scores for the SP parameter indicate that the deflection amplitude is not constant across the sand, but remains near the maximum deflection amplitude in the Prue section in Well C. Porosity (*Phi*), and invasion factor (R_i/R_d) parameters are ranked with a predominance of (3s) and (4s), indicating fair to good reservoir quality. The gas effect (*DN*) parameter is ranked with a predominance of scores of (4s) and (5s), indicating this Prue Sand is a gas-saturated reservoir.

Scores for the *FMOP* and *PhiResA* hydrocarbon detection and movability parameters indicate the sand is saturated with movable hydrocarbons, with virtually no indication of excess conductivity in the reservoir. The *MHI* parameters are ranked with all (4s) and (5s). Relative permeability to gas and S_{wa} parameters show scores of 100% (5s). The S_{wa} : S_{wr} parameter (Figure 7.23) indicates that over 90% of the S_{wa} values fall within the range of S_{wr} values, adding confidence that the calculated S_{wa} values are a valid representation of actual saturation conditions in this sand. With a score of (3), the *BVW_SD* parameter indicates minimal scatter in *BVW* data, constrained within two adjacent sediment grain size classes, as indicated by the *BVW* parameter. The scores of (3) and (2) for the *BVW* parameter suggest the reservoir is grain size graded from very fine to fine-grained sands, which is confirmed by the *Amplified BVW* curve on the log data chart for this sand. The predominance of scores of (4s) and (5s) shown on the

ranking histogram indicate the zone should be highly productive, and these scores are supported by the strong production rates established for this zone, similar to those in Well A.

Prue Sand 2

The second Prue Sand tested in Well C was perforated from 11,401 ft to 11,416 ft. It was production tested and it swabbed [unmeasured gas + 41 barrels of water]. The sand was not completed. Figure 7.24 is the ranking histogram for this sand. Porosity and gas effect parameters are ranked with a predominance of (3s), indicating fair reservoir quality. Scores for the hydrocarbon detection and movability parameters are predominantly (5s), indicating the sand is well saturated with movable hydrocarbons, much like the petrophysical character of the upper sand illustrated in Figure 7.23. The ranking of the *BVW_SD* parameter, with a score of (4), indicates BVW data scatter is minimal, and suggests the reservoir is at irreducible water saturation.

The poor test results established from this Prue Sand indicate that these scores can not be correct; poor scores from two parameters stand out from all the good scores on Figure 7.24. The score for the SP parameter is 100% (1s) indicating the amplitude of the SP deflection in this sand is uniformly much less than the maximum SP deflection in the Prue in Well C. The score for S_{wpat} (Patchett Sw) is 100% (2s), indicating the reservoir is very shaly, or the R_w used in evaluating this sand is invalid relative to the R_{mf} value in the well. Scores from both these parameters are a cause for caution in the interpretation.

The value for R_w used in the analysis of this lower sand shown on Figure 7.24, is 0.065, an R_w value commonly used in the analysis of Prue sands. Examination of the SP parameter scores for the upper Prue Sand in Well C on Figure 7.23 demonstrates the scores are predominantly (4s) and (5s). Amplitude of the SP deflection in the upper Prue Sand is as great as, or exceeds deflection amplitude in all other Prue Sands in Well C. SP parameter scores in this lower sand indicate that the SP deflection is considerably less than other Prue Sands in Well C. Scores for the *FMOP* and *PhiResA* parameters indicate

that excess conductivity is limited, indicating that shaliness is not significantly affecting SP amplitude in this sand, but unrecognized variable R_w could be a problem.

Petrophysical analysis was re-run across the lower sand, using a value of R_w in the analysis that was calculated from the SP deflection across the lower sand. In the first analysis, the R_w value was used because it was a commonly accepted value for the Prue. Now the interpretation makes use of the information available in the logging data, the SP, rather than assuming a value for this critical petrophysical parameter. The new R_w value used, 0.21, and the results from the new petrophysical analyses are shown on Figure 7.25, the new ranking histogram for this lower Prue Sand in Well C. Scores for the hydrocarbon detection and movability parameters on Figure 7.25 are now predominantly (2s), signaling very poor movability of any saturating hydrocarbons. Scores for the S_{wa} parameter are nearly 100% (2s) although only about 45% correlation with the range of S_{wr} values. The *BVW_SD* parameter indicates very little scatter in the *BVW* data, which is a reflection of the consistent score populations for the S_{wa} and *Phi* parameters in this sand: S_{wa} with (2s) and *Phi* with (3s). The S_{wpat} parameter is now 80% (5s); Patchett agrees with the higher values of S_{wa}, based on the increased R_w.

Figure 7.26 is a further revaluation of this sand, using a value of 1.965 for the Archie empirical parameter m and 0.0675 for the z-factor. With this very slight modification to the analysis, the (0) scores are virtually eliminated from the FMOP_Ri and PhiResA_Ri parameters, indicating minimized excess conductivity, and the $S_{wa} : S_{wr}$ parameter indicates there is now over 70% correlation between S_{wa} and the range of S_{wr} values. Based on this ranking histogram, using a value for R_w from the SP rather than an assumed constant (low) value, the scores would direct an interpreter to not include this sand in the testing program for the well.

Summary: Ranking Histogram Charts

Ranking histogram examples from three different productive Prue Sands have been examined in this review. The ranking histograms show a range of scores among the three sands that provides an accurate representation of the actual range in production

testing results from the three sands. Scores on the ranking histograms for the productive sands from Wells A and C, Figures 7.12 and 7.23, respectively, would indicate each of the sands to be valid test candidates with low risk and expected high production rates. Well A scored better than Well C and produced better, although both had good test results.

The initial potential and cumulative production values from the productive sand in Well B, with 14 ft of perforations, are about half the values for IP and cumulative production in Well A, with 11 ft of perforations. Scores on the ranking histogram for the productive Prue Sand in Well A (Figure 7.12) are uniformly and dominantly (5s), while ranking scores for the productive Prue Sand in Well B (Figures 7.15 through 7.18) exhibit a range of scores that indicate the presence of movable hydrocarbons in a heterogeneous reservoir. The difference in the ranking histograms illustrate the difference in reservoir quality and production potential that is confirmed by the production difference from the two Prue Sand completions

Three Prue Sands were reviewed that were tested and not completed, two in Well B, illustrated in Figures 7.19 – 7.22, and one in well C, illustrated on Figures 7.24 – 7.26. The ranking histograms from each of these three Prue Sands exhibit petrophysical characteristics indicating weak potential for movable hydrocarbons that was confirmed by completion attempts that were abandoned. Examination of the Prue Sand that was tested in the interval 11,401-ft to 11,416-ft in Well C demonstrated the potential risk for failed completions in Prue Sands that can result from assuming a constant R_w in petrophysical evaluation in the Prue.

Permian Basin Carbonates

Petrophysical Parameter Charts

Basic log data was examined from two wells that tested Permian Basin carbonate reservoirs, a Fusselman dolomite and Canyon Lime. As with the Prue Sands, four separate petrophysical parameter charts are used to illustrate the results of the petrophysical analysis in each well. The Siluro-Devonian Fusselman was tested and

completed for 1305 BOPD + 1.5 mmcfgpd and no water. The completed Fusselman reservoir was described as a cherty, limy dolomite with intercrystalline and vuggy porosity (Asquith,1995, p. 78). In a separate well, a production test was run in the vuggy limestone of the Pennsylvanian Canyon Reef; it produced only water and was not completed (Asquith, 1985, p. 7-8). The following petrophysical parameter charts illustrate the distinct petrophysical characteristics of these carbonate reservoirs and the ranking histograms illustrate the difference in productive potential between the Fusselman and Canyon reservoirs.

Fusselman

Standard Log Data Chart

Figure 7.27, the first of the four petrophysical parameter charts, is the plot of basic log data across the Fusselman reservoir, plus the *Amplified BVW* curve [BVW x 1000]. Log data available for the Fusselman include SP and standard gamma ray data, a dual induction – laterolog 8 log, a density–neutron log and a sonic log. The SP curve delineates a permeable zone from about 9,087-ft to 9,126-ft, across which the density-neutron combination indicates about 18%-20% total porosity. The standard dolomite separation of the neutron and density curves is affected by the siliceous-limy nature of the Fusselman dolomite and is obscured by the small scale of the plot. Sonic log data is shown as travel time, and tracks the density-neutron trend. The deep and shallow resistivity curves show very little separation, and in fact exhibit an annulus tendency. The *Amplified BVW* curve is very consistent in the top half of the SP-defined reservoir interval, suggesting it is at irreducible water saturation. It increases somewhat from that trend in the bottom half, suggesting some textural or lithologic variability in the lower part of the SP-defined reservoir interval.

FMOP Chart

Figure 7.28, is the FMOP chart for the SP-defined Fusselman reservoir shown on Figure 7.27. As in Figure Figure 7.2, there are five curves on this chart, the SP curve and

four *FMOP* curves. The *FMOP* curves include the empirical formation resistivity factor curve, F(*DN*), and three apparent formation resistivity factor curves, F(R_{xoc}), F(R_i) and F(R_d), identified in Equations 6.7 and 6.8. The SP curve is referenced to the chart top scale, while the formation resistivity factor curves are referenced to the chart bottom scale. The only curve on this chart affected by the Archie empirical parameter m is the F(*DN*) curve; it was calculated using a fixed value for $m = 2.0$. The three other FMOP curves are simple formation resistivity ratios, no empirical parameter is required in their computation.

The FMOP curves from the flushed and invaded zone, F(R_{xoc}) and F(R_i), respectively, nearly overlay the empirical F(*DN*) curve, indicating the reservoir is either wet or very well flushed of original hydrocarbon saturation. The large separation between the F(*DN*) and F(R_d) curves indicates that the reservoir is well saturated with hydrocarbons. Therefore, before any water saturation information is available, this plot indicates the Fusselman is a well flushed, hydrocarbon saturated reservoir. It would be very encouraging for the zone as a potential test candidate.

Resistivity Porosity-Movable Hydrocarbon Index Chart

Figure 7.29, the third of the four petrophysical parameter charts, is the Resistivity Porosity-MHI chart and includes five porosity curves: three resistivity porosity curves, a density–neutron porosity curve and a sonic porosity curve. Two movable hydrocarbon index (MHI) curves are also displayed.

The density-neutron porosity curve, Phi (*DN*), represents total formation porosity and the sonic porosity curve, Phi (*Son*), represents interconnected matrix porosity. When the two logs yield similar readings, it indicates the pore system is largely composed of interconnected voids. As the sonic and density-neutron log readings diverge, it indicates an increasing presence of secondary porosity, isolated vugs, is represented in the total porosity of the reservoir.

The resistivity porosity curves include Phi (R_{xoc}), Phi (R_i) and Phi (R_d), and represent water-filled, interconnected matrix porosity at different depths of investigation

across the invasion profile. All the porosity curves are referenced to the chart top scale. The two movable hydrocarbon index (MHI) curves are developed from shallow resistivity log data, the MHI (R_i) curve, and from calculated R_{xo} data, the MHI (R_{xoc}) curve. The MHI curves are referenced to the chart bottom scale.

Density-neutron porosity (total formation porosity) falls in a range of about 16% to about 23%. Sonic porosity tracks total porosity almost exactly, although about four porosity units (PU's) less than total porosity. This relationship indicates there is some poorly connected secondary porosity in this reservoir, but intercrystalline porosity is the primary pore type in this Fusselman dolomite. The calculated flushed zone resistivity porosity curve, Phi (R_{xoc}), virtually overlays the sonic porosity curve, indicating the matrix porosity in this reservoir is wet or completely flushed. The invaded zone resistivity porosity curve, Phi (R_i), is 7 or 8 PU's less than Phi (R_{xoc}) and sonic porosity. This demonstrates that the invaded zone is less completely flushed than the flushed zone, as should be expected, and documents the presence of movable hydrocarbons in this reservoir. The deep resistivity porosity curve, Phi (R_d), indicates that water-filled porosity in the uninvaded zone is about 8 to 12 PU's less than matrix porosity and 5-7 PU's less than Phi (R_i). The relationship of the resistivity porosity and formation porosity curves indicates the reservoir is saturated with movable hydrocarbons.

The values of the MHI curves are running at about 0.15 to 0.30, indicating water saturation in the flushed and invaded zones is much greater than water saturation in the uninvaded zone, and indicate the presence of movable hydrocarbons. Asquith (1982, p. 97) indicates that an MHI ratio value of about 0.6 represents the onset of reservoir conditions suitable to producible hydrocarbons in carbonate reservoirs.

Variable *m*. If the Fusselman dolomite represents a dual pore system with intercrystalline porosity and isolated vug porosity, it would be expected that the value of the empirical parameter *m* should be greater than 2.0. This is exactly the case. With density, neutron and sonic logs available, the Nugent method for calculating variable *m* is appropriate. The range of values for the empirical parameter *m* calculated using the Nugent relationship in this reservoir interval is about 2 to 2.5, with an average value of

2.25. This seems reasonable in a pore system identified as predominantly intercrystalline with some isolated vugs.

Figure 7.30 contains all the same parameters as Figure 7.29, however resistivity porosity on this chart was calculated using the variable *m* values from the Nugent relationship. The empirical parameter *m* is not part of the density-neutron or sonic porosity relationships, or the MHI relationship; therefore, these curves are not affected by the changed values in *m*. However, Phi (R_{xoc}) now overlays the density-neutron porosity curve rather than the sonic porosity curve as it did on Figure 7.29. This indicates that water-filled porosity now equals total porosity by mathematically accounting for the discrepancy between the pore body to pore throat ratio in the Fusselman through the use of a variable *m*. Also, the Phi (R_i) and Phi (R_d) curves have increased in value slightly, indicating slightly greater water-filled porosity, and hence slightly less hydrocarbon-filled porosity, in the reservoir. Considerable separation remains among the resistivity porosity curves, indicating that the reservoir is saturated with movable hydrocarbons.

Water Saturation-Relative Permeability Chart

Figure 7.31 is the Water Saturation-RelPerm petrophysical parameters chart, and includes six curves: two Ratio water saturation curves, two Archie water saturation curves and two Relative Permeability curves. The four water saturation curves are referenced to the chart top scale and all four fall within a narrow range of values from about 0.05 to about 0.20. The two outside curves, the lowest and highest, are the two Ratio water saturation curves, S_{wr} *(1/2)* and S_{wr} *(1/5)*, respectively. The two inside curves are two Archie water saturation curves, one calculated using a fixed value of the empirical parameter $m = 2.0$, the other using the variable *m* value from the Nugent relationship. Archie water saturation from fixed $m = 2.0$ is nearly identical in value to Archie water saturation from variable *m* because the difference in the effect of $m = 2.0$ and $m = 2.25$ on the computation of S_{wa} is not significant. The fact that the Archie saturation curves fall inside the Ratio water saturation curves improves confidence in all the input data and assumptions used to develop the curves. Archie water saturation

computed from variable *m* provides direct information on the hydrocarbon saturation in the reservoir that was illustrated qualitatively on Figures 7.28-7.30

The two relative permeability curves are referenced to the chart bottom scale and were generated from water saturation data based on variable *m* values. The strong separation of the relative permeability curves supports the idea that a test of this interval should produce a water-free completion, which it did.

Canyon Lime

Standard Log Data Chart

This Canyon Lime well was perforated from 4035-ft to 4082-ft. It was tested and the test produced only water and the zone was not completed. Figure 7.32, is the plot of basic log data across the Canyon Lime reservoir, plus the Amplified BVW curve for the interval. Log data available for the Canyon Lime include SP and standard gamma ray data, a dual induction–laterolog 8 log and a density log. Neutron and sonic logs available in the Fussleman well were not run in this Canyon well, which makes the recognition of poorly connected secondary porosity more difficult.

The SP and *GR* curves identify the reservoir interval, across which density porosity, *DenPhi*, ranges from about 18% to 28% and averages about 22%. Deep and shallow resistivity curves show strong separation, supporting the indication from the SP that the zone has permeability. Variability in the *Amplified BVW* curve indicates that if the zone is at irreducible water saturation, then textural or lithological variability should be evident across the reservoir interval to explain the variable *BVW*.

FMOP Chart

Figure 7.33 is the FMOP chart for the SP-defined reservoir interval shown on Figure 7.32. The response of the $F(R_{xoc})$ and $F(R_i)$ curves from this Canyon Reef reservoir is distinct from their character in the Fusselman. Rather than overlaying the empirical formation resistivity factor curve, F(*Den*), the $F(R_{xoc})$ and $F(R_i)$ curves rise above the curve Archie developed to be able to recognize a wet formation, indicating the

invaded zone contains hydrocarbons that were not moved during invasion. The separation between *F(R_d)* and *F(Den)* indicate the zone is saturated with hydrocarbons, but, on comparison of figures 7.28 and 7.33, it is clear that hydrocarbon saturation and movability will certainly not be of the same quality as was found in the Fusselman. The FMOP scale difference between the two reservoirs is a further reflection of the difference in formation resistivity between the Canyon Lime and Fusselman reservoirs.

Resistivity Porosity-Movable Hydrocarbon Index Chart

Figure 7.34 is the Resistivity Porosity-MHI chart for the Canyon Lime. It includes only four porosity curves, the three resistivity porosity curves noted on Figure 7.29, but only one formation porosity curve, total porosity from the formation density log, because no sonic log was run in this well. The two MHI curves are also displayed. The porosity and MHI curves are referenced to the chart top and bottom scales, respectively, as indicated on the chart legend.

The density log porosity curve, representing total formation porosity, illustrates the highly porous nature of this reservoir. The deep resistivity porosity curve, *Phi (R_d)*, is about 10 - 20 PU's less than total porosity, indicating water-filled porosity in the reservoir is much less than total formation porosity, and the reservoir is apparently hydrocarbon saturated. However, interconnected water-filled porosity in the flushed and invaded zones, as shown by *Phi (R_{xoc})* and *Phi (R_i)*, are also considerably less than total formation porosity, as they approach the deep resistivity porosity curve. If the uninvaded zone in this reservoir is hydrocarbon saturated, that saturation is nearly the same as in the flushed and invaded zones, indicating extremely poor movability of any hydrocarbons in the reservoir. The *MHI* curves are running along between 0.7 and 0.8, greater than the 0.6 cutoff noted by Asquith (1982, p. 97), supporting the information illustrated by the resistivity porosity curves.

The poor hydrocarbon movability apparent on Figure 7.34 could be an indication that this highly porous reservoir is not highly permeable. Furthermore, the very low values of interconnected, water-filled porosity in the flushed zone (Figure 7.34) suggests

that much of the Canyon Lime porosity is comprised of isolated vugs. Any hydrocarbons saturating the pore system of this reservoir will be virtually unproducible. Data from a sonic log, in addition to the density log, would have added excellent support to the interpretation in determining the character of the porosity in the Canyon Reef in this well.

Variable *m*. The use of the standard value for the Archie empirical parameter *m* requires the assumption that the reservoir pore system is predominantly one of interconnected voids associated with interparticle porosity. If examination of the petrophysical parameters suggests that the pore geometry of the Canyon Lime reservoir is not well connected, then the use of a fixed value for Archie's empirical parameter $m = 2.0$ in developing the data plotted on the charts in Figures 7.33 and 7.34 is incorrect. Consequently, values for the petrophysical parameters that include *m* in their calculation would be incorrect, and an interpretation that the results indicate a hydrocarbon-saturated reservoir would be invalid. It would warrant petrophysical analysis using a variable *m* in developing the multiple parameter approach.

The only porosity log available in this well is density porosity, therefore the Nugent method for variable *m* can not be used. However, the method of Focke and Munn (1987) can be applied in vuggy carbonates with one porosity log. The Focke and Munn relationships for vuggy limestones, Rock Type 4, Permeability Class 2 and 3, were used in this well to compute values for variable *m* in this Canyon limestone reservoir.

Figure 7.35 is a Resistivity Porosity-MHI chart for the Canyon Reef in which the resistivity porosity calculations for the reservoir interval were revised using a variable *m* value that ranged from 2.6 to 3.9,with an average of 3.2. Now, Phi (R_{xoc}) and Phi(R_i) nearly overlay Phi (*Den*), indicating water-filled porosity in the flushed and invaded zones nearly equals total formation porosity, and water-filled porosity in the uninvaded zone is only 3-6 PU's less that total porosity. These results indicate that water saturation in the effective porosity of the reservoir is high and hydrocarbon saturation is low, in contradiction of the data on Figure 7.34, which indicated a reservoir thoroughly saturated with poorly moved hydrocarbons.

Water Saturation-Relative Permeability Chart

Figure 7.36 is the Water Saturation-RelPerm chart for the Canyon Reef reservoir. The curves and scale references are the same as on Figure 7.31. Note the difference between Archie water saturation curve developed using a fixed value for Archie's empirical parameter $m = 2.0$ and the Ratio water saturation curve. Values computed for S_{wa} using a fixed m = 2.0 range from 0.20 to 0.40, and average 0.29, while S_{wr} values range from about 0.5 to 0.7. When values for Archie water saturation fall well below Ratio water saturation, it indicates that the value used for the empirical parameter m in the water saturation calculation could be too low due to the presence of vuggy porosity. The poor hydrocarbon movability indicated on Figure 7.34 could be a result of vuggy porosity in which there is a variable pore body to pore throat ratio across the extent of the reservoir, and a variable m is required. It represents a hydraulically as well as an electrically heterogeneous pore system.

Note the second Archie water saturation curve on Figure 7.36 developed using the variable m from Focke and Munn, with an average water saturation value of 0.68. The water saturation computed using a variable m relationship falls within the upper limit of the range of Ratio water saturation values. Ratio water saturation is calculated without using a value for the Archie empirical parameter m, and supports the S_{wa} values computed using variable m as a more accurate representation of actual saturation conditions in the Canyon Lime.

The two relative permeability curves were developed using water saturation from variable m. One would expect a very highly water cut production stream at best with this relative permeability relationship.

Production-Calibrated Ranking System Histograms

The Permian Basin carbonate reservoirs examined in this study were not part of a field study like the Prue, correlated to wells with a range of production results. It was an attempt to determine if the multiple parameter approach to petrophysical analysis can be applied to reservoirs beyond the Prue. Values in some of the parameter ranges had to be

adjusted, but the logic and direction of the ranges established in the Prue were maintained. The examples of these Permian Basin carbonates represent the kind of approach that would be required in an exploration setting, where general parameter logic and ranges would be needed, rather than the controlled evaluation appropriate in a field development setting. As the multiple parameter approach is applied more broadly in field studies, its value in exploration should be enhanced.

Figure 7.37 is the legend for the Petrophysical Interpretation Ranking System Histogram charts for the Permian Basin carbonate reservoirs. As with the Prue Sands, histograms of scored output from individual petrophysical parameters examined in the carbonates are arranged across each ranking system chart. The left side of a chart begins with the four reservoir quality parameters noted on Figure 7.37. Seven petrophysical parameters intended to detect the presence and movability of hydrocarbons and the presence of excess conductivity follow to the right of the four reservoir quality parameters. Seven additional petrophysical parameters to evaluate aspects of water saturation are displayed toward the right side of the chart. In each of the individual parameter histograms, the scores represented by the vertical columns decrease progressively from *5* to *–1*, proceeding from left to right across each histogram. Not all scores will be present on each histogram; a legend to identify the scores represented by the individual vertical columns in each histogram has been placed on each chart.

Fusselman

Figure 7.38 is the ranking histogram for the Fusselman well. The results scored on this chart are based on petrophysical calculations using a fixed value for Archie's empirical parameter $m = 2.0$. Scores for the reservoir quality parameters SP and *Phi* are 85% to 90 % (4s) and (5s). The measure of secondary porosity, *Phi(Son/Den)*, is about 90% (4s) and (5s), indicating the reservoir has very little isolated secondary porosity, although about 5 – 10% of formation porosity could be secondary vugs. The shallow to deep resistivity ratio, a measure of invasion, is scored 90% (1s) and (2s), and suggests the reservoir could be low permeability with minimal invasion. Alternativly, if the invaded

zone of a reservoir is well swept, with minimal residual hydrocarbon saturation, then the hydrocarbon and saline connate water-filled pores in the uninvaded zone could be as resistive as the mud filtrate-filled pores in the invaded zone. Results from the hydrocarbon detection and movability parameters and water saturation assessment parameters suggest that that is a reasonable interpretation.

Scores for the FMOP, Resistivity Porosity and MHI indicators are all in the range of 75% to 95% (5s). Scores for the relative permeability to oil parameter, *kr* is 100% (5s). The methods have detected the presence of well-saturated, highly movable hydrocarbons in this Fusselman reservoir. Scores for water saturation parameters are all 90% to 100% (5s). The S_{wr} : S_{wa} Consistency Comparator indicates that over 95% of the Archie water saturation values based on a fixed $m = 2.0$, fall within the range of Ratio water saturation values and promotes confidence in the calculated water saturation values. The score of (4) for the *BVW_SD* parameter demonstrates there is very little scatter in the BVW data, suggesting the reservoir is at irreducible water saturation. If the reservoir is at irreducible water, then score of (4) for the BVW parameter indicates the reservoir pore type is predominantly vuggy + intercrystalline porosity.

Figure 7.39 is the ranking histogram for the Fusselman with the petrophysical parameters calculated using variable *m* values determined by the Nugent method. There is very little difference between the petrophysical parameter scores on this chart and those on Figure 7.38. As noted on Figure 7.31, the average value for variable *m* in the Fusselman is 2.25, not significantly different from the fixed $m = 2.0$. Some excess conductivity is suggested by the (0) scores in *FMOP_*R_{xoc} and *PhiResA(*R_{xoc}*)* parameters. Consistent with its description as a cherty dolomite, the excess conductivity could be the result of some microporous chert in the Fusselman mode. The S_{wr} : S_{wa} consistency comparator, predominantly ranked with a score of (3), indicates that Archie water saturation from variable *m* is a bit more neutral in the range of Ratio water saturation values than was Archie water saturation from fixed $m = 2.0$. Comparing scores for the *BVW_SD* parameter on Figures 7.38 and 7.39 indicates there is more scatter in bulk volume water data calculated from Archie water saturation based on a variable *m* than

was found in bulk volume water data calculated Archie water saturation based on a fixed m. The increased scatter is a response to what appears to be more variability in pore types in the reservoir. The percentage of (3') and (4s) in the BVW parameter in this analysis indicates about 55% of the pore system is intercrystalline and 40% is vuggy + intercrystalline. This range of pore types supports the finding that the average variable m value of 2.25 represents a pore system dominated by regular pore throat-pore body interconnections.

Canyon Lime

Figure 7.40 is the ranking histogram for the Canyon Reef reservoir based on petrophysical parameters calculated using a fixed value for Archie's empirical parameter $m = 2.0$. The Canyon reservoir scored over 65% (5s) for the SP and *Phi* parameters and the invasion parameter, R_i/R_d, is over 80% (4s) and (5s), indicating good reservoir quality. Because there is no sonic data, the secondary porosity parameter is blank.

The *FMOP*, *PhiResA* and *MHI* parameters all score 95% (2s), which is a very weak indicator for the presence of movable of hydrocarbons in the reservoir. However, Archie water saturation from fixed $m = 2.0$, $S_{wa}F_{xd}\_m$, is scored 100% (4s) and (5s) and *Kr*, based on $S_{wa}F_{xd}\_m$ is scored 100% (5s). The ranking difference between the hydrocarbon movability and saturation petrophysical parameters indicates that the Canyon Lime reservoir is saturated with hydrocarbons of limited movability Furthermore, there is a discrepancy between $S_{wa}F_{xd}\_m$ and S_wVar_m parameters. Scores for S_wVar_m are predominantly (2s) and Ratio water saturation values, $S_{wr}1/2$ and $S_{wr}1/5$, are predominantly (2s) and (3s). The score for the $S_{wr} : S_{wa}$ parameter is predominantly (–1s), which indicates a marked discrepancy between Archie water saturation calculated using a fixed $m = 2.0$ and the Ratio water saturation data. This discrepancy represents a condition that requires the interpreter's attention to reexamine the Archie and Ratio water saturation calculations.

A score of (2) in the *BVW_SD* parameter indicates that scatter in the bulk volume water data is high. However, if the reservoir is at irreducible water saturation and BVW

data represents the texture of this Canyon Lime reservoir, then scores of (1) and (0) for the BVW parameter indicate that the predominant pore type would be extremely fine chalky porosity, possibly in an argillaceous lime matrix. In contrast, with the value of the Ratio water saturation parameters much greater than Archie water saturation (Figure 7.36), it indicates the value of the empirical parameter *m* used to calculate Archie water saturation may be too low. If that is the case, it indicates the porosity of the Canyon Lime reservoir should be vuggy rather than chalky (Asquith, 1985). At this point, sample descriptions from a core or cuttings can provide valuable input to petrophysical interpretation to determine if chalky porosity represents the dominant pore type in this Canyon Reef reservoir. If it does not, then the bulk volume water data scatter is probably associated with a reservoir in or below the transition zone and strong water cut should be expected.

Figure 7.41 is the ranking histogram for the Canyon reservoir with all parameters based on variable *m* values generated from the Focke and Munn relationships. The reservoir quality parameters are unchanged from Figure 7.40 because the value for empirical parameter *m* is not used in any of those relationships.

The FMOP, PhiRes and MHI parameters, with scores in excess of 90% 2*s*, indicate poor hydrocarbon movability in this reservoir. With (0) representing over 50% of the RelPerm scores, it indicates the RelPerm to water is greater than RelPerm to oil across most of the Canyon reservoir and the RelPerm to oil parameter scores appear much worse than on Figure 7.40.

Archie water saturation from variable *m* is scored with over 90% (2s). The Ratio water saturation parameters do not use the empirical parameter *m* and are unchanged from Figure 7.40. The $S_{wr} : S_{wa}$ parameter indicates that about 60% of the Archie water saturation from variable *m* values fall within the range of Ratio water saturation values, which improves confidence in those values from those Archie water saturation values calculated with a fixed $m = 2.0$. Figure 7.36 demonstrates that the Archie water saturation values from variable *m* that are higher than the range of Ratio water saturation

values are only slightly higher, and probably represent reasonable values of calculated water saturation for this Canyon Reef reservoir.

A score of (0) for the BVW_SD parameter shows that the scatter of BVW data calculated from S_{wa} *Var_m* is very high. If the scatter in BVW data represented texture at irreducible water saturation conditions, the BVW parameter indicates that the associated pore type would have to be an extremely fine chalky-argillaceous reservoir. If that is not a reasonable characterization of the texture of this reservoir, then the BVW scatter represents a reservoir that is not at irreducible water saturation.

Summary: Permian Basin Carbonates

A multiple parameter approach to petrophysical analysis in Permian Basin carbonates has accurately identified a Fusselman dolomite as a reservoir with a predominantly intercrystalline pore system, that is well saturated with highly movable hydrocarbons. Interpretation of the analytical results through a scored ranking system showed that the Fusselman earned a very high percentage of the highest score representing a producible accumulation of hydrocarbons. This would provide an operator the basis not only to recommend the zone be tested, but to expect top rate results from the test.

The Canyon Reef was identified as a reservoir that could confound standard petrophysical analysis, in which the highly porous character could mislead an interpretation to incorrectly assess its value. Even without a sonic log, the multiple parameter approach identified the potential problem with the standard analysis, lack of movable hydrocarbons and the potential for significant secondary pore volume, with consequent effect on the value of *m*. Uncritical reliance on standard assumptions in texturally complex reservoirs and relying only on only one analytical parameter, standard Archie water saturation, led to interpretation failure in this reservoir. Those problems were highlighted in the multiple parameter approach, which also provided the means to develop analytical results that fairly represent the petrophysical character of the reservoir. The interpretation through the ranking histograms demonstrated that the Canyon should

not have been recommended as a test candidate. If tested, this Canyon reservoir would produce water, which is exactly what it did produce on test.

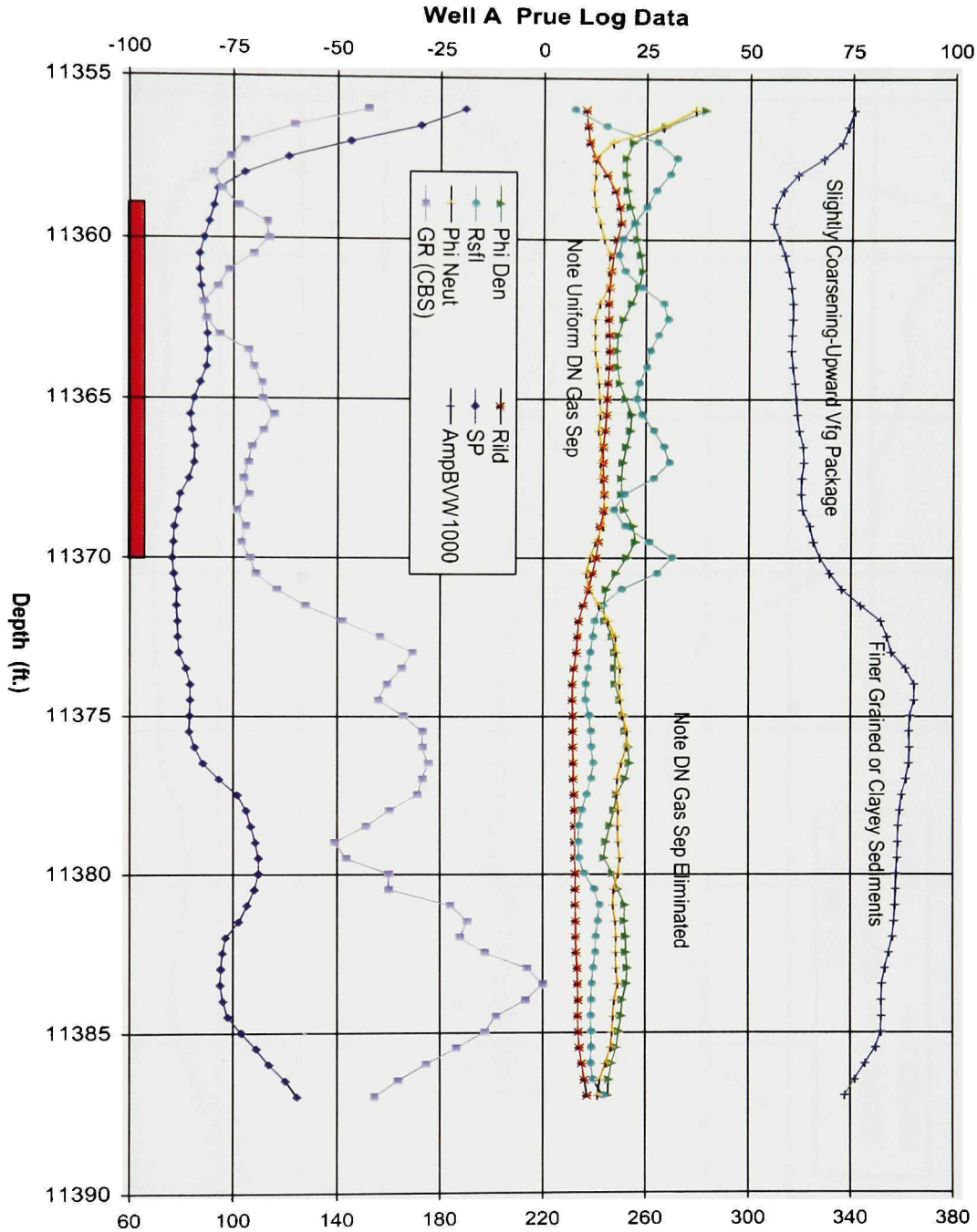

Figure 7.1 Well A Petrophysical Parameters Chart: Plot of Prue Basic Log Data and Amplified *BVW* (x 1000) Curve. IP = 4.9 mmscfd + 30 bcpd and No Water. Cumulative Production = 2.9 bcfg Over 78 Months.

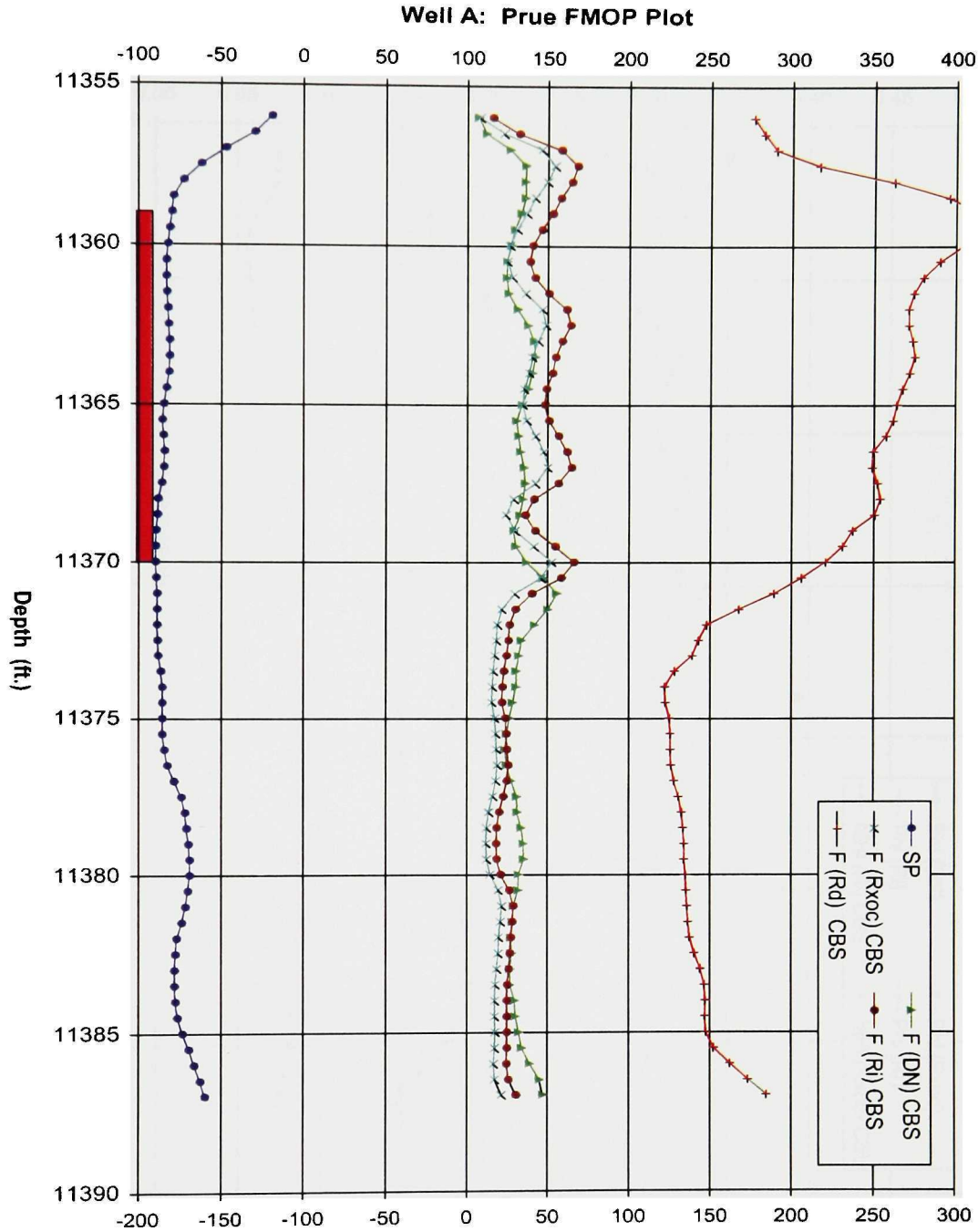

Figure 7.2 Well A Petrophysical Parameters Chart: FMOP. IP = 4.9 mmscfd + 30 bcpd and No Water. Cumulative Production = 2.9 bcfg Over 78 Months.

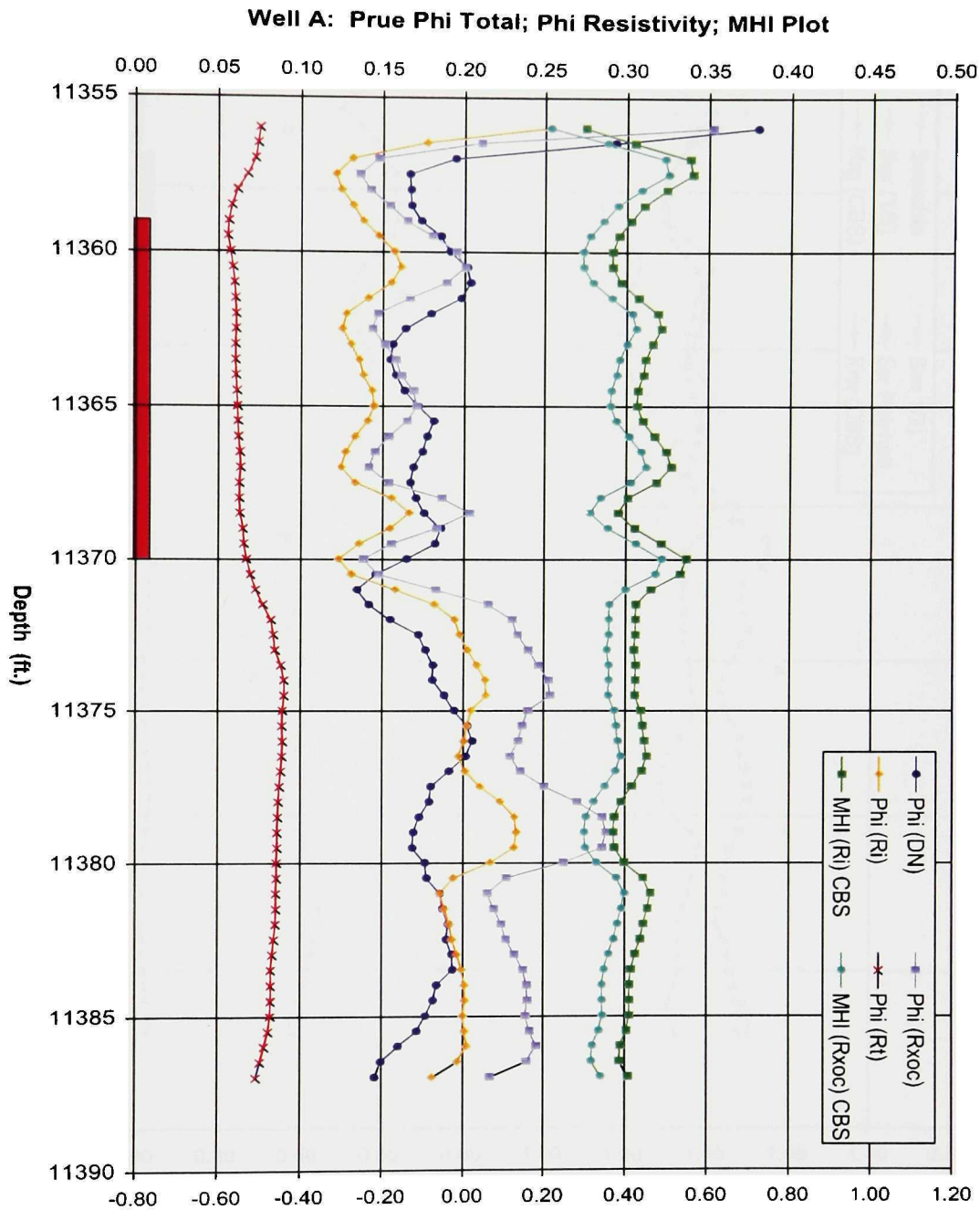

Figure 7.3 Well A Petrophysical Parameters Chart: Plot of Resistivity Porosity and Movable Hydrocarbon Index. IP = 4.9 mmscfd + 30 bcpd and No Water. Cumulative Production = 2.9 bcfg Over 78 Months.

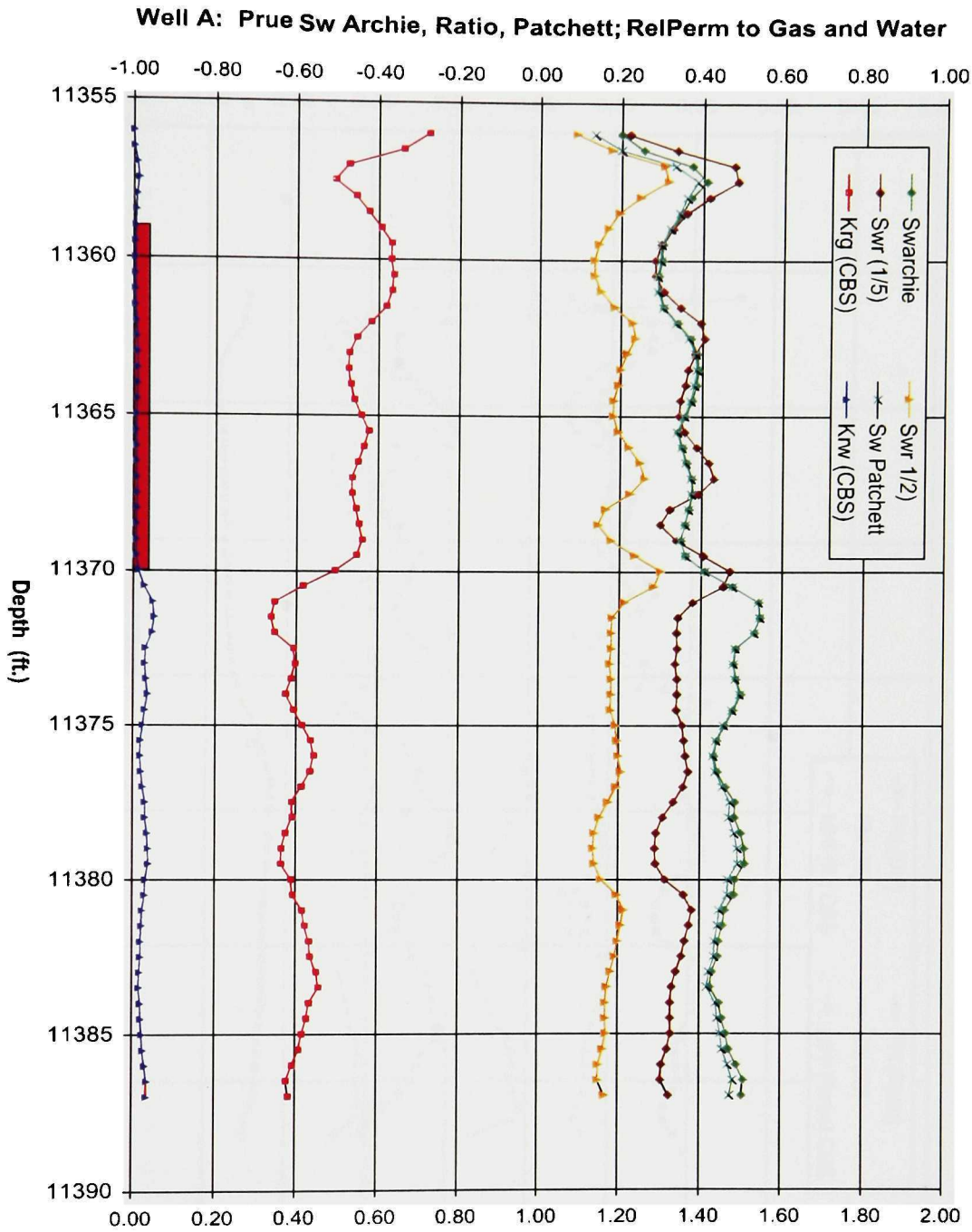

Figure 7.4 Well A Petrophysical Parameters Chart: Plot of Calculated Water Saturation Values and Relative Permeability to Gas and Water. IP = 4.9 mmscfd + 30 bcpd and No Water. Cumulative Production = 2.9 bcfg Over 78 Months.

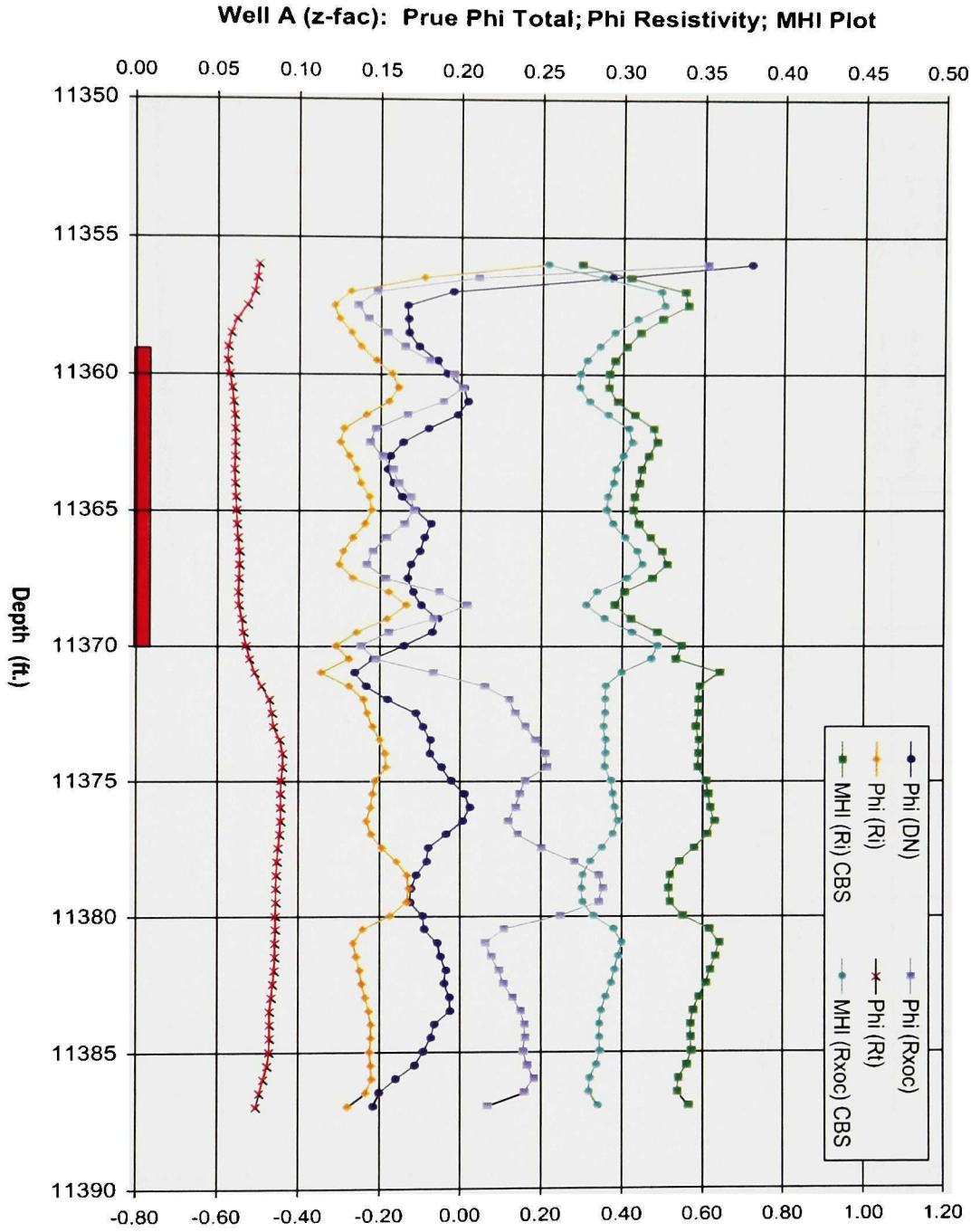

Figure 7.5 Well A Petrophysical Parameters Chart: Applied AEP m = 2.0 and Z Factor = 0.175 to PhiRes and MHI. IP = 4.9 mmscfd + 30 bcpd and No Water. Cumulative Production = 2.9 bcfg Over 78 Months.

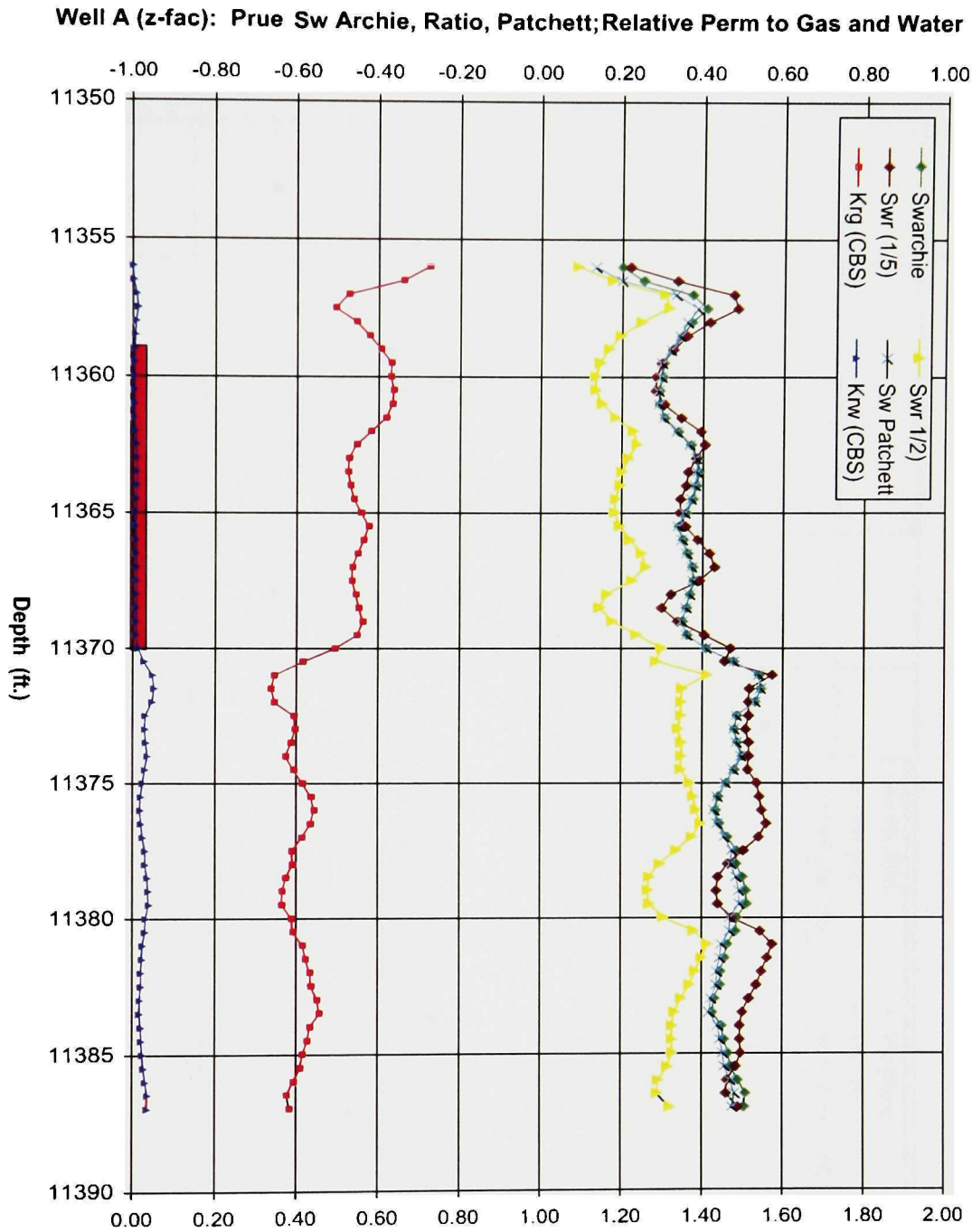

Figure 7.6 Well A Petrophysical Parameters Chart: Applied AEP m = 2.0 to Swa and Swptcht and Z Factor = 0.175 to Swr. IP = 4.9 mmscfd + 30 bcpd and No Water. Cumulative Production = 2.9 bcfg Over 78 Months.

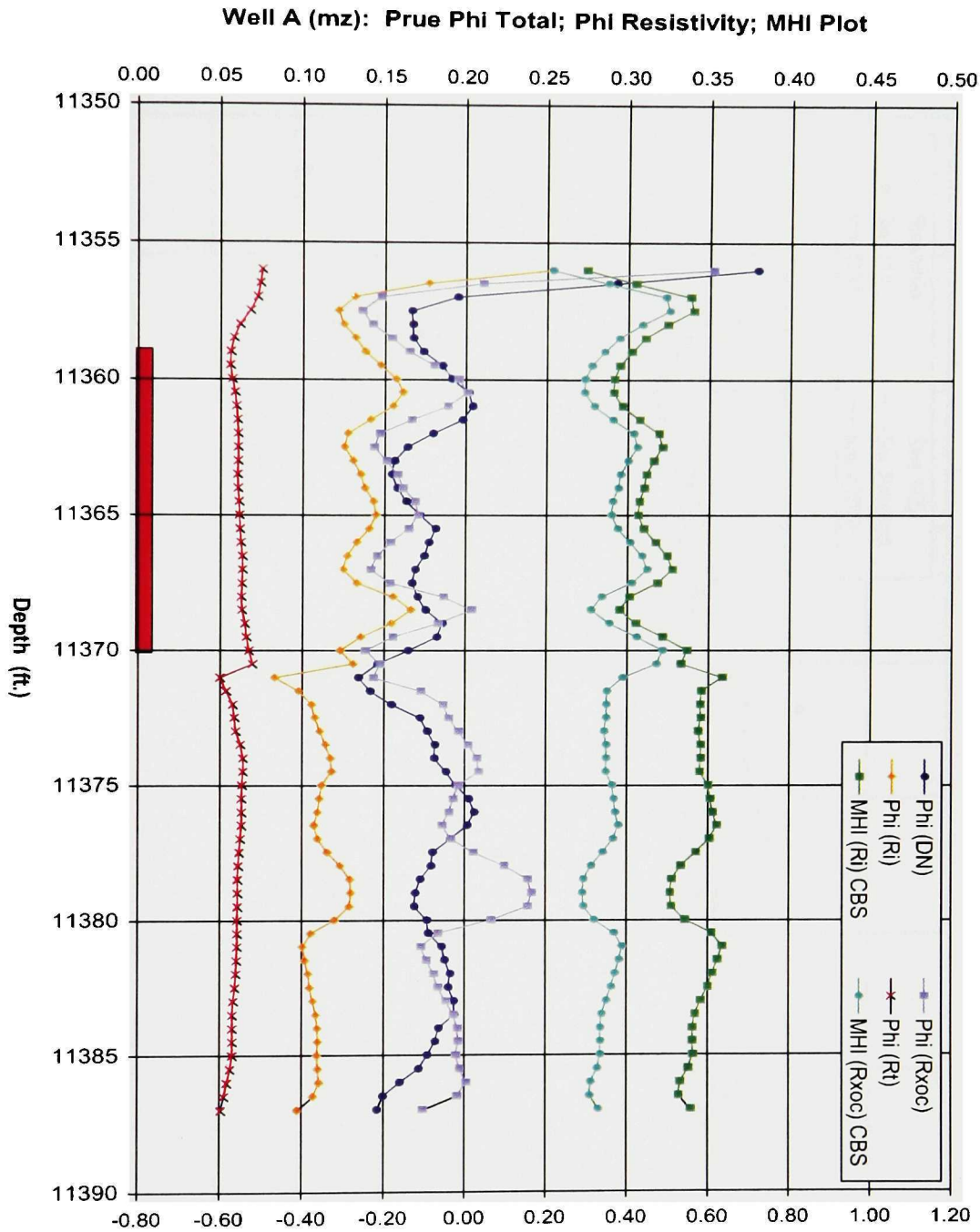

Figure 7.7 Well A Petrophysical Parameters Chart: Applied AEP m = 1.75 and Z Factor = 0.175 to PhiRes and MHI. IP = 4.9 mmscfd + 30 bcpd and No Water. Cumulative Production = 2.9 bcfg Over 78 Months.

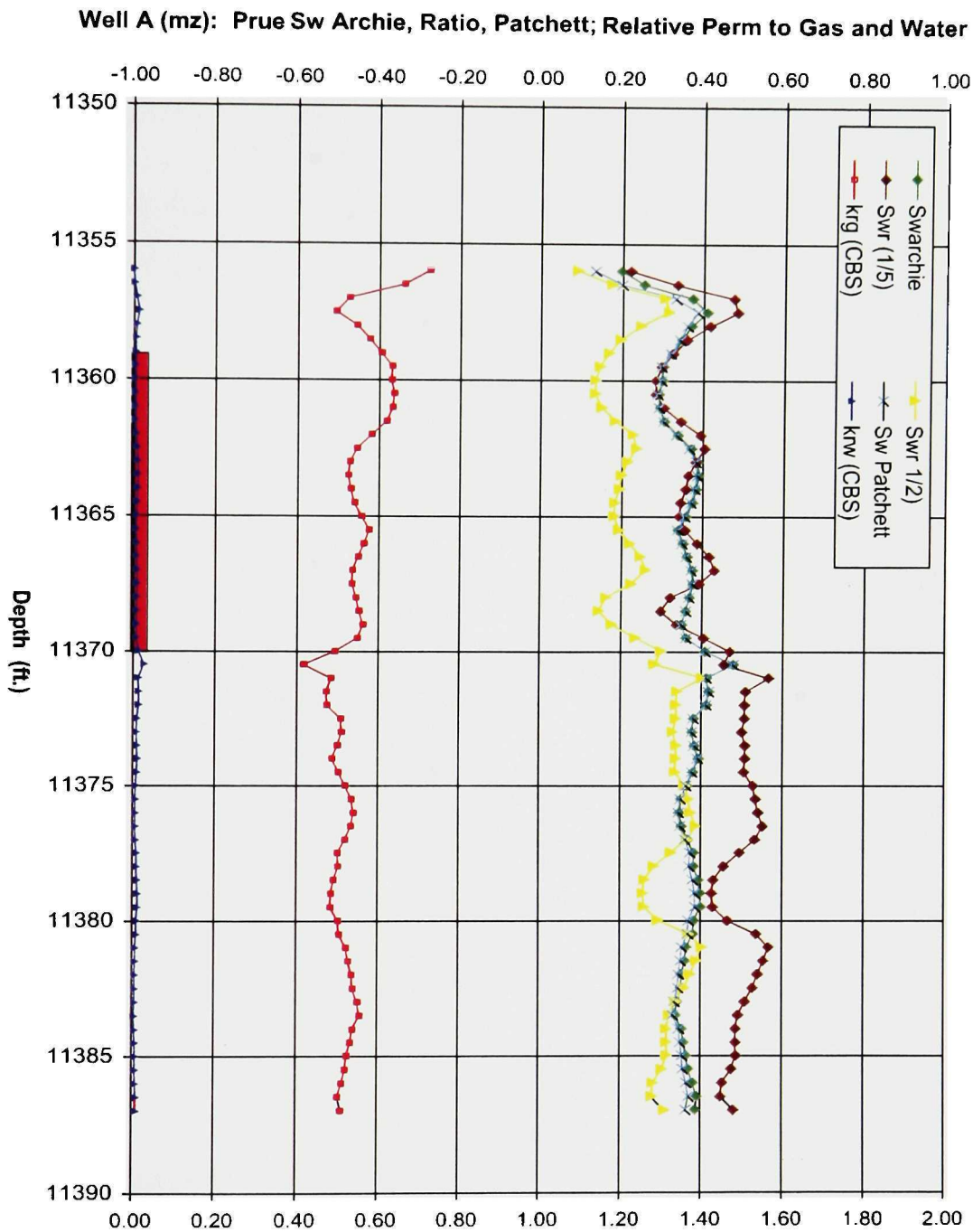

Figure 7.8 Well A Petrophysical Parameters Chart: Applied AEP m = 1.750 to Swa and Swptcht and Z Factor = 0.175 to Swr. IP = 4.9 mmscfd + 30 bcpd and No Water. Cumulative Production = 2.9 bcfg Over 78 Months.

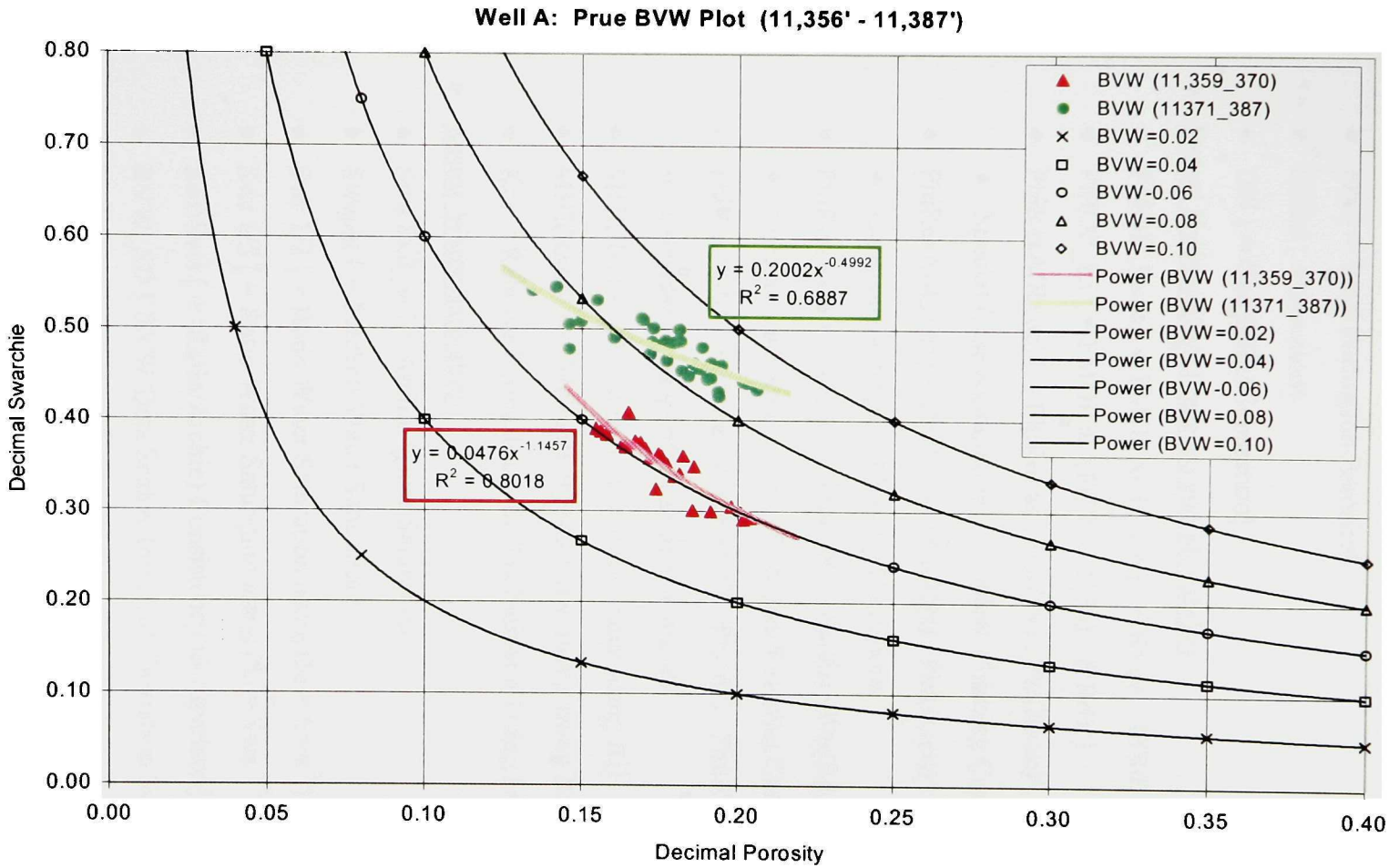

Figure 7.9 Well A Buckles -Type BVW Plot For Separate Intervals, 11,359 ft. - 11,370 ft. And 11, 371 ft. - 11,387 ft.

- Assess Reservoir Quality
  - SP
  - Phi [= Total Formation Porosity]
  - Ri/Rd [= Invasion]
  - DN [= Gas Effect Separation]
- Detect Hydrocarbon Presence and Movability
  - FMOP_Rxoc [= FMOP as {F(DN) : F(Rxoc) : F(Rd)}]
  - FMOP_Ri [= FMOP as {F(DN) : F(Ri) : F(Rd)}]
  - PhiResA(Rxoc) [= PhiRes as {Phi(DN) : Phi(Rxoc) : Phi(Rd)}]
    - Special Case Assumption: Excellent Flushing Condition
  - PhiResA(Rxoc) [= PhiRes as {Phi(DN) : Phi(Rxoc) : Phi(Rd)}]
    - Considers a range of Flushing Conditions
  - PhiRes(Ri) [= PhiRes as {Phi(DN) : Phi(Ri) : Phi(Rd)}]
    - Special Case Assumption: Excellent Flushing Condition
  - PhiResA(Ri) [= PhiRes as {Phi(DN) : Phi(Ri) : Phi(Rd)}]
    - Considers a range of Flushing Conditions
  - MHI(Ri) [= Movable Hydrocarbon Index using Ri]
  - MHI(Rxoc) [= Movable Hydrocarbon Index using Rxoc]
  - Kr [= Relative Permeability to Gas Indicator Using krw/krg) Ratio]
- Assess Water Saturation
  - Swa Fxd_m [= Archie Water Saturation]
  - Swapat [= Patchett Water Saturation]
  - Swr 1/2 [= Ratio Water Saturation using (Si = Swa $^{1/2}$) Assumption]
  - Swr 1/5 [= Ratio Water Saturation using (Si = Swa $^{1/5}$) Assumption]
  - Swr:Swa [= (Ratio/Archie) Consistency Comparison]
  - BVW_SD [BVW Data Scatter from Std. Deviation Screen]
  - BVW [= Grain Size Group Assuming Reservoir @ Swirr]

Figure 7.10 Legend for Petrophysical Parameters Reported on the Ranking Calibration Histograms.

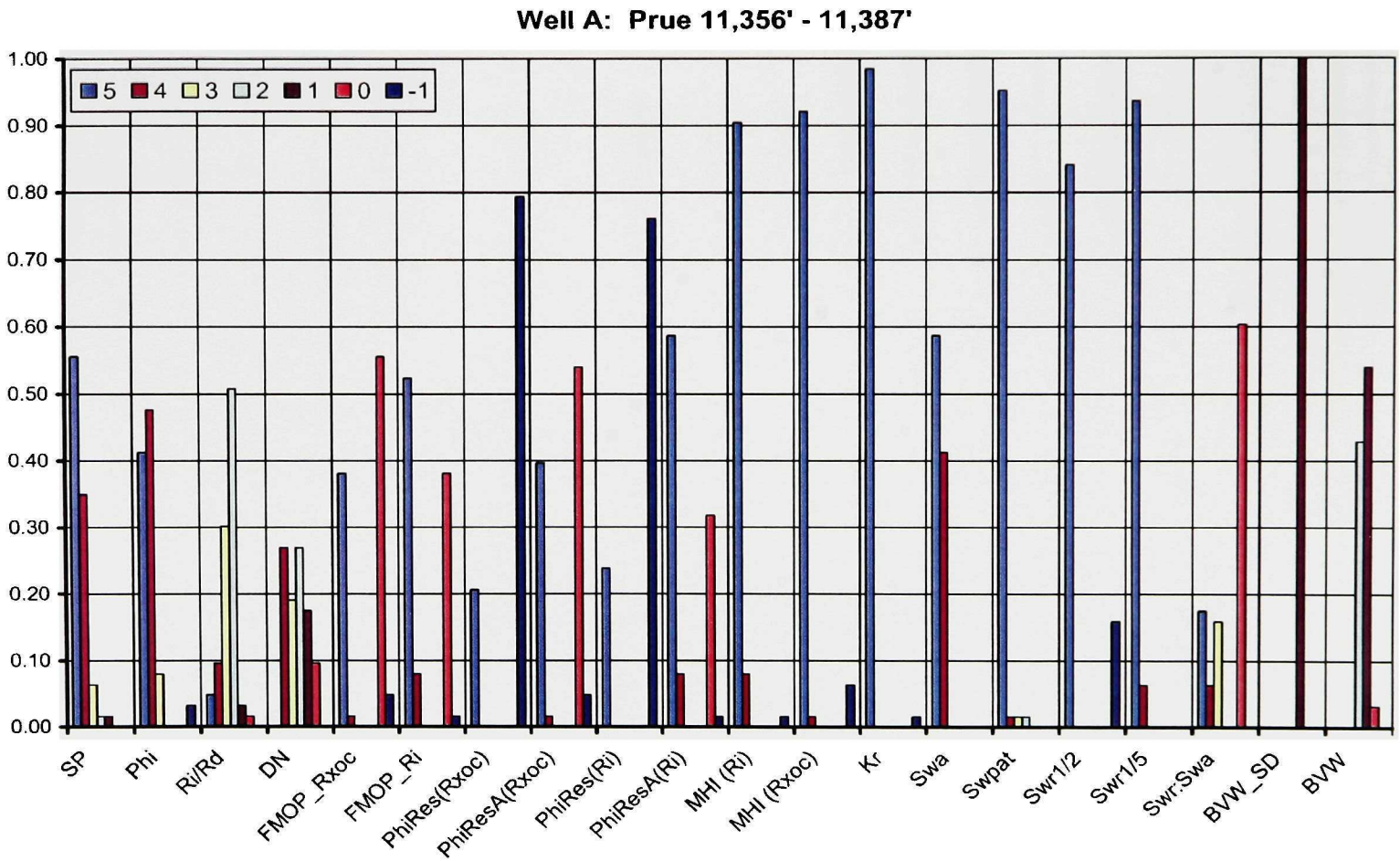

Figure 7.11 Production-Calibrated Ranking System Histogram for the SP - Defined Reservoir Interval, 11,356 ft - 11,387 ft, Represented by Figures 7.1-7.4.

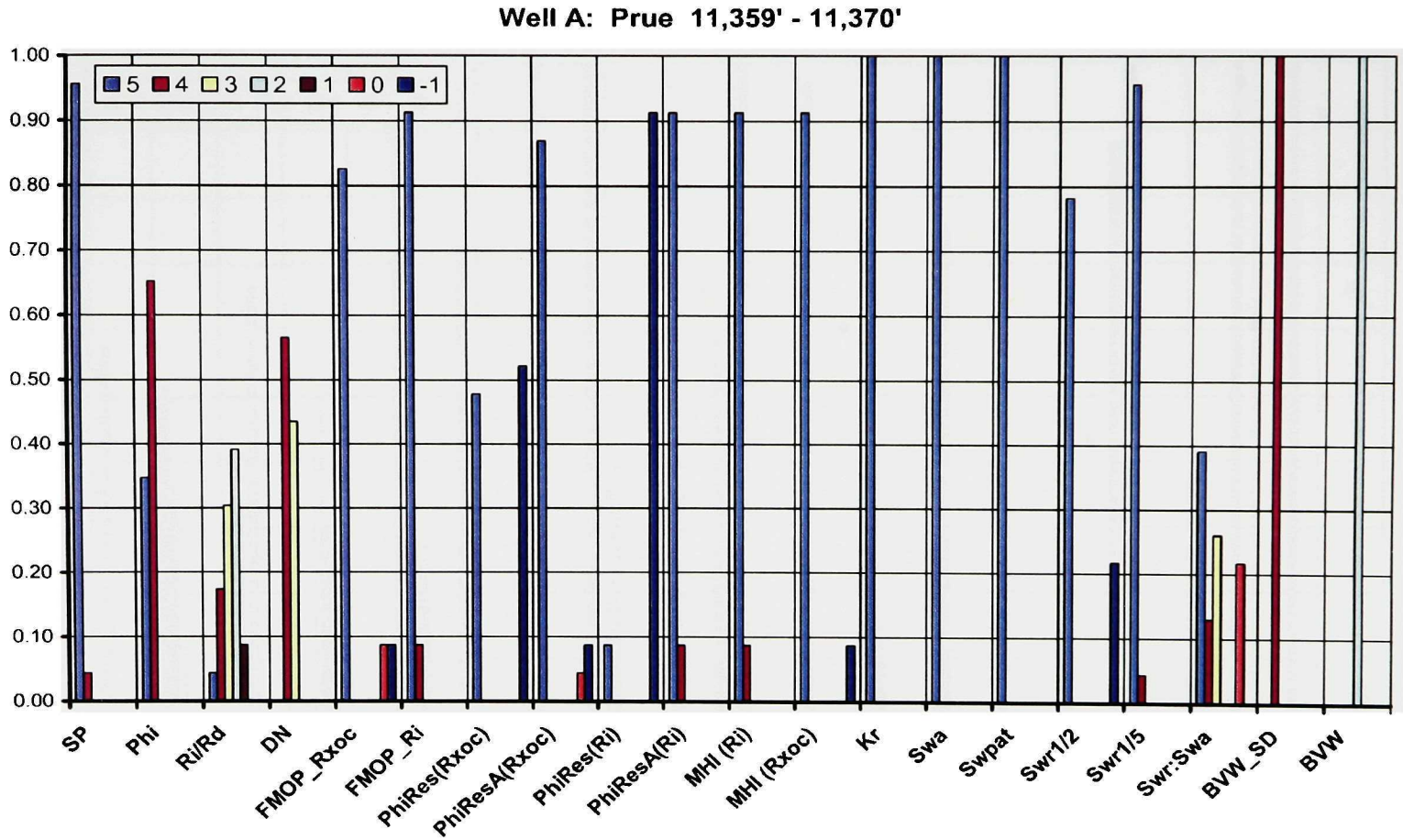

Figure 7.12 Well A Production-Calibrated Ranking System Histogram for the SP-Defined Reservoir Interval, 11,359 ft. - 11,370 ft., Represented by Figures 7.1-7.4. IP = 4.9 mmscfd + 30 bcpd and No Water. Cumulative Production = 2.9 bcfg Over 78 Months.

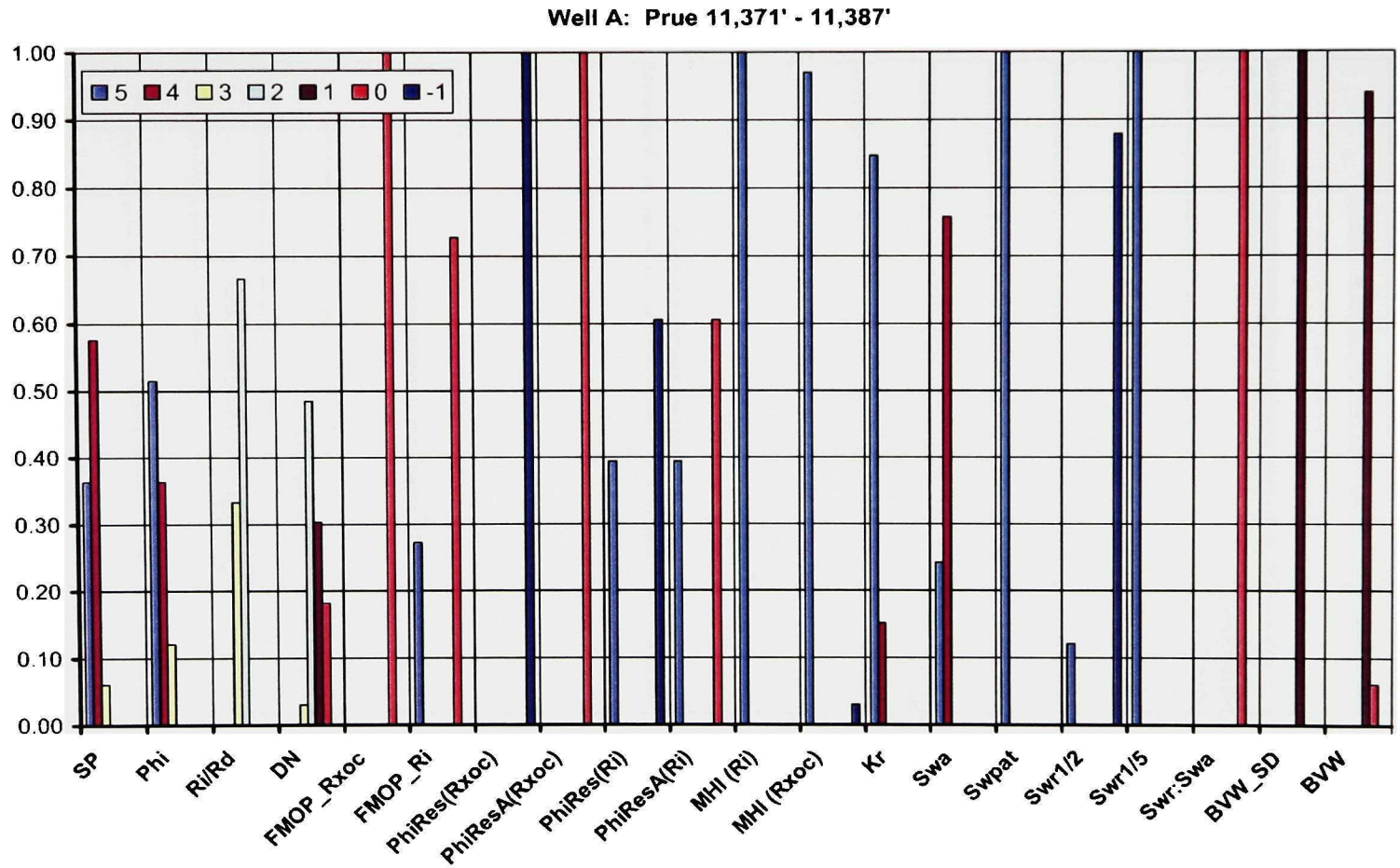

Figure 7.13 Well A Production-Calibrated Ranking System Histogram for the lower half of the SP-Defined Reservoir Interval, 11,371 ft.-11,387 ft.

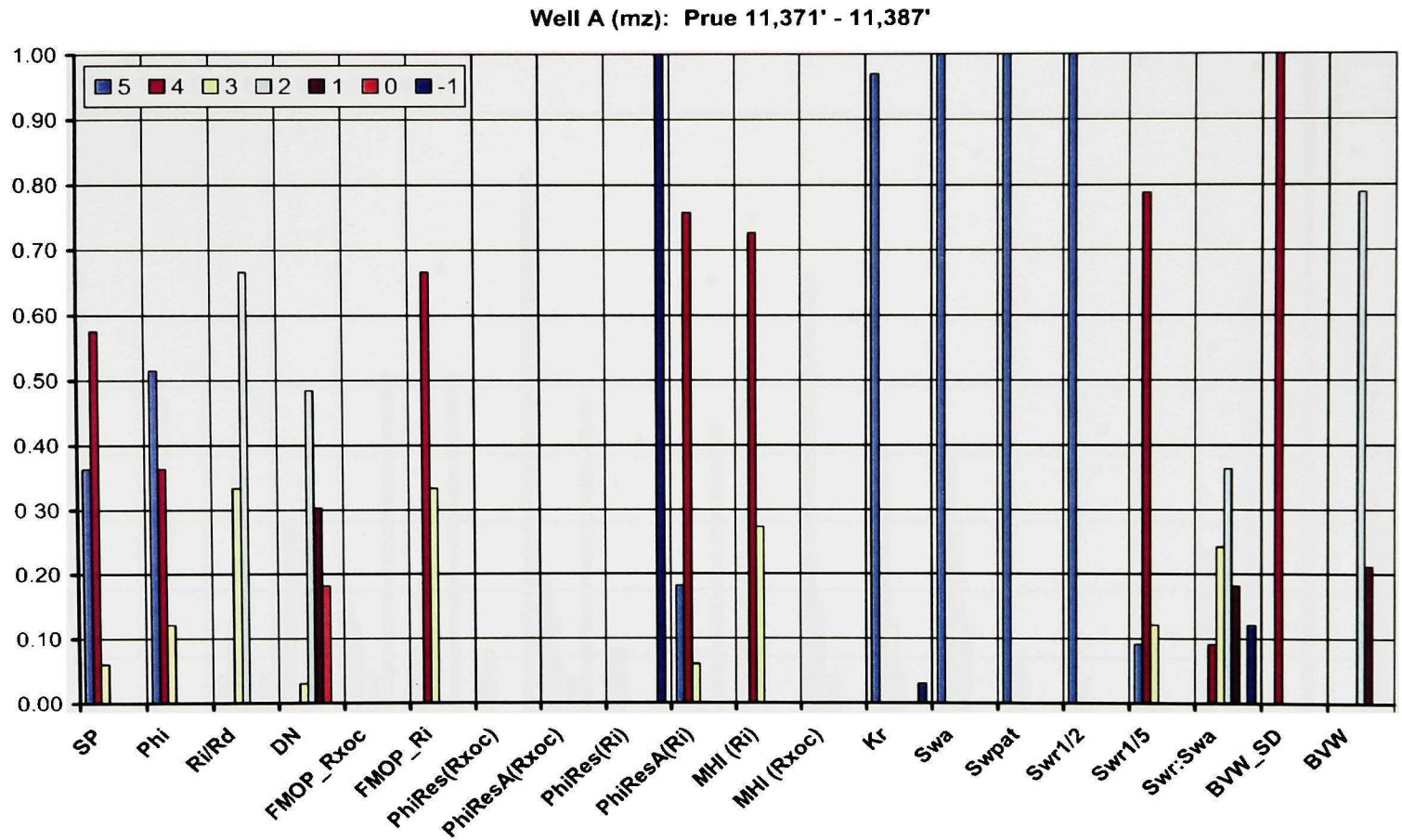

Figure 7.14 Well A Production-Calibrated Ranking System Histogram for the lower half of the SP-Defined Reservoir Interval, 11,371 ft.-11,387 ft., With Modified *m* and *z*.

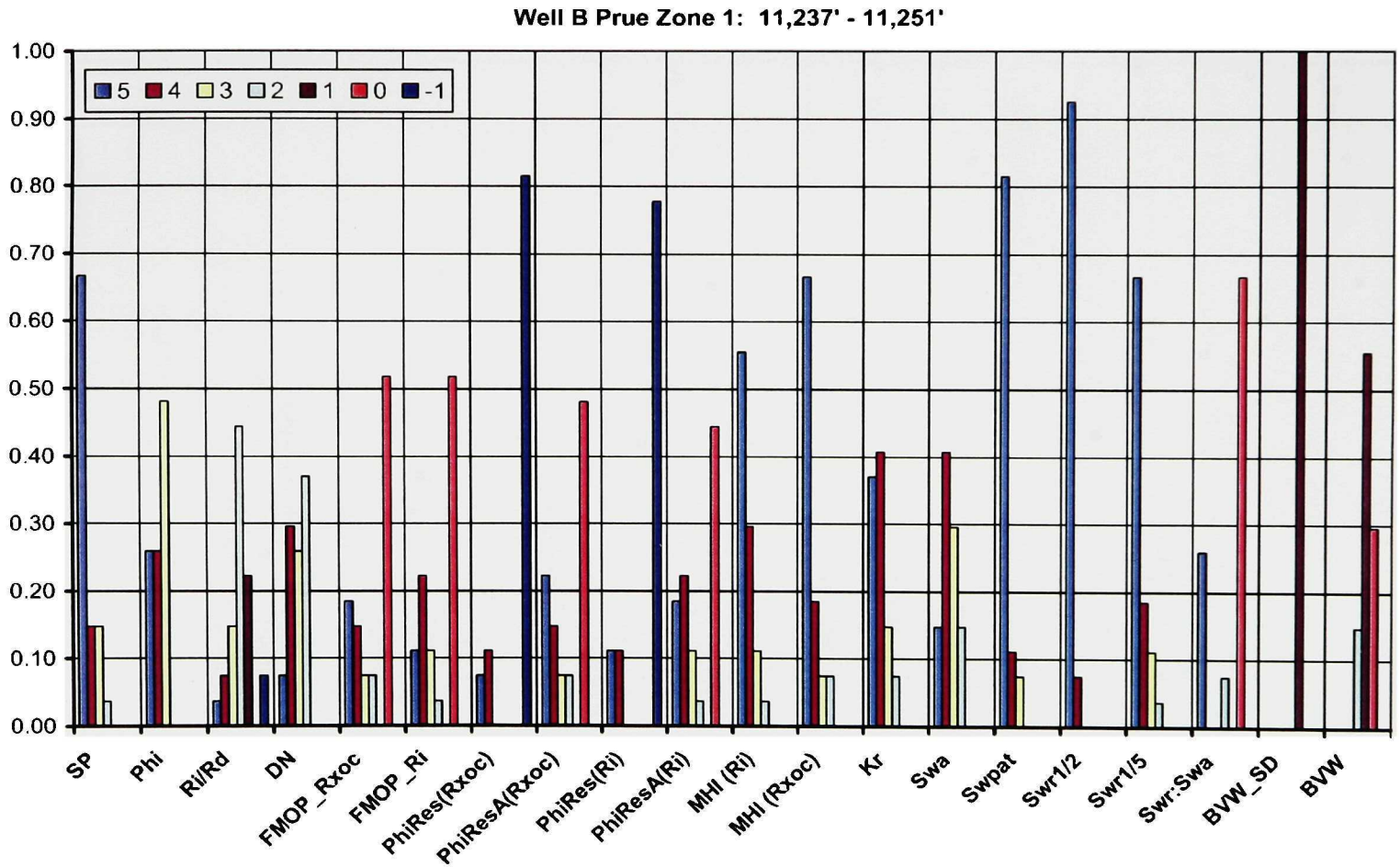

Figure 7.15 Well B Production-Calibrated Ranking System Histogram for the Perforated Interval, 11,237 ft. - 11,251'. IP = 2.46 MMSCFPD + 30 BCPD and No Water. Cumulative Production =1.45 BCFG over 112 Months.

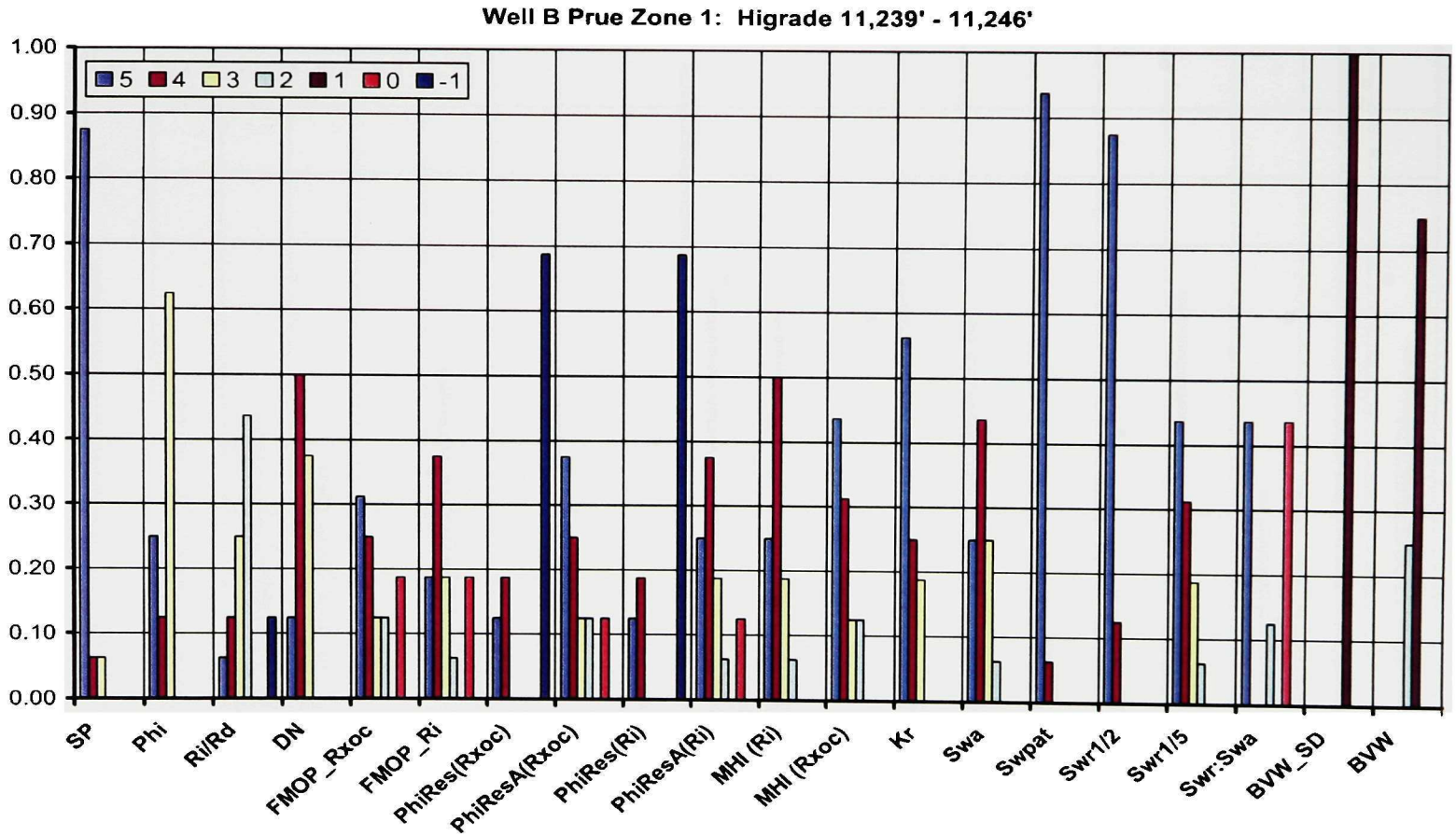

Figure 7.16 Well B Production-Calibrated Ranking System Histogram for the High Graded Interval, 11,239' to 11,246'. Perforated 11,237' - 11,251' with IP = 2.46 MMSCFPD + 30 BCPD and No Water. Cumulative Production =1.45 BCFG over 112 Months.

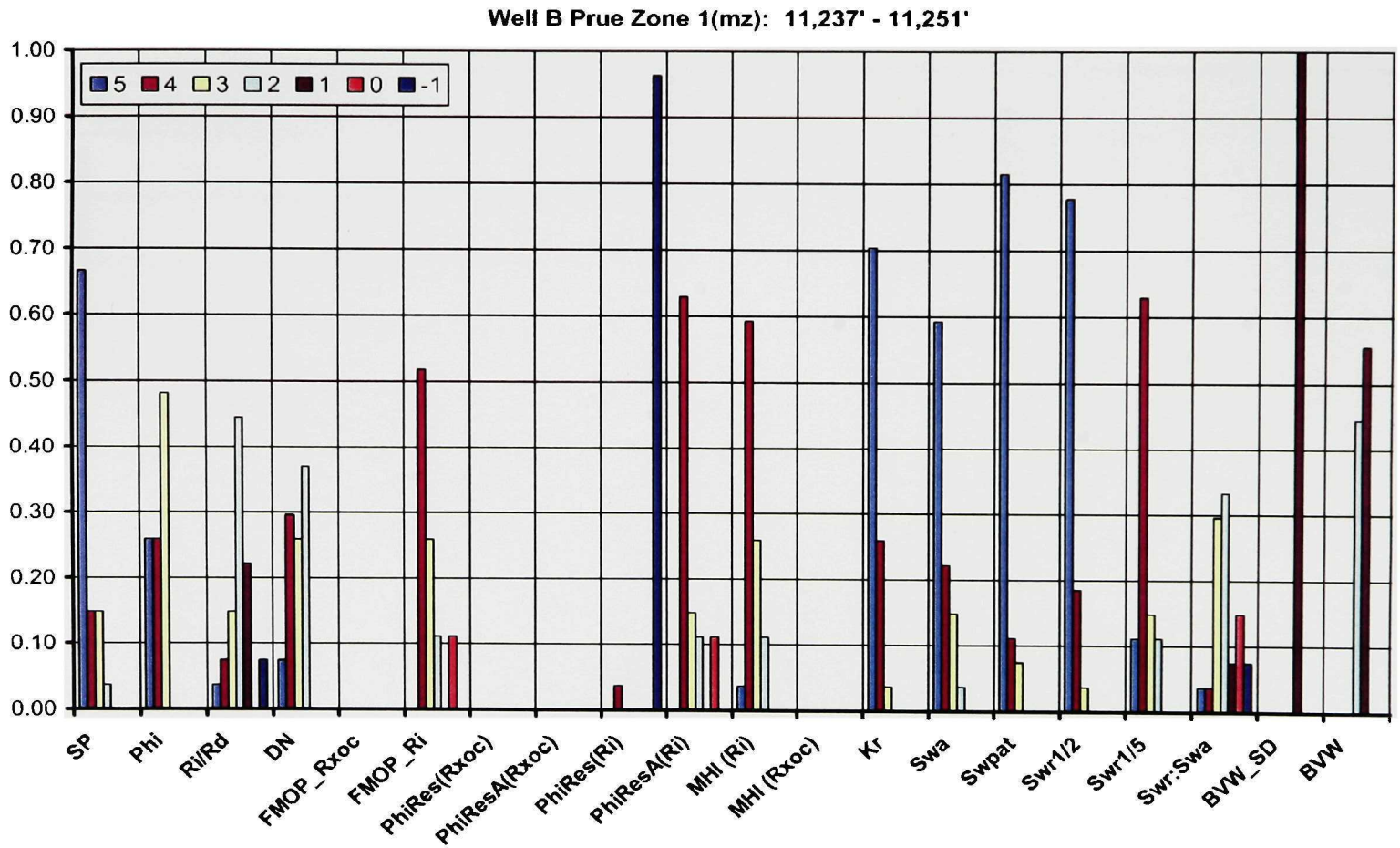

Figure 7.17 Well B Production-Calibrated Ranking System Histogram for the Perforated Interval, 11,237' - 11,251'. Modified Empirical Parameter *m* and *z*-factor for Excess Conductivity. IP = 2.46 MMSCFPD + 30 BCPD and No Water. Cumulative Production =1.45 BCFG over 112 Months.

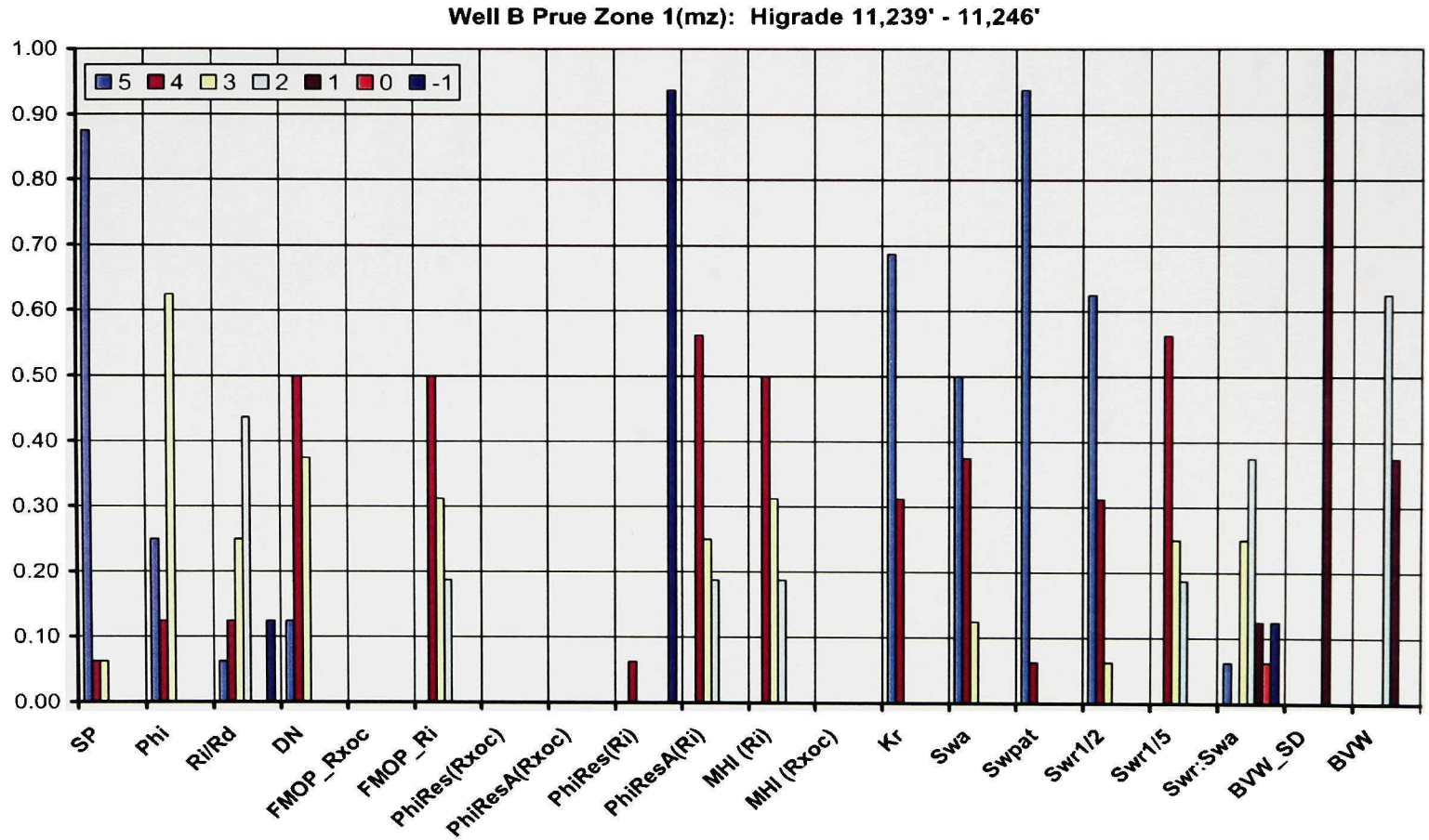

Figure 7.18 Well B Production-Calibrated Ranking System Histogram for the High Graded Interval, 11,239' to 11,246'. Modified Empirical Parameter *m* and *z*-factor for Excess Conductivity. Perforated, 11,237' - 11,251' with IP = 2.46 MMSCFPD + 30 BCPD and No Water. Cumulative Production =1.45 BCFG over 112 Months.

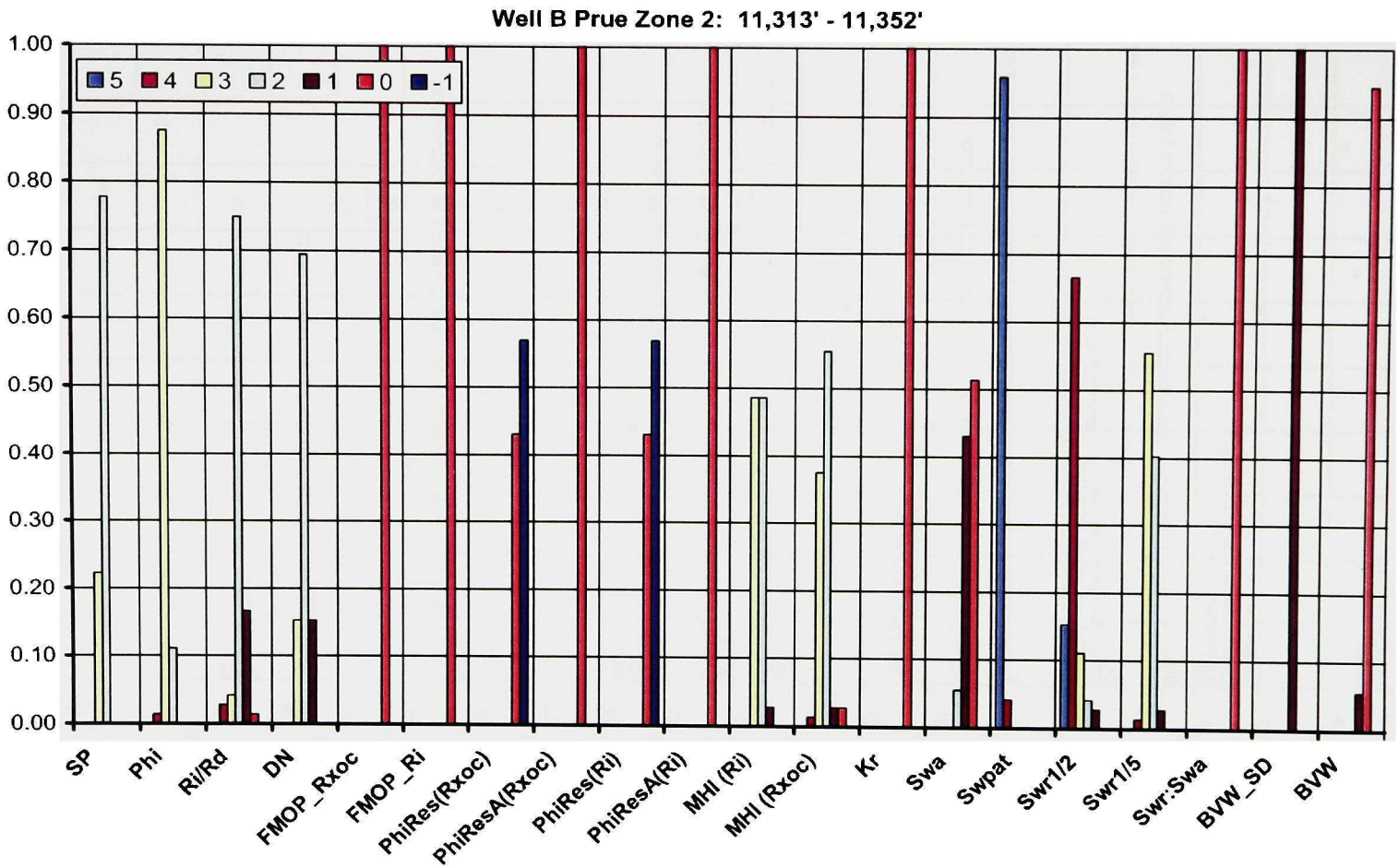

Figure 7.19 Well B Production-Calibrated Ranking System Histogram for the Second Prue Sand tested in Well B. Well was Hydraulically Fractured and Production Tested; No Results were Reported, but the Zone was Not Completed.

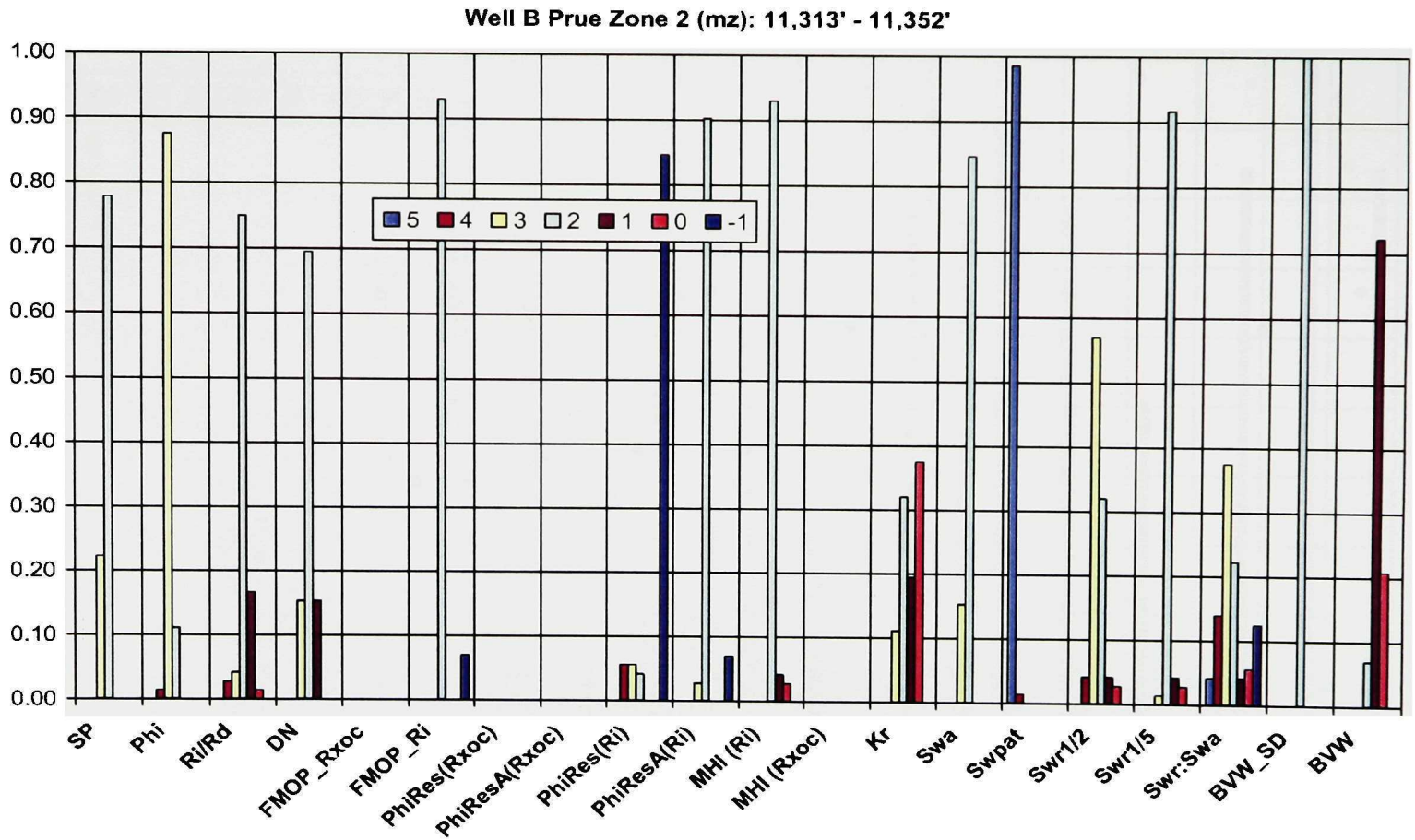

Figure 7.20 Well B Production-Calibrated Ranking System Histogram for the Second Prue Zone tested in Well B, With Modified *m* and *z*. Well was Hydraulically Fractured and Production Tested; No Results were Reported, but the Zone was Not Completed.

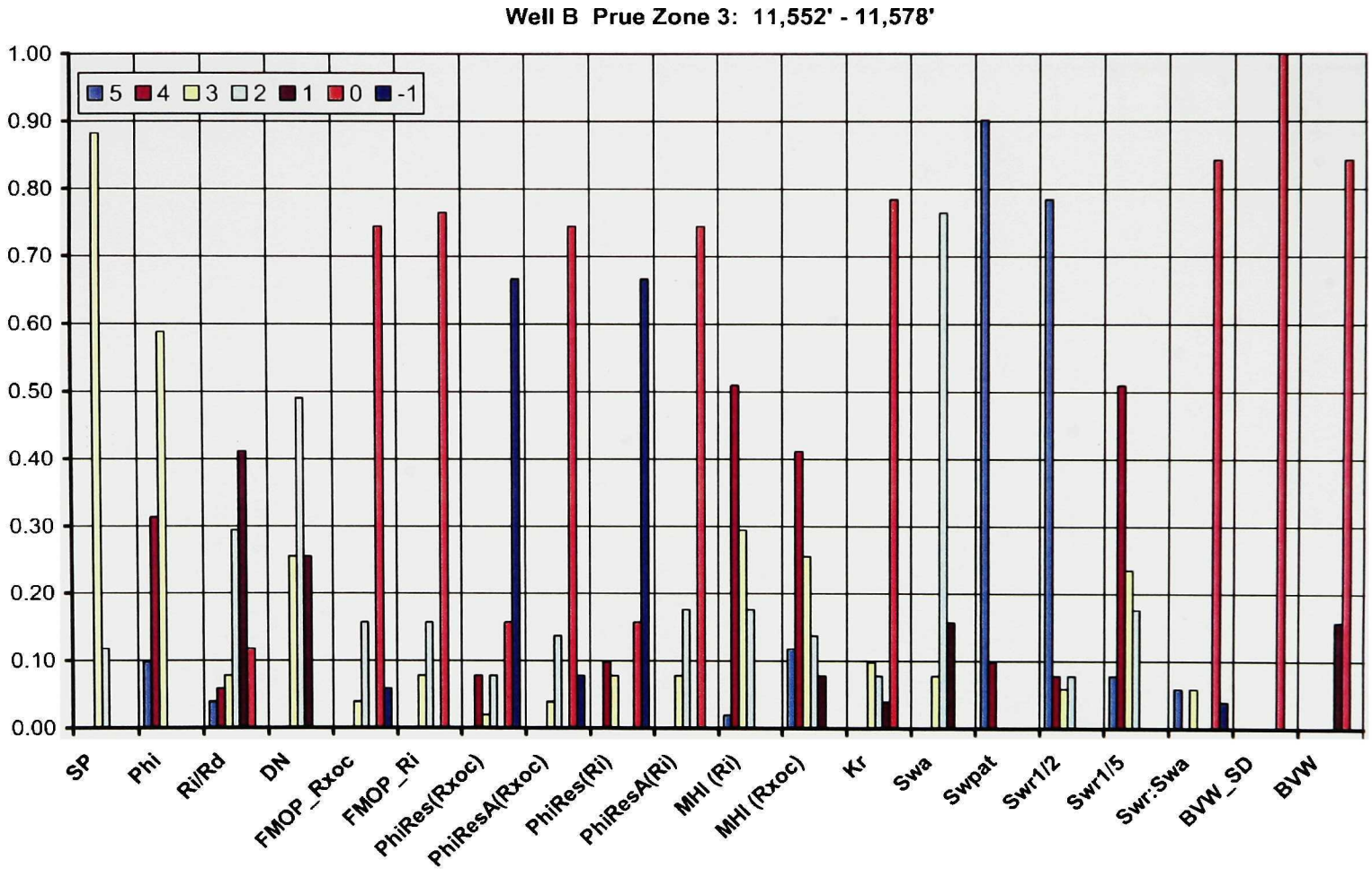

Figure 7.21 Well B Production-Calibrated Ranking System Histogram for the Third Prue Sand Tested in Well B. Well was Hydraulically Fractured and Production Tested ARO 0.353 MMCFGPD + 356 BW; Zone was Not Completed.

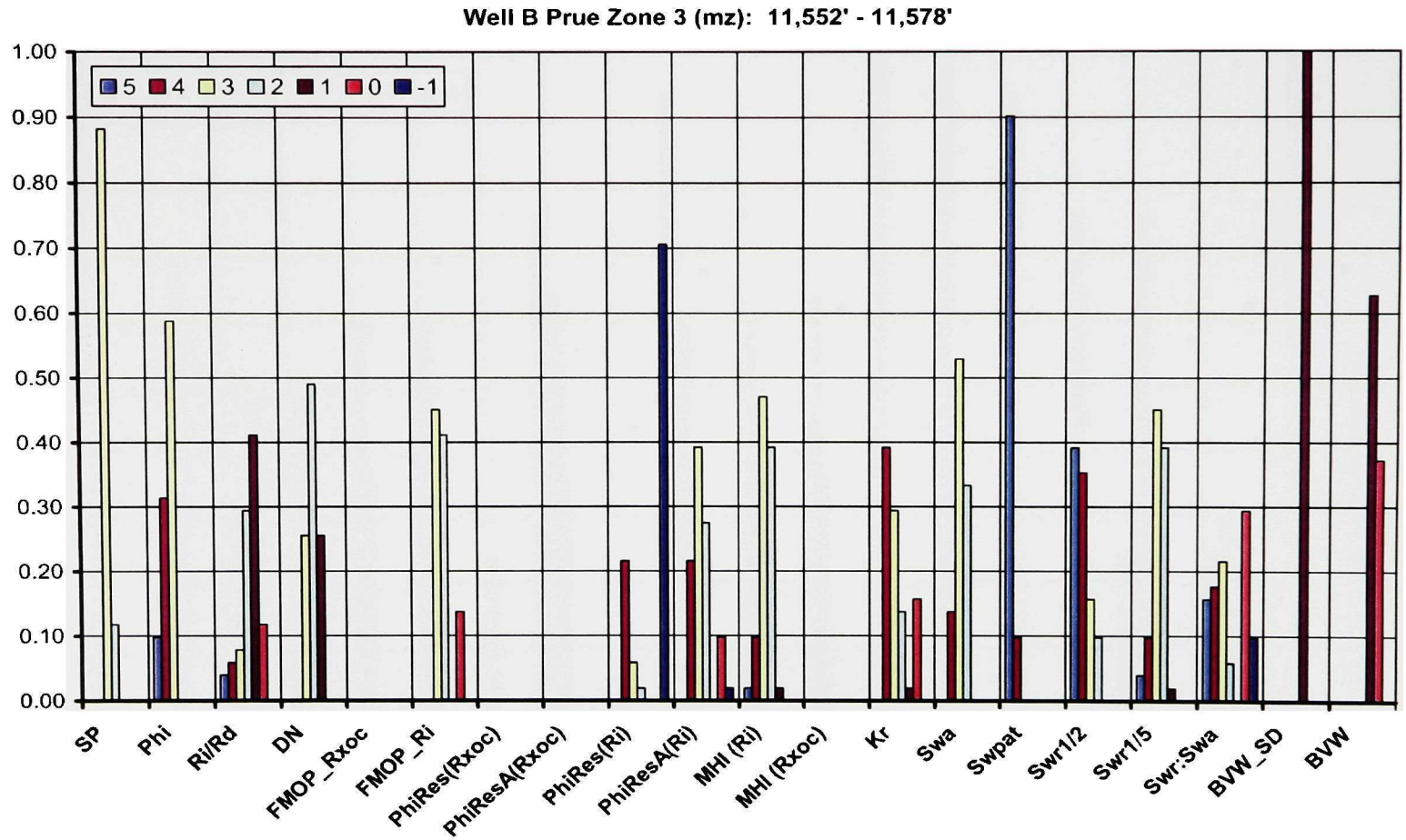

Figure 7.22 Well B Production-Calibrated Ranking System Histogram for the Third Prue Zone Tested in Well B, With Modified *m* and *z*. Well was Frac'd and Production Tested ARO 0.353 MMCFGPD + 356 BW; Zone was Not Completed.

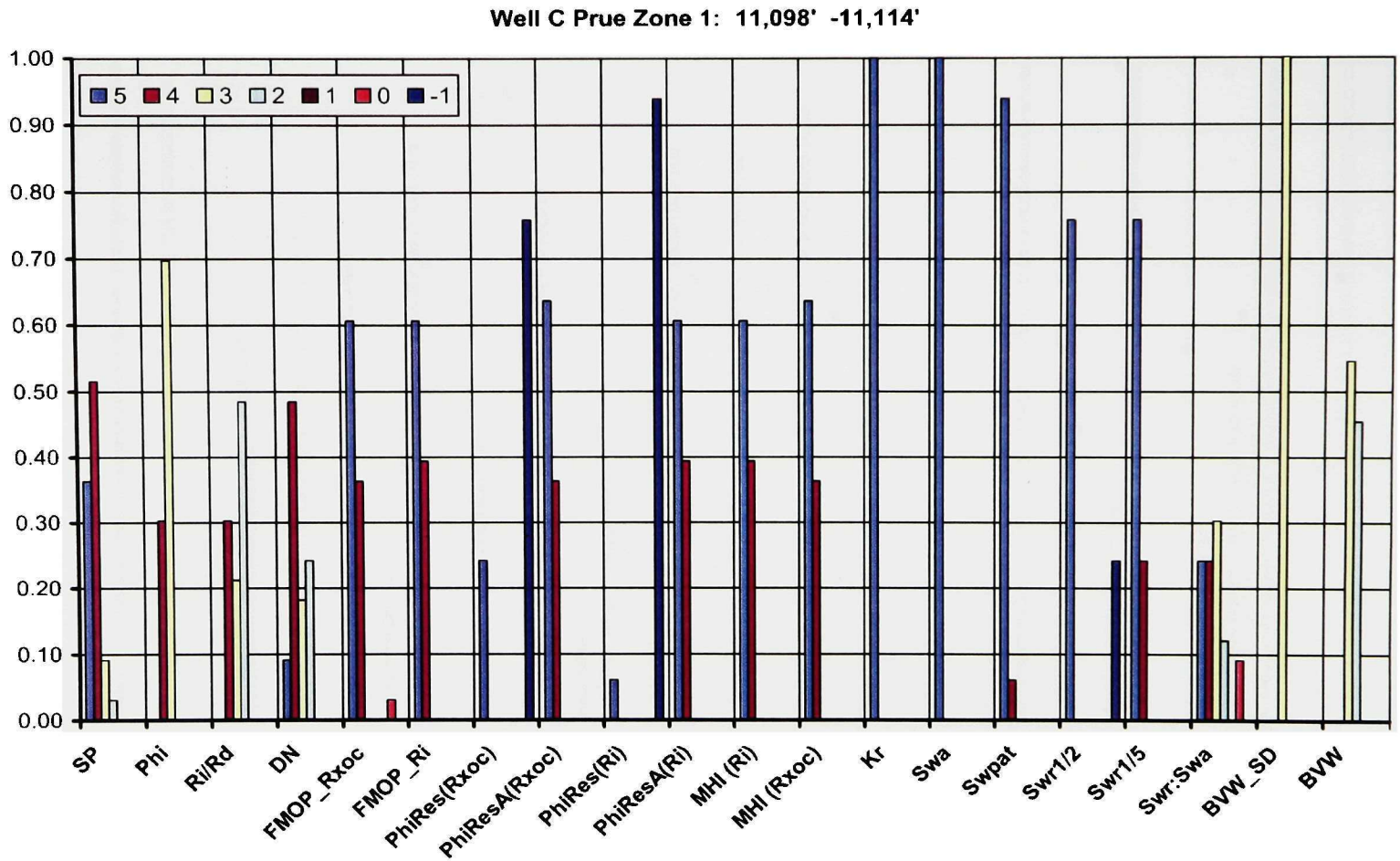

Figure 7.23 Well C Production-Calibrated Ranking System Histogram for the Perforated Interval 11,098 ft. to 11,114 ft. IP = 3.7 MMSCFPD + 43 BCPD and no water. Cumulative Production = 1.95 BCFG over 78 months.

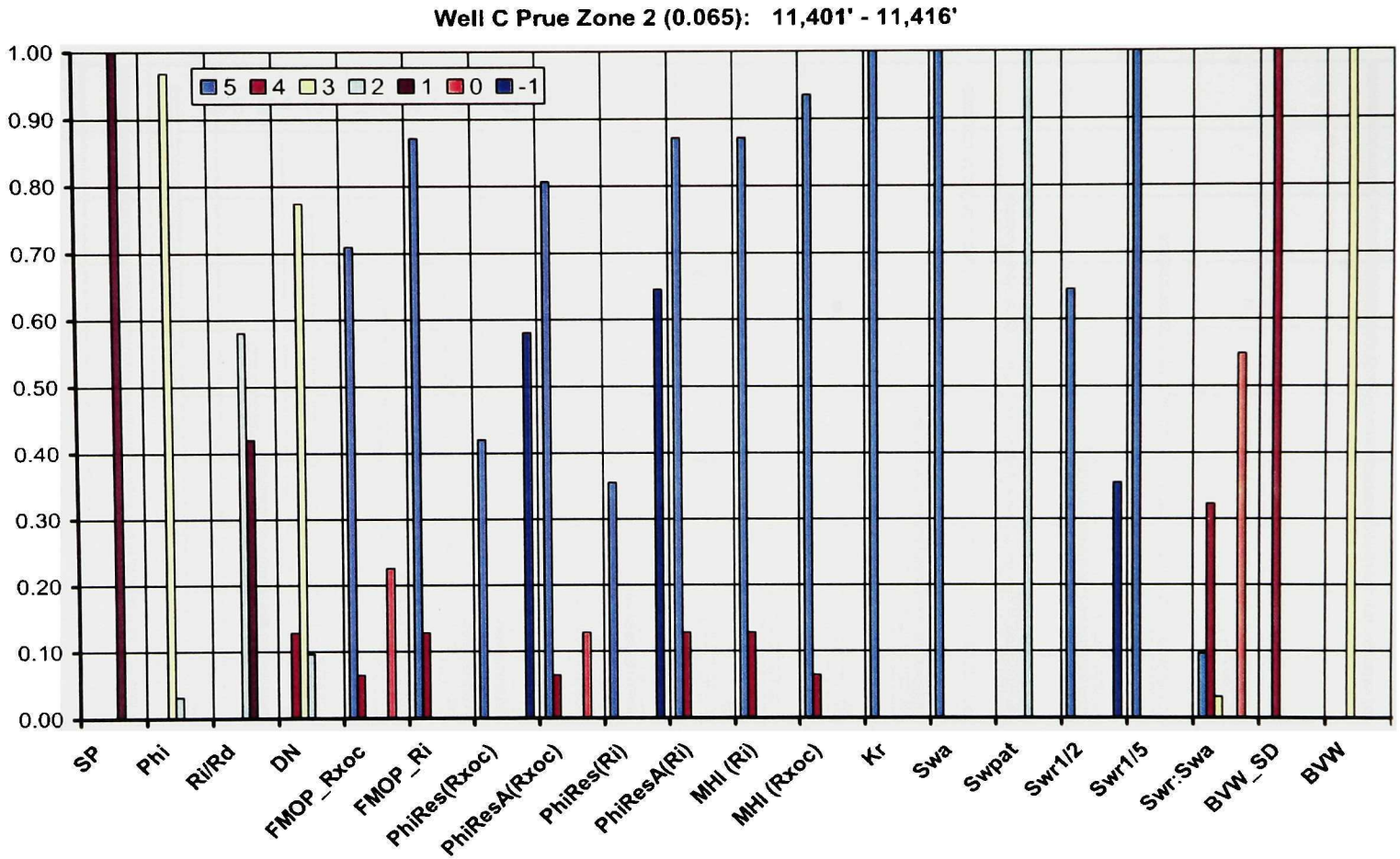

Figure 7.24 Well C Production-Calibrated Ranking System Histogram for the Perforated Interval 11,401 ft. - 11,416 ft., Using Rw = 0.065. Production Test Swabbed [Unmeasured Gas + 41 Barrels of Water]. The Sand was Not Completed.

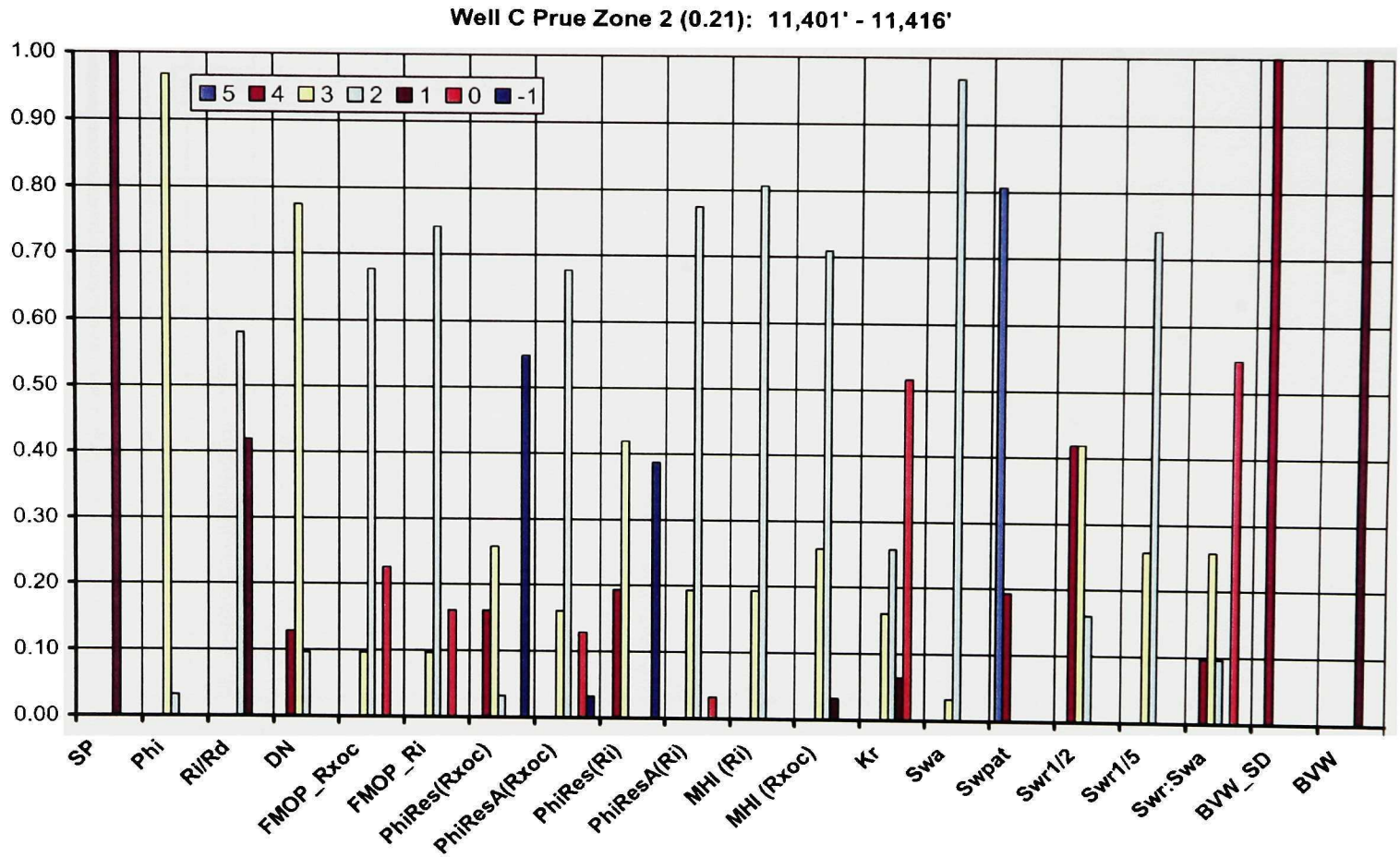

Figure 7.25 Well C Production-Calibrated Ranking System Histogram for the Perforated Interval 11,401 ft. - 11,416 ft., Using Rw = 0.21. Production Test Swabbed [Unmeasured Gas + 41 Barrels of Water]. The Sand was Not Completed.

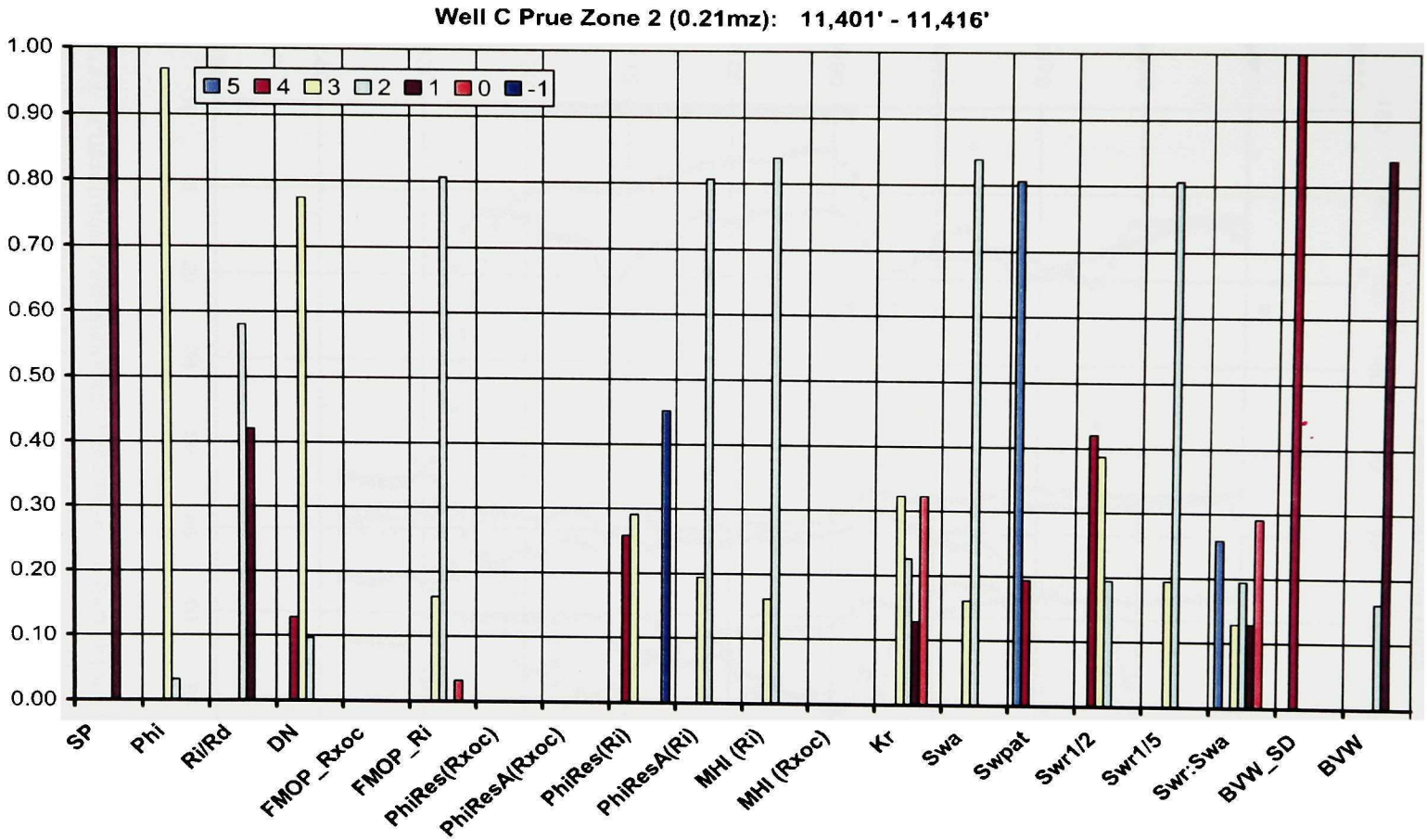

Figure 7.26 Well C Production-Calibrated Ranking System Histogram for the Perforated Interval 11,401 ft. - 11,416 ft., Using Rw = 0.21, Revised *m* and *z*-Factor Parameters. Production Test Swabbed [Unmeasured Gas + 41 Barrels of Water]. The Sand was Not Completed.

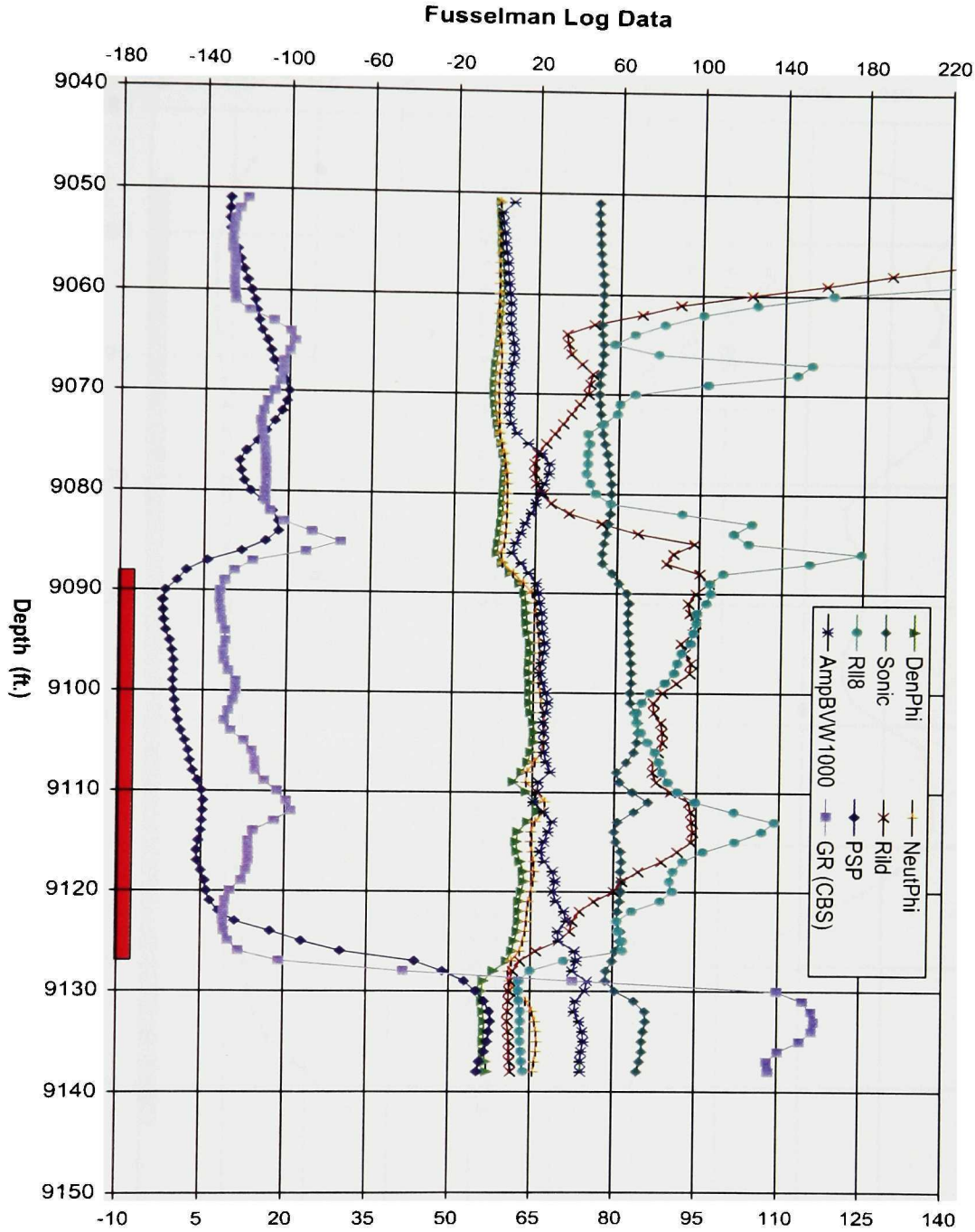

Figure 7.27 Fusselman Petrophysical Parameters Chart: Plot of Basic Log Data and Amplified *BVW* (x 1000) Curve. Perforated Interval 9088' - 9126', IP Flowing 1305 BOPD + 1.5 MMSCFGPD and No Water. Red Bar Marks the Perforated Interval.

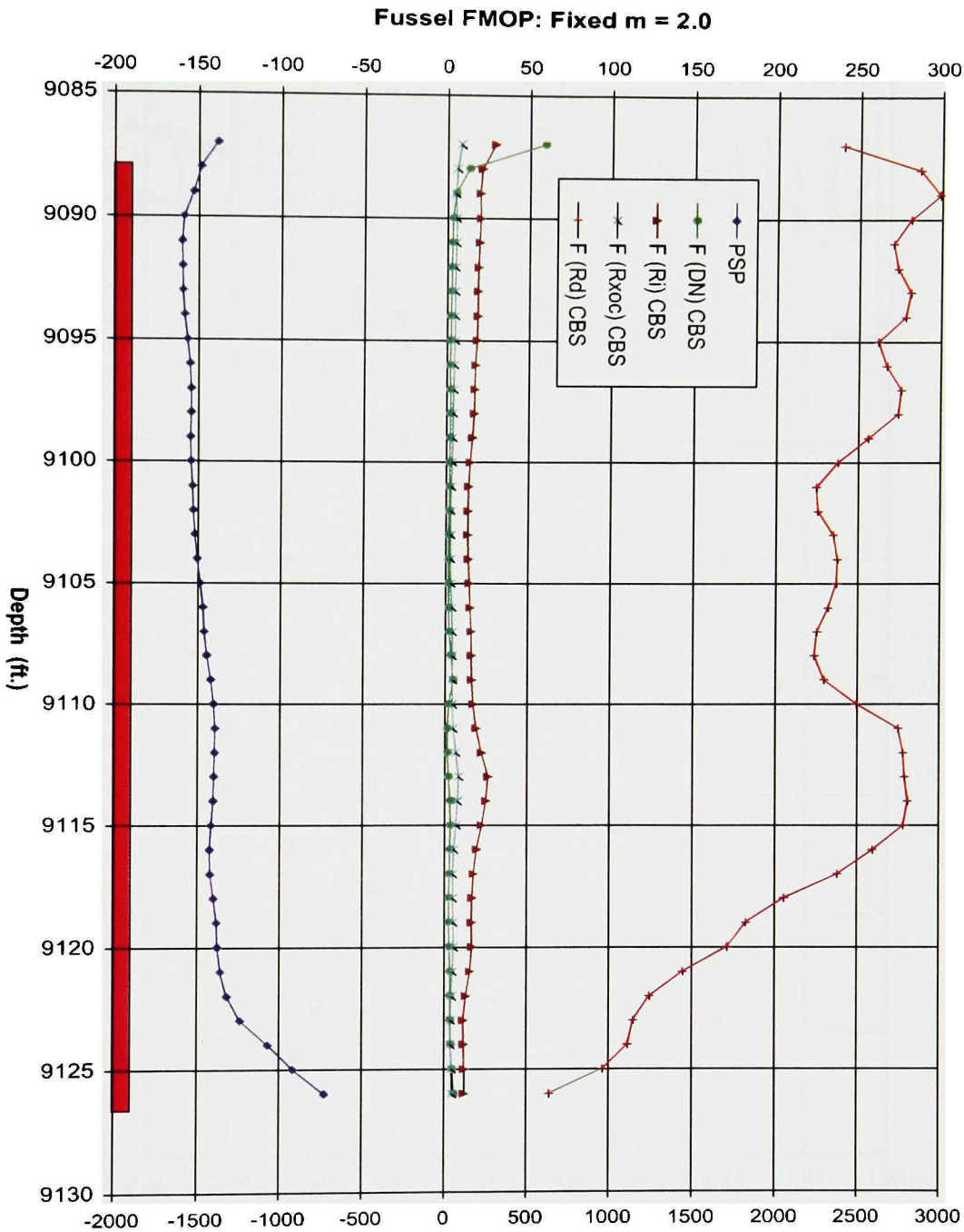

Figure 7.28 Fusselman Petrophysical Parameters Chart: FMOP with Fixed m = 2.0. Perforated Interval 9088' - 9126', IP Flowing 1305 BOPD + 1.5 MMSCFGPD and No Water. Red Bar Marks the Perforated Interval.

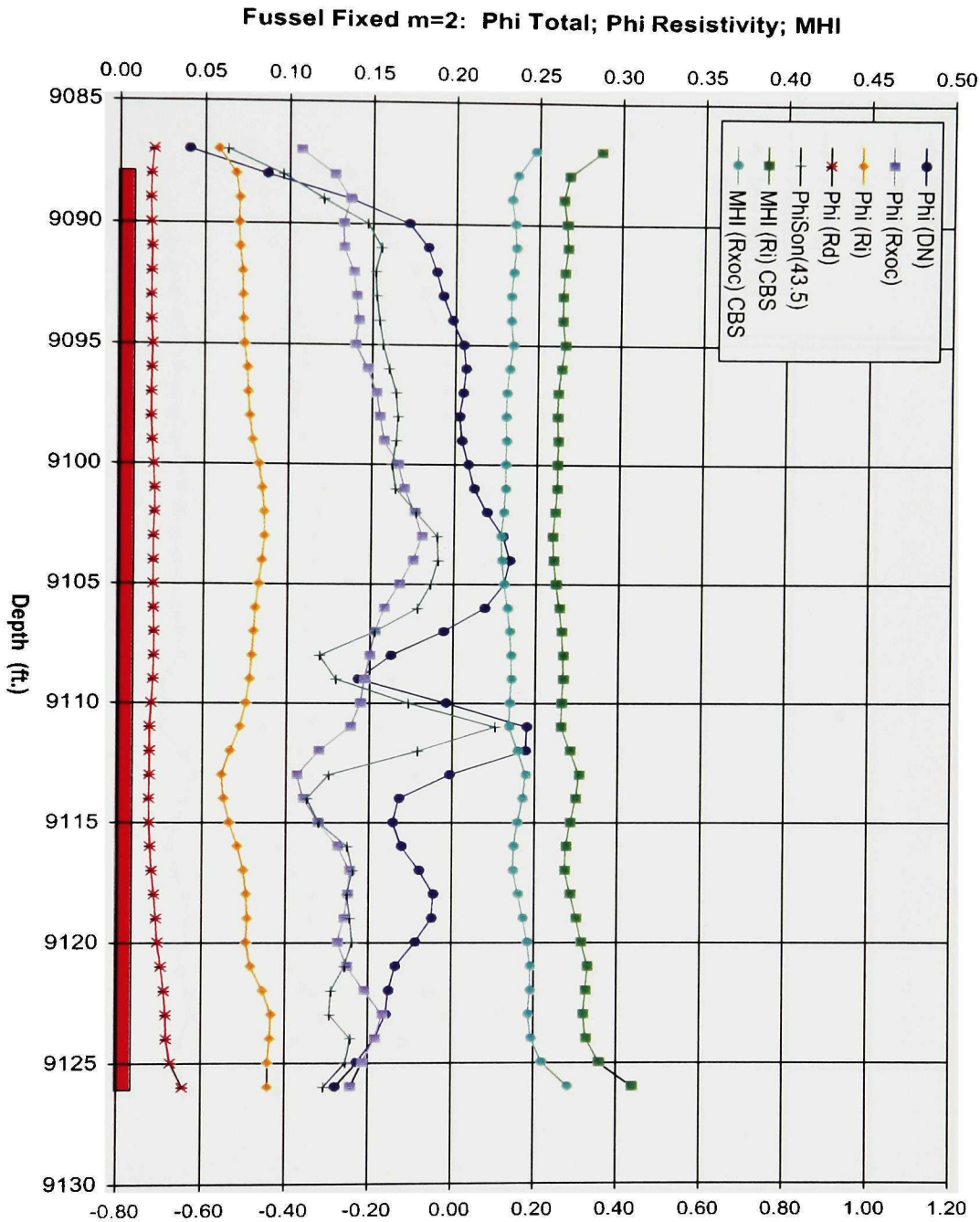

Figure 7.29 Fusselman Petrophysical Parameters Chart: Plot of Resistivity Porosity and Movable Hydrocarbon Index with Fixed m = 2.0. Perforated Interval 9088' - 9126', IP Flowing 1305 BOPD + 1.5 MMSCFGPD and No Water. Red Bar Marks the Perforated Interval.

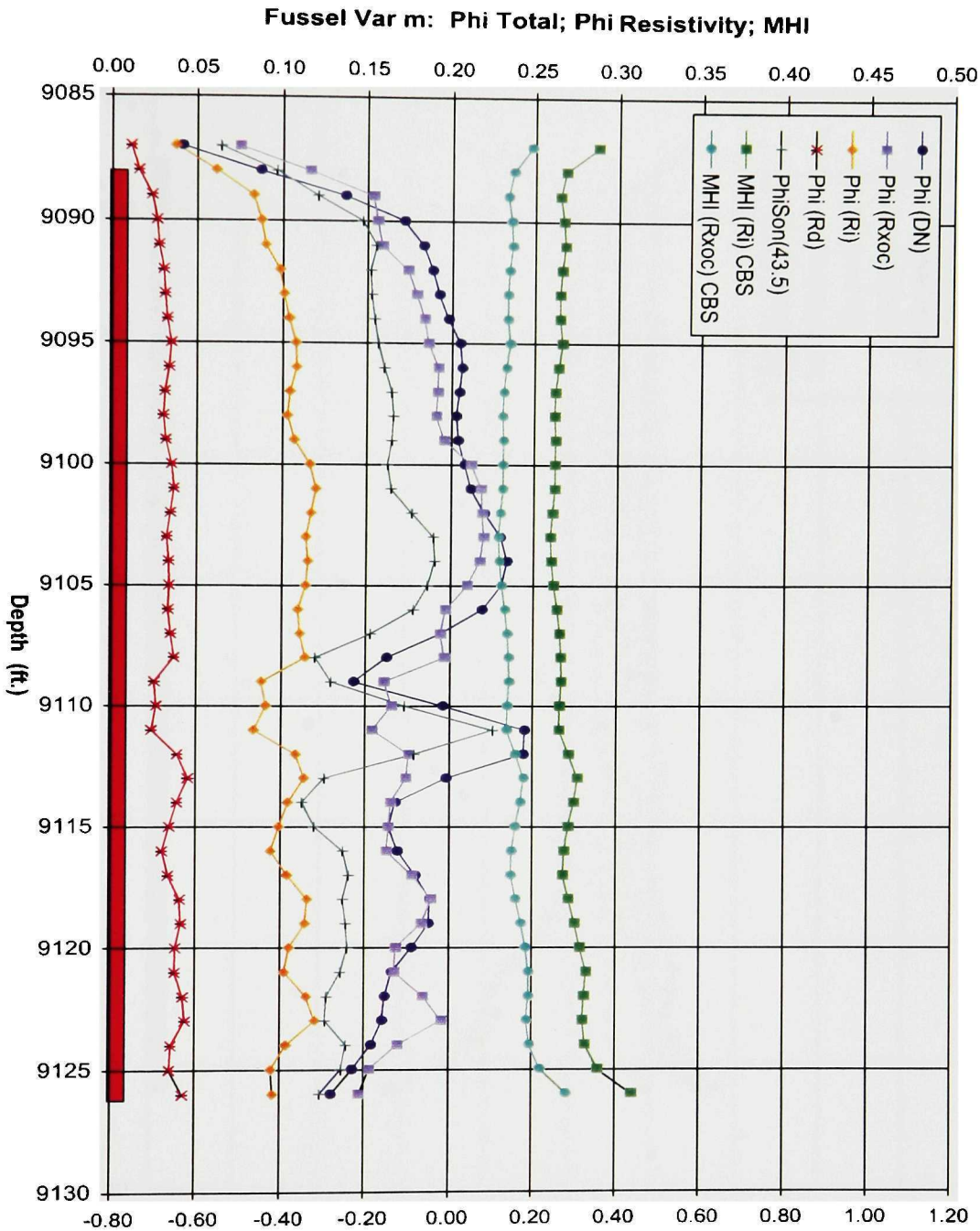

Figure 7.30 Fusselman Petrophysical Parameters Chart: Plot of Resistivity Porosity and Movable Hydrocarbon Index with Variable m. Perforated Interval 9088' - 9126', IP Flowing 1305 BOPD + 1.5 MMSCFGPD and No Water. Red Bar Marks the Perforated Interval.

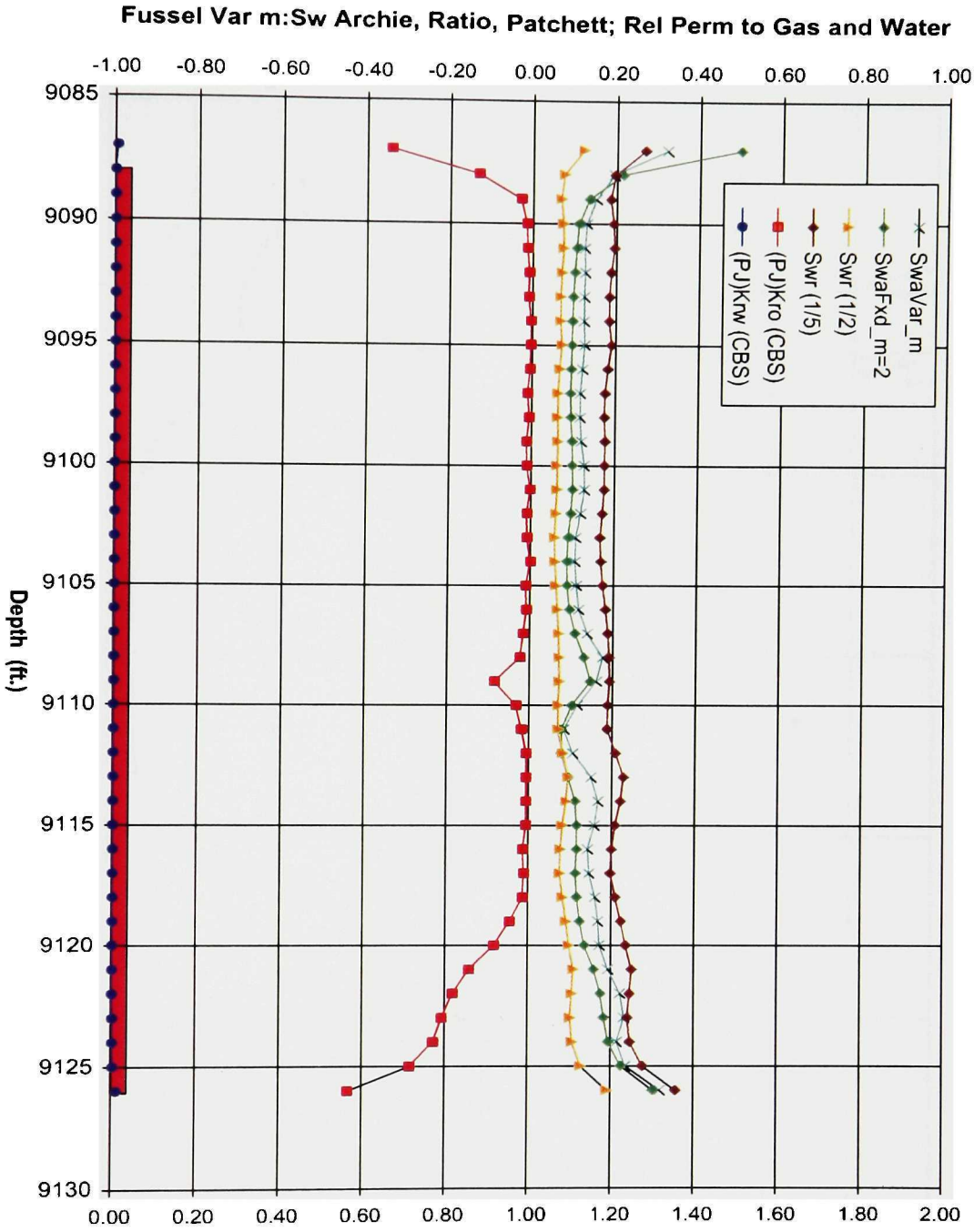

Figure 7.31 Fusselman Petrophysical Parameters Chart: Plot of Calculated Water Saturation Values and Relative Permeability to Gas and Water with Variable m. Perforated Interval 9088' - 9126', IP Flowing 1305 BOPD + 1.5 MMSCFGPD and No Water. Red Bar Marks the Perforated Interval.

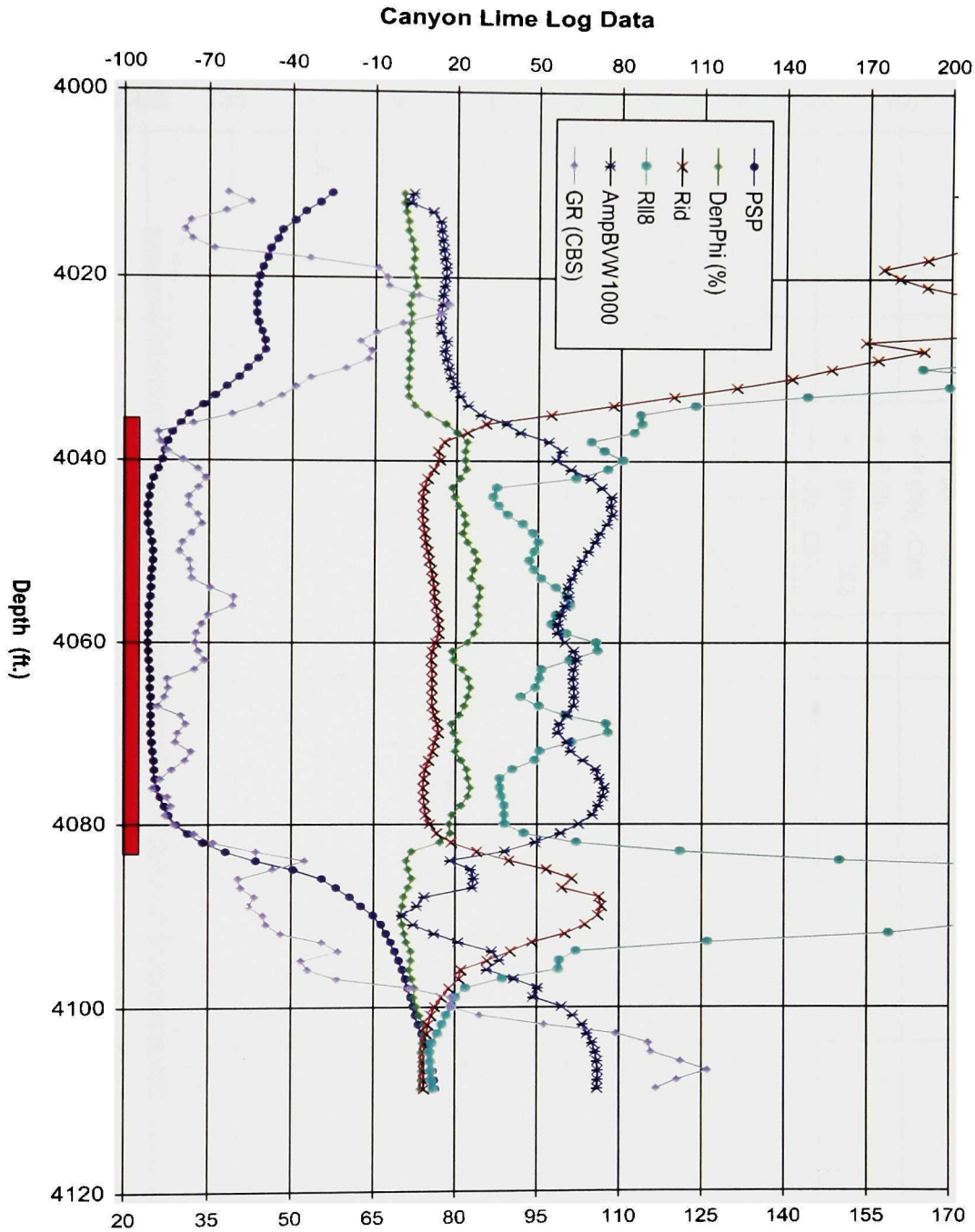

Figure 7.32 Canyon Lime Petrophysical Parameters Chart: Plot of Basic Log Data and Amplified *BVW* (x 1000) Curve. Perforated Interval 4035' - 4082'. Production Test Produced Only Water. Red Bar Marks the Perforated Interval.

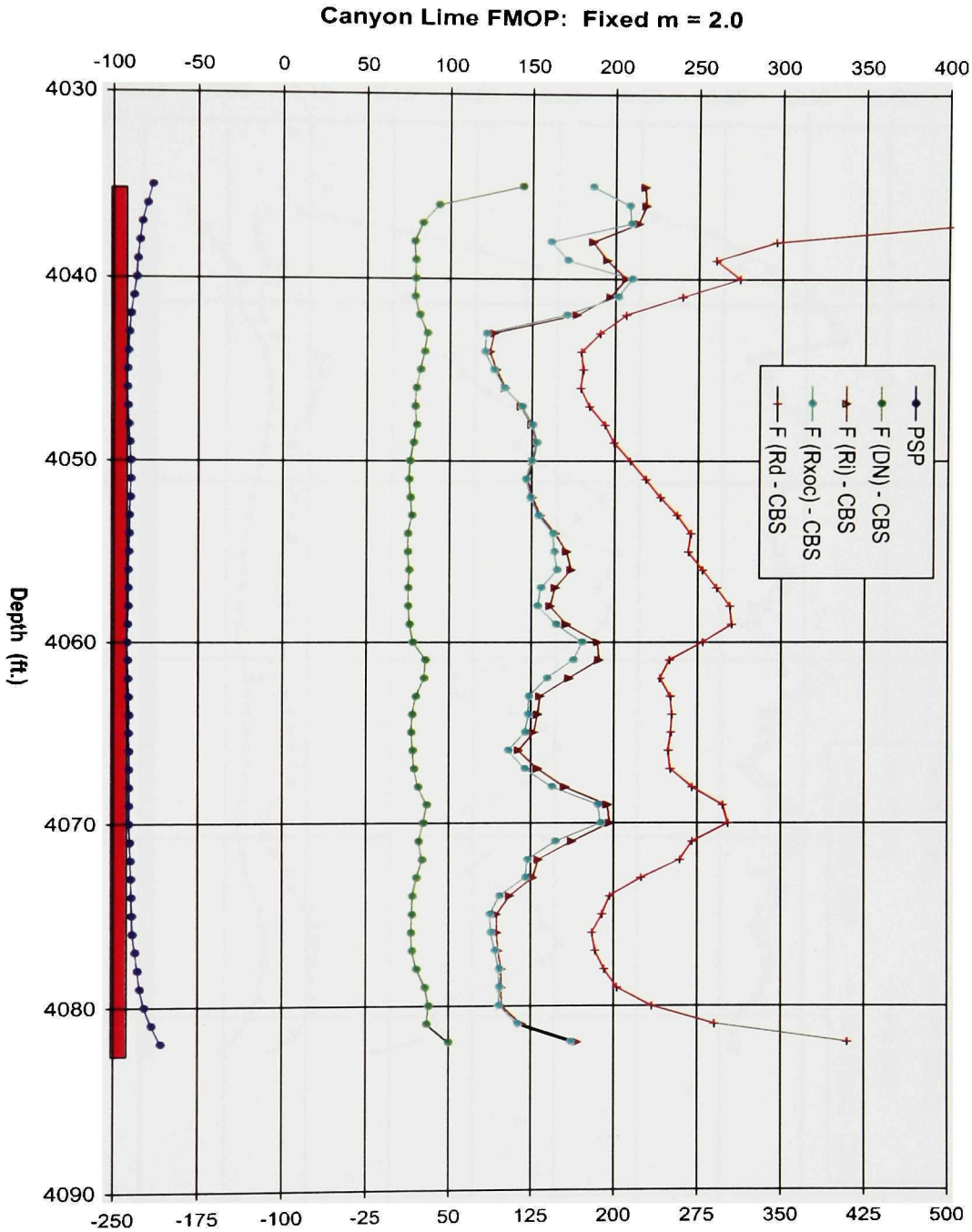

Figure 7.33 Canyon Lime Petrophysical Parameters Chart: FMOP Using Fixed $m = 2.0$. Perforated Interval 4035' - 4082'. Production Test Produced Only Water. Red Bar Marks the Perforated Interval.

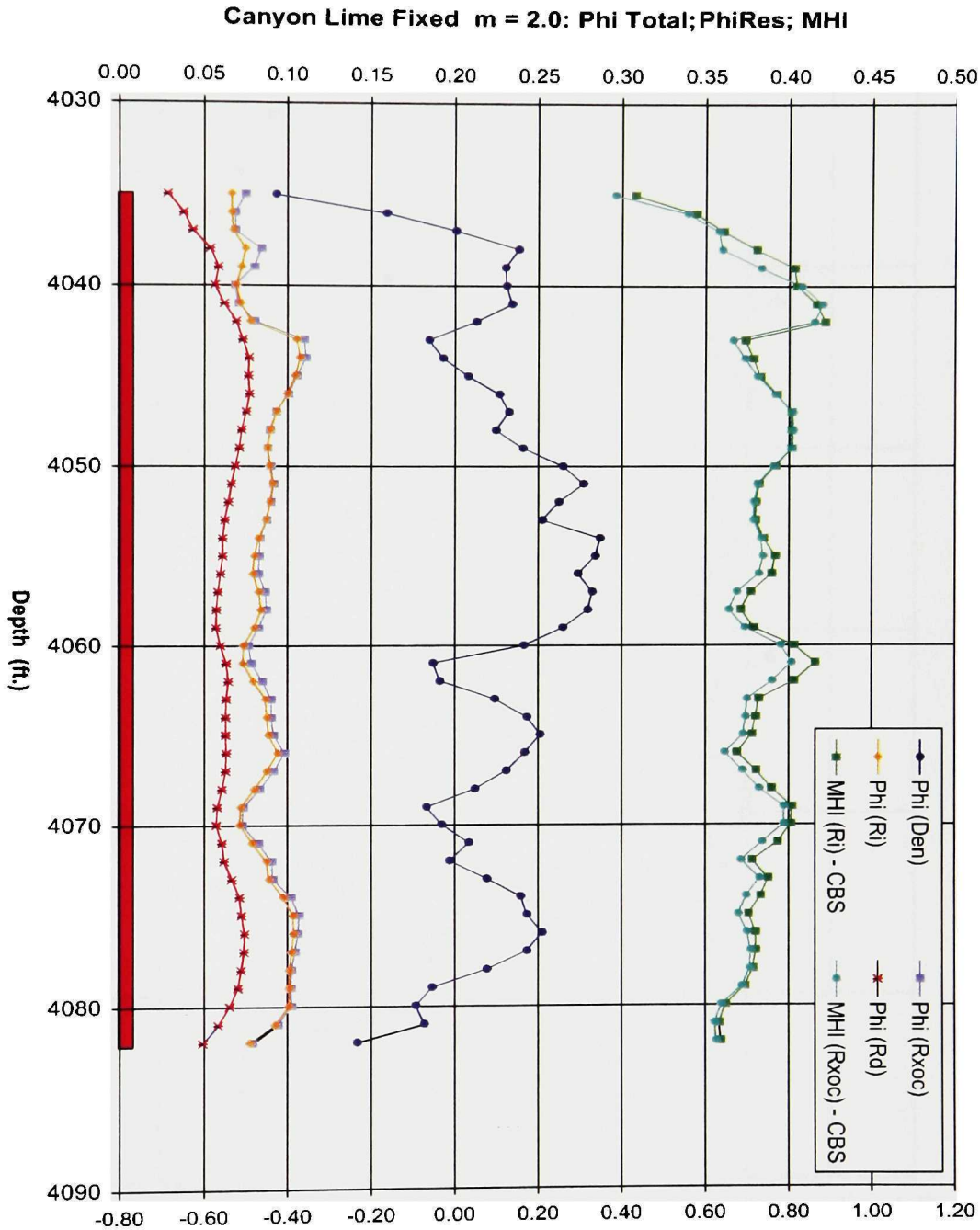

Figure 7.34 Canyon Lime Petrophysical Parameters Chart: Plot of Resistivity Porosity and Movable Hydrocarbon Index Using Fixed $m = 2.0$. Perforated Interval 4035' - 4082'. Production Test Produced Only Water. Red Bar Marks the Perforated Interval.

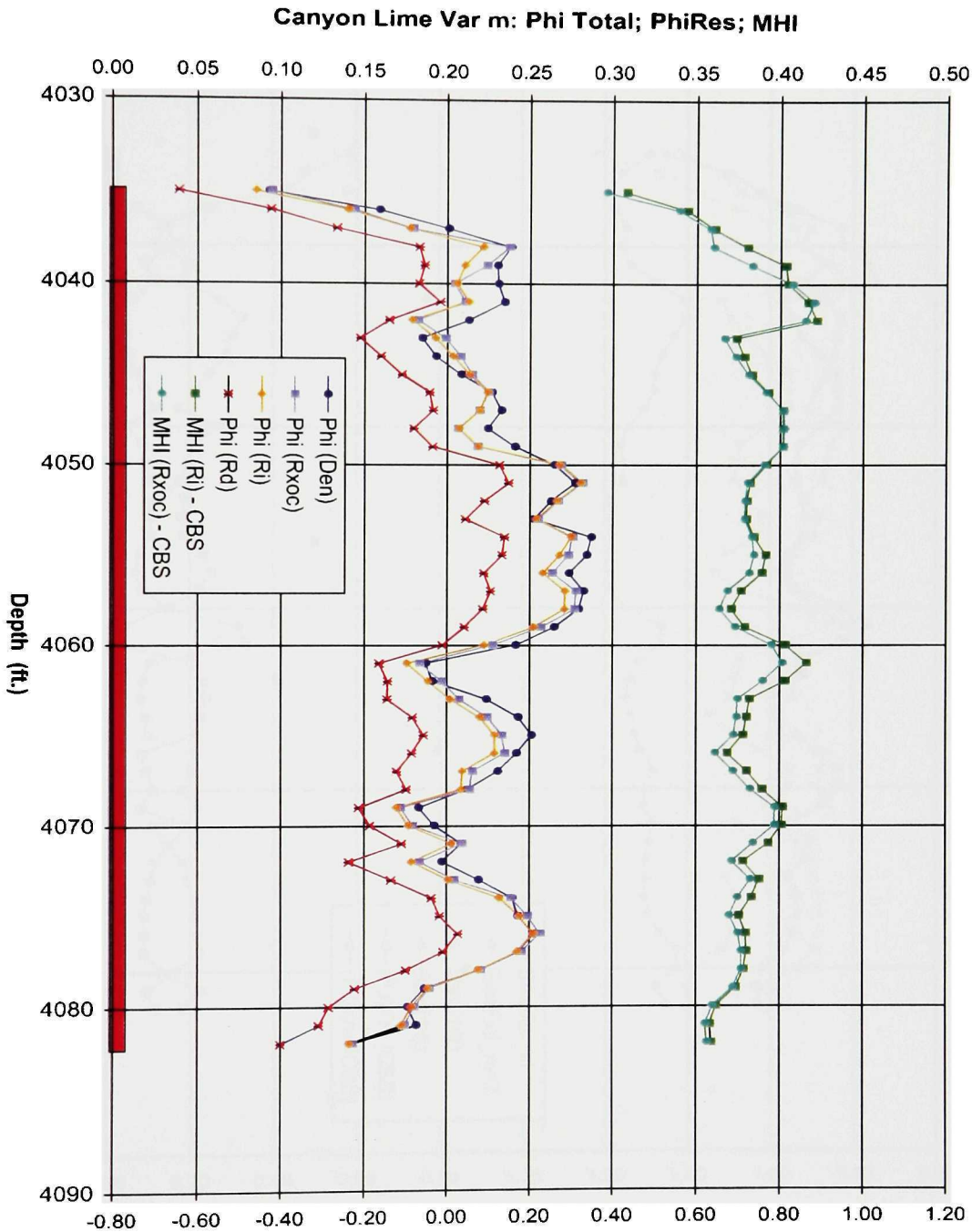

Figure 7.35 Canyon Lime Petrophysical Parameters Chart: Plot of Resistivity

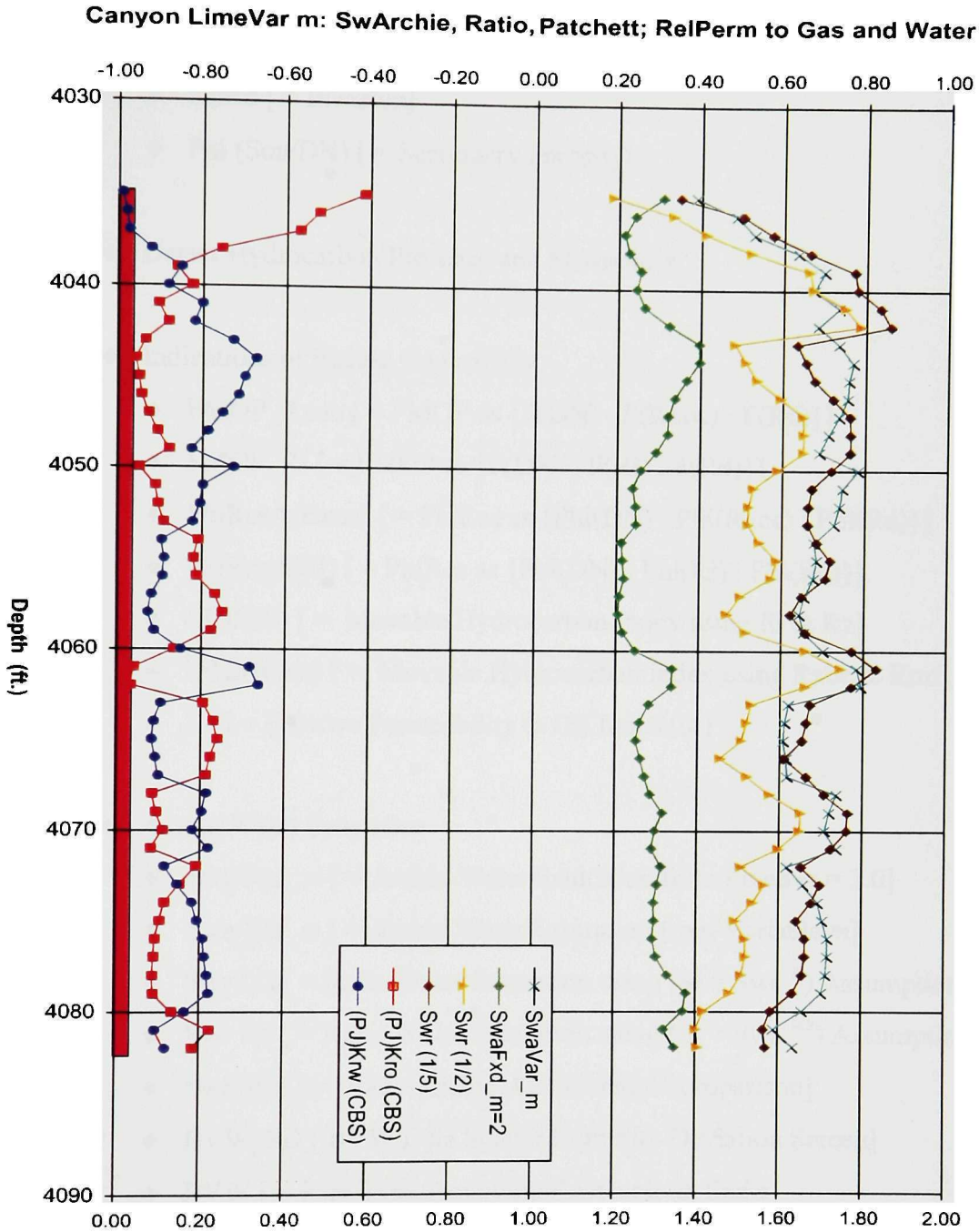

Figure 7.36 Canyon Lime Petrophysical Parameters Chart: Plot of Calculated Water Saturation Values and Relative Permeability to Gas and Water Using Variable *m*. Perforated Interval 4035' - 4082'. Production Test Produced Only Water. Red Bar Marks the Perforated Interval.

- Assess Reservoir Quality
  - SP
  - Phi [= Total Formation Porosity]
  - Ri/Rd [= Invasion]
  - Phi (Son/DN) [= Secondary Porosity]

- Detect Hydrocarbon Presence and Movability

- Indications of Excess Coductivity
  - FMOP_Rxoc [= FMOP as {F(DN) : F(Rxoc) : F(Rd)}]
  - FMOP_Ri [= FMOP as {F(DN) : F(Ri) : F(Rd)}]
  - PhiResA(Rxoc) [= PhiRes as {Phi(DN) : Phi(Rxoc) : Phi(Rd)}]
  - PhiResA(Ri) [= PhiRes as {Phi(DN) : Phi(Ri) : Phi(Rd)}]
  - MHI(Ri) [= Movable Hydrocarbon Index using Ri & Rz]
  - MHI(Rxoc) [= Movable Hydrocarbon Index using Rxoc & Rmf]
  - Kr [= Relative Permeability to Oil Indicator}

- Assess Water Saturation
  - Swa Fxd_m [= Archie Water Saturation from Fixed m = 2.0]
  - Swa Var_m [= Archie Water Saturation from Variable m]
  - Swr 1/2 [= Ratio Water Saturation using (Si = Swa $^{1/2}$) Assumption
  - Swr 1/5 [= Ratio Water Saturation using (Si = Swa $^{1/5}$) Assumption
  - Swr:Swa [= (Ratio/Archie) Consistency Comparison]
  - BVW_SD [BVW Data Scatter from Std. Deviation Screen]
  - BVW [= Pore Type Assuming Reservoir @ Swirr]

Figure 7.37 Legend for Carbonate Ranking System Histogram Charts.

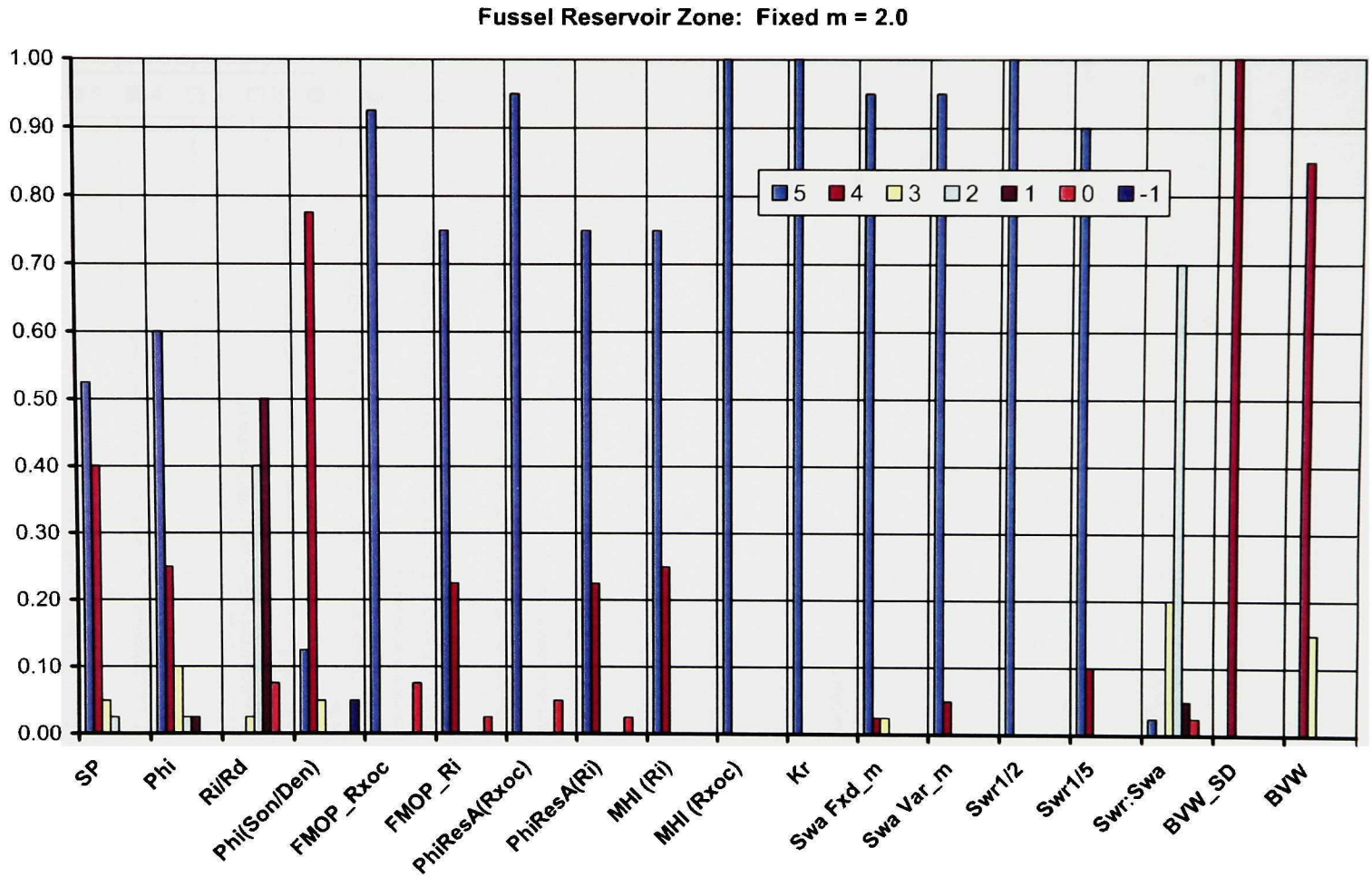

Figure 7.38 Fusselman Reservoir Production-Calibrated Ranking System Histogram for the Perforated Interval 9088' - 9126', Using Fixed m = 2.0. IP Flowing 1305 BOPD + 1.5 MMSCFGPD and No Water.

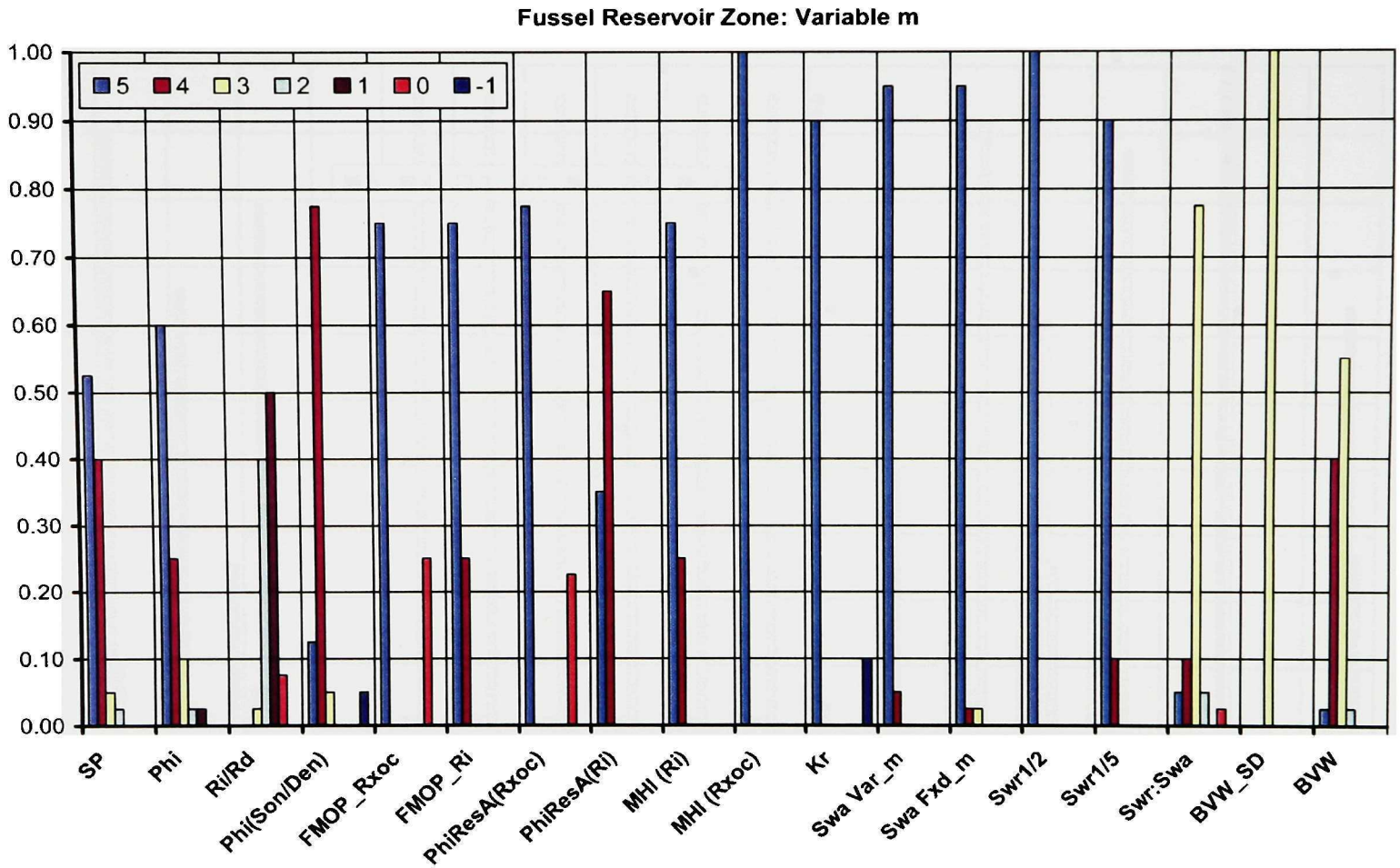

Figure 7.39 Fusselman Reservoir Production-Calibrated Ranking System Histogram for the Perforated Interval 9088' - 9126', Using Variable m. IP Flowing 1305 BOPD + 1.5 MMSCFGPD and No Water.

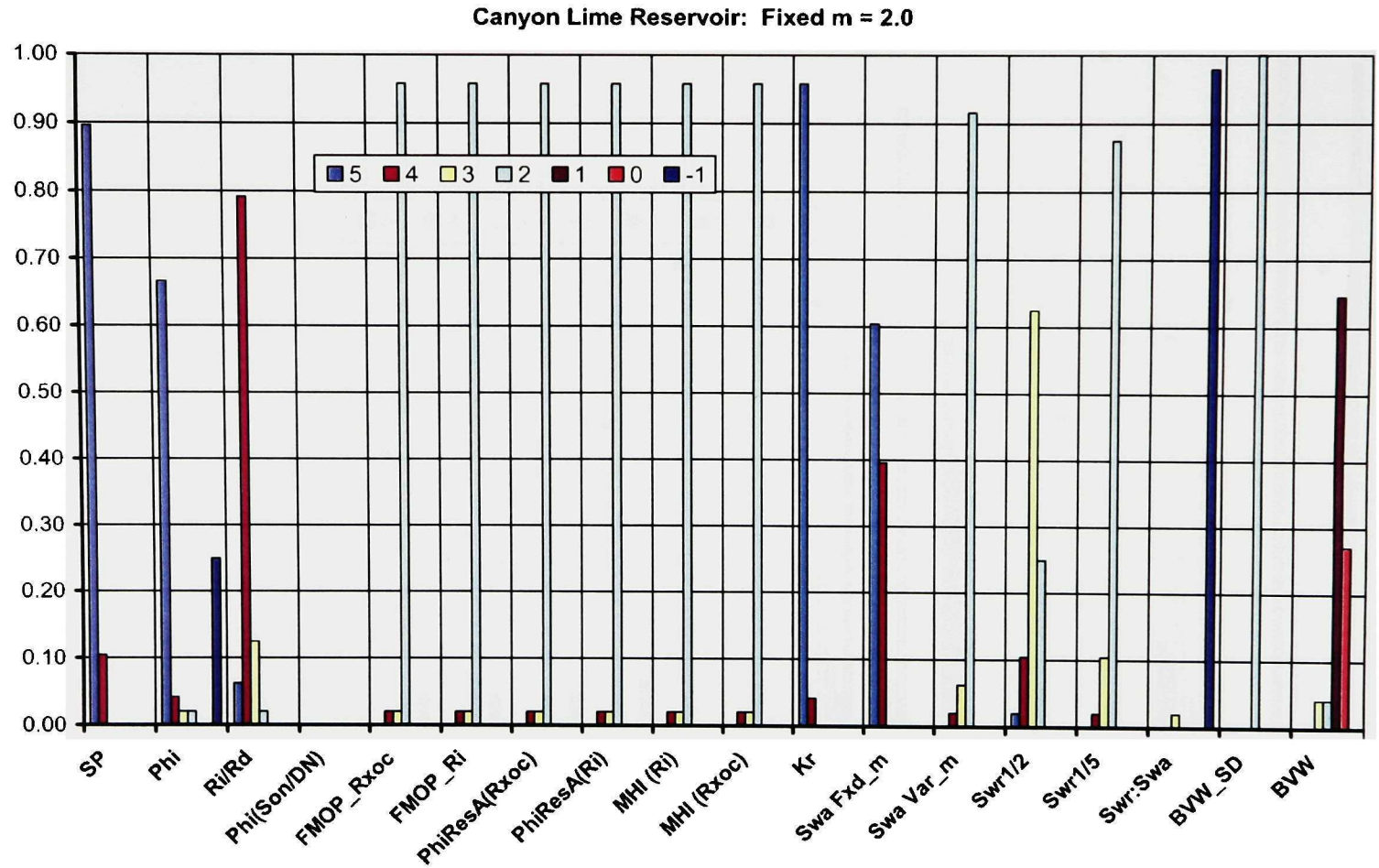

Figure 7.40 Canyon Lime Reservoir Production-Calibrated Ranking System Histogram for the Perforated Interval 4035-ft. to 4082-ft., Using Fixed m = 2.0. Production Test Produced Only Water.

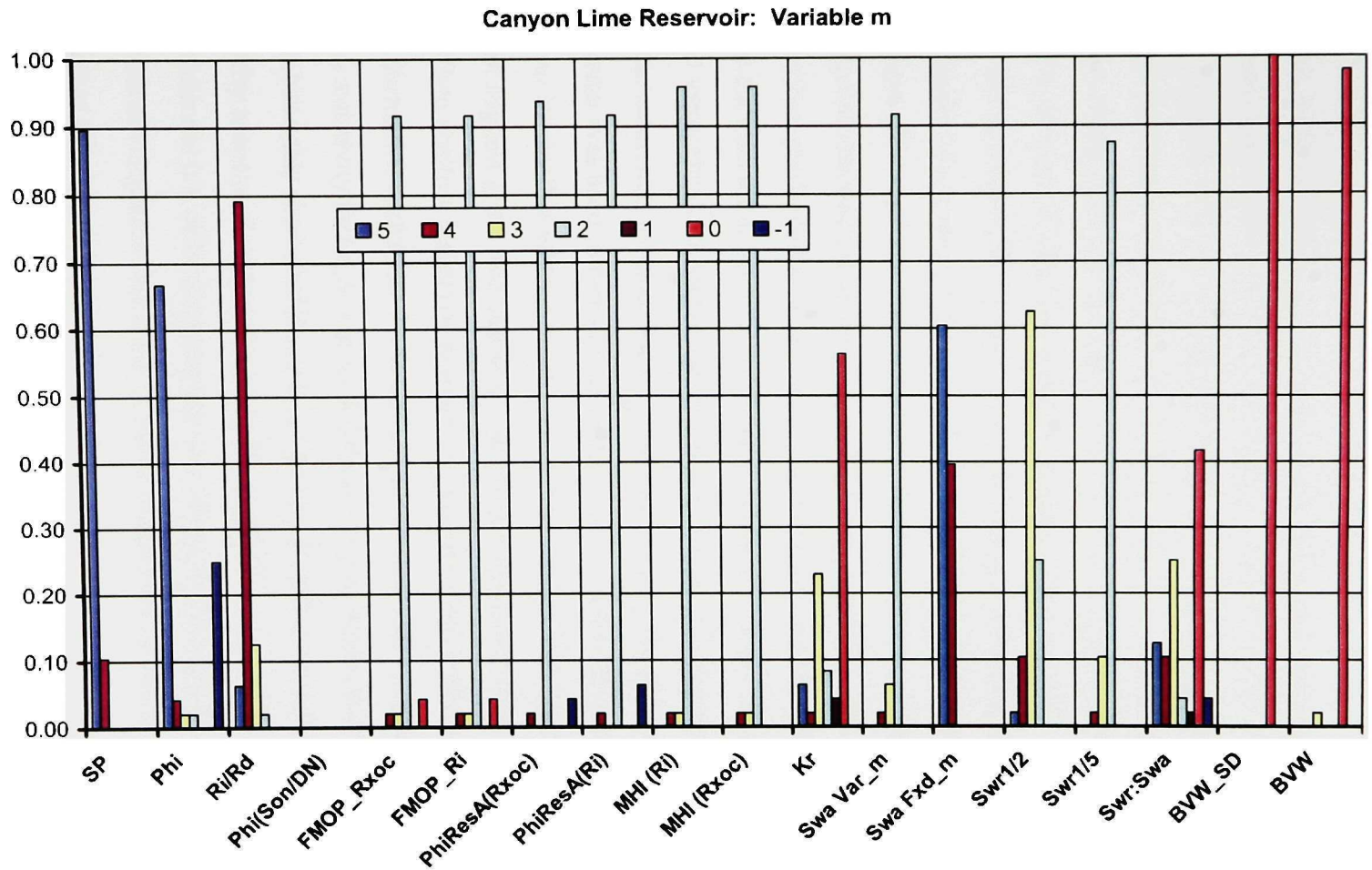

Figure 7.41 Canyon Lime Reservoir Production-Calibrated Ranking System Histogram for the Perforated Interval 4035-ft. to 4082-ft., Using Variable m. Production Test Produced Only Water.

CHAPTER VIII
CONCLUSIONS

This study has shown that a production-calibrated multiple parameter approach to petrophysical analysis and interpretation, using a standard suite of logging data, can be used to distinguish variation in production potential in Prue Sands in the study area. Calculated water saturation alone is not a good indicator of hydrocarbon producibility in the Prue. A recognition that the value of R_w can vary among the stacked Prue Sands was necessary to properly distinguish variation in production potential.

In the context of the multiple parameter approach to petrophysical analysis, two reservoir quality parameters, SP and porosity, were useful production quality indicators, while the gas effect and invasion parameters were less effective. The FMOP, PhiResA, and MHI parameters demonstrated that hydrocarbon movability is a successful indicator of hydrocarbon producibility in the Prue, and the relative permeability parameter supported the indication from the movability indicators. Water saturation values calculated using standard Archie that fell within a range of values developed from the Ratio water saturation method, were representative of hydrocarbon producibility. Bulk volume water was used in two separate parameters to assess the relationship of a Prue reservoir to irreducible water saturation, and showed that Prue Sands can exhibit textural trends that suggest grain size variability across an individual reservoir zone.

When shallow resistivity porosity values exceeded formation porosity and the apparent formation resistivity factors from the invaded zone were less than the empirical formation resistivity factor, it was an indication of poor producibility. Poor producers often exhibited this characteristic, and it was interpreted as an indication of excess conductivity associated with shaliness in the reservoir.

Shaliness is a difficult parameter to evaluate in Prue granite wash sands. A method was developed in this study in which the amount of excess porosity from ϕ_{Rxoc} over ϕ_{DN} was eliminated by decreasing the value of the empirical parameter m to bring values of ϕ_{Rxoc} and ϕ_{DN} to near equality. The revised value of m was used to adjust the

value of the z factor in R_z calculations and analyses were rerun to attempt to develop an effective water saturation value and movability of hydrocarbons through the effective porosity. The results in three wells suggest it can produce results supported by production. It certainly requires validation from further study, including core analysis.

The multiple parameter approach demonstrates the flexibility to be used in other formations and lithologies, as was illustrated by its application in Permian Basin carbonates. It requires calibration to the reservoir under investigation.

It would be useful going forward in evaluation of the Prue, for a Prue reservoir R_w map to be constructed. This would involve correlation of individual Prue reservoir sands, with R_w values then calculated across the correlation section for each Prue reservoir. Such a map could be used to investigate the mechanism responsible for R_w variability and could help identify R_w values that are out of the expected range for any individual sand. If a value is outside the expected range, can it be explained as a valid phenomenon, or does it represent poor data, such as improperly measured R_{mf} data?

It would also be useful to undertake experiments to determine if excess conductivity identified in this study can be attributed to shaliness or microporosity, as was done in Asquith (1995). This would require actual sample material, preferably core material, that could be examined for mineralogy and electrical properties across a zone that exhibits excess conductivity as identified in this study.

Analysis of movable hydrocarbons as an indicator of hydrocarbon presence and producibility is an important part of the multiple parameter approach to log analysis in Prue Sands in the deep Anadarko Basin. Were the multiple parameter method applied in reservoirs in other basins, such as highly porous Gulf Coast Tertiary sands, where invasion may be intrinsically shallow, hydrocarbon movability could be difficult to detect. In order to be effective, it is important to understand the rock-fluid mechanisms that underlie the petrophysical parameters prior to application of the multiple parameter approach. Alternate parameters or altered assumptions for the current parameters may be required as the method is used in different reservoirs with different petrophysical characteristics.

REFERENCES CITED

Adisoemarta, P. S., Anderson, G. A., Frailey, S. M., and Asquith, G. B., 2000, Historical use of M and A in Well Log Interpretation: Is Conventional Wisdom Backwards: Permian Basin Oil and Gas Recovery Conference, Society of Petroleum Engineers, SPE 59699, 7 p.

Adisoemarta, P. S., Anderson, G. A., Frailey, S. M., and Asquith, G. B., 2001, Saturation Exponent *n* in Well Log Interpretation: Another Look at the Permissible Range: Permian Basin Oil and Gas Recovery Conference, Society of Petroleum Engineers, SPE 70043, 4 p.

Al-Shaieb, Zuhair; Puckette, J. O.; Abdalla, A. A.; and Ely, P. B., 1994, Megacompartment Complex in the Anadarko Basin: A Completely Sealed Overpressured Phenomenon, *in* Ortoleva, P. J. (ed.), Basin Compartments and Seals: American Association of Petroleum Geologists Memoir 61, p. 55–68.

Amyx, J.W., Bass, D.M., and Whiting, R.L., 1960, Petroleum Reservoir Engineering Physical Properties, McGraw - Hill Book Company, New York, p. 610.

Anderson, G.A., Asquith, G.B., and Frailey, S.M., 2002a, A Petrophysical Study of the Prue Sands in Washita Co., Oklahoma: A Multiple Parameter Approach to Log Analysis, *in* Boyd, D., (ed.), Finding and Producing Cherokee Reservoirs in the Southern Midcontinent, Oklahoma Geological Survey Circular 108, p. 135-159.

Anderson, G.A., Asquith, G.B., and Frailey, S.M., 2002b, A Comprehensive Quicklook Method to Log Analysis in Permian Basin Carbonates, *in* Hunt, T.J., and Lufholm, P.H. (eds.), The Permian Basin: Preserving Our Past - Securing Our Future, Publication # 02-111, West Texas Geological Society Fall Symposium, October 9-10, 2002, p. 143-175.

Andrews, R. D.; et al., 1996, Fluvial-dominated deltaic (FDD) Oil Reservoirs in Oklahoma: the Skinner and Prue plays: Oklahoma Geological Survey Special Publication 96-2, 118 p.

Archie, G. E., 1942, The Electrical Resistivity Log as an Aid in Determining Some Reservoir Characteristics: Transactions of the American Institute of Mining and Metallurgical Engineers (AIME), v. 146, p. 54–62.

Archie, G. E., 1950, Introduction to Petrophysics of Reservoir Rocks: American Association of Petroleum Geologists Bulletin, v. 34, no. 5, May, p. 943–961.

Asquith, G.B., 1980, Log Analysis by Microcomputer, PennWell Books, Tulsa, OK, p. 105.

Asquith, G. B., 1985, Handbook of Log Evaluation Techniques for Carbonate Reservoirs: American Association of Petroleum Geologists, Methods in Exploration Series No. 5, 47 p.

Asquith, G.B., 1991, Log Evaluation of Shaly Sandstones: A Practical Guide: Continuing Education Course Note Series # 31, American Association of Petroleum Geologists, Tulsa, OK, 59 p.

Asquith, G. B., 1995, Determining Carbonate Pore Types from Petrophysical Logs: in, Pause, P.H. and Candelaria, (Eds.) Carbonate Facies and Sequence Stratigraphy: Practical Applications of Carbonate Models, PBS-SEPM Publication 95-36, Midland, TX, p. 69-79.

Asquith, G. B.; with Gibson, C., 1982, Basic Well Log Analysis for Geologists: American Association of Petroleum Geologists, Tulsa, Oklahoma, 216 p.

Asquith, G. B.; Thomerson, M. D.; and Saha, S., 1992, Petrophysical Study of the Permian Tannehill Sandstone, Knox County, Texas, *in* Mruk, D. H.; and Curran, B. C. (Eds.) Permian Basin Exploration and Production Strategies: Applications of Sequence Stratigraphic and Reservoir Characterization Concepts: West Texas Geological Society Symposium, November 5–6, 1992, Publication 92-91, p. 123–133.

Ball, M.M., Henry, M.E., and Frezon, S.E., 1991, Petroleum Geology of the Anadarko Basin Region, Province (115), Kansas, Oklahoma, and Texas: U.S. Geological Survey Open-File Report 88-450W, 36 p.

Bassiouni, Z., 1994, Theory, Measurement, and Interpretation of Well Logs: Society of Petroleum Engineers Textbook Series, v. 4, 372 p.

Bateman, R.M., 1985, Open-Hole Log Analysis and Formation Evaluation: International Human Resources Development Corporation, Boston, MA, 647 p.

Bateman, R.M., and Konen, C.E., 1977, The Log Analyst and the Programmable Pocket Calculator: The Log Analyst, September-October, 1977, p. 3-11.

Breeze, A., 1972, Abnormal-Subnormal Pressure Relationships in the Morrow Sands of Northwestern Oklahoma: Oklahoma Geology Notes, February, 1972.

Buckles, R. S., 1965, Correlating and Averaging Connate Water Saturation Data: The Journal of Canadian Petroleum Technology, January–March, p. 42–52.

Burke, J. A., Curtis, M. R. and Cox, J. T., 1966, Computer Processing of Log Data Enables Better Production in Chaveroo Field: Society of Petroleum Engineers of AIME Paper No. SPE - 1576.

Campbell, W.M., and Martin, J.L., 1955, Displacement Logging -- A New Exploratory Tool: *in*, Petroleum Transactions, AIME, v. 204, T.P. 4178, p. 233-239.

Chase, G.W., Frederickson, E.A., Ham, W.E., 1956, Resume′ of the Geology of the Wichita Mountains, Oklahoma: Petroleum Geology of Southern Oklahoma, v. I, p. 36–55, American Association of Petroleum Geologists, Tulsa, Oklahoma, p. 402.

Cheng, M.L., Leal, M.A., and McNaughton, D., 1999, Productivity Prediction from Well Logs in Variable Grain Size Reservoirs, Cretaceous Qishn Formation, Republic of Yemen: The Log analyst, Vol. 40, No. 1, Jan. - Feb., p. 24 - 32.

Choquette, P.W., and Pray, L.C., 1970, Geologic Nomenclature and Classification of Porosity in Sedimentary Carbonates: Bulletin of the American Association of Petroleum Geologists, v. 54, no. 2 (February, 1970), p. 207-250.

Coalson, E.B., Hartmann, D.J., and Thomas, J.B., 1987, Productive Characteristics of Common Reservoir Porosity Types: *in*, Reservoirs I: Properties, Treatise of Petroleum Geology Reprint Series No. 3; compiled by Foster, N.H. and Beaumont, E.A., American Association of Petroleum Geologists, Tulsa, OK, p. 419.

Core Lab, 1973, Fundamentals of Core Analysis: Core Laboratories, Inc., Dallas, TX, p. 265.

Desmond, R. J.; Steidtmann, J. R.; and Cardinal, D. F., 1984, Stratigraphy and depositional environments of the Middle Member of the Minnelusa Formation, Central Powder River Basin, Wyoming, *in* Goolsby, J.; and Morton, D. (eds.), The Permian and Pennsylvanian geology of Wyoming: Wyoming Geological Association Guidebook, p. 213–239.

Dewan, J. T., 1983, Essentials of Modern Open-Hole Log Interpretation: PennWell Books, Tulsa, Oklahoma, 361 p.

Dickey, P.A., 1986, Petroleum Development Geology, 3rd ed., PennWell Books, Tulsa, OK, p. 530.

Dickey, P.A., and Soto, C., 1974, Chemical Composition of Deep Subsurface Waters of the Western Anadarko Basin: Society of Petroleum Engineers of AIME Paper No. SPE - 5178, 17 p.

Doll, H.G., 1949, The S.P. Log: Theoretical Analysis and Principles of Interpretation: Society of Petroleum Engineers Reprint Series No. 21, Openhole Well Logging, p. 21–40.

Doll, H. G., 1950, The Microlog—A New Electrical Logging Method for Detailed Determination of Permeable Beds: Society of Petroleum Engineers Reprint Series No. 21, Openhole Well Logging, p.74–83.

Doll, H.G., and Martin, M., 1954, How to Use Electrical Log Data to Determine Maximum Producible Oil Index in a Formation: The Oil and Gas Journal, July 5, p. 120 - 129.

Doll, H.G., Dumanoir, J.L., and Martin, M., 1960, Suggestions for Better Electric Log Combinations and Improved Interpretations; Geophysics, v. XXV, no. 4 (August 1960), p. 854 - 882.

Dorin, A.H., Chase, A.E., and Linke, W.A., 1968, A Guide to Improved Formation Evaluation In Carbonates of Northwestern Alberta: Transactions of the Formation Evaluation Symposium, Canadian Well Logging Society, Calgary, May 6, 1968.

Dresser Atlas, 1982, Well Logging and Interpretation Techniques: The Course for Home Study [3rd edition]: Dresser Atlas, Dresser Industries, Inc., 211 p.

Dresser Atlas, 1983, Log Interpretation Charts: Dresser Atlas, Dresser Industries, Inc., 149 p.

Dresser Atlas, 1985, Log Interpretation Charts: Atlas Wireline Services, Western Atlas International, Inc., 203 p.

Dunham, R.J., 1962, Classification of Carbonate Rocks According to Depositional Texture: *in* W. E. Ham (ed.), Classification of Carbonate Rocks, A Symposium; AAPG Memoir 1, American Association of Petroleum Geologists, Tulsa, OK, p. 108-121.

Dutton, S. P., 1982, Pennsylvanian Fan-Delta and Carbonate Deposition, Mobeetie Field, Texas Panhandle: American Association of Petroleum Geologists Bulletin, v. 66, p. 389–407.

Dutton, S. P.; and Land, L. S., 1985, Meteoric Burial Diagenesis of Pennsylvanian Arkosic Sandstones, Southwestern Anadarko Basin, Texas: American Association of Petroleum Geologists Bulletin, v. 69, p. 22–38.

Edwards, A. R., 1959, Facies Changes in Pennsylvanian Rocks along the North Flank of Wichita Mountains: Petroleum Geology of Southern Oklahoma, v. II, p. 142–155, American Association of Petroleum Geologists, Tulsa, Oklahoma, 341 p.

Evans, J.L., 1979, Major Structural and Stratigraphic Features of the Anadarko Basin, *in* Hyne, N.J., (ed.), Pennsylvanian Sandstones of the Mid-Continent: Tulsa Geological Society Special Publication No. 1, p. 97-113.

Feray, D.E., Heuer, E., and Hewatt, W.G., 1962, Biological, Genetic, and Utilitarian Aspects of Limestone Classification: *in* W. E. Ham (ed.), Classification of Carbonate Rocks, A Symposium; AAPG Memoir 1, American Association of Petroleum Geologists, Tulsa, OK, p. 20-32.

Fertl, W. H.; and Hammack, G. W., 1972, A Comparative Look at Water Saturation Computations in Shaly Pay Sands: The Log Analyst, March–April, v. XIII, No. 2, p. 12–20.

Frank, R.W., 1986, Prospecting With Old E-Logs; Schlumberger Educational Services, Houston, TX, p. 161.

Frost, E., Jr.; Allen, T.; and Fertl, W. H., 1982, Formation Evaluation in Granite Wash Reservoirs: World Oil, September, p. 121–132.

Garber, M., 1999, Abstract from "Improved Interpretation in the Granite Wash Features Combined Measurements": Presentation to Panhandle Geological Society, Amarillo, Texas, March, 31, 1999. Panhandle Geological Society Meeting Announcement, March 31, 1999; 2 p.

Gondouin, M., Tixier, M.P., and Simard, G.L., 1957, An Experimental Study on the Influence of the Chemical Composition of Electrolytes on the SP Curve: Society of Petroleum Engineers Reprint Series No. 21, Openhole Well Logging, p. 59–73.

Gondouin, M., Heim, A., 1964, Experimentally Determined Resistivity Profiles in Invaded Water and Oil Sands for Linear Flows, Journal of Petroleum Technology, March, 1964, p. 337-348, SPE 712.

GRI, 1991, Regional Geology of the Low-Permeability, Gas-Bearing Cleveland Formation, Western Anadarko Basin, Texas Panhandle: Lithologic and Depositional Facies, Structure and Sequence Stratigraphy; Gas Research Institute Tight Gas Sands Topical Report (Bureau of Economic Geology Contract No. 5082-211-0708).

Ham, W.E., and Pray, L.C., 1962, Modern Concepts and Classifications of Carbonate Rocks: *in* W. E. Ham (ed.), Classification of Carbonate Rocks, A Symposium; AAPG Memoir 1, American Association of Petroleum Geologists, Tulsa, OK, p. 2-19.

Hamilton, R.G., 1960, Application of the Proximity Log, Transactions of the Society of Professional Well Log Analysts First Annual Logging Symposium, May 16-17, 1960, Paper F (VI).

Hassan, M., Shu, Z., and Frailey, S.M., 1994, PE 3113 Laboratory Work Manual: Department of Petroleum Engineering, Texas Tech University, p. 67.

Hilchie, D. W., 1979, Old (pre-1958) Electrical Log Interpretation: Douglas W. Hilchie, Inc., Golden, Colorado, 165 p.

Hilchie, D. W., 1982, Advanced Well Log Interpretation: Douglas W. Hilchie, Inc., Golden, Colorado, p. I-1 to XI-14, 359 p.

Houston Geological Society Study Group, 1939, Electrical Well Logging: Bulletin of the American Association of Petroleum Geologists, v. 23, no. 9, September 1939, p. 1287-1313.

Johnson, H.M., 1961, A History of Well Logging: Transactions of the Society of Professional Well Log Analysts Second Annual Logging Symposium, May 18-19, 1961, p. i-vi, 1-27.

JPT, 1999, Formation Evaluation: Logging and Testing: JPT, v. 51, no. 11, November, 1999, p. 20-26.

Keike, E.M., and Hartmann, D.J., 1974, Detecting Microporosity to Improve Formation Evaluation, Journal of Petroleum Technology, October, 1974, p. 1080-1086.

Kenyon, W.E., Howard, J.J., Sezginer, A., Straley, C., Matteson, A., Horkowitz, K., and Ehrlich, R., 1989, Pore Size Distribution and NMR in Microporous Cherty Sandstones: Transactions of the Society of Professional Well Log Analysts Thirtieth Annual Logging Symposium, Paper LL. p. 20.

Lucia, J.F., 1995, Rock-Fabric/Petrophysical Classification of Carbonate Pore Space for Reservoir Characterization, American Association of Petroleum Geologists Bulletin, v. 79, no. 9 (September 1995), p. 1275-1300.

Luo, P., and Machel, H.G., 1995, Pore Size and Pore Throat Types in a Heterogeneous Dolostone Reservoir, Devonian Grosmont Formation, Western Canada Sedimentary Basin, American Association of Petroleum Geologists Bulletin, v. 79, no. 11 (November, 1995), p. 1698-1720.

Martin, M., 1956, S.P. and Conventional Resistivity Logs: *in*, Fundamentals of Logging, University of Kansas Petroleum Engineering Conference, April 2-3, 1956, p. 15-42.

Mason, B., 1966, Principles of Geochemistry, 3rd ed., John Wiley and Sons, Inc., New York, p. 329.

Maxson, R. R., 1969, Three Porosity Movable Oil Plot Vs. Single Porosity Movable Oil Plot to Improve Completion Results in the Wasson field: Society of Petroleum Engineers of AIME Paper No. SPE - 2472, 6 p.

McConnell, D.A., and Gilbert, M.C., 1986, Calculations for Cambrian Extension of the Southern Oklahoma Aulacogen, *in* M.C.Gilbert, (ed.), Petrology of the Cambrian Wichita Mountains Igneous Suite, Oklahoma Geological Survey Guidebook 23, 188 p.

Millican, M.L., Raymer, L.L., and Alger, R. P., 1964, Wellsite Recording of Movable Oil Plot: Transactions of Society of Professional Well Log Analysts Fifth Annual Logging Symposium, Paper F, 11 p.

Morris, R. L.; and Biggs, W. P., 1967, Using Log-Derived Values of Water Saturation and Porosity: Transactions of the Society of Professional Well Log Analysts Eighth Annual Logging Symposium, Paper X. 26 p.

Patchett, J. G.; and Rausch, R. W., 1967, An Approach to Determining Water Saturation in Shaly Sands: Journal of Petroleum Technology, October, p. 1395 – 1405.

Pettijohn, F.J., Potter, P.E., and Siever, R., 1972, Sand and Sandstone, Springer-Verlag, New York, NY, p. 618.

Pirson, S. J.; Boatman, E. M.; Nettle, R. L., 1963, Prediction of Relative Permeability Characteristics of Intergranular Reservoir Rocks from Electrical Resistivity Measurements: Transactions of Society of Professional Well Log Analysts Fourth Annual Logging symposium, Paper VIII, 23 p.

Pittman, E.D., 1971, Microporosity in Carbonate Rocks: American Association of Petroleum Geologists Bulletin, v. 55, no. 10 (October, 1971), p. 1873-1881.

Rascoe, Bailey, Jr.; and Adler, F. J., 1983, Permo–Carboniferous Hydrocarbon Accumulations, Mid-continent, U.S.A.: American Association of Petroleum Geologists Bulletin, v. 67, p. 979–1001.

Raymer, L.L., Salisch, H.A., 1970, The Contribution of Flushed Zone Measurements to Formation Evaluation: The Log Analyst, v. 11, no. 3 (May-June 1970), p. 17-25.

Schlumberger, 1958, Introduction to Schlumberger well logging: Schlumberger Document Number 8, Schlumberger Well Surveying Corporation, 176 p.

Schlumberger, 1972, Log Interpretation Volume I - Principles, Schlumberger, Ltd., New York, NY, p. 113.

Schlumberger, 1974, Log Interpretation Volume II - Applications, Schlumberger, Ltd., New York, NY, p. 116.

Schlumberger, (Edmundson) 1988, Archie's Law: Electrical Conduction in Clean, Water-Bearing Rock: Technical Review, October, v. 36, no. 3, p. 4 – 13.

Schlumberger, 1989a, Log Interpretation Principles/Applications: Schlumberger Educational Services, Houston, TX, p. 1-1 to 13-19, p. 227.

Schlumberger, 1989b, Archie III: Electrical Conduction in Shaly Sands: Oilfield Review, October, v. 1, no. 3, p. 43–53.

Schlumberger, 1989c, Log Interpretation Charts: Schlumberger Educational Services, Houston, TX, p. 227.

Scholle, P.A., 1979, A Color Illustrated Guide to Constituents, Textures, Cements, and Porosities of Sandstones and Associated Rocks: AAPG Memoir 28; American Association of Petroleum Geologists, Tulsa, OK, p. 201.

Singer, J.M., and Barber, T.D., 1988, The Effect of Transition Zones on the Response of Induction Logs: Transactions of the Society of Professional Well Log Analysts Twenty Ninth Annual Logging Symposium, June 5–8, 1988, v. I, Paper L, p. 13.

SPE, 1975, Survey of Resistivities of Water from Subsurface Formations in Oklahoma; Oklahoma City Section, Society of Petroleum Engineers of AIME.

Suau, J., Grimaldi, P., Poupon, A., and Souhaite, P., 1972. The Dual Laterolog - R_{xo} Tool: Society of Petroleum Engineers Reprint Series No. 21, Openhole Well Logging, p.121–132.

Swanson, B.F., 1985, Microporosity in Reservoir Rocks - Its Measurement and Influence on Electrical Resistivity: Transactions of the Society of Professional Well Log Analysts Twenty Sixth Annual Logging Symposium, June 17–20, 1985, v. I, Paper F, p. 17.

Tiab, D. and Donaldson, E.C., 1999, Petrophysics, Gulf Publishing Company, Houston, TX, p. 706.

Tixier, M. P., 1949, Electric Log Analysis in the Rocky Mountains: The Oil and Gas Journal, June 23, v. 48, no. 7, p. 143, 145, 146, 148, 217, 219.

Tixier, M.P., Alger, R.P., and Tanguy, D.R., 1960, New Developments in Induction and Sonic Logging: Society of Petroleum Engineers Reprint Series No. 21, Openhole Well Logging, p.148–173.

Tixier, M. P.; Morris, R. L.; and Connell, J.G., 1968, Log Evaluation of Low Resistivity Pay Sands in the Gulf Coast: The Log Analyst, November-December, v. IX, no. 6, p. 3–20.

Ver Wiebe, W., 1930, Ancestral Rocky Mountains: American Association of Petroleum Geologists Bulletin, v. 14, no. 6, June, p. 765–788.

Walsh, J. W., Brown, S. L., and Asquith, G. B., 1994, Analyzing Well Logs from the Montoya LimeUsing a New Carbonate Well Log Interpretation Procedure: Permian Basin Oil and Gas Recovery Conference, Society of Petroleum Engineers, SPE 27645, p. 291 - 299.

Wang, F.P., and Lucia, J.F., 1993, Comparison of Empirical Models for Calculating the Vuggy Porosity and Cementation Exponent of Carbonates from Log Responses, Geological Circular 93-4, Bureau of Economic Geology, Austin, TX, p. 27.

Watney, W.L., Guy, W.J., Byrnes, A.P., 2001, Characterization of the Mississippian Chat in South-central Kansas: American Association of Petroleum Geologists Bulletin, v. 85, no. 1 (January 2001), p. 85-113.

White, H.E., 1966, Modern College Physics, D. Van Nostrand Company, Inc., Princeton, NJ, p. 765.

Wichmann, P. A., 1986, What's the real Rw?, *in* Problematic Overview: A Series of Six Studies on Difficult Log Analysis: Transactions of the Society of Professional Well Log Analysts Twenty Seventh Annual Logging Symposium, June 9–13, 1986, v. II, Paper NNN, 25 p.

Winsauer, W.O., Shearin, H.M., Masson, P.H., and Williams, M., 1952, Resistivity of Brine-Saturated Sands in Relation to Pore Geometry: *in*, Bulletin of the American Association of Petroleum Geologists, v. 36, no. 2 (February 1952), p. 253-257.

Worthington, P.F., Pallatt, N., Toussaint-Jackson, J.E., 1989, Influence of Microporosity on the Evaluation of Hydrocarbon Saturation: SPE Formation Evaluation, v. 4, no. 2 (June 1989), p. 203-209.

Wyllie, M.R.J., 1949, A Quantitative Analysis of the Electrochemical Component of the S.P. Curve: Society of Petroleum Engineers Reprint Series No. 21, Openhole Well Logging, p. 41–50.

Wyllie, M. R. J., 1954, The Fundamentals of Electric Log Interpretation [1st edition]: Academic Press, New York, New York, 126 p.

Wyllie, M. R. J., 1963, The Fundamentals of Well Log Interpretation [3rd edition]: Academic Press, New York, New York, 238 p.

Zanier, A. M.; and Timko, D. J., 1970, Prediction of Morrow Sand Performance and Geological Environment by Well Log Salinity: API Mid-Continent District Spring Meeting, April 8-10, 1970, Wichita, Kansas; Mid-Continent Division of Production, American Petroleum Institute, Paper No. 851-44–B, 16 p.

APPENDIX A

R_w CALCULATION PROCESS

Permeable zones can be recognized from the spontaneous potential log, SP, where the SP curve takes a negative excursion away from the shale base line. The shale base line is the response recorded on the SP log opposite a thick shale bed. It represents the zone of constant potential measured through a shale section and is called the shale base line. The magnitude of the SP deflection in a permeable bed is measured with reference to the base line developed through the adjacent shale (Wyllie, 1963, p. 37).

The method of Wyllie (1963, p. 37-39) was followed in drawing the shale base line on well logs analyzed in this study. An interval beginning several thousand feet above the zone of interest was examined on the correlation depth scale of the log print. A straight edge was used to draw a line through the deflection minima that are most representative of the shale potential, and the line was extended down through the Prue Sand section. All SP values for Prue Sands used to calculate an R_w value for the sand were determined relative to the shale base line.

According to Doll (1949, p. 21), the SP log is a measurement of the potential drop or change recorded at the contact between a shale and a permeable bed that has been traversed by a mud-filled wellbore. The SP log responds to the natural electrochemical potential developed at such a contact.

Gondouin et al. (1957, p. 61), showed that the electrochemical response of the SP can be characterized by the activities of Na^{+1}, Ca^{+2}, and Mg^{+2} cations in solution in connate water and mud filtrate. The problem in petrophysical analysis examined by Gondouin et al., however, was not to characterize the SP by cation activities from compositional analysis, but to determine the resistivity of connate water from the SP. The concept of equivalent resistivity was introduced by Gondouin et al. to address that problem.

The parameter R_{we}, equivalent connate water resistivity, is a function of the activities of the cations in connate water that was developed empirically by Gondouin, et

al. It was necessary to account for the content of divalent ions and monovalent ions in the connate water, which affects the magnitude of the SP response at low and high salinities, respectively. Gondouin et al. (1957, p. 61, 63) stated that equivalent resistivity values should not be used for mud filtrate unless the mud is known to be calcic, as in a calcium chloride mud or a gypsum-based mud, and presented the following relationship for the quantitative interpretation of the electrochemical spontaneous potential recorded by the SP log.

$$SSP = -K\left[\log\left(\frac{R_{mf}}{R_{we}}\right)\right] \qquad \text{A.1}$$

To calculate the value for R_w in a Prue Sand using this relationship established for the electrochemical potential, it is necessary to use the total *emf* generated by the electrochemical potential. Therefore, it is necessary to use the Static SP, SSP, in the calculation.

According to Doll (1949, p. 23), the Static SP corresponds to the condition in the wellbore mud in which no current is flowing, i.e., a condition of electrically static wellbore mud. Electrical currents from the membrane and liquid junction potentials generated at the contact between a shale and a permeable bed are set in motion in the wellbore mud as a current loop extending some vertical distance above and below the contact. Current loops of opposite direction develop around the upper and lower contacts of the permeable bed within the encasing shale. If a permeable bed is too thin, the extent of the current loops flowing in the mud around the upper and lower contacts can exceed the thickness of the permeable bed and current will flow in the mud across the entire face of the permeable bed. In that case, electrically static conditions can not exist in the wellbore adjacent to that permeable bed, and, therefore, the *S*SP can not be measured by the SP log in that permeable bed. If a permeable bed is too thin for the *S*SP to have developed, then a thin-bed correction to the SP is required.

Dresser Atlas (1982, p. 74) included a relationship, shown here as Equation A.2, to calculate a thin bed correction factor (SP_{CF}) for SP data, which follows SP Correction

Chart 9-1 (Dresser Atlas, 1982, p. 74). Reservoir bed thickness, h, is determined from the upper and lower inflection maxima on the SP curve that define the reservoir bed boundaries (Doll, 1949, p. 24). A value for R_i is read from the shallow induction log across the reservoir bed and R_m is read from the log header and corrected to formation temperature. All R_w calculations completed in this study used this thin bed correction.

$$SP_{CF} = \left[\frac{\left(4\left(\left(R_i/R_m\right)+2\right)\right)^{\frac{1}{3.65}} - 1.5}{h - \left(\frac{\left(\left(R_i/R_m\right)+11\right)}{0.65} \right)^{\frac{1}{6.05}} - 0.1} \right] + 0.95 \qquad \text{A.2}$$

The correction factor is used with the SP data read from the log to determine the SSP value.

$$SSP = SP \times SP_{CF} \qquad \text{A.3}$$

Resistivity is inversely proportional to temperature, therefore, it is necessary to correct the R_{mf} value recorded on the log header to formation temperature. This step requires that formation temperature be determined first, using the general relationship for a temperature gradient shown in Equation A.4 (Asquith, 1982, p. 5).

$$Tgrad = \frac{(BHT - MAST)}{\left(Logger's\ TD/100\right)} \qquad \text{A.4}$$

Where: Tgrad = Geothermal Gradient, °F / 100 ft

BHT = Bottom hole Temperature (recorded on Log Header), °F

MAST = Mean Annual Surface Temperature (Assumed 60° F for this study)

Logger's TD = Total Depth Reached by Logger to record the BHT (recorded on Log Header), ft.

The temperature gradient is applied to the depth at the center of the Prue Sand under investigation to determine formation temperature.

After the formation temperature is determined, the R_{mf} on the log header must be calculated at formation temperature, and the following relationship (Asquith, 1982, p. 26) was used for that purpose:

$$R_{T2} = \frac{[R_{T1} \times (T_1 + 7)]}{(T_2 + 7)} \qquad \text{A.5}$$

Where : T_1 = Temperature Recorded on Log Header for *Rmf* Measurement

R_{T1} = Resistivity at Measured Temperature recorded on Log Header

T_2 = Formation Temperature

R_{T2} = Resistivity at Formation Temperature

With Values for SSP and R_{mf} at formation temperature, the remaining unknown in the SP equation is the constant *K*. Wyllie (1949) indicated the constant *K* was known to be a function of certain electrical properties of the ions in solution and the temperature of the solution. Martin (1956, p. 16) provided an explicit characterization of the constant *K*, shown in Equation A.6, in a solution of pure sodium chloride.

$$K_{millivolts} = 2303 \frac{RT}{F}\left(1 + \frac{u - v}{u + v}\right) \qquad \text{A.6}$$

Where : R = Universal Gas Constant, joules

T_2 = Absolute Temperature, °K

F = the Faraday, coulumbs

u and *v* = Mobilities of the Chloride and Sodium ions, respectively

A theoretical derivation of the value of K that is a form commonly used in the logging industry with only very slight variation among operators, was provided by Bassiouni (1994, p. 131) where T = formation temperature in °F.

$$K = 61.3 + 0.133T \qquad \text{A.7}$$

The SP equation can be rewritten in terms of the value for R_{we}, and note that the SP value used in the relationship is negative.

$$R_{we} = \left[R_{mf} \left(10^{\frac{-SSP}{K}} \right) \right] \qquad \text{A.8}$$

The equation to determine R_{we} used in this study shown below (Dresser Atlas, 1982, p. 75).

$$R_{we} = Rmf \left[10^{\frac{-SSP}{(60+0.133T_f)}} \right] \qquad \text{A.9}$$

The mud filtrate resistivity was used in the relationship, as according to Gondouin et al. (1957, p. 61, 63), R_{mfe} should not be used unless the mud is known to be calcium chloride or gypsum-based mud.

With a value for R_{we}, it is necessary to correct that term to R_w. Two different methods were used to provide an internal check on the results. The first method used is from Dresser Atlas (1982, p. 76) and is shown by Equation A.10.

$$R_w = \frac{R_{we} + \left[0.131 \times 10^{\left(\left(\frac{1}{\log\left(T_f/19.9\right)}\right)^{-2}\right)}\right]}{(-0.5 \times R_{we}) + 10^{\left(\frac{0.0426}{\log\left(T_f/50.8\right)}\right)}} \qquad \text{A.10}$$

The second method used to calculate a value for R_w from R_{we} is from Bateman and Konen (1977), referenced in Asquith (1982, p. 29). Bateman and Konen developed this SP algorithm to duplicate the method of Gondouin et al. (1957) and to match chartbook curves. The algorithm includes two separate equations; which equation is appropriate is determined by the value of R_{we} at 75° F. Equation A.11 should be used if $R_{we} < 0.12$ Ω-m @ 75° F, and Equation A.12 should be used if $R_{we} > 0.12$ Ω-m @ 75° F.

$$R_w @ 75^\circ F = \frac{((77 \times R_{we}) + 5)}{(146 - (377 \times R_{we}))} \qquad \text{A.11}$$

$$R_w @ 75^\circ F = -\left(0.58 - 10^{\,(0.69 R_{we} - 0.24)}\right) \qquad \text{A.12}$$

Figures A.1 through A.3 illustrate the character of the computed results from the Dresser Atlas and Bateman and Konen methods, in a format following the Dresser Atlas Chartbook, Chart 2-3 (1985). Figure A.1 illustrates the case for the Dresser Atlas and Bateman-Konen algorithms at 75° F. *DARw* data represents the Dresser Atlas method shown as Equation A.10. *Asq1Rw* and *Asq2Rw* data represent results from the Bateman-Konen algorithm shown as Equations A.11 and A.12, respectively.

DARw data and *Asq1Rw* data match very well on Figure A.1 and provide a good representation of the correlation shown in the higher salinity portion of Chart 2-3. *DARw* data and *Asq2Rw* data provide a good representation of the two correlations shown in the lower salinity portion of Chart 2-3. *DARw* data represent the correlation for "mostly NaCl" formation water, while *Asq2Rw* data represents the correlation for fresher formation waters influenced by divalent cations, Ca^{+2} and Mg^{+2}.

Figures A.2 and A.3 illustrate the case for the Dresser Atlas and Bateman-Konen algorithms at 150° F and 200° F, respectively. Calculated formation temperatures for Prue Sands examined in this study ranged from 160° F to 195° F. Correlations on both figures hold very well through $R_{we} = 0.60$ at formation temperature, with the "mostly NaCl" correlation deteriorating somewhat above that value to one that would indicate the presence of some divalent cations in solution. The highest Prue Sand R_{we} value at formation temperature in the study was 0.62. The great majority of R_{we} values at formation temperature for Prue Sands in this study fell into the range 0.04 - 0.40, with less than 6% falling between 0.4 and 0.62. The value for R_w calculated from the Dresser Atlas method was used in all petrophysical calculations in this study.

In addition to applying an effective R_w from SP algorithm, it is also critical to the analysis to insure that the values for R_m and R_{mf} provided by the logging service companies are accurate. Operators should emphasize to service companies the importance placed on these values in petrophysical analysis in the Prue.

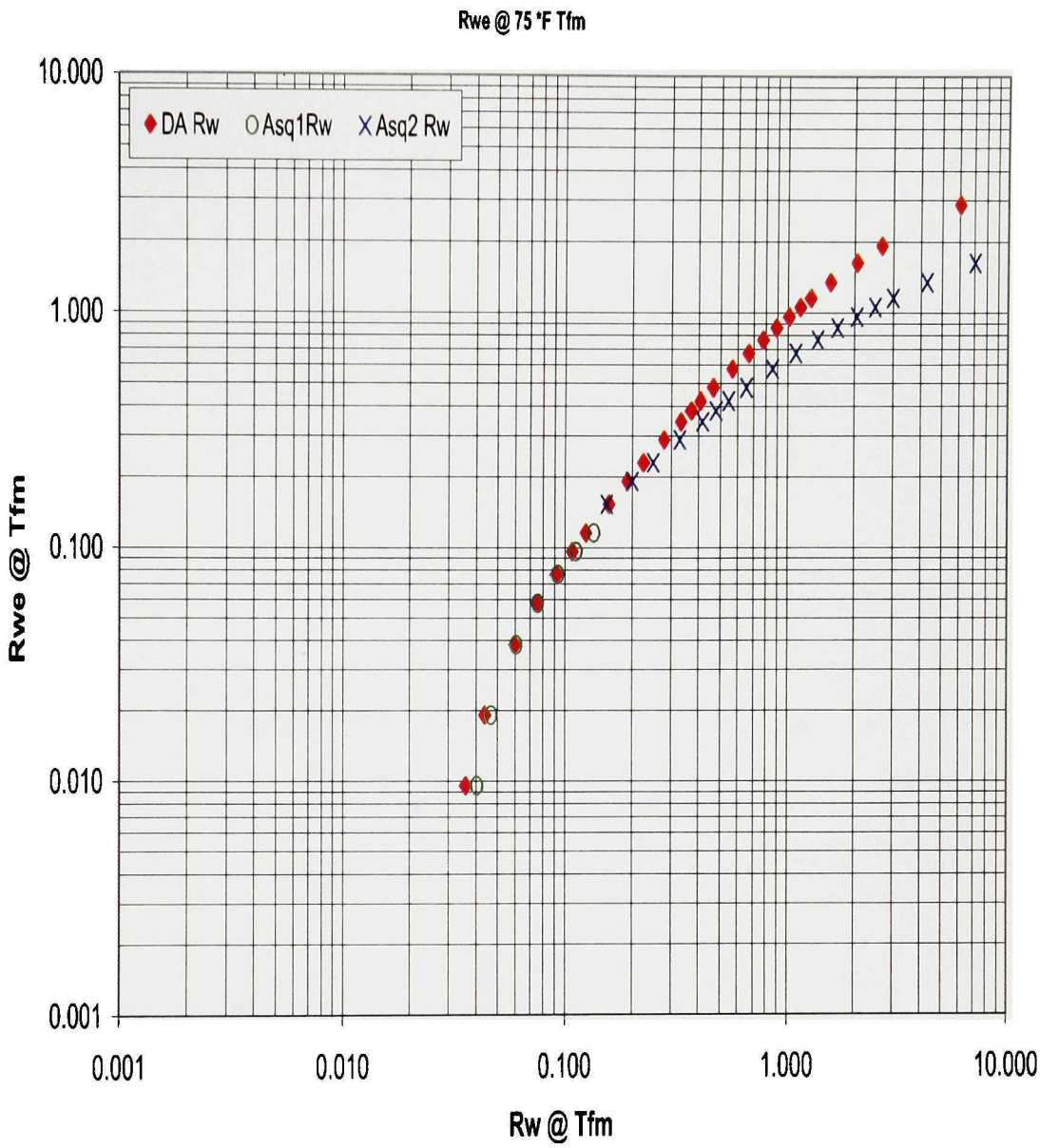

Figure A.1 Relationship between Dresser Atlas and Bateman-Konen Algorithms for R_w from R_{we} at 75° F, Following the Format of Dresser Atlas Chart 2-3. *DARw* Data Represents the Dresser Atlas Method Shown as Equation A.10. *Asq1Rw* and *Asq2Rw* Data Represent Results from the Bateman-Konen Algorithm Shown as Equations A.11 and A.12, Respectively.

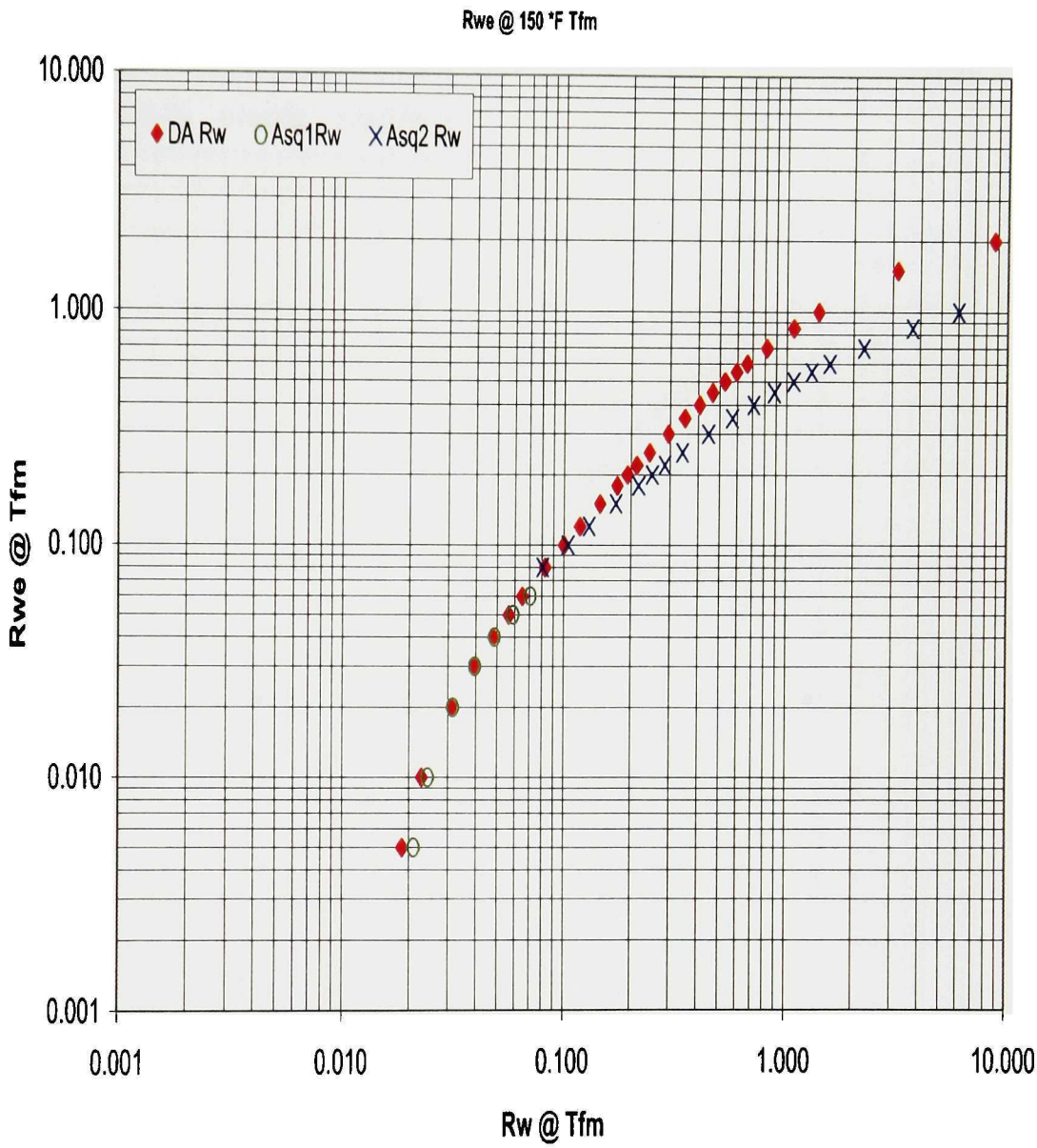

Figure A.2 Relationship between Dresser Atlas and Bateman-Konen Algorithms for R_w from R_{we} at 150° F, Following the Format of Dresser Atlas Chart 2-3. *DARw* Data Represents the Dresser Atlas Method Shown as Equation A.10. *Asq1Rw* and *Asq2Rw* Data Represent Results from the Bateman-Konen Algorithm Shown as Equations A.11 and A.12, Respectively.

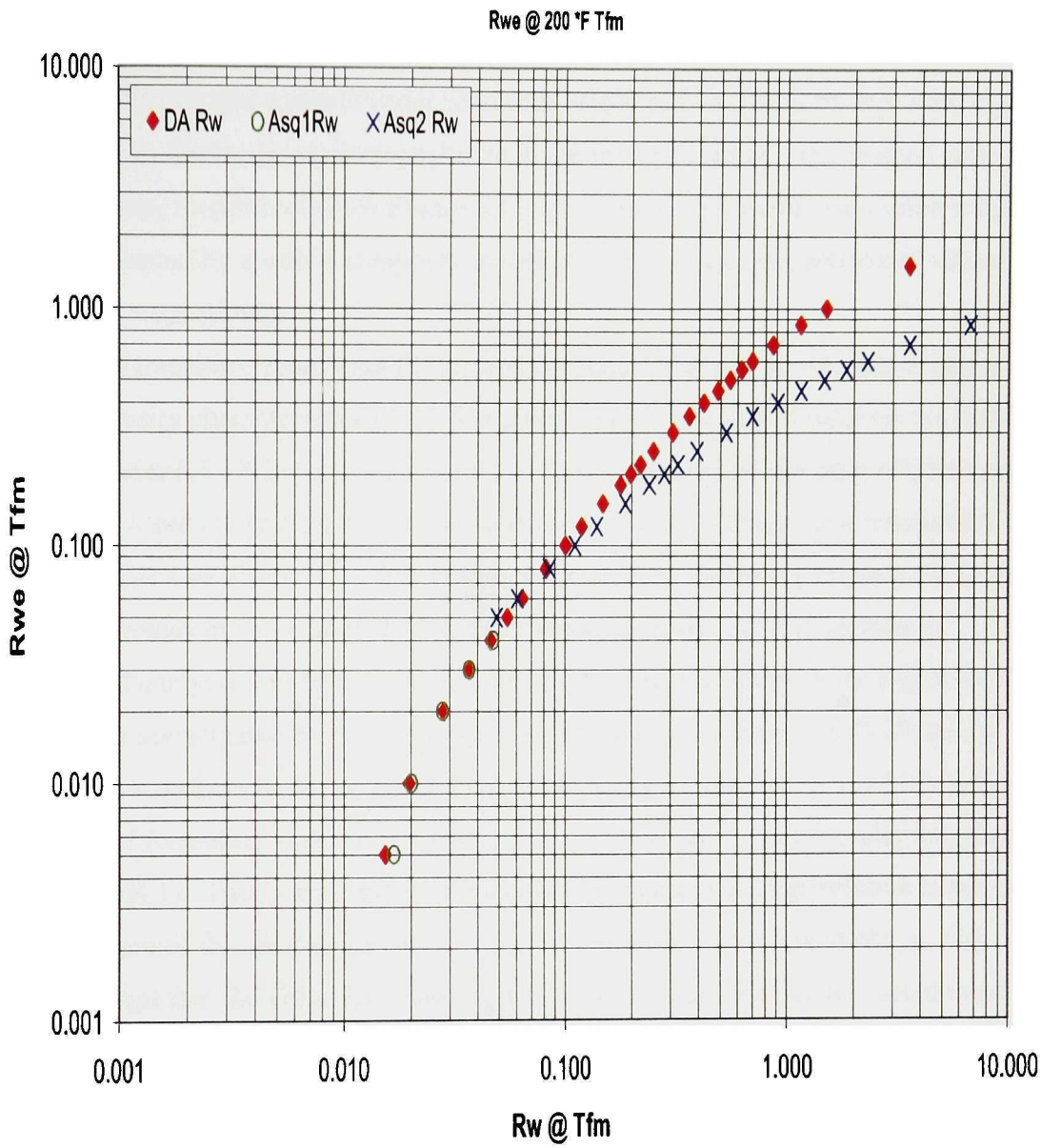

Figure A.3 Relationship between Dresser Atlas and Bateman-Konen Algorithms for R_w from R_{we} at 200° F, Following the Format of Dresser Atlas Chart 2-3. *DARw* Data Represents the Dresser Atlas Method Shown as Equation A.10. *Asq1Rw* and *Asq2Rw* Data Represent Results from the Bateman-Konen Algorithm Shown as Equations A.11 and A.12, Respectively.

APPENDIX B
DEVELOPMENT OF THE z FACTOR AND Rz FOR INVADED ZONE RESISTIVITY ANALYSIS

Mud filtrate and connate water represent brines of two distinctly separate origins, and occupy two distinctly separate positions in the invasion profile, the flushed zone and uninvaded zone, respectively (see Figure 5.11). In that environment, each brine solution can be represented by specific compositional character with distinct resistivity values, *Rmf* and *Rw*, respectively.

In the transition zone, mud filtrate and connate water mix to varying degrees, based on porosity characteristics of the formation, which acts as a control on the depth of invasion. Tixier (1949) introduced a factor, *z*, which represented the ratio of [the volume of formation water] to [the total water volume] in the invaded zone. In a transitional invasion profile (see Figure 5.6), that ratio is very small immediately beyond the flushed zone and increases in value approaching the uninvaded zone. As it is applied in petrophysical analysis, the factor *z* is the percent of formation water in the region of the invaded zone investigated by the shallow resistivity log as a measure of *Ri* (Frank, p. 50).

Several authors have presented a range of values for the factor, *z*, which indicate the volume of formation water in this part of the invasion profile is generally less than 10% (Figure B.1). This is reasonable if the depth of invasion is large relative to the depth of investigation of the shallow resistivity log that measures *Ri*. Frank (1986, p. 50) makes the point that the value for *z* used in petrophysical analysis can be varied to suit conditions in different Basins and rock types, but should be related to formation porosity which affects depth of invasion. Asquith ties the appropriate value for *z* to depth of invasion. Smaller values of *z* accompany deeper invasion because deeper invasion indicates a greater pore volume of invaded filtrate available at any point along the invasion profile compared to shallower invasion. As the depth of invasion decreases, the pore volume of mud filtrate diminishes more rapidly across the invasion profile than in

deeper invasion, and the compensatory pore volume of connate water increases more rapidly.

When an appropriate value for the *z* factor is determined for the reservoir in question, then it is used to calculate a value for *Rz*, which, according to Tixier, is the resistivity of the mixed water in the invaded zone. There are three representative brine resistivity values across the invaded zone, *Rz* is analogous to *Rmf* and *Rw*. Equation B.1, from Schlumberger (1989, p. 8-7) was used in this study to calculate necessary *Rz* values. This same relationship is also published in Frank (1986, p. 50) and Hilchie (1982, p. III-6).

$$\frac{1}{R_z} = \frac{z}{R_w} + \frac{1-z}{R_{mf}} \qquad \text{B.1}$$

The equation for *Rz* was developed by Tixier (1949), and is shown in its original form in Equation B.2. The factor *Rm* represents *Rmf* in Tixier's equation.

$$\frac{R_z}{R_w} = \frac{R_m / R_w}{(1-z) + \left[z \left(R_m / R_w \right) \right]} \qquad \text{B.2}$$

The following sequence of factoring relationships demonstrates the equivalence of Equations B.1 and B.2.

$$\frac{R_z}{R_w}\left(\frac{R_w}{R_{mf}}\right) = \left[\left(\frac{1}{(1-z) + \left(z \left(R_{mf} / R_w \right) \right)}\right)\right]$$

$$\frac{R_z}{R_{mf}} = \left[\left(\frac{1}{(1-z)+\left(z\left(R_{mf}/R_w\right)\right)}\right)\right]$$

$$\frac{R_{mf}}{R_z} = \left[(1-z)+\left(z\left(R_{mf}/R_w\right)\right)\right]$$

$$\frac{1}{R_z} = \frac{\left[(1-z)+\left(z\left(R_{mf}/R_w\right)\right)\right]}{R_{mf}}$$

$$\frac{1}{R_z} = \left[\left(\frac{1-z}{R_{mf}}\right)+\left(\frac{z\left(R_{mf}/R_w\right)}{R_{mf}}\right)\right]$$

$$\frac{1}{R_z} = \left[\left(\frac{1-z}{R_{mf}}\right)+\left(\frac{z}{R_w}\right)\right]$$

For convenience, the final equation can be rewritten as Equation B.3, in terms of *Rz* rather than reciprocal *Rz*.

$$R_z = \frac{1}{\left(1 - z/R_{mf} + z/R_w\right)} \qquad \text{B.3}$$

Sedimentary Rock Type	Porosity (%)	Z Factor	Depth of Invasion
M. P. Tixier (1949) Recommended Values			
Rocky Mountain Reservoirs	Shaly Sand	> 0.100	
Rocky Mountain Reservoirs	Average Rocky Mountain Reservoir	0.100	
Rocky Mountain Reservoirs		0.075	
Rocky Mountain Reservoirs		0.050	
Rocky Mountain Reservoirs	Below Average	0.025	
R. Hamilton (1960) Recommended Values			
		$(1/F_R)^{(1/2.05)}$	Slight Flushing
		$(1/F_R)^{(1/1.41)}$	Average Flushing
		$(1/F_R)$	Extreme Flushing
S. Pirson (1963, p. 57) Recommended Values			
	> 25	0.100	
	18 - 25	0.075	
	10 - 18	0.050	
R. Frank (1986, p. 50) Recommended Values			
Gulf Coast "Soft" Sands	30 - 35	0.150	Shallow
	20 - 25	0.100	Shallow
Mid-Continent Sands	15 - 25	0.080	Moderate
Carbonates & Tight Sands	10 - 15	0.050	Deep
	5 - 10	0.030	Deep
Dr. G. Asquith (TTU Adv. Petrophysics) Recommended Values:			
	Higher	0.100	Very Shallow (< 20")
	↓	0.075	Shallow (20"– 30")
	↓	0.050	Average (30" – 60")
	↓	0.035	Deep (60" – 80")
	Lower	0.025	Very Deep (> 80")

Figure B.1 For comparison, values for the factor, *z*, percent connate water in the invaded zone, based on specified rock-fluid property relationships, published by several different authors.

APPENDIX C
DEVELOPMENT OF RESISTIVITY POROSITY

Schlumberger (1958, p. 18) presented the following relationship for the computation of formation porosity from resistivity measurements.

$$\phi = \frac{1}{S_{xo}} \left(\frac{R_{mf}}{R_{xo}} \right)^{1/2} \qquad \text{C.1}$$

Asquith (1982, p. 45) illustrated the development of that relationship, using the equation for calculating water saturation in the flushed zone, Sxo, based on the Archie equation for water saturation in the uninvaded zone (Equation C.2).

$$S_w{}^n = \frac{F_R R_w}{R_t} \quad \Rightarrow \quad S_{xo}{}^n = \frac{F_R R_{mf}}{R_{xo}} \qquad \text{C.2}$$

If the value for the empirical parameter, n, is assumed 2.0, then the Equation C.2 can be rewritten as Equation C.3, which can be followed mathematically to Equation C.4.

$$F_R = \frac{a}{\phi^m} = S_{xo}{}^2 \left(\frac{R_{xo}}{R_{mf}} \right) \qquad \text{C.3}$$

$$\phi^m = \left(\frac{a}{S_{xo}{}^2} \right) \left(\frac{R_{mf}}{R_{xo}} \right) \Rightarrow \phi = \left[\frac{1}{S_{xo}{}^2} \left(\frac{aR_{mf}}{R_{xo}} \right) \right]^{\frac{1}{m}} \qquad \text{C.4}$$

Equation C.4 is the relationship used to determine formation porosity, corrected for residual hydrocarbon saturation. When the parameter a is assumed to be 1.0 and the reservoir is assumed to be wet, so that $S_{xo} = 1.0$, then Equation C.4 reduces to Equation C.5, the relationship for resistivity porosity using flushed zone resistivity measurements.

$$\phi_{Rxo} = \left(\frac{R_{mf}}{R_{xo}} \right)^{\frac{1}{m}} \qquad \text{C.5}$$

If the reservoir is hydrocarbon-bearing, then the porosity value computed from Equation C.5 will be reduced by the amount of residual hydrocarbon saturation that would have been accounted for in Equation C.3. For example, assume a formation where $R_{mf} = 0.50$ Ω-m, $R_{xo} = 15$ Ω-m, $S_{xo} = 0.70$, and the empirical parameter $m = 2.0$. Then $\phi_{Rxo} = 0.26$ from Equation C.3, but from Equation C.5, $\phi_{Rxo} = 0.18$, indicating true formation porosity in the assumed formation is 26% and water-filled porosity in the flushed zone = 18%. A check confirms that 0.18 / 0.26 = 0.7 = S_{xo}.

APPENDIX D
METHOD IN ESTIMATION OF IRREDUCIBLE WATER SATURATION

Equation D.1 is used to estimate irreducible water saturation, *Swirr*, for a "clean" (i.e. clay free) medium - coarse grained (0.5mm) sandstone.

$$S_{wirr} = \sqrt{\frac{F_R}{2000}} \qquad \text{D.1}$$

Coarse-grained grain packs have less grain surface area than finer-grained grain packs, consequently, coarser grained packs have lower irreducible water saturation values than do finer-grained packs. Therefore, if the assumption of coarse grain size is not representative of the actual formation texture, and is too coarse, the consequent estimated irreducible water saturation values, *Swirr*, will be too low for the actual texture of the formation. Therefore, calculated Archie water saturation values, *Swa*, applied in Equation 5.21 will be greater than the estimated *Swirr* values, and the consequent calculated relative permeability to water, *krw*, will be greater than zero. Further, the calculated relative permeability to gas, *krg*, will be less than 1.0, even if the formation actually is at *Swirr*. It appears, however, that in such a case, calculated *krg* values will be reasonably consistent, albeit at values less than 1.0. For example, the reservoir could exhibit consistent calculated *krg* values about 0.40, and *krw* near zero. The ratio of *krw* to *krg* will be very small.

Equations D.2 through D.4 illustrate the basis for estimating the irreducible water saturation as given in Equation D.1. This *Swirr* estimation relationship is based on the bulk volume water relationship, $BVW = S_w\phi$, for a coarse grained sand, which, according to Asquith (1982, p. 98, Table 8) has a range of values from 0.02 to 0.025. Further, it assumes that $a = 1.0$, $m = 2.0$ in the F_R relationship; n is not a part of this relationship. Note that the exponent 2 is introduced to correlate *Sw* to $F_R = 1/\phi^2$,

therefore the exponent relates to the value for the empirical parameter *m*, not *n*. A value for BVW = 0.022, from the midrange of values shown by Asquith for coarse grained BVW values, is used in the example illustrated below, and emphasizes that this method to determine irreducible water saturation is an estimate based on an approximation. Using a BVW value of 0.02236 results in the equation shown in D.1.

$$BVW_{irr} = 0.022 = S_{wirr} \times \phi \Rightarrow (0.022)^2 = (S_{wirr} \times \phi)^2 = {S_{wirr}}^2 \times {\phi}^2 \qquad \text{D.2}$$

$$4.84 \times 10^{-4} = Swirr^{\,2} \times \phi^{\,2} \;\Rightarrow\; \frac{1}{4.84 \times 10^{-4}} = \frac{1}{{S_{wirr}}^2} \times \frac{1}{\phi^2} \;\Rightarrow\; \left[F_R = \frac{1}{\phi^2} \right] \qquad \text{D.3}$$

$$2066 \times {S_{wirr}}^2 = F_R \;\Rightarrow\; {S_{wirr}}^2 = \frac{F_R}{2066} \;\Rightarrow\; S_{wirr} = \sqrt{F_R / 2066} \qquad \text{D.4}$$

$$@\,Cgr\ BVW_{irr} \;\Rightarrow\; S_{wirr} = \sqrt{F_R / 2066} \qquad \text{D.5}$$

A Quick Look method to convert a BVW value to the appropriate value for the denominator in the *Swirr* estimation relationship:

1. If the empirical parameter $m = 2.0$ and $a = 1.0$,
2. Square the BVW value
3. Invert the squared value
   - BVW = 0.022
   - $0.022^2 = 4.84 \times 10^{-4}$
   - $1/(4.84 \times 10^{-4}) = 2066$
4. If the empirical parameter a, assumed to be 0.81, then
   - BVW = 0.02
   - $0.02^2 = 4 \times 10^{-4}$
   - $0.81/(4 \times 10^{-4}) = 2025$

Table D.1 Relationships to Estimate Irreducible Water Saturation for Different Siliciclastic Grain Size Ranges (See Table 8, Asquith, 1982, p.98)

Swirr Eqn. @	BVW =	for Grain Size
$(F_R / 2000)^{0.5}$	0.022	Coarse (Cgr)
$(F_R / 1111)^{0.5}$	0.030	Medium (Mgr)
$(F_R / 750)^{0.5}$	0.037	Fine, Upper (Fgru)
$(F_R / 500)^{0.5}$	0.045	Fine, Lower (Fgrl)
$(F_R / 275)^{0.5}$	0.060	Very Fine (Vfgr)
$(F_R / 150)^{0.5}$	0.082	Silt

APPENDIX E
STANDARD DEVIATION SCREEN IN ESTIMATION OF BVW SCATTER AS AN INDICATOR OF IRREDUCIBLE WATER SATURATION

A series of computer-generated reservoirs with synthetic porosity and water saturation pairings were developed and cross plotted to evaluate how well the Sw - Phi data fit a hyperbolic trend. The standard deviation of the BVW values from each synthetic reservoir was computed and is shown on each respective porosity - water saturation cross plot.

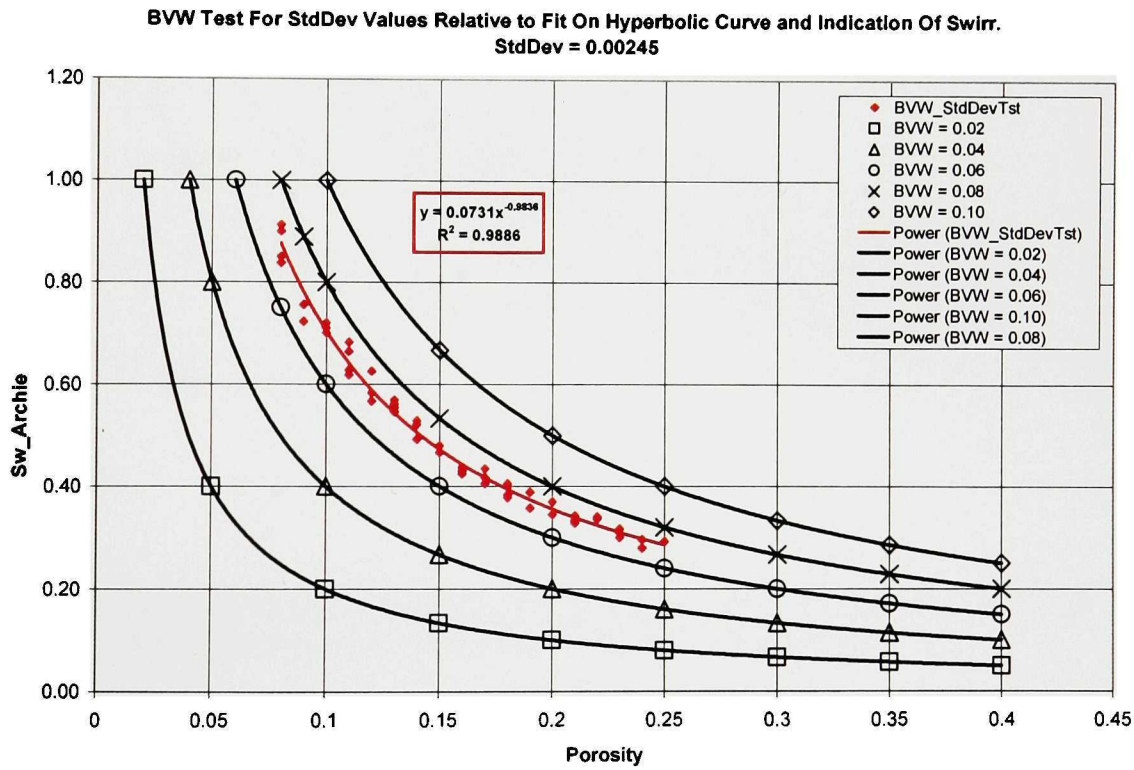

Figure E.1 Standard Deviation Screen for Minimal Scatter along a Hyperbolic Trendline.

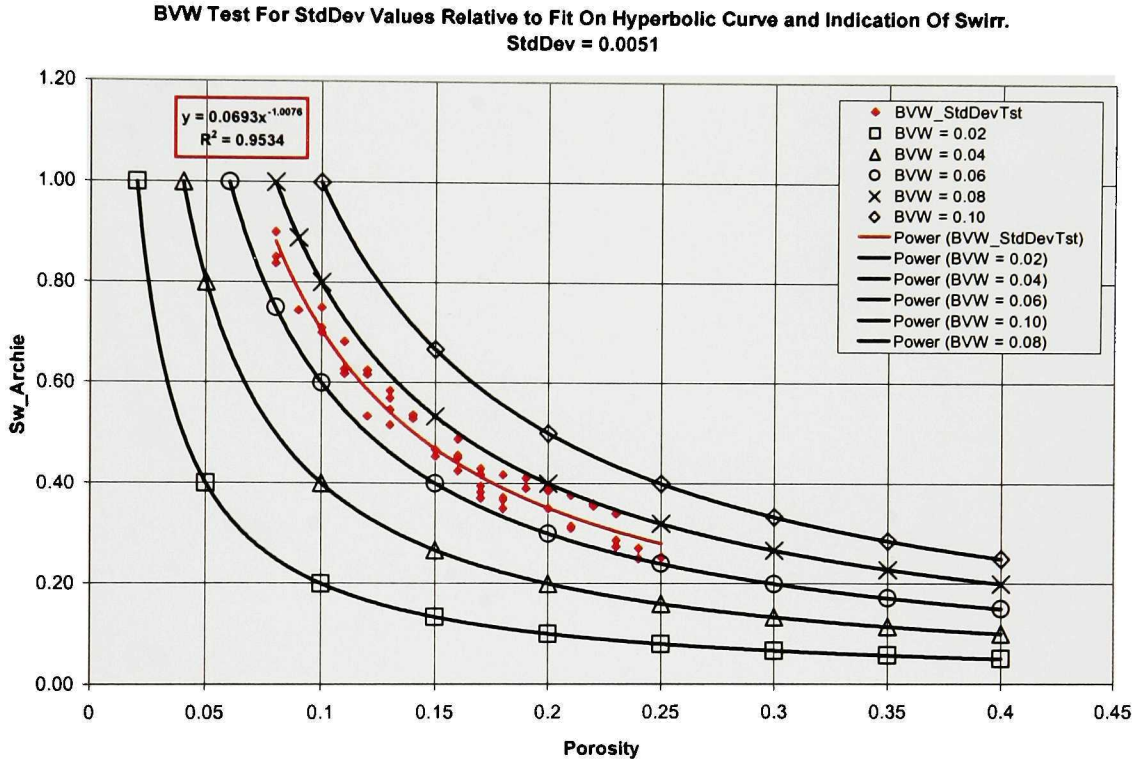

Figure E.2 Standard Deviation Screen for Slight Scatter Along a Hyperbolic Trendline Within the First Pair of Standard BVW Bounding Curves.

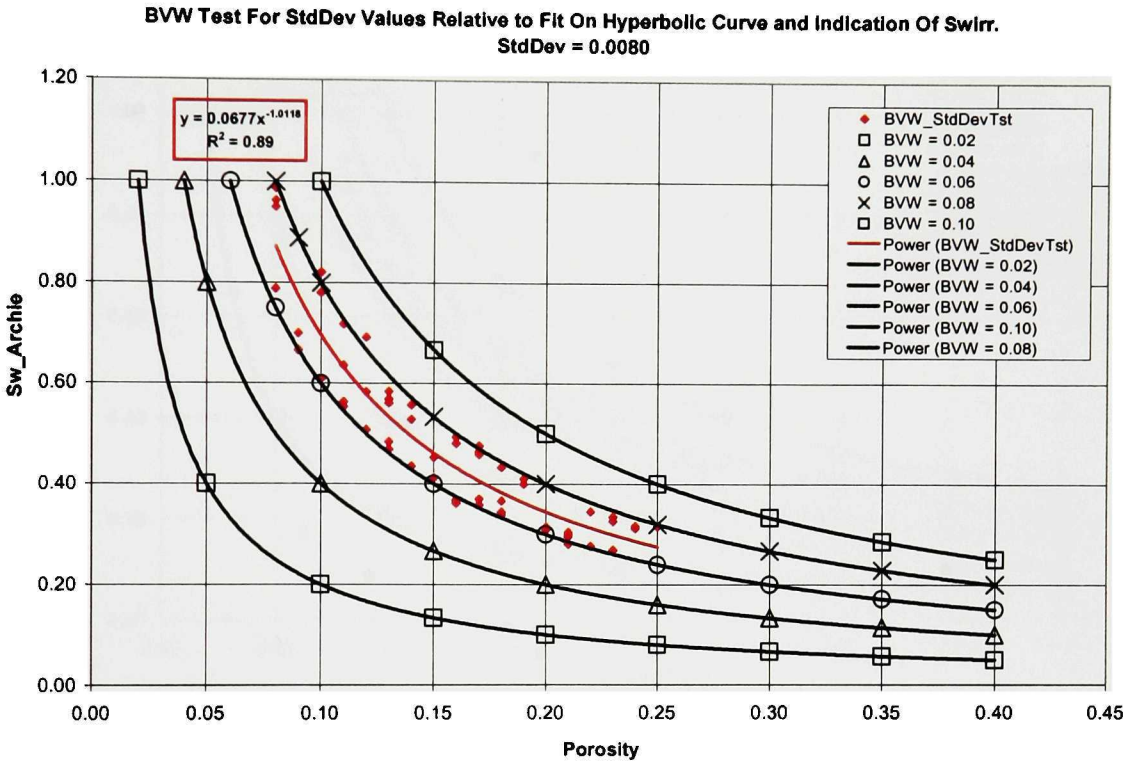

Figure E.3 Standard Deviation Screen for Moderate Scatter about a Hyperbolic Trendline, with Scatter Spread to First Pair of Standard Bounding Curves.

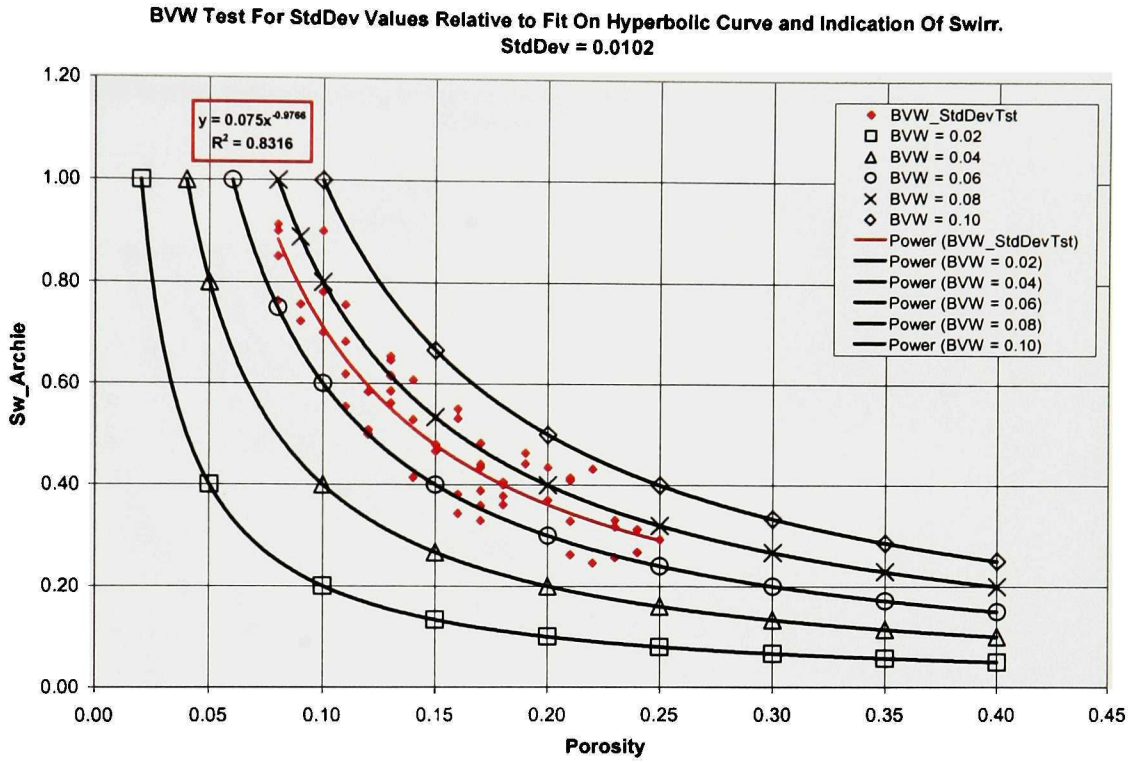

Figure E.4 Standard Deviation Screen for High Scatter about a Hyperbolic Trendline, with Scatter Exceeding First Pair of Standard Bounding Curves.

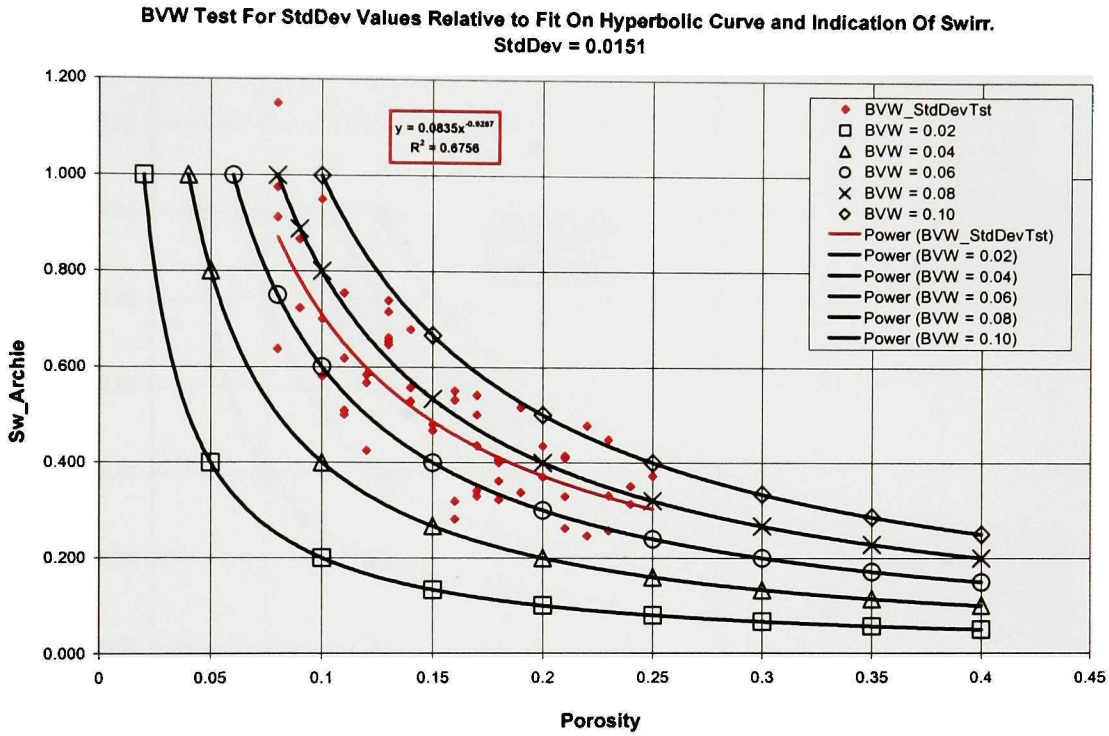

Figure E.5 Standard Deviation Screen for Very High Scatter about a Hyperbolic Trendline, with Scatter Approaching the Second Pair of Standard Bounding Curves.

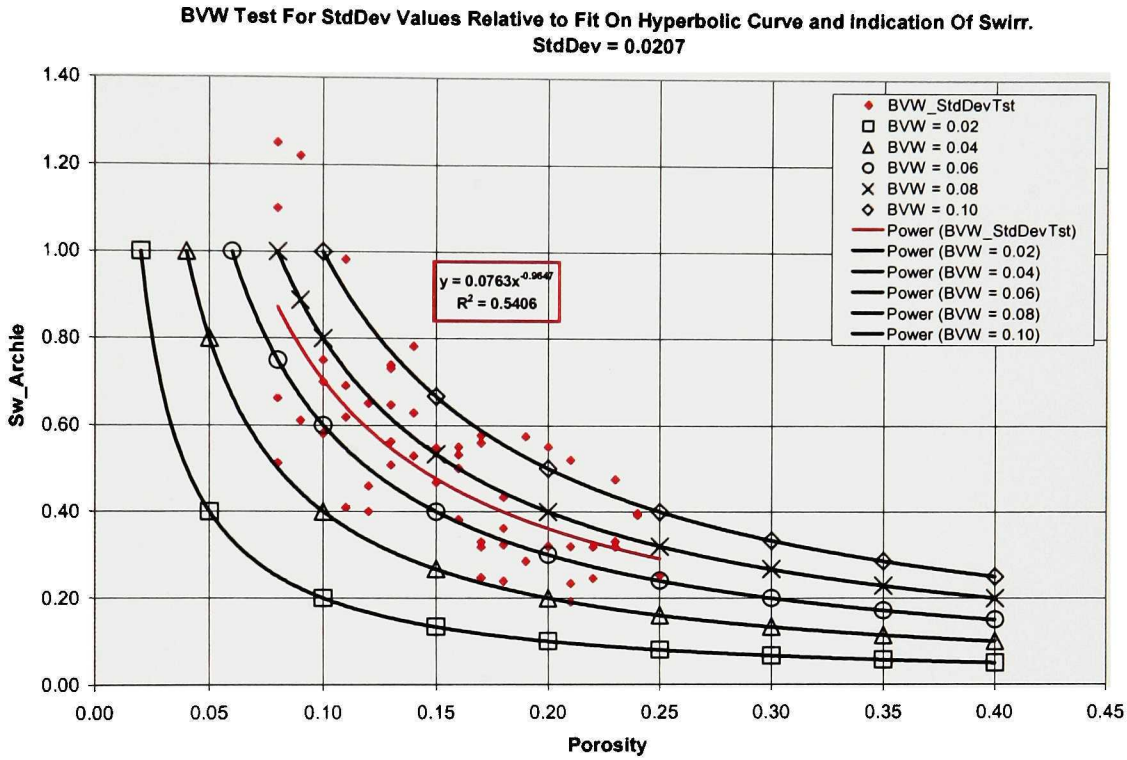

Figure E.6 Standard Deviation Screen for Extremely High Scatter about a Hyperbolic Trendline, with Scatter Exceeding the Second Pair of standard Bounding Curves.